The Functions of Rictor, Pten, and p53 Signaling Pathways in Brain Tumors and Brain Development

by

Seckin Akgul

A dissertation submitted in partial fulfillment
of the requirements for the degree of
Doctor of Philosophy
(Cellular and Molecular Biology)
in the University of Michigan
2015

Doctoral Committee:

Professor Yuan Zhu, Co-Chair
Professor Eric R. Fearon, Co-Chair
Professor Mark L. Day
Associate Professor Diane C. Fingar
Associate Professor Ivan P. Maillard

Dedication

This thesis is dedicated to my beloved family, including my mom Birgül Akgül, my dad M. Zeki Akgül, my brother Meriç Akgül, my grandma Fevziye Atay, and my granddad Muammer Atay, and to patients who suffer from brain disorders.

Acknowledgements

I would like to thank my academic adviser Professor Yuan Zhu, who has contributed tremendously to my academic progress over the years. This thesis would have not been possible without his generous support and valuable guidance. Our almost-everyday scientific discussions and personal conversations made my graduate school years full of excellent memories.

My co-adviser Professor Eric R. Fearon and the rest of my thesis committee members, including Professor Mark L. Day, Associate Professor Diane C. Fingar and Associate Professor Ivan P. Maillard have committed remarkable amount of time and effort in my doctorate studies. I consider myself very lucky to have them as my teachers. Each of them has been a role model for my academic and personal life.

I would like to acknowledge the Watersons, especially my former roommate Michael J. Waterson, who have been a family for me in the U.S. It would have been very difficult to pursue my academic career if it was not for them.

Thanks to my lovely friends, I have built so many great memories during my graduate school years. Zeynep Akgöç, Merih Angın, Pelin Angın, Tayfun Bilgin, Cansu Çimen, Hanife Broome, Nilüfer Esen-Bilgin, Jeremy Johns, Hande Koçak, Gürkan Muş, and Diego A. Ortiz Parra have been the most special friends bringing me joy and happiness over the years.

Undergraduate students Vinay Guduguntla, Emily Li, and Cristal Lee, and medical school student Gerald Tomasek have contributed significantly to the projects described

here. Thanks to their great work, many experiments have been completed in a short time period.

I had the chance to collaborate with many great scientists both in the USA and Europe. I deeply appreciate their help and contribution to my projects. Specifically, I would like to thank to Drs. Roeland G. W. Verhaak, Siyuan Zheng, Kun-Liang Guan, Tsuneo Ikenoue, Stefan M. Pfister, Marcel Kool, Sebastian Stark, Sandra Camelo-Piragua, James F. Gusella, Yiping Shen, and Yinghua Li.

I am also grateful to Zhu Laboratory members, particularly Dr. SunJung Kim, Dr. Yuan Wang and Daniel M. Triesman for their generous friendship and significant contributions to my graduate work.

I owe many thanks to our former program administrator Cathy Mitchell and current administrator Margarita Bekiares, who have been generously taking care of us without a hesitation. None of this academic and friendly environment would have happened without their hard work. Furthermore, our former program director Dr. Jessica Schwartz and current director Dr. Robert Fuller have created an atmosphere filled with friendship, success stories, motivation, and fun. Thanks to them, I will always consider CMB program as my home.

And finally, I would like to acknowledge the most special people in my life, my family. My mom Birgül, my dad Zeki, my brother Meriç, my grandma Fevziye and my granddad Muammer have been the biggest motivation and happiness in my life. I owe all of my accomplishments to their ever-lasting love and strong principles that have guided me for over 29 years.

Table of Contents

List of Tables

List of Figures

Abstract

The Functions of Rictor, Pten, and p53 Signaling Pathways

in Brain Tumors and Brain Development

by

Seckin Akgul

Glioblastoma is the most common malignant neoplasm of the central nervous system. Despite intense treatment plans and supportive care, the median survival rate remains approximately 12-15 months. Comprehensive analyses have demonstrated that approximately 90% of glioblastomas have elevated PI3K/AKT signaling accompanied by chromosome-10 (chr10) loss. We, therefore, investigated the clinical implications of genetically inhibiting Rictor/mTORC2, a positive regulator of the PI3K/AKT pathway. We show that mutant-*p53* driven mouse gliomas undergo independent but concurrent loss of chr19 and chr7, syntenic to human chr10q, which results in *Pten* deletion and hyperactivation of PI3K/Akt. Removal of *Rictor*, and by extension PI3K/Akt signaling, exerts significant tumor suppressive activity in both initiation and progression of high-grade gliomas. However, this oncogenic pathway is not absolutely required for a group of gliomas, calling for a need to identify the other molecular events that may lead to tumor resistance and recurrence.

Unpredictably, embryonic inactivation of Rictor/mTORC2 increases the frequency of mutant-*p53* driven medulloblastoma development. In contrast to glioblastoma, which is mostly associated with adult oncology cases, medulloblastoma is largely a pediatric malignancy of the cerebellum affecting infants and children. Our analyses suggest that

Rictor loss delays the cell cycle exit and neuronal differentiation in a subset of cerebellar progenitors leading to an increased predisposition to mutant-*p53* induced medulloblastoma formation. These tumors exhibit distinctive genomic alterations that are associated with poor clinical outcome, providing a platform to study alternative treatment options for incurable kids.

Given the cell type-specific roles of Rictor/mTORC2/Akt signaling in brain tumorigenesis, our additional analyses aimed to understand its roles in different neuronal populations during the brain development. We show that intact Pten functions, including the regulation of PI3K/Akt signaling, are required for the proper neuronal layering, and the generation and/or survival of a subset of projection neurons in the cerebral cortex. These findings provide valuable insight into cognitive and neurodevelopmental defects observed in patients with germline *PTEN* mutations.

Together, this thesis work identifies Rictor/mTORC2 as a signaling pathway with opposing roles in adult and pediatric brain tumors, and uncovers novel roles for Pten in the formation of neuronal architecture during the brain development.

Chapter I: Introduction

1.1 Malignant gliomas and glioblastoma

Malignant gliomas are the most common and lethal primary brain tumors (Furnari et al., 2007; Louis, 2006). These deadly intracranial tumors can occur in all age groups, however, they are mostly observed in adult patients over the age of forty-five, making them the most common adult neuro-oncology cases (Louis, 2006; Watkins and Sontheimer, 2012). Gliomas are divided into different degrees of malignancy based on World Health Organization (WHO) classification criteria: Grade I gliomas are considered to be benign and can be cured with a successful surgical resection, however, grade II-IV gliomas (i.e. malignant gliomas) exhibit gradually increased anaplasia, malignancy, and proliferation (Furnari et al., 2007). Consequently, while grade-II and grade-III gliomas are often associated with 5-15 years and less than 3 years of overall survival rates, respectively, grade-IV gliomas (also known as glioblastoma) are highly resistant to conventional radiotherapy and chemotherapy leading to extremely low survival rates of approximately 12-15 months. (Huse et al., 2013; Louis, 2006; Louis et al., 2007). Overall, approximately 60-70% of the malignant gliomas are glioblastomas, while 10-15% are anaplastic astrocytomas, and 10% are anaplastic oligodendriogliomas and oligoastrocytomas. The remaining rare portion includes anaplastic ependymomas and anaplastic gangliogliomas (Wen and Kesari, 2008).

Approximately 90% of glioblastomas develop rapidly without any preceding clinical or histological evidence of a less malignant lesion (e.g. grade I-III). These *de novo* tumors are called “primary glioblastoma” and they mostly manifest in elderly patients.

"Secondary glioblastoma", on the other hand, gradually progress from an already-detected low-grade diffuse astrocytoma or anaplastic astrocytoma. These tumors are mostly found in younger patients and mostly associated with comparatively better clinical outcomes (Furnari et al., 2007; Ohgaki and Kleihues, 2013). Even though these two types of glioblastomas have very similar histopathologic features, recent studies identified different cell-of-origin and genetic alterations required for their formation (Brennan et al., 2013; Nobusawa et al., 2009).

Approximately 10,000 new patients are diagnosed with glioblastoma in the USA each year (Cloughesy et al., 2014). Typical symptomatic presentation includes headaches, seizures, focal neurological deficits, memory loss, confusion and personality changes (Watkins and Sontheimer, 2012). As these tumors exhibit extremely aggressive growth characterized by infiltration and widespread invasion surrounding the brain, it is virtually impossible to surgically resect the tumor mass completely (Cloughesy et al., 2014). Even though the subsequent treatments including ionizing radiation, cytotoxic chemotherapy with alkylating agent temozolomide and intense supportive care can increase the survival, tumors typically recur after an average of only 6.9 months (Huse et al., 2013; Watkins and Sontheimer, 2012). As a result, the overall 5-year survival rate of glioblastoma patients remains less than 5%, which is even worse for older patients (Chen et al., 2012b). Poor drug delivery and tumor heterogeneity are considered to be the other main factors that limit the effectiveness of the current treatment strategies (Sottoriva et al., 2013). The presence of intratumor and intertumor heterogeneity, in particular, suggests that molecularly distinct tumors might exhibit differences in progression, prognosis, and clinical implications (see below) (Phillips et al., 2006; Verhaak et al., 2010).

1.2 Molecular signature of glioblastoma and key pathway alterations

How does a perfectly normal and functional cell transform into a malignant cell, and what are the roles of molecular alterations that it acquires during the initiation and/or progression of a disease? Answering these questions requires detailed and careful

analyses of the tumor cells, and accurate interpretation of the findings. Integrated multi-dimensional investigations, including large-scale genomic, transcriptomic and epigenetic analyses have been performed to increase our knowledge of the molecular basis of glioblastoma. For instance, sequencing analyses identified *PTEN*, *TP53*, *NF1*, *RB1* (tumor suppressor genes), *EGFR*, *PIK3CA*, *PIK3R1*, *PDGFRA* (oncogenes) and *IDH1* as the significantly mutated genes in glioblastoma (Table 1) (Brennan et al., 2013; Cancer Genome Atlas Research, 2008; Parsons et al., 2008). Copy number analyses uncovered amplifications in many important oncogenes including *EGFR*, *MET*, *CDK6*, *CDK4*, *MDM2* and *PDGFRA*. In addition, frequent gains of *AKT3*, *SOX2*, *MYCN*, *CCDN1* and *CCNE2* have also been detected. Deletions, which are more frequent than amplifications, include *CDKN2A/B*, *PTEN*, *CDKN2C*, *RB1*, *PARK2* and *NF1* (Table 1). These altered genes normally function in three major signaling pathways. As a result, 90% of the glioblastomas have alterations in PI3K/RTK signaling, 86% in p53-signaling and 79% in Rb-signaling, underlining the landscape of pathway alterations in glioblastomas (Brennan et al., 2013; Cancer Genome Atlas Research, 2008; Parsons et al., 2008).

Table 1. **Most common somatic alterations and deregulated core signaling pathways in human glioblastomas.**

Gene name	Location	Frequency	Molecular event	Assoc. pathway
CDKN2A/B	Chr9	61 %	Deletion/mutation	p53 & Rb
EGFR	Chr7	57 %	Amplification/mutation	PI3K/RTK
PTEN	Chr10	41 %	Deletion/mutation	PI3K/RTK
TP53	Chr17	28 %	Deletion/mutation	p53
PIK3C/R *	Multiple chr.	25 %	Amplification/mutation	PI3K/RTK
CDK4	Chr12	14 %	Amplification/mutation	Rb
PDGFRA	Chr4	10 %	Amplification/mutation	PI3K/RTK
NF1	Chr17	10 %	Deletion/mutation	PI3K/RTK
MDM2	Chr12	7.6%	Amplification/mutation	p53
RB1	Chr13	7.6 %	Deletion/mutation	Rb
MDM4	Chr1	7.2 %	Amplification/mutation	p53
CDKN2C	Chr1	5.6 %	Deletion/mutation	Rb

*PIK3C/R is a combination of multiple genes, including *PIK3CA, PIK3R1, PIK3C2G, PIK3CG, PIK3CB, PIK3C2B, PIK3C2A* and *PIK3R2,* which encode for PI3K family.

In addition to signaling pathway-associated genes, several epigenetic control genes are also deregulated. Of those, *IDH1*, which is a chromatin modifier and associated with lower grade gliomas or secondary glioblastoma, is mutated in 5% of the total cases. SWI/SNF complex gene *ATRX* is also mutated in 6% of the tumors, most of which co-occurred with *IDH1* alterations. Other epigenetic regulators are listed in Table 2 (Brennan et al., 2013). Deregulation of these genes lead to abnormalities in gene expression as a result of altered accessibility of regulatory transcription machinery to regulatory DNA sites (Berdasco and Esteller, 2010).

Table 2. Epigenetic regulatory genes that are frequently mutated in glioblastoma.

Gene name	Epigenetic function
IDH1 (5%), *ATRX* (6%), *SETD2* (2%), *CREBBP* (2%), *TEP1*, *SETD1A*, *TERT*, *BAP1*, *SRCAP*, *TET2*	Chromatin modifier
MLL3 (3%), *MLL2* (2%), *MLL4* (2%), *MLL*, *BMI1*, *EHMT2*, *EZH2*	Histone methyltransferase
HLTF, *SMARCA2*, *ARID1A*, *SMARCA5*, *SARCAL1*, *SMARCC2*	SWI/SNF complex
KDM2B, *KDM1B*, *KDM4D*, *KDM5A*, *KDM5C*, *KDM6A*, *KDM6B*, *KDM5B*, *MYSM1*	Histone demethylase
HDAC2, *HDAC9*	Histone deacetylase

Alteration frequency is approximately 1% for each gene, unless indicated otherwise in parenthesis.

1.3 Intertumor heterogeneity and molecular profiling of glioblastoma

Recent studies identified significantly varying genetic and phenotypic profiles between tumors from different individuals (intertumor heterogeneity) and also within a single tumor mass (intratumor or cellular heterogeneity) (Burrell et al., 2013). As reflected by its original name “glioblastoma multiforme”, glioblastoma is a disease of heterogeneity. Numerous efforts to develop effective therapies have been greatly challenged as a result of this variation. Though, it has been suggested that classifying tumors from different patients into subgroups may help interpreting molecular complexity of the disease, which would subsequently allow tailor precise and novel treatment plans (Parsons et al., 2008). Glioblastomas, therefore, have been categorized based on their distinct gene mutations,

genome-wide DNA copy number changes, protein or RNA expression profiles, DNA methylation status and chromosomal alterations. (Brennan et al., 2013; Noushmehr et al., 2010; Phillips et al., 2006; Sturm et al., 2012; Verhaak et al., 2010). Current classification system for glioblastomas predicts four molecularly distinct subgroups based on their gene expression profiles: Proneural, Classical, Mesenchymal and Neural (Verhaak et al., 2010). The Proneural subgroup is mainly associated with murine oligodendrocytic gene expression signature, high expression levels of *OLIG2,* amplifications in *PDGFRA* gene and *TP53* mutations (Phillips et al., 2006; Verhaak et al., 2010). Based on promoter CpG island hypermethylation status, Proneural group is further divided into two subgroups: "G-CIMP" tumors (glioma-CpG island methylator phenotype) associated with concerted global hypermethylations at numerous loci and others as "non-G-CIMP" tumors (Noushmehr et al., 2010). G-CIMP tumors are tightly associated with *IDH1* mutation, which is a signature molecular event for secondary glioblastomas (Nobusawa et al., 2009) and they represent approximately 30% of all Proneural glioblastomas (Noushmehr et al., 2010). DNA methylation of O^6-methylguanine-DNA methyltransferase (*MGMT*) gene promoter, in particular, is enriched in G-CIMP tumors (79% in G-CIMP versus 46% in non-G-CIMP) (Brennan et al., 2013). It is worth noting that epigenetic silencing of *MGMT* through this hypermethylation leads to better clinical outcomes in the presence of alkylating agent cancer therapy (Hegi et al., 2005). Accordingly, Proneural G-CIMP patients had significantly longer survival compared to Proneural non-G-CIMP patients (150 weeks versus 42 weeks) (Noushmehr et al., 2010). Despite this favorable prognosis, only one third of the G-CIMP patients survived more than three years (Brennan et al., 2013). Classical group glioblastomas are characterized by murine astrocytic gene expression signature and extensive chr7 amplifications. *EGFR* amplification located in this chromosome and the presence of constitutively active "EGFR deletion mutant variant III" (EGFRvIII) are typical molecular events for Classical group tumors (Huse et al., 2013). Consistently, glioblastomas associated with EGFRvIII were found to be sensitive to EGFR kinase inhibitors, gefitinib and erlotinib, given that PTEN expression was intact (Mellinghoff et al., 2005). Abnormalities in *PDGFRA*, *IDH1* and *TP53* are notably uncommon in this group as opposed to Proneural tumors. However, deletion of *CDKN2A*

was significantly associated with Classical group tumors, which underlines the distinct ways of p53-signaling inactivation in different subgroups (Brennan et al., 2013; Verhaak et al., 2010). Mesenchymal glioblastomas predominantly undergo hemizygous deletions at a region in chr17q11.2, which harbors *NF1* gene. In addition, these tumors highly expressed mesenchymal markers *YKL40* and *MET*, and other genes in the tumor necrosis factor superfamily and NF-KB pathways, which are attributed to the high incidence of necrosis and inflammatory responses observed in Mesenchymal group glioblastomas (Bhat et al., 2013; Phillips et al., 2006; Verhaak et al., 2010). Lastly, Neural subgroup tumors were categorized mostly based on their gene expression of neuron markers, including *NEFL*, *GABRA1*, *SYT1* and *SLC12A5* (Verhaak et al., 2010). These tumors had mutations in many genes similar to other three groups and there are not any specific alterations attributed to this group alone. Thus, it still remains a debate as to whether Neural subgroup is a genuine category or it just represents a combination of the other three glioblastoma groups and normal brain (Huse et al., 2013).

As well as the genomic and transcriptomic alterations, epigenetic changes can vary significantly among the glioblastomas, as discussed earlier for Proneural G-CIMP and non-G-CIMP tumors. Accordingly, six epigenetic glioblastoma subgroups with distinct methylation profiles have been identified: IDH, G34 (*H3F3A* G34R/V mutation), K27 (*H3F3A* K27M mutation), RTK I (PDGFRA), Mesenchymal, and RTK II (Classic) (Sturm et al., 2012). Consistent with the previous findings, IDH group exhibits concerted, global hypermethylation along with *IDH1* mutations, similar to G-CIMP tumors (Noushmehr et al., 2010). G34 subgroup, on the other hand, display widespread hypomethylation, particularly in non-promoter regions and at chromosome ends, and therefore called “CpG hypomethylator phenotype (CHOP)” tumors. Interestingly, G34 and K27 glioblastomas are pediatric/young adult patients while the remaining four groups are significantly enriched for elderly patients (Schwartzentruber et al., 2012; Sturm et al., 2012). In addition, K27 tumors are mostly found in thalamus, pons and spinal cord while the remaining groups are almost exclusively in the cerebral hemispheres (Sturm et al., 2012). This finding indicates a different biological subtype with different cellular origins

and/or signaling pathway alterations required for tumor growth. It has also been suggested that G34- and K27-mutant H3.3 lead to abnormal patterns of chromatin remodeling, which results in distinct gene expression profiles for G34 and K27 mutant glioblastomas (Schwartzentruber et al., 2012). Accordingly, K27 patients have significantly shorter overall survival than G34 patients. These findings altogether suggest that epigenetic alterations may exert further tumor heterogeneity, especially between pediatric/young adult and older patients, in terms of tumor cell-of-origin, oncogenic pathways leading to tumorigenesis, clinical outcome and drug sensitivity.

These comprehensive studies helped us draw a molecular map of glioblastomas, which includes critical alterations distinguishing each clinical case, diverging/converging core signaling pathways responsible for tumorigenesis (further discussed in the next sections), and connections between transcriptomic, genomic and epigenetic events. The major information extrapolated from these studies to the clinical platform is: 1) G34 epigenetic group and Proneural group, especially those with *IDH1* mutations, may not benefit from intensive chemotherapy and radiation compared to less aggressive therapies (Sturm et al., 2012; Verhaak et al., 2010), 2) Tumors with epigenetic silencing of *MGMT* gene may benefit more from treatment plans that include alkylating agents such as temozolomide (Hegi et al., 2005), 3) Pediatric and adult glioblastomas may be different entities that require distinct clinical approach and treatment. However, other studies found that some tumors have the ability to switch their molecular profile upon the occurrence of certain molecular events. For instance, *Nf1* loss (Ozawa et al., 2014) or NF-κB activation (Bhat et al., 2013) shifted Proneural profile to Mesenchymal, which was associated with poor radiation response and shorter survival in glioblastoma patients. Furthermore, Proneural to Mesenchymal shift has been reported in glioblastomas after recurrence (Phillips et al., 2006), which suggests a tumor evolution. Thus, it still remains a challenge as to whether and how the identification of molecular subgroups can be translated into novel therapies that would actually reflect to the clinical outcome.

1.4 Intratumor heterogeneity of glioblastoma and its clinical impact

The study of tumors as a bulk provides large-scale information gained from a mixture of heterogeneous tumor population. Accordingly, in addition to the molecular complexities pertaining to the molecular differences between individual glioblastoma cases, recent studies have also identified individual tumor cells associated with different subgroups or with different molecular characteristics within a single tumor mass. For instance, surgical multisampling allowed analyses of the spatially separated tumor fragments from each glioblastoma patient. Interestingly, each fragment from the same patient belonged to different glioblastoma subtype with unique and common copy number alterations (Sottoriva et al., 2013). Another study extended the depth of the analysis by isolating 96 to192 single cells from each glioblastoma tissue and examining the cells individually. Surprisingly, while most of the cells exhibited a molecular profile similar to their original tumor mass, many of the cells actually crossed into the molecular profile of another tumor, which is different from their original tumor mass (Patel et al., 2014). Both of these studies and many others (Bonavia et al., 2011; Shi et al., 2012; Snuderl et al., 2011) suggest the emergence and maintenance of an extensive level of intratumor heterogeneity and tumor evolution.

Intratumoral heterogeneity is a remarkable feature of glioblastoma that is strongly relevant to clinical field and current therapies. For instance, recent studies have uncovered a mosaic and mutually exclusive amplification of receptor Receptor Tyrosine Kinase (RTK) genes (*EGFR*, *MET*, *PDGFRA*) in different subpopulations of single tumors, raising the question of whether multiple kinase inhibitors are required to eradicate the tumor (Little et al., 2012; Snuderl et al., 2011; Szerlip et al., 2012). Similarly, another single-cell investigation revealed that each cellular clone with different genetic profile has variable sensitivity to known cancer drugs (Meyer et al., 2015). This finding not only emphasizes the presence of intratumor heterogeneity, but also calls for a need to identify the resistant clones for a better clinical outcome. Lastly, molecular comparison of the original gliomas to matched recurrent tumors extended tumor

heterogeneity concept to temporal and spatial clonal evolution. It has been shown that both initial and recurrent tumors exist as a mixture of heterogeneous populations formed as a result of cellular evolution, and that recurrent tumors might be seeded by an early-formed clone of the original tumor, which has not acquired many of the mutations found in subsequent clones (Deng et al., 2014). This discovery further complicates the use of comprehensive genome studies, which presents the full set-of molecular alterations as a whole found in a tumor mass.

Intratumor heterogeneity is thought to be formed by multiple cellular mechanisms, including 1) clonal evolution, 2) cancer stem cell model 3) microenvironment and interclonal cooperativity (Bonavia et al., 2011). According to the clonal evolution, tumor cells gain a diversity of molecular alterations throughout the tumor expansion and increase the tumor heterogeneity. Upon a selective pressure, such as chemotherapy or radiotherapy, only the clones that have acquired treatment-resistant features survive and reform a new heterogeneous tumor population, while the others perish or stay dormant (Greaves and Maley, 2012). Cancer stem cell model predicts a small population of cancer cells with indefinite self-renewing ability, and these cells give rise to a heterogeneous progeny that composes the major bulk of the tumor mass (Singh et al., 2004). The relatively quiescent cancer stem cells are considered to be drug-resistant population and they are thought to be the origin of the recurring tumors after the removal of the daughter cells (Vanner et al., 2014). Lastly, interclonal cooperativity defines a mixture of heterogeneous population formed either through clonal evolution or cancer stem cell model. The interaction of the genetically diverse cells with one another may provide drug resistance, invasion, migration, angiogenesis, growth enhancement and immunosuppression. Accordingly, it has been shown that a minor EGFRvIII-expressing tumor cell population drives the tumorigenic potential of the entire tumor mass by inducing wild type EGFR expression in neighboring cells through secreted IL-6 and LIF cytokines (Inda et al., 2010). Regardless of the way that it is formed, intratumor heterogeneity in glioblastoma still represents one of the major machineries for tumor

resistance and ineffective personalized therapies (Almendro et al., 2013), as discussed above.

1.5 Oncogene addiction and the Achilles' heel of glioblastoma

The regulation of numerous genes and signaling pathways is disrupted in cancer cells as a result of multiple genomic, epigenetic and chromosomal abnormalities accumulating over time in a complex set of events. However, recent studies have identified a phenomenon called "oncogene addiction", which suggests that cancer cells largely depend on a single oncogenic pathway for their survival, proliferation, and malignancy. This notion has been subsequently supported by various experimental systems and clinical trials in chronic myeloid leukemia, breast cancer, gastrointestinal stromal tumor, head and neck cancer, pancreas cancer, melanoma, and non-small-cell lung cancer. Therefore, uncovering the "Achilles' heel" of cancer cells is essential to treat the patients effectively even in the presence of multiple genetic and epigenetic alterations (Huse et al., 2013; Sharma and Settleman, 2007; Weinstein, 2002; Weinstein and Joe, 2006). However, it should be noted that cancer cells can escape from their addiction to a specific molecular event and acquire further genomic instability accompanied by new oncogenic signals. As the original approach will no longer be effective, it is critical to identify the new oncogenic pathway(s) and design therapeutic approaches accordingly (Weinstein, 2002).

Glioblastoma displays extreme degrees of intertumor and intratumor heterogeneity accompanied by severe molecular alterations (see sections 1.3 and 1.4). As a result, glioblastoma remains an incurable disease while many attempts to develop more effective therapeutics have been hampered. However, a gain of several chr7 copies (86%) and a loss of at least one chr10 copy (90%) remain the most common molecular events in a majority of glioblastomas from numerous patients, regardless of the molecular classification. More importantly, these two chromosomal abnormalities were consistently found in every tumor cell isolated from several glioblastoma samples, even though it has been emphasized that distinct molecular profiles and drug sensitivities exist within a

single mass (Meyer et al., 2015; Ozawa et al., 2014; Patel et al., 2014). Gain of several chr7 and deletion of chr10 are strongly associated with the amplification of *EGFR* and *PDGFA,* and the loss of *PTEN*, respectively (Ozawa et al., 2014; Verhaak et al., 2010). Consistently, even though significant intratumor heterogeneity has been detected in spatially separated tumor fragments in a single tumor mass, *EGFR* amplification and *PTEN* deletion has been observed in all and majority of the tumor fragments, respectively (Sottoriva et al., 2013). These results, altogether, support the previous findings showing that PI3K/RTK pathway is altered in 90% of human glioblastomas, leading to highly active AKT signaling (Brennan et al., 2013; Cancer Genome Atlas Research, 2008; Furnari et al., 2007). The inhibition of PI3K and/or AKT signaling, therefore, has been of particular interest in many cancer studies, including glioblastoma (Altomare and Testa, 2005; Bellacosa et al., 2005; Cully et al., 2006; Momota et al., 2005; Testa and Bellacosa, 2001; Wen and Kesari, 2008).

1.6 PI3K/RTK/AKT signaling and glioblastoma

1.6.1 PI3K family and activation of RTK/PI3K signaling pathway

Phosphatidylinositol 3-kinases (PI3Ks) are large family of lipid kinases that provide a connection between the extracellular signals such as growth factors, cytokines and other environmental cues, and the intracellular signals that regulate proliferation, growth, motility, differentiation, migration, trafficking and metabolism (Katso et al., 2001). Class IA PI3Ks are heterodimers of one of the three catalytic isoforms (p110α (encoded by *PIK3CA*), p110β (*PIK3CB*) and p110δ (*PIK3CD*)) that associates with one of the five regulatory isoforms (p85α, p55α, p50α (*PIK3R1*), p85β (*PIK3R2*), and p55γ (*PIK3R3*)). Class IB PI3Ks are heterodimers of one catalytic subunit (p110γ (*PIK3CG*)) coupled with one of the two regulatory isoforms (p101 (*PIK3R5*) and p87 (*PIK3R6*)). Class II RTKs are monomeric and formed by one of the three catalytic isoforms, PI3K-C2α (*PIK3C2A*), PI3K-C2β (*PIK3C2B*), and PI3K-C2γ (PIK3C2*G*). Class III RTKs are only a dimer of

VPS34 (*PIK3C3*) and VPS15 (*PIK3R4*). Relatively less is understood about the functions and regulations of Class II and Class III PI3Ks (Thorpe et al., 2015).

In the absence of a stimulus, p85 regulatory subunit of a Class IA PI3K interacts with p110 catalytic subunit and blocks its kinase activity. Upon binding of an activating ligand to a membrane-bound growth factor receptor tyrosine kinase (RTK), dimerized and autophosphorylated RTK can activate Class IA PI3Ks in at least three different ways, all of which requires a physical interaction between a Src homology 2 (SH2)-domain-containing molecule with the RTK: 1) Regulatory p85 subunit of PI3K can directly bind to a specific phosphorylated site on RTK, leading to the activation of p110 catalytic subunit. 2) An adaptor molecule, such as insulin receptor substrate (IRS1), can form a bridge between the RTK and PI3Ks leading to activation of p110 catalytic subunit. 3) Ras or other small GTPases can integrate signals to activate p110 catalytic subunit of PI3Ks independently of the p85 regulatory domain (Cully et al., 2006; Vanhaesebroeck et al., 2010). Class IB PI3Ks do not have p85 family regulatory subunit, therefore, they are not regulated by RTKs. Rather, they are exclusively activated by G-protein-coupled receptors (GPCRs) as a result of a physical interaction between p101 or p87 regulatory domains of PI3K and Gβγ subunit of trimeric G proteins (Engelman et al., 2006). Upon activation by one of these mechanisms, PI3Ks generate a second messenger, lipid phosphatidylinositol (3,4,5) triphosphate (PtdIns(3,4,5)P_3), by phosphorylating phosphatidylinositol (4,5) bisphosphate (PtdIns(4,5)P_2). PtdIns(3,4,5)P_3, in turn, activates downstream components of RTK/PI3K signaling, including AKT (also known as PKB), PDK1, GRP1, BTK1, and TEC, by serving as a membrane recruitment site (Miao et al., 2010; Park et al., 2008). Of those, the protein serine/threonine kinase AKT is considered to be the major target of PtdIns(3,4,5)P_3 and, by extension, of RTK/PI3K signaling (Sparks and Guertin, 2010). Tumor suppressor PTEN, on the contrary, is a phosphatase, which removes the 3' phosphate from PtdIns(3,4,5)P_3 and generates PtdIns(4,5)P_2 to inactivate RTK/PI3K signaling pathway (see next section for details) (Song et al., 2012).

Aberrant PI3K signaling, leading to AKT hyperactivation, has been found frequently in a wide range of cancer cases including glioblastoma (see Table 1), making this oncogenic pathway as a major therapeutic target. Thus, many pharmaceutical companies are making an effort to design more effective pan-PI3K inhibitors, dual pan-PI3K/mTOR inhibitors, and isoform-specific PI3K inhibitors. Recent studies have emphasized the potential benefits of isoform-specific inhibitors of PI3Ks or inhibitors of downstream molecules, such as AKT, which may have better specificity and reduced toxicity compared to pan-PI3K inhibitors (Lino and Merlo, 2011; Thorpe et al., 2015).

1.6.2 Alterations in *PTEN* tumor suppressor gene and abnormal PI3K/AKT signaling

PTEN is the major negative regulator of PI3K/AKT signaling, underlining the fact that 41% of the human glioblastomas have mutation/deletion in *PTEN*, and 90% have loss of at least one copy of chr10q, which normally harbors *PTEN* gene (Brennan et al., 2013; Ozawa et al., 2014). Similar to *TP53*, *PTEN* is known as one of the most frequently mutated/altered tumor suppressor genes in human cancers today (Salmena et al., 2008). Identification of *PTEN* gene dates back to 1984, when loss of chr10 in malignant gliomas, concomitantly with amplification of chr7, was first reported (Bigner et al., 1984). Subsequent studies identified a novel tumor suppressor gene, *PTEN*/*MMAC1*/*TEP1*, at the 10q23 locus (Li and Sun, 1997; Li et al., 1997; Steck et al., 1997), which functions as a lipid phosphatase that opposes the PI3K/AKT signaling pathway by dephosphorylating and converting PtdIns(3,4,5)P_3 to PtdInst(4,5)P_2 (Maehama and Dixon, 1998; Stambolic et al., 1998). In addition to its lipid phosphatase activity, PTEN also functions as a protein phosphatase, which can dephosphorylate serine, threonine and tyrosine residues of protein substrates. PTEN protein has a phosphatase (catalytic) domain and a lipid membrane-binding C2 domain, both of which are required for its complete tumor suppressor functions. Protein modifications (e.g. phosphorylation) at additional two regions, PDZ-binding domain and C-terminal tail

(contains two PEST motifs) have been associated with protein stability and activity (Hollander et al., 2011; Salmena et al., 2008).

Both germline and somatic alterations in *PTEN* gene can lead to a wide range of diseases including multiple cancer types in different organs. Autosomal dominant syndromes as a result of germline mutations can cause developmental disorders, neurological deficits, multiple hamartomas and increased susceptibility to develop breast, thyroid, and endometrial cancers. These disorders altogether are called "PTEN hamartoma tumor syndromes (PHTS)", which includes Cowden syndrome, Bannayan-Riley-Ruvalcaba syndrome, Lhermitte-Duclos disease and Proteus and Proteus-like syndromes. While these syndromes have similar clinical representations, Cowden syndrome, particularly, is associated with the development of malignant tumors, including breast, endometrial and thyroid cancer (Salmena et al., 2008; Sulis and Parsons, 2003). Approximately 60-70% of *PTEN* mutations in Cowden syndrome are found in its phosphatase domain (in exons 5, 7, 8), while mutations in C-terminal tail (in exon 9), promoter region (both leads to reduced expression) and splice donor/acceptor sites (leads to truncated protein) have also been detected (Song et al., 2012).

Somatic alterations of *PTEN* include mutations, deletions, insertions, allelic or complete gene loss, promoter methylation (epigenetic silencing), miRNA silencing, alternative splicing and chromosomal (chr10q) loss. Mutations, insertions and deletions occur throughout the gene, however alterations in Arg130 (mostly in endometrial and ovarian cancers), Arg173 (mostly in CNS tumors) and Arg233 have been frequently observed and referred as hotspot mutations (Hollander et al., 2011; Song et al., 2012). Approximately 90% of the human glioblastomas have chromosomal loss in at least one copy of chr10q, suggesting that at least 90% of the tumors will have monoallelic *PTEN* loss (Ozawa et al., 2014). In addition, 41% the glioblastomas have homozygous deletions or mutation, resulting in biallelic *PTEN* loss (Brennan et al., 2013). Recent studies have also shown that overexpression of a non-coding miRNA, miR-26a, targets *PTEN* transcript and cause a reduction in PTEN expression in high-grade gliomas. It has been further demonstrated

that miR-26a overexpression is due to amplification in *miR-26a-2* locus and that this event is strongly associated with monoallelic *PTEN* loss (Huse et al., 2009). Similarly, other studies have shown that PTEN expression is repressed by miR-21, leading to tumor proliferation and inhibition of apoptosis (Meng et al., 2007). Other mechanisms, including posttranslational modification, promoter methylation and protein delocalization might lead to loss of PTEN function (Salmena et al., 2008). These results, altogether, suggest that *PTEN* loss of heterozygosity (LOH) can be achieved functionally by various mechanisms other than direct genetic alterations; raising the possibility that biallelic inactivation of *PTEN* in glioblastoma might be more than previously estimated. Inactivation of PTEN by any of the mechanisms listed above leads to a balance change in the phospholipid molecules, resulting in accumulation of PtdIns(3,4,5)P_3 on the cellular membrane. Excess levels of PtdIns(3,4,5)P_3 promote recruitment of PH-domain containing proteins, including AKT and PDK1 (Phosphoinositide-dependent kinase), to the cell membrane. Once positioned in the membrane, AKT is activated (hyperactivated in this case) upon phosphorylation by PDK1 and mTORC2 (see next section for details) (Salmena et al., 2008; Sarbassov et al., 2005).

1.6.3 AKT signaling and its oncogenic functions

PI3K-generated PtdIns(3,4,5)P_3 serves as a lipid second messenger that activates many downstream molecules by binding to their pleckstrin-homology (PH) domain. As discussed earlier, AKT is considered to be the major downstream effector of the RTK/PI3K signaling pathway. A physical interaction between AKT and PtdIns(3,4,5)P3 allows AKT to be recruited to the membrane, where it is subsequently phosphorylated by PDK1 at Threonine-308 (Thr^{308}) in the kinase activation loop (T-loop), and by mTORC2 at Serine-473 (Ser^{473}) in the hydrophobic motif of the carboxyl-terminal tail, respectively (see next section for details) (Alessi et al., 1997; Engelman et al., 2006; Guertin et al., 2006; Ikenoue et al., 2008; Sarbassov et al., 2005; Testa and Bellacosa, 2001). These two phosphorylation events are required for full activation of AKT, which in turn phosphorylates multiple downstream proteins that function in various cellular functions,

including survival, proliferation, cell size/growth, metabolism, and angiogenesis (Table 3) (Manning and Cantley, 2007). Phosphorylation by AKT changes the activity and/or localization of these proteins. Most of the AKT substrates are inhibited upon phosphorylation (e.g. FOXO family, BAD, CASP9, AS160, TSC2, PRAS40, p27, GSK-3β), while a few of them are activated (e.g. eNOS and MDM2) (Table 3) (Engelman et al., 2006; Manning and Cantley, 2007; Testa and Bellacosa, 2001). Once activated, AKT signaling can be terminated upon dephosphorylation of Ser^{473} on AKT by a protein phosphatase PHLIPP (Gao et al., 2005).

Table 3. Downstream targets of AKT signaling and implications for cancer when deregulated.

Substrate	Normal function	Regulation by AKT signaling	Implications for cancer
FOXO family (FOXO1, FOXO3A, FOXO4)	Apoptosis, cell-cycle arrest, induction of pro-apoptotic genes such as FasL and Bim)	Inhibition	Cell survival
BAD	Pro-apoptotic	Inhibition	Cell survival
CASP9	Pro-apoptotic	Inhibition	Cell survival
MDM2	TP53 degradation	Activation	Cell survival
p27 (encoded by *CDKN1B*) and p21 (encoded by *CDKN1A*)	Cell-cycle inhibitors	Inhibition	Cell proliferation
GSK-3α/β	Cell-cycle regulation by inhibiting cyclin D, cyclin E, Myc and c-Jun functions	Inhibition	Cell proliferation
GSK-3 α/β	Negative regulator of glycogen synthesis	Inhibition	Cell metabolism (glycogen synthesis)
TSC2	Negative regulator of mTORC1 signaling	Inhibition	Cell metabolism (protein synthesis)
PRAS40 (encoded by *AKT1S1*)	Negative regulator of mTORC1 signaling	Inhibition	Cell metabolism (protein synthesis)
AS160	Inhibition of GLUT4 activity and glucose uptake	Inhibition	Cell metabolism (glucose uptake)
eNOS	Vasodilation, vascular remodeling and angiogenesis	Activation	Angiogenesis

Several studies have revealed that hyperactivation of AKT signaling as a result of sporadic molecular alterations, alone or in cooperation with other abnormalities, can cause to human malignancies in numerous organ systems (Bellacosa et al., 2005). More specifically, deletion/mutation/downregulation of *PTEN* and *NF1*, amplification/mutation/upregulation of *EGFR*, *PDGFRA*, *PDGF* and PIK3C genes, mutations in PIK3R genes, autocrine or paracrine stimulation of RTKs and aberrant activation of Ras are the most common sporadic events that lead to hyperactivation of AKT signaling, especially in glioblastomas (see Table 1). In addition, dominantly inherited cancer syndromes associated with germline mutations in *PTEN*, *LKB1*, *TSC2/TSC1*, *NF1* and *VHL* lead to aberrant AKT activation, suggesting that several tumor suppressor genes are negative regulators of AKT signaling (Altomare and Testa, 2005).

1.6.4 RICTOR/mTOR complex is a major positive regulator of AKT signaling

mTOR (originally "mammalian target of rapamycin", now "mechanistic target of rapamycin") is a serine/threonine protein kinase, which interacts with several other proteins to form two important complexes called "mTOR complex 1 (mTORC1)" and "mTOR complex 2 (mTORC2)" (Table 4). While mTORC1 is regulated by various signals, including nutrients (e.g. amino acids), growth factors, oxygen, cellular energy and stress pathways, mTORC2 is mainly regulated by growth factors (Laplante and Sabatini, 2012; Sparks and Guertin, 2010). Downstream cellular processes of mTORC1 signaling include protein and lipid synthesis, cellular metabolism, ATP production, cellular growth, and inhibition of autophagy and lysosome biogenesis. Main functions of mTORC2, on the other hand, are regulating cell survival, cell proliferation and cytoskeletal organization (Table 4) (Foster and Fingar, 2010; Laplante and Sabatini, 2012).

mTORC2 regulates several members of AGC kinase family, including AKT, SGK1 (serum- and glucocorticoid-induced protein kinase 1), and PKC-α (protein kinase C-α) by phosphorylating their hydrophobic motif at Ser^{473} of AKT, Ser^{422} of SGK1, and Ser^{657} of PKC-α (Foster and Fingar, 2010). It should be noted that these protein kinases are further phosphorylated by PDK1 in their activation loop at Thr^{308} of AKT, Thr^{256} of SGK1, and Thr^{500} of PKC-α (Newton, 2003; Sparks and Guertin, 2010). Upon activation, AKT involves in various cellular processes including proliferation, cell survival, metabolism, angiogenesis and growth (Table 3, also see the previous section).

Table 4. Common and unique protein components of mTORC1 and mTORC2, and their functions within the complexes.

Protein component	Function	Complex
mTOR	Serine/threonine kinase.	mTORC1 mTORC2
DEPTOR (DEP domain containing mTOR-interacting protein)	mTOR inhibitor.	mTORC1 mTORC2
mLST8 (mammalian lethal with sec-13 protein 8, aka GβL)	Unknown function, may not be essential for mTORC1, essential for mTORC2.	mTORC1 mTORC2
Tti1/Tel2 complex	Scaffold complex for the assembly and stability of mTORC1.	mTORC1 mTORC2
RPTOR (regulatory-associated protein of mammalian target of rapamycin)	Scaffold protein regulating the assembly, localization, and the substrate binding.	mTORC1
PRAS40 (proline-rich AKT substrate)	mTORC1 inhibitor	mTORC1
RICTOR (Rapamycin-insensitive companion of mTOR)	Scaffold protein regulating the assembly and the substrate binding.	mTORC2
mSIN1 (mammalian stress-activated map kinase-interacting protein 1)	Scaffold protein for mTORC2 assembly and its interaction with SGK1. Contains PH-domain at its C-terminus.	mTORC2
PROTOR1/2 (Protein observed with with Rictor 1 and 2)	Increases mTORC2-mediated activation of SGK1	mTORC2

SGK1, on the other hand, regulates ion transport (e.g. Sodium), growth, motility and apoptosis. SGK1 has approximately 80% similarity to AKT in its kinase domain, and it

also shares similar substrate specificity requirements with AKT, suggesting that SGK1 involves in cellular processes in a comparable fashion to AKT. Furthermore, since the same upstream signals regulate SGK1 and AKT, alterations that trigger AKT signaling would, therefore, activate SGK1 concomitantly (Gao et al., 2010; Moniz and Vanhaesebroeck, 2013). Even though AKT is considered to be the major mediator of the RTK/PI3K signaling pathway, recent studies uncovered critical roles of SGK1 and its downstream substrate NDRG1 (N-Myc downstream regulated gene 1) in tumor resistance to AKT inhibitors and alkylating chemotherapy. Particular interest is the finding that SGK1-activated NDRG1 binds to and stabilizes methyltransferase MGMT, which consequently renders glioblastoma cells resistant to alkylating agent Temozolomide. Consistently, silencing methylation of *MGMT* promoter was no longer associated with better prognosis in patients who concurrently received corticosteroids, which are known to activate SGK1 signaling, compared to the patients without steroid administration (Moniz and Vanhaesebroeck, 2013; Sommer et al., 2013; Weiler et al., 2014). Lastly, PKC-α is a calcium- and phospholipid-dependent kinase, and upon activation by mTORC2 and PDK1, PKC-α is involved in actin cytoskeleton to determine the cellular shape and structure. In addition to AGC kinases, mTORC2 phosphorylates Rho GTPases and Paxillin in regulation of actin cytoskeleton dynamics (Laplante and Sabatini, 2012).

RICTOR is a critical and defining subunit of mTORC2, as all known mTORC2 functions require intact RICTOR protein. Furthermore, its interaction with SIN1 is thought to be required for mTORC2 stability and function. Accordingly, *Rictor*-deficient mice die in early embryogenesis, emphasizing the crucial roles of Rictor/mTORC2 during the development (Guertin et al., 2006; Huang et al., 2013; Sarbassov et al., 2005; Sparks and Guertin, 2010). It has been shown that functional loss of *Rictor* is sufficient to block Akt activation and tumor growth in various cancer models. In the first study, it has been shown that mouse prostate epithelial cells transform into prostate cancer in the absence of *Pten* gene, and concurrent *Rictor*-loss can prevent this tumorigenesis mainly by blocking Akt signaling (Guertin et al., 2009). Interestingly, *Rictor*-loss alone does not affect the structural maintenance of normal prostate epithelium, suggesting that tumor cells

characterized by elevated Akt signaling are dependent on this molecule for survival, and are thus vulnerable to Akt inhibition (Bellacosa et al., 2005; Koul et al., 2006). In a similar study, *Rictor* deletion blocked the *Pten*-deficiency induced leukemogenesis and hematopoietic stem cell depletion in adult mice, underlining the important roles of Rictor/mTORC2, and by extension Akt signaling, in stem cell self-renewal and tumorigenesis. *Rictor*-loss alone had minimal effect on the function of normal hematopoietic stem cells (Magee et al., 2012). There oncogenic activity of Rictor/mTORC2 signaling has been confirmed in an opposite manner to the previous two studies. Accordingly, it has been shown that glial cell specific overexpression of *Rictor*, with or without oncogenic *EGFRvIII* expression, causes oligodendrioglioma-like or mixed astrocytic-oligodendrial tumors in the mouse brain (Bashir et al., 2012).

In addition to model organisms, the important roles of Rictor/mTORC2 signaling in tumorigenesis are further demonstrated using human tumor samples. For instance, it has been uncovered that protein and mRNA levels of RICTOR, as well as the protein levels of $pAKT^{Ser473}$ are elevated in human glioblastoma samples. It has been concluded that increased RICTOR expression promotes mTORC2 assembly, tumor cell proliferation, migration and invasiveness (Masri et al., 2007). Accordingly, RNAi mediated inhibition of *RICTOR* has reversed mTORC2 activity, and consequently impaired cell growth and migration ability of the tumor cells, including glioblastoma cell lines (Hietakangas and Cohen, 2008; Masri et al., 2007). Furthermore, knockdown of *RICTOR* in xenograft model of human glioblastoma cells has reduced the tumor cell proliferation, but more importantly, reversed the chemotherapy resistance to DNA-crosslinking agent cisplatin. This finding suggests that mTORC2 inhibition sensitizes the tumor cells to chemotherapy-induced DNA-damage, resulting in tumor shrinkage (Tanaka et al., 2011). The molecular mechanisms for this phenomenon might be explained by studies from yeast models, which have suggested that mTORC2 (tor1 in yeast) has roles in maintaining the stability of the genome and telomere length in DNA-damaging conditions. As such, inhibition of mTORC2 signaling by targeted mutagenesis renders the cells extremely sensitive to DNA-damaging reagents (Schonbrun et al., 2009;

Shimada et al., 2013). It is worth noting that mTORC2 signaling might have other oncogenic roles independent of its functions in PI3K/AKT signaling pathway. For instance, it has been demonstrated that RICTOR/mTORC2 signaling can inhibit FoxO activity via acetylation, and upregulate c-Myc expression, which in turn positively affects proliferation and glycolytic metabolism in glioblastoma cells (Masui et al., 2013). These emerging evidences for the critical roles of RICTOR/mTORC2 in human cancer offer a potential therapeutic strategy that aims to inhibit/reduce the activity of RICTOR/mTORC2. However, there is not any pharmacological means of targeting mTORC2 complex specifically, as it shares many protein components with mTORC1, including the catalytic domain mTOR (Laplante and Sabatini, 2012).

Other than its roles pertaining to tumor formation and progression, RICTOR/mTORC2 is involved in several neurodevelopmental processes. Multiple studies have shown that alterations in mTORC2 activity can lead to several cognitive disorders including Huntington's disease, Parkinsonism, Alzheimer-type dementia and autism spectrum disorders. It is thought that deregulation of actin polymerization in neurons, as a consequence of altered mTORC2 and/or AKT signaling, might be one of the major mechanisms behind these disorders. A recent study has also demonstrated that, genetic inactivation of mouse *Rictor* gene in postnatal forebrain prevents actin polymerization and actin regulatory signaling, which in turn leads to a block in conversion of a short-term synaptic process into a long-term memory (Huang et al., 2013). In a second study, deletion of *Rictor* in dorsal neural progenitors leads to decreased size of neurons and a thinner corpus callosum linked to a decrease in the expression of myelin-associated proteins. Subsequent behavioral studies revealed that *Rictor*-mutant mice displayed reduced anxiety-like behaviors, though they were hyperactive, suggestive of attention-deficit hyperactivity disorders (Carson et al., 2013). It has also been revealed that deletion of *Rictor* in cerebellar Purkinje cells leads to a reduction in cell size, a change in cell morphology, and abnormal synaptic connectivity, which may altogether lead to cerebellar motor deficits and ataxia (Thomanetz et al., 2013). Lastly, *Rictor* deletion in other organ systems have caused a wide range of abnormalities, including defective development in

T-lymphocytes, defective glucose transport in skeletal muscle, mild hyperglycemia and glucose intolerance in pancreas β-cells, and increased body size, insulin-resistance, and hyperinsulinemia in adipose tissue (reviewed in (Oh and Jacinto, 2011)).

1.7 Cell of origin and mouse models for glioblastoma

Identifying the cell of origin for glioblastoma is as imperative as understanding the molecular mechanisms promoting the tumor formation and progression. Therefore, mouse models provide a unique platform to delineate the complexity of glioblastoma formation and progression. Currently, four cells types have been reported to have potential to initiate malignant gliomas, and thus they are thought to be the cell of origin for glioblastoma. These cells are neural stem/progenitor cells (NSCs), oligodendrocyte precursor cells (OPCs), mature astrocytes and neurons (Friedmann-Morvinski et al., 2012; Zong et al., 2015).

Due to their self-renewal ability and multi-lineage developmental potential, NSCs have been one of the most susceptible cell types that can give rise to malignant gliomas. Accordingly, viral infection of constitutively active *Ras* and *Akt* genes to nestin-expressing (encoded by *Nes*) NSCs in a tissue specific manner has resulted in high-grade gliomas with histological features of human glioblastoma (Holland et al., 2000). Furthermore, various combinations of mutations in *p53*, *Pten* and *Nf1* tumor suppressor genes in genetically engineered mouse models allow embryonic NSCs to develop malignant astrocytomas with high penetrance (Chen et al., 2012a; Kwon et al., 2008; Wang et al., 2009; Zheng et al., 2008; Zhu et al., 2005). Additional investigations revealed that, adult NSCs also have the potential to form malignant-gliomas in the presence of inactivating *p53*, *Nf1*, *Pten* and *Rb* mutation combinations or activating *K-ras* mutations (Alcantara Llaguno et al., 2009; Jacques et al., 2010; Munoz et al., 2013).

As OPCs are the major proliferating cell population in the adult brain and their number is significantly higher than NGCs, it has been a particular interest to test their capacity to

form malignant gliomas (Zong et al., 2015). A unique system called "mosaic analysis with double markers (MADM)" provides the most definitive evidence demonstrating the tumorigenic potential of OPCs (Liu et al., 2011). In this system, the mutant or wild-type allele of a gene is tagged with sequences encoding different fluorescent molecules. As the cells divide, the sibling cells are labeled with different colors based on their allele content. For instance, the mutant sibling is green while the wild type is red. This system, consequently, enables investigators to determine whether a gene mutation provides a growth advantage to a cell type towards tumorigenesis. Detailed analyses have implicated that green OPCs ($p53^{-/-}$;$Nf1^{-/-}$) outgrow their red wild type siblings by more than 100-fold. However, such difference between siblings of mutant and wild type NSCs, astrocytes and neurons has not been detected. Consistently, introducing p53 and Nf1 mutations directly into OPCs results in highly penetrant gliomagenesis (Liu et al., 2011). Other evidences include the prominent expression of OPC-specific markers (e.g. Olig2, NG2, O4) in human glioma samples, and the similarity between the molecular profile of OPCs and the proneural subtype of human glioblastoma samples (Zong et al., 2015).

Mature astrocytes have long been thought to be the only replicative cells in the adult brain, thus they were also believed to be the cell of origin for glioblastoma. After the discovery of neural progenitor cells, several studies tried to determine whether mature astrocytes could actually give rise to tumors (Stiles and Rowitch, 2008). Interestingly, tamoxifen induced deletion of *p53* and *Pten* genes with or without *Rb* deletion in mature GFAP-Cre^{ER} mice has allowed mature astrocytes to develop high-grade gliomas that shares molecular signatures with human counterparts (Chow et al., 2011). Even though GFAP promoter is active in NSCs as well, tumor formation in non-germinal zones, including brain stem, cortex, cerebellum and spinal cord, raises the possibility that mature astrocytes in these regions are the cell of origin for the observed gliomas. (Chow et al., 2011) Lastly, a recent study has also demonstrated that both mature neurons in the cortex and mature astrocytes can be transformed into glioma cells by specific genetic modifications, such as concomitant knockdown of *Nf1* and *p53* tumor suppressor genes in respective cell compartments (Friedmann-Morvinski et al., 2012). These results

altogether suggest that many cell types in the brain can be targets of particular genetic alterations leading to malignant glioma formation, consistent with the fact that glioblastoma is a very complex and heterogeneous disease. Even though these studies provide valuable information that elucidates the tumorigenic potential of each cell compartment, they still lack a definitive evidence of cell of origin for human glioblastomas.

1.8 Medulloblastoma and its pathogenesis

In contrast to glioblastoma, which mainly occurs in adulthood, medulloblastoma is largely a childhood malignancy as it predominantly occurs in infants (≤ 3 years old) and children (4-17 years old). Medulloblastoma is an embryonic neuroepithelial tumor of the cerebellum and it is the most common pediatric brain malignancy, as it accounts for approximately 20-25% of all childhood brain tumors. Patients with the presence of metastasis (or leptomeningeal dissemination) at diagnosis or of residual disease after the surgical operation are classified as "high-risk groups", while the others are as "average-risk groups". Current treatment protocols include surgical removal of the tumor mass, craniospinal irradiation, and chemotherapy (Gajjar and Robinson, 2014; Northcott et al., 2012a). Accordingly, patients younger than 3-5 years old are treated in the absence of radiation protocols, while older patients with metastatic disease or imperfect surgical resection receive high doses of craniospinal radiation and aggressive chemotherapy. Patients with non-disseminating tumors and with near-complete removal of the tumor mass receive a combination of low dose irradiation and chemotherapy (Tabori et al., 2010). Stratification of the patients based on this system improved therapeutic strategies, as reducing the treatment exposure in average-risk patients results in decreased toxicity. Furthermore, this approach has increased the cure rates for high-risk patients (Gajjar and Robinson, 2014). Despite the increased overall survival rates reaching up to 70-80%, a significant portion of the treated patients still suffers from long-term adverse sequelae, including neurological, neuroendocrine and psychosocial deficits, as well as various problems in fertility, cardiopulmonary fitness, hearing, and physical performance. Post-

treatment cognitive problems, in particular, are common in younger patients. For instance, a child's IQ can drop as much as 30 points after a 36 Gy of craniospinal irradiation, or 10-15 points reduction by a lower dose of 24 Gy. Furthermore, tumor heterogeneity of medulloblastoma represents a major obstacle to current treatment strategies - a phenomenon frequently seen in glioblastoma (Ellison, 2010; Gajjar and Robinson, 2014; Northcott et al., 2012a).

Histopathologic analysis based on 2007 WHO classification of CNS tumors categorizes medulloblastomas into classic histology and four additional variants: Desmoplastic nodular (D/N), medulloblastoma with extensive nodularity (MBEN), anaplastic medulloblastoma, and large cell medulloblastoma. Due to their shared features, D/N and MBEN are often grouped together as desmoplastic, and also anaplastic and large cell medulloblastomas are classified together as large cell/anaplastic (LC/A) medulloblastoma (Gajjar and Robinson, 2014; Louis et al., 2007). Classic medulloblastomas consist of small rounded cells with a high nuclear-to-cytoplasmic content ratio. D/N and MBEN medulloblastomas contain nodular and internodular regions, some of which are filled with chains of cells in MBEN tumors. LC/A medulloblastomas have extensive nuclear pleomorphism, cell wrapping, apoptotic cells, prominent mitotic figures, large tumor nuclei and easily noticeable nucleoli (Ellison, 2010). Majority of the medulloblastomas (70%) have classic histology, while 16% are desmoplastic and 10% are LC/A. In general, desmoplastic tumors have better prognosis (especially in infants), followed by classic tumors. LC/A tumors, however, behave the most aggressively with the presence of metastasis and consequently they predict a poor outcome. However, histological categorization along with the molecular profiles (see next section 1.10) may exhibit a more complex situation (Kool et al., 2012).

Recent studies and clinical findings have suggested that a more comprehensive understanding of medulloblastoma based on its molecular and genetic nature is urgently needed to treat patients in a more systematic and effective way than the current protocols,

which are mainly based on general clinical representation of the disease and sometimes histologic features of the tumors (Gajjar and Robinson, 2014).

1.9 Familial syndromes reveal the molecular basis of medulloblastoma

The genetic makeup that triggers the formation of medulloblastomas has been initially uncovered by the studies pertaining to familial syndromes. In the 1990s, human homolog of drosophila *patched* (*PTCH1* in humans) gene was discovered in Gorlin's syndrome (aka the nevoid basal cell carcinoma syndrome - NBCCS), which is an autosomal dominant disorder characterized by predisposition to developmental defects and various cancers, including medulloblastoma (Hahn et al., 1996). Concordantly, the frequency of medulloblastoma increases approximately from 2/million to 4/hundred in Gorlin's syndrome patients (< 18 years old) (Wetmore et al., 2001). Subsequent studies revealed that many sporadic medulloblastomas indeed carry somatic *PTCH1* mutations (Kool et al., 2012). *PTCH1* product is a tumor suppressor protein that negatively regulates Sonic Hedgehog (SHH) signaling pathway by inhibiting the release of another transmembrane protein Smoothened (encoded by *SMO*), which otherwise activates downstream signaling cascade. Thus, inactivating mutations or loss of *PTCH1* gene leads to aberrantly activated SHH signaling, which in turn promotes proliferation and inhibits terminal differentiation of the granule neuron precursor cells of the cerebellum (Taipale and Beachy, 2001). The therapeutic potentials of SMO-inhibitors, therefore, have been extensively studied in order to overcome the oncogenic SHH signaling in medulloblastoma and other SHH-associated malignancies (Amakye et al., 2013). The second heritable form of medulloblastoma occurs in Turcot's syndrome patients, who have germline inactivating mutations in adenomatous polyposis coli (*APC*) gene. *APC* is a tumor suppressor gene and its protein product functions in WNT signaling pathway as a negative regulator of the oncogene *CTNNB1* (encodes CTNNB1 or β-Catenin), which normally regulates cell-to-cell adhesion and also functions as a transcription factor (Fearon, 2011; Northcott et al., 2012a). APC controls β-catenin levels by regulating its degradation, thus inactivating *APC* mutations leads to stabilized β-catenin proteins in the cell nucleus, and subsequent

hyperactivation of WNT signaling pathway. Consistently, approximately 95% of the medulloblastomas with aberrant WNT signaling have activating somatic mutations in *CTNNB1* gene, which encodes for mutant β-catenin proteins that are resistant to phosphorylation-induced degradation. (Gajjar and Robinson, 2014; Hajra and Fearon, 2002; Northcott et al., 2012a). Aberrant SHH and WNT signaling pathways are observed in approximately 25-30% and 10% of all medulloblastoma patients, respectively. It should be noted that SHH signaling is also altered in about 50% of the basal cell carcinoma patients, and aberrant WNT signaling is found in roughly 90% of colorectal cancer patients (Fearon, 2011; Taipale and Beachy, 2001). Lastly, Li-Fraumeni patients with germline *TP53* mutations are predisposed to several malignancies, including soft tissue sarcomas, osteosarcoma and chondrosarcoma, breast cancer, adrenocortical carcinoma, leukemia, and brain tumors - glioblastoma and medulloblastoma (Birch et al., 2001). Including the somatic mutations, approximately 10% of the medulloblastomas have *TP53* mutations, while 40% of samples display p53 protein expression, indicating the presence of dysfunctional/malfunctioning p53 protein (Tabori et al., 2010; Zhukova et al., 2013). Furthermore, loss of chromosome 17p, which harbors *TP53* gene, is observed in 30-50% of the medulloblastomas. This phenomenon is mostly linked to gain of 17q, which consequently causes "isochromosome 17q" (Huse and Holland, 2010). Interestingly, concurrent *TP53* mutation and SHH activation in medulloblastomas has been reported as an adverse prognostic factor associated with poor survival (further discussed in next section) (Tabori et al., 2010; Zhukova et al., 2013).

1.10 Molecular classification enhances our understanding of medulloblastoma

Similar to glioblastomas, molecular stratification of medulloblastomas is critical in the comprehension of the disease and implementation of targeted therapies based on the genetic makeup that defines individual cases (Northcott et al., 2012a; Taylor et al., 2012). The current consensus of molecular classification predicts four subgroups with specific mutations and genetic alterations, each of which are associated with different survival rates (Jones et al., 2012; Kool et al., 2008; Northcott et al., 2011; Northcott et al., 2012b;

Pugh et al., 2012; Robinson et al., 2012; Thompson et al., 2006). Wnt-group tumors (10%) have the best outcome with 5-year overall survival (OS) of 95% followed by Shh-group (30%) and Group-4 (35%) tumors with approximately 75% OS. The worst outcome was seen in Group-3 or Myc (25%) patients with approximately 50% OS (Table 5) (Gajjar and Robinson, 2014; Kool et al., 2012; Northcott et al., 2012a).

WNT medulloblastoma has the best prognosis among the four subgroups, as the long-term survival rates for these patients reach 95% with the current treatment protocols (Table 5). However, it is the least common subtype of the medulloblastoma with the frequency of only about 10% of all cases. Virtually all of the WNT medulloblastomas have classic histology, while very rare cases of LC/A histology is also observed (Kool et al., 2012). WNT signaling pathway as a result of nuclear accumulation of β-catenin proteins characterizes WNT medulloblastomas, and consistently, over 90% of these tumors have *CTNNB1* mutation, which renders β-catenin protein resistant to degradation by APC-Axin-GSK3β-CK1α destruction complex. WNT tumors are considered to have relatively balanced genome, except for the monosomy 6 (presence of only one chr6 copy) observed in almost all of the WNT medulloblastomas, and *TP53* mutations detected in approximately 13% of the patients (Jones et al., 2012; Northcott et al., 2012a). Even though concurrent SHH signaling and *TP53* mutations are associated with worse prognosis compared to *TP53* wild type cases, *TP53* status seems not to have a prognostic factor for WNT medulloblastomas (Zhukova et al., 2013).

SHH medulloblastoma represent roughly 30% of all medulloblastoma cases, and the 5-year overall survival rate for patients with SHH tumors is approximately 75% (Table 5). Classic tumor histology is prominent in this subgroup, followed by desmoplastic and LC/A tumors. It is worth noting that desmoplastic histology is almost exclusively observed in SHH medulloblastomas (Kool et al., 2012). Characteristic SHH signaling pathway can appear as a result of various genomic and epigenetic alterations in this pathway, including germline and somatic inactivating mutations in *PTCH1* and *SUFU* genes, somatic activating mutations in *SMO,* and copy number amplifications in *N-MYC*,

GLI1, *GLI2* and *SHH* genes. Furthermore, *TP53* mutations (14-21%) and broad chromosomal losses of 17p (harbors *TP53* gene) are detected in SHH medulloblastomas. Other chromosomal aberrations include loss of 9q (harbors *PTCH1*), loss of 10q (harbors *PTEN*), and gain of chromosomes 3q and 9p (Kool et al., 2012; Northcott et al., 2011).

As discussed earlier, SHH medulloblastomas with *TP53* mutations (SHH/*TP53*^{mut}) are associated with early recurrence and extremely poor outcome with a 5-year survival rate of 41% compared to 81% in SHH/*TP53*^{wt} patients. Especially in children between the ages of 5-18, *TP53* mutation accounts for 72% of the deaths (Tabori et al., 2010; Zhukova et al., 2013). Remarkably, *TP53* mutations seem to be a critical alteration exclusive to childhood (4-17 years old) SHH tumors, as almost 50% of the childhood SHH medulloblastomas had *TP53* alterations, while similar events were virtually absent in the remaining SHH cases, as well as Group-3 and Group-4 medulloblastomas (Kool et al., 2014; Zhukova et al., 2013). These findings altogether suggest that the presence of *TP53* mutation is one of the most decisive adverse prognostic factors in medulloblastoma (Tabori et al., 2010; Zhukova et al., 2013). Interestingly, SHH/*TP53*^{mut} medulloblastomas were found to undergo "chromothripsis" (concurrent severe fragmentation of divergent chromosomal regions and a subsequent reassembly in an imperfect or random manner), resulting in catastrophic DNA rearrangements and also "tetraploidy" (having a chromosome number four times the monoploid number). Even though approximately 13-16% of the WNT medulloblastomas also carry *TP53* mutations, none of them have been found to undergo chromothripsis, which underlines the context dependent consequences of *TP53* loss. Importantly, medulloblastoma oncogenes, *N-MYC*, *GLI2*, and *BOC* are amplified in SHH/*TP53*^{mut} medulloblastomas as a result of chromothripsis (Jones and Jallepalli, 2012; Rausch et al., 2012). Since both *N-MYC* and *GLI2* products are downstream components of the SHH signaling pathway, amplifications in these genes are thought to render the tumors inherently resistant to SMO-inhibitors. Consistently, SHH medulloblastomas with *N-MYC* and *GLI2* amplification have worse prognosis compared to their wild type counterparts, and even the presence of high dose craniospinal radiation

and adjuvant chemotherapy is mostly ineffective (Gajjar and Robinson, 2014; Kool et al., 2014; Northcott et al., 2012a; Northcott et al., 2012b; Pfister et al., 2009).

Approximately 25% of the medulloblastomas belong to Group-3, which has the worst clinical outcome of the four subgroups with a 50% 5-year overall survival rate (Table 5). These tumors are characterized by classic and LC/A histology, metastasis with 40-45% frequency, and occurrence in pediatric patients exclusively, all of which might underline the aggressive nature of the disease (Gajjar and Robinson, 2014; Kool et al., 2012). Group-3 medulloblastomas are also called "MYC medulloblastomas" due to the fact that almost all of them have aberrant MYC expression and approximately 17% of them acquire high-level amplifications in *MYC* oncogene. Recent studies have also uncovered the presence of *PVT1-MYC* fusion genes, which is thought to promote tumorigenesis in a combinatory manner (Northcott et al., 2012b). In addition, alterations in chromatin remodeling and histone modification genes, including *SMARCA4* (11%), *KMT2D* (4%), *MLL2* (4%), and *KDM6A* are noticeable in Group-3 medulloblastomas (Pugh et al., 2012; Robinson et al., 2012). Group-3 tumors, particularly, exhibit severe genomic alterations that include loss of chromosomes 8, 10q, 11, 16q, and 17p, and gain of chromosomes 1q, 7, and 17q (isochromosome 17q), and 18.

Group-4 tumors are the most common subgroup of all medulloblastomas (35%) (Table 5). Interestingly, these tumors are three times as likely to manifest in males compared to females. Classic histology is predominantly observed in Group-4 medulloblastomas, while rare cases of LC/A tumors are also reported. Similar to SHH medulloblastomas, Group-4 tumors have approximately 75% survival rate in general, though the adult patients have significantly worse clinical outcome (Kool et al., 2012; Taylor et al., 2012). The biologic disposition underlying the disease formation and/or progression is less understood compared to other three subgroups, and there is not a signaling pathway associated with Group-4 tumors either. However, amplifications in *N-MYC* (6%) and *CDK6* (5%) genes are thought to be among the driver events, and isochromosome 17q is detected in majority of the Group-4 medulloblastomas, making this genomic alteration as

a hallmark event (Kool et al., 2012; Northcott et al., 2012a; Northcott et al., 2011). Similar to Group-3 tumors, somatic alterations in many chromatin modifier genes, including *KDM6A* (13%), *MLL3* (5%), *KMT2C* (5%), *CDK6* (5%), *ZMYM3* (4%), and *CHD7* (2%) are typical to Group-4 medulloblastomas (Pugh et al., 2012; Robinson et al., 2012). Lastly, Group-4 medulloblastomas are also distinguished with their extensive genomic alterations, including losses of chromosomes 8, 10, 11, and 17p, and gains of chromosomes 4, 7, 17q (isochromosome 17q), and 18 (Kool et al., 2012).

Even though both Group-3 and Group-4 medulloblastomas undergo extensive chromosomal alterations and oncogenic chromatin remodeling, recurrent somatic gene mutations are mostly rare (Table 5). In general, only aberrant MYC and N-MYC signaling is associated with Group-3 and Group-4 medulloblastomas, respectively. Thus, identifying the oncogenic driver mutations or signaling pathways, particularly for these two subgroups, remain essentially unrevealed (Northcott et al., 2012a). Interestingly, recent studies have revealed that activation of an oncogene can be achieved by unusual mechanisms in addition to sole gene mutations or amplifications. According to these studies, the expression of growth factor independent 1 family proto-oncogenes, *GFI1* and *GFI1B*, are hyperactivated upon genomic redistribution of the active enhancers in Group-3 (25-41%) and Group-4 (5-10%) medulloblastomas. More specifically, "enhancer hijacking" occurs when *GFI1* and *GFI1B* loci are genetically redistributed from the regions in transcriptionally silent chromatin to regions that are occupied with active enhancers by various mechanisms, including deletion, inversion, tandem duplication (local enhancer hijacking), and translocation and intrachromosomal structural variation (distal enhancer hijacking) (Northcott et al., 2014). These findings implicate the potential oncogenic drivers in relatively less understood medulloblastoma subgroups, and pave the way for the pursuit of targeted therapy.

Table 5. Molecular and clinical properties of medulloblastoma subgroups.

		WNT	SHH	Group-3	Group-4
Overall frequency		~10%	~30%	~25%	~35%
Age distribution	Infant: Child: Adult:	**–** **++** **+**	**+++** **+** **+++**	**+++** **++** **–**	**+** **+++** **++**
Gender distribution	Male: Female:	1 1	1.5 1	2 1	3 1
Predominant histology		Classic	Classic > desmoplastic > LC/A	Classic > LC/A	Classic
Frequency of metastasis		~ 5-10%	~ 15-20%	~ 40-45%	~ 35-40%
5-year OS rate		~ 95%	~ 75%	~ 50%	~ 75%
Signaling pathway-specific alterations		*CTNNB1* (91%)	*PTCH1* (28%) *N-MYC* (8%) *GLI2* (5%)	*MYC* (17%)	*N-MYC* (6%)
Recurrently mutated chromatin modifiers	*SMARCA4*: *MLL2*: *KMT2D*: *BCOR*: *LDB1*: *KDM6A*: *MLL3*: *CDK6*: *ZMYM3*: *KMT2C*:	26% 13% 12% - - - - - - -	- 13% 13% 8% 7% - - - - -	11% 4% 4% - - - - - - -	- - - - - 13% 5% 5% 4% 5%
Other recurrent alterations		*DDX3X* (50%)	*DDX3X* (12%) *TCF4* (6%)	*PVT1* (12%) *OTX2* (8%) *CTDNEP1* (5%) *LRP1B* (5%)	*SNCAIP* (10%)
***TP53* mutation**		13-16%	14-21%	-	-
Loss of chr17p		-	25%	42%	63%
Chromosomal alterations	1q + 3q + 6 – 7 + 8p – 8q + 9q – 10q – 12q + 16q – 17q + 18 +	- - 85% - - - - - - - - -	- 27% - - - - 47% 26% - - - -	35% - - 55% 33% 22% 21% 49% 17% 50% 62% 26%	- - - 47% 41% - - 15% 20% - 73% 16%

1.11 RTK/PI3K signaling in medulloblastoma

The role of RTK/PI3K/AKT signaling in medulloblastoma formation/progression is relatively less studied and understood. Previous research has revealed that the mutations and copy number alterations in key pathway components, including *PTEN*, *PIK3CA*, *IGF1R* and *IRS2* were enriched in SHH medulloblastomas (Northcott et al., 2012a; Northcott et al., 2012b; Robinson et al., 2012). Nevertheless, these alterations were still rare, as only 10% of the SHH medulloblastomas had copy number changes associated with RTK/PI3K/AKT signaling (Northcott et al., 2012b). Furthermore, none of the childhood SHH medulloblastomas carried mutations in *PIK3CA*, *PTEN* and *PIK3C2G* genes, making these alterations restricted to adults (≥ 18 years old) and infants (Kool et al., 2014). Consistently, only less than 10% of the childhood SHH tumors were immunoreactive to $pAKT^{S473}$, while majority of the positive cases were found in the adult tumors (Kool et al., 2014), suggesting that AKT activation is mostly associated with adult tumorigenesis. In contrast to relatively normal PI3K/AKT signaling, almost 50% of the childhood SHH tumors had *TP53* alterations, while similar events were virtually absent in the remaining SHH medulloblastomas, as well as Group-3 and Group-4 medulloblastomas. It is, thus, essential to understand the role of PI3K/AKT signaling within the context of *TP53* alterations in SHH medulloblastomas in order to design and implement more effective targeted therapies.

1.12 Cerebellar development, germinal zones and neurogenesis

The vertebrate central nervous system arises from the neural plate, which subsequently closes and forms the neural tube. During the development, morphologically distinct vesicles are generated along the anterior-posterior axis of the neural tube. The most anterior end of the neural tube forms forebrain (prosencephalon), which is further divided into two parts named as telencephalon (gives rise to anterior forebrain structures, including cerebral cortex, hippocampus, basal ganglia, and olfactory bulb) and diencephalon (gives rise to posterior forebrain structures, including thalamus,

hypothalamus, and pituitary gland). More posterior to forebrain, neural tube forms the midbrain (mesencephalon), hindbrain (rhombencephalon) and spinal cord. The hindbrain is further divided into eight segments called rhombomeres (r1-r8). While the anterior region (r1-r3) is named as metencephalon (forms pons and cerebellum), the remaining rhombomeres in the posterior hindbrain (r4-r8) are referred to as myelencephalon (forms medulla oblongata). The mouse cerebellar primordium arises from the hindbrain r1 at around E7-8. Signaling molecules secreted from isthmic organizer (e.g. Fgf and Wnt), a ring-like structure that encircles the neural tube at midbrain-hindbrain junction, and IV ventricle roof plate (e.g. Bmp, Wnt, retinoic acid) are important for the development, maintenance, and regional specification of the midbrain and hindbrain (Marzban et al., 2014; Millen and Gleeson, 2008). Other molecules including, the homeobox gene products engrailed 1 (En1) and En2, and the paired box gene products Pax2 and Pax5 also have essential functions in the maintenance of the primordial cerebellum (White and Sillitoe, 2013). Two primary germinal zones are established in the embryonic cerebellum: neuroepithelium of IV ventricle (the ventricular zone - VZ) located at the inner germinal layer, and neuroepithelium of the rhombic lip located at the roof plate. These two germinal zones are labeled by two distinct bHLH transcription factors: while pancreas specific transcription factor 1a (Ptf1a) identifies VZ progenitors, Atonal homolog 1 (Atoh1) identifies rhombic lip progenitors (Hoshino et al., 2005; Machold and Fishell, 2005). Both of these neuroepithelia disappear at birth, however secondary germinal zones derived from them continue to populate the postnatal cerebellum (Leto et al., 2012).

Initial expansion of the VZ progenitors requires Wnt signaling pathway, while subsequent proliferation relies on SHH signaling pathway (White and Sillitoe, 2013). Apart from labeling the VZ progenitors, Ptf1a transcription factor has important roles in proper differentiation of VZ progenitors to generate GABAergic neurons, as it has been shown that loss of *Ptf1a* causes a failure in producing GABAergic neurons in the cerebellum. Interestingly, *Ptf1a*-deficient VZ progenitor cells acquire rhombic lip expression profile, including Atoh1, Reelin and Zic1/2, suggesting that GABAergic neuron fate is mainly regulated by Ptf1a activity (Pascual et al., 2007). Notch signaling

components and Mash1 transcription factor have also been indicated as other factors facilitating the differentiation of the VZ progenitors. All inhibitory GABAergic neurons, including basket and stellate cells of the molecular layer, Golgi and Lugaro cells of the internal granular layer, Purkinje cells in the Purkinje layer, and nucleo-olivary neurons are derived from VZ progenitors. While the projections neurons Purkinje cells (major output neuron of the cerebellum) are formed around E1-E13, the interneurons stellate, basket and Golgi cells are born postnatally (Leto et al., 2012; White and Sillitoe, 2013).

The rhombic lip progenitors are highly proliferative cells that are positioned along the dorsal edge of the IV ventricle. As mentioned earlier, this region is divided into eight subunits called rhombomeres (r1-r8). The most anterior rhombomere (r1) is termed as upper rhombic lip (URL), while posterior r2-r8 is called lower rhombic lip (LRL), which is further divided into auditory rhombic lip (r2-r5) and precerebellar rhombic lip (r6-r8) (Grammel et al., 2012; Marzban et al., 2014). Rhombic lip progenitors are distinguished with *Atoh1* expression, which is induced by Bmp signaling from the IV ventricle roof plate. Atoh1 is essential for the subsequent generation of the excitatory glutamatergic neuronal lineage; accordingly, it has been shown that inactivation of Atoh1 gene results in substantial loss of rhombic lip progeny (Machold and Fishell, 2005; Millen and Gleeson, 2008). Rhombic lip undergoes three waves of cell formation at distinct developmental stages: 1) Between E10.5-E12.5, rhombic lip progenitors give rise to glutamatergic projection neurons of deep cerebellar nuclei under the control of Tbr1, Tbr2, Pax6 and NeuroD signals. Upon their formation, these cells migrate rostrally to nuclear transitory zone. 2) Between E14-E21, another glutamatergic excitatory neuron type, unipolar brush cell, is generated under the control of Bmp, Pax6, Math1 and Lmx1a. 3) Lastly, a tangential migration of cerebellar granule cell progenitors (CGNPs) from rhombic lip takes place in late embryogenesis to early postnatal stages. Various signaling molecules, including Bmi1, N-myc, cyclin D2, Zic and Wnt accompany this critical migratory wave (Leto et al., 2012; Marzban et al., 2014).

After their tangential migration from the rhombic lip, CGNPs form a thick layer of a secondary germinal zone called external germinal zone or external granular layer (EGL) located at the subpial surface of the developing cerebellum. This transient structure forms as early as E15 and undergoes an extensive proliferation, mainly regulated by SHH secreted from Purkinje cells (Gilbertson and Ellison, 2008; Marzban et al., 2014). Activation of SHH signaling induces Gli1 and subsequently N-myc and Ccnd1/2 transcription factors leading to CGNP proliferation and inhibition of cell cycle exit. Wnt and Notch2 signaling pathways are also shown to have roles in CGNP proliferation via induction of Myc family and Atoh1, respectively. Bmp2/4 and NeuroD1 signaling, on the other hand, are considered as negative growth regulators, as their activity leads to inhibition of Atoh1 and activation of $p27^{Kip1}$ and $p16^{Ink4a}$, which results in cell cycle exit and neuronal differentiation (Hatten and Roussel, 2011; Roussel and Hatten, 2011). The main cell type that CGNPs give rise to is excitatory glutamatergic interneurons granule cells, which are generated only from CGNPs. A minor population of Golgi cells and astroglial cells are also produced from CGNPs (Marzban et al., 2014). Even though P8 is the peak of granule neuron generation, loss of EGL structure starts as early as P0 due to an inward radial migration of the post-mitotic granule cells through molecular layer (ML). The newly formed granule neurons migrate against the Bergmann glia fibers, pass through Purkinje cells and locate themselves in internal granular layer (IGL). Various signals such as neuropeptide somatostatin and NMDA receptor activation by glutamate are important for the formation and proper migration of the granule neurons (White and Sillitoe, 2013). Once granule cell formation and migration is completed at around P20, cerebellar foliation takes its final structure, which corresponds to depletion of CGNPs, and therefore EGL. Another secondary germinal zone in the white matter of the postnatal cerebellum has been characterized. These $CD133^{+}$; $Nestin^{+}$ multipotent neural stem cells are thought to generate astrocytes, oligodendrocytes, and neurons (except for granule neurons) (Lee et al., 2005).

1.13 Mouse models and cell of origin for medulloblastoma

In addition to uncovering chromosomal alterations, gene mutations, epigenetic abnormalities, and the specifics of the oncogenic signaling pathways leading to tumorigenesis, it is essential to untangle in which cell(s) these tumorigenic events are taking place and causing transformation. Therefore, revealing the cell of origin for medulloblastoma will expose the cellular context of the oncogenic signals, and consequently will allow the pharmacologic approaches to be more precise and effective. Current studies utilizing mouse models of medulloblastoma have implied different cell of origins for three of the medulloblastoma subgroups (WNT, SHH, Group-3), while efforts to understand the cellular origin of Group-4 medulloblastomas continue (Table 6) (Northcott et al., 2012a).

Tumor location can provide clues about the origin of the tumors. Almost all of the human WNT medulloblastomas are located within the IV ventricle, and they infiltrate the dorsal surface of the brain stem. Studies utilizing mouse models have concordantly shown that WNT medulloblastomas arise from the lower rhombic lip progenitor cells of the dorsal brainstem (in rhombomeres r2-r8) (Table 6). Tissue specific expression of mutant *Ctnnb1* gene in mouse dorsal brainstem progenitors (*Blbp-Cre*$^{+/-}$; *Ctnnb1*$^{+/lox(ex3)}$) has caused aberrant accumulation of lower rhombic lip cells, which initiate medulloblastoma formation only in the presence of additional *Trp53* mutations (*Ctnnb1*-mutant; *Trp53*$^{flox/flox\ (OR\ +)}$). Interestingly, mutant *Ctnnb1* expression or the *Apc*-deficiency in EGL cells of the cerebellum (*Atoh1-Cre*$^{+/-}$; *Ctnnb1*$^{+/lox(ex3)}$ or *Atoh1-Cre*; *Apc*$^{flox/flox}$) do not lead to hyperplasia or cerebellar masses, consistent with the notion that EGL cells are the cell of origin for SHH medulloblastomas, which are not associated with WNT signaling pathway (Gibson et al., 2010; Lorenz et al., 2011). Even though these studies have clearly shown the cell of origin for WNT medulloblastomas, only 4-15% of the *Ctnnb1*/*Trp53*-mutant mice form medulloblastomas. In contrast, introduction of an additional activating mutation into *Pik3ca* gene (*Blbp-Cre*; *Ctnnb1*$^{+/lox(ex3)}$; *Trp53*$^{+/flox}$; *Pik3ca*^{E545K}) has increased the medulloblastoma frequency up to 100% by three months of age. It is suggested that consequent elevation in Akt signaling has roles in tumor progression, rather than tumor initiation (Robinson et al., 2012).

Cerebellar granule neuron precursors (CGNPs) located in the external granule cell layer (EGL) are well-characterized cell types that can give rise to SHH medulloblastomas (Table 6). Almost all of the mouse models of SHH medulloblastoma rely on the genetic manipulations of SHH signaling pathway, and they carry genetically mutated *Ptch1* or *Smo* alleles (Northcott et al., 2012a). More specifically, *Ptch1* heterozygous mice (*Atoh1-GFP*; $Ptch1^{+/-}$) form GFP-expressing cerebellar pre-neoplastic cells and consequently medulloblastomas, indicating that both early tumor-initiating cells and the end-stage tumors have come from *Atoh1* expressing, therefore GFP^{+}, CGNP lineage (Oliver et al., 2005). Even though only 16% of these mice form medulloblastoma, additional *Trp53* loss ($Ptch1^{+/-}$; $Trp53^{-/-}$) can increase the tumor penetrance to greater than 95% (Wetmore et al., 2001). More definitive studies using tissue-specific knockout of *Ptch1* gene have confirmed that not only the progenitor cells of the cerebellum (*Atoh1-Cre*; $Ptch1^{flox/flox}$), but also the neural stem cells of the ventricular zone (*hGFAP-Cre*; $Ptch1^{flox/flox}$) can give rise to SHH medulloblastomas in the absence of *Ptch1* gene. It is worth nothing that both cerebellar progenitor cells and the VZ neural stem cells eventually acquire a CGNP phenotype rather than a stem cell profile (Yang et al., 2008). Similar to *Ptch1* mutation, tissue specific expression of constitutively active *Smo* gene in CGNPs (*ND2-SmoA1/+* or *ND2-SmoA1/SmoA1*) leads to persistent proliferation of CGNPs at postnatal stages, which eventually form medulloblastomas with high frequency (> 90%). Interestingly, some of these medulloblastomas are found to display leptomeningeal spread within the brain and/or spine, mimicking metastasis in human counterparts (Hatton et al., 2008). In addition to previously identified CGNPs as the origin of SHH medulloblastomas, a recent study has suggested that granule cell precursors of the cochlear nuclei of the dorsal brainstem can also lead to medulloblastoma formation in the presence of constitutively active *Smo* gene (*hGFAP-cre*::$SmoM2^{Fl/+}$ or *Atoh1-cre*::$SmoM2^{Fl/+}$). This finding suggests that two molecular subgroups of medulloblastomas arise from the lower rhombic lip, as opposed to the former conclusions that lower rhombic lip initiates only WNT tumors: Cochlear granule neuron precursors (in rhombomeres r2-r5) of the lower rhombic lip can form SHH medulloblastomas, while the pontine grey neuron precursors (in rhombomeres

r6-r8) of the lower rhombic rip can form WNT medulloblastomas (Grammel et al., 2012). Consistent with these findings, a recent study has suggested that Olig1^{+} progenitor cells (in rhombomeres r2-r4) of the lower rhombic lip, which give rise to both oligodendrocyte precursors and granule neuron lineage cells, initiate SHH medulloblastomas in the absence of *Gnas* (*Olig1-Cre*; *Gnas*$^{flox/flox}$) - a gene which encodes heterotrimeric stimulatory G-protein alpha subunit (Gα_s). In accordance with their origin, these tumors are enriched between the caudal posterolateral lobe and the dorsal brainstem around the IV ventricle, as opposed to the medulloblastomas confined to the cerebellum in *hGFAP-Cre*; *Gnas*$^{flox/flox}$ mice. Interestingly, even though many somatic tumor types in humans acquire gain-of-function mutations in *GNAS* gene, Gα_s seems to function as a tumor suppressor in cerebellum by controlling the ciliary trafficking of SHH signaling pathway components, and also regulating the activation/processing of Gli2 and Gli3. Consistently, the chromosomal region containing the *GNAS* gene is notably lost in human medulloblastomas, and *GNAS* expression is strongly correlated with decreased overall survival within SHH subgroup (He et al., 2014). These studies, altogether, suggest that there might be multiple cell of origins for SHH medulloblastomas: cerebellar granule neuron precursors of the external granule layer and cochlear nucleus of the lower rhombic lip, and neural stem cells of the subventricular zone. Detecting the origin of the tumors might, therefore, reflect the clinical outcome and treatment response even though they belong to the same subgroup (Gajjar and Robinson, 2014).

Group-3 medulloblastomas can be generated from at least two types of cells: cerebellar granule neuron precursors and prominin1^{+}/lineage^{-} cerebellar neural stem cells (Table 6). Two recent studies have successfully shown that orthotopic transplantation of Atoh1^{+} CGNPs or prominin1^{+}lineage^{-} cerebellar stem cells infected with proto-oncogene *Myc* can give rise to aggressive LC/A medulloblastomas in immunocompromised mice with median survival rates of 39 or 48 days, respectively. It is, however, important to note that both of these models require concurrent loss of *Trp53* functions in order to overcome the Myc-induced apoptosis in CGNPs or cerebellar stem cells (Kawauchi et al., 2012; Pei et al., 2012). Since *TP53* is not directly mutated in human Group-3 medulloblastomas with

MYC amplification, it is currently unknown about at what degree these two models recapitulate human disease, even though their molecular profiling shares similarities with human counterparts (Northcott et al., 2012a). A third study might address these concerns by utilizing genetically engineered mouse models that reflect the genomic alterations of human medulloblastomas. This study relies on the findings that *GFI1* and *GFI1B* genes are hyperactivated upon genomic redistribution of the active enhancer elements in Group-3 (25-41%) and Group-4 (5-10%) medulloblastomas, and that a subset of Group-3 medulloblastomas are characterized by simultaneous *MYC* amplification and *GFI1* activation (see Section 1.10). Accordingly, prominin1^{+} cerebellar stem cells that are concurrently infected with *GFI1* (or *GFI1B*) and *MYC* expressing retroviruses are orthotopically transplanted into the cerebella of immunocompromised mice. Both *MYC*/*GFI1* and *MYC*/*GFI1B* expressing cerebellar stem cells, but not *MYC* alone or *GFI1* (or *GFI1B*) alone, formed aggressive medulloblastomas in approximately 90% of the animals with median survival rates of 38 and 26 days, respectively. Transcriptional profiling has demonstrated prominent similarities between these mouse tumors and human Group-3 medulloblastomas. Furthermore, 30-50% of the animals from both models have exhibited metastatic dissemination, a phenomenon that is frequently observed in Group-3 medulloblastomas (Northcott et al., 2014).

Currently, there is not an established mouse model for Group-4 medulloblastomas, and it is still unknown which cells give rise to these tumors (Eberhart, 2012). However, it has been shown that overexpression of *N-Myc* in the developing posterior hindbrain can lead to the formation of LC/A medulloblastomas, consistent with the fact that *N-MYC* amplification is observed in both SHH (8%) and Group-4 (6%) medulloblastomas (Northcott et al., 2012a). According to this model (*glutamate transporter 1-tetracycline transactivator*; *tetracycline response element-N-myc*/*luciferase* OR *Glt1-tTA*;*TRE-N-myc*/*Luc* OR GTML mice), *Glt1* promoter drives the expression of tTA, which subsequently activates the expression of N-myc only in the absence of doxycycline. Thus, N-myc expression can be controlled by administrating doxycycline, which binds to tTA and halts its activity on *TRE* promoter upstream of *N-myc* (Table 6) (Swartling et al.,

2010). The tumors formed in this model are considered as SHH-independent medulloblastomas, as they lack the expression of SHH downstream target molecules Gli1 and Sox9, CGNP marker Atoh1, and SHH medulloblastoma identifier SFRP1. Furthermore, GTML medulloblastomas are not correlated with WNT and Group-3 medulloblastoma identifiers, DKK1 and NPR3, respectively. In stark contrast, GTML medulloblastomas display significant expression of Group-4 identifier KCNA1. These results altogether suggest that N-myc overexpression in developing cerebellum form medulloblastomas, which partly resemble Group-4 medulloblastomas, while display divergent features from other three subgroups (Swartling et al., 2012). Additional studies have suggested that N-myc activation in different cell types gives rise to medulloblastomas of different molecular subgroups: while expression of mutationally stabilized *N-Myc* (*N- myc*^{T58A}) in postnatal (P0) cerebellar stem cells give rise to SHH-independent medulloblastomas, its activation in embryonic (E16) cerebellar stem cells causes medulloblastomas with characteristic components of SHH signaling pathway (Swartling et al., 2012).

Table 6. Representative mouse models and characterized cell of origin for medulloblastoma subgroups.

Genotype/model	Proposed cell of origin	Molecular subgroup	Reference
Blbp-Cre$^{+/-}$; *Ctnnb1*$^{+/lox(ex3)}$; *Trp53*$^{flox/flox\ (OR\ +)}$	Lower rhombic lip progenitor cells (r2-8)	WNT	(Gibson et al., 2010)
Blbp-Cre; *Ctnnb1*$^{+/lox(ex3)}$; *Trp53*$^{+/flox}$; *Pik3ca*^{E545K}	Lower rhombic lip progenitor cells (r2-r8)	WNT	(Robinson et al., 2012)
Ptch1$^{+/-}$	Cerebellar granule neuron precursors	SHH	(Oliver et al., 2005)
Ptch1$^{+/-}$; *Trp53*$^{-/-}$	Not defined.	SHH	(Wetmore et al., 2001)
Atoh1-Cre; *Ptch1*$^{flox/flox}$	Cerebellar granule neuron precursors	SHH	(Yang et al., 2008)
hGFAP-Cre; *Ptch1*$^{flox/flox}$	Ventricular zone neural stem cells	SHH	(Yang et al., 2008)
ND2-SmoA1/+ or *ND2-SmoA1/SmoA1*	Cerebellar granule neuron precursors	SHH	(Hatton et al., 2008)
hGFAP-cre::*SmoM2*$^{Fl/+}$ or *Atoh1-cre*::*SmoM2*$^{Fl/+}$	Cochlear granule neuron precursors of the lower rhombic lip (r2-r5)	SHH	(Grammel et al., 2012)
Olig1-Cre; *Gnas*$^{flox/flox}$	Olig1^{+} progenitor cells of the lower rhombic lip (r2-r4)	SHH	(He et al., 2014)
hGFAP-Cre; *Gnas*$^{flox/flox}$	Neural stem/progenitor cells	SHH	(He et al., 2014)
Atoh1-GFP; *Trp53*$^{-/-}$ CGNPs infected with *Myc-RFP* retrovirus	Cerebellar granule neuron precursors	Group-3	(Kawauchi et al., 2012)
prominin1^{+}lineage^{-} cerebellar stem cells infected with *Myc*^{T58A} and *DNp53* retroviruses	prominin1^{+}lineage^{-} cerebellar stem cells	Group-3	(Pei et al., 2012)
prominin1^{+} cerebellar stem cells infected with *GFI1* (or *GFI1B*) and *MYC* retroviruses	prominin1^{+} cerebellar stem cells	Group-3	(Northcott et al., 2014)
Glt1-tTA;*TRE-N-myc*/*Luc* (aka GTML mice)	Developing posterior hindbrain	Group-4?	(Swartling et al., 2010)
Postnatal cerebellar NSCs infected with *N-Myc*^{T58A}	Postnatal cerebellar NSCs	Group-4?	(Swartling et al., 2012)

1.14 References

Alcantara Llaguno, S., Chen, J., Kwon, C. H., Jackson, E. L., Li, Y., Burns, D. K., Alvarez-Buylla, A. and Parada, L. F. (2009). Malignant astrocytomas originate from neural stem/progenitor cells in a somatic tumor suppressor mouse model. *Cancer cell* **15**, 45-56.

Alessi, D. R., James, S. R., Downes, C. P., Holmes, A. B., Gaffney, P. R., Reese, C. B. and Cohen, P. (1997). Characterization of a 3-phosphoinositide-dependent protein kinase which phosphorylates and activates protein kinase Balpha. *Current biology : CB* **7**, 261-269.

Almendro, V., Marusyk, A. and Polyak, K. (2013). Cellular heterogeneity and molecular evolution in cancer. *Annual review of pathology* **8**, 277-302.

Altomare, D. A. and Testa, J. R. (2005). Perturbations of the AKT signaling pathway in human cancer. *Oncogene* **24**, 7455-7464.

Amakye, D., Jagani, Z. and Dorsch, M. (2013). Unraveling the therapeutic potential of the Hedgehog pathway in cancer. *Nature medicine* **19**, 1410-1422.

Bashir, T., Cloninger, C., Artinian, N., Anderson, L., Bernath, A., Holmes, B., Benavides-Serrato, A., Sabha, N., Nishimura, R. N., Guha, A., et al. (2012). Conditional astroglial Rictor overexpression induces malignant glioma in mice. *PloS one* **7**, e47741.

Bellacosa, A., Kumar, C. C., Di Cristofano, A. and Testa, J. R. (2005). Activation of AKT kinases in cancer: implications for therapeutic targeting. *Advances in cancer research* **94**, 29-86.

Berdasco, M. and Esteller, M. (2010). Aberrant epigenetic landscape in cancer: how cellular identity goes awry. *Developmental cell* **19**, 698-711.

Bhat, K. P., Balasubramaniyan, V., Vaillant, B., Ezhilarasan, R., Hummelink, K., Hollingsworth, F., Wani, K., Heathcock, L., James, J. D., Goodman, L. D., et al. (2013). Mesenchymal differentiation mediated by NF-kappaB promotes radiation resistance in glioblastoma. *Cancer cell* **24**, 331-346.

Bigner, S. H., Mark, J., Mahaley, M. S. and Bigner, D. D. (1984). Patterns of the early, gross chromosomal changes in malignant human gliomas. *Hereditas* **101**, 103-113.

Birch, J. M., Alston, R. D., McNally, R. J., Evans, D. G., Kelsey, A. M., Harris, M., Eden, O. B. and Varley, J. M. (2001). Relative frequency and morphology of cancers in carriers of germline TP53 mutations. *Oncogene* **20**, 4621-4628.

Bonavia, R., Inda, M. M., Cavenee, W. K. and Furnari, F. B. (2011). Heterogeneity maintenance in glioblastoma: a social network. *Cancer research* **71**, 4055-4060.

Brennan, C. W., Verhaak, R. G., McKenna, A., Campos, B., Noushmehr, H., Salama, S. R., Zheng, S., Chakravarty, D., Sanborn, J. Z., Berman, S. H., et al. (2013). The somatic genomic landscape of glioblastoma. *Cell* **155**, 462-477.

Burrell, R. A., McGranahan, N., Bartek, J. and Swanton, C. (2013). The causes and consequences of genetic heterogeneity in cancer evolution. *Nature* **501**, 338-345.

Cancer Genome Atlas Research, N. (2008). Comprehensive genomic characterization defines human glioblastoma genes and core pathways. *Nature* **455**, 1061-1068.

Carson, R. P., Fu, C., Winzenburger, P. and Ess, K. C. (2013). Deletion of Rictor in neural progenitor cells reveals contributions of mTORC2 signaling to tuberous sclerosis complex. *Human molecular genetics* **22**, 140-152.

Chen, J., Li, Y., Yu, T. S., McKay, R. M., Burns, D. K., Kernie, S. G. and Parada, L. F. (2012a). A restricted cell population propagates glioblastoma growth after chemotherapy. *Nature* **488**, 522-526.

Chen, J., McKay, R. M. and Parada, L. F. (2012b). Malignant glioma: lessons from genomics, mouse models, and stem cells. *Cell* **149**, 36-47.

Chow, L. M., Endersby, R., Zhu, X., Rankin, S., Qu, C., Zhang, J., Broniscer, A., Ellison, D. W. and Baker, S. J. (2011). Cooperativity within and among Pten, p53, and Rb pathways induces high-grade astrocytoma in adult brain. *Cancer cell* **19**, 305-316.

Cloughesy, T. F., Cavenee, W. K. and Mischel, P. S. (2014). Glioblastoma: from molecular pathology to targeted treatment. *Annual review of pathology* **9**, 1-25.

Cully, M., You, H., Levine, A. J. and Mak, T. W. (2006). Beyond PTEN mutations: the PI3K pathway as an integrator of multiple inputs during tumorigenesis. *Nature reviews. Cancer* **6**, 184-192.

Deng, Q., Ramskold, D., Reinius, B. and Sandberg, R. (2014). Single-cell RNA-seq reveals dynamic, random monoallelic gene expression in mammalian cells. *Science* **343**, 193-196.

Eberhart, C. G. (2012). Three down and one to go: modeling medulloblastoma subgroups. *Cancer cell* **21**, 137-138.

Ellison, D. W. (2010). Childhood medulloblastoma: novel approaches to the classification of a heterogeneous disease. *Acta neuropathologica* **120**, 305-316.

Engelman, J. A., Luo, J. and Cantley, L. C. (2006). The evolution of phosphatidylinositol 3-kinases as regulators of growth and metabolism. *Nature reviews. Genetics* **7**, 606-619.

Fearon, E. R. (2011). Molecular genetics of colorectal cancer. *Annual review of pathology* **6**, 479-507.

Foster, K. G. and Fingar, D. C. (2010). Mammalian target of rapamycin (mTOR): conducting the cellular signaling symphony. *The Journal of biological chemistry* **285**, 14071-14077.

Friedmann-Morvinski, D., Bushong, E. A., Ke, E., Soda, Y., Marumoto, T., Singer, O., Ellisman, M. H. and Verma, I. M. (2012). Dedifferentiation of neurons and astrocytes by oncogenes can induce gliomas in mice. *Science* **338**, 1080-1084.

Furnari, F. B., Fenton, T., Bachoo, R. M., Mukasa, A., Stommel, J. M., Stegh, A., Hahn, W. C., Ligon, K. L., Louis, D. N., Brennan, C., et al. (2007). Malignant astrocytic glioma: genetics, biology, and paths to treatment. *Genes & development* **21**, 2683-2710.

Gajjar, A. J. and Robinson, G. W. (2014). Medulloblastoma-translating discoveries from the bench to the bedside. *Nature reviews. Clinical oncology* **11**, 714-722.

Gao, D., Wan, L., Inuzuka, H., Berg, A. H., Tseng, A., Zhai, B., Shaik, S., Bennett, E., Tron, A. E., Gasser, J. A., et al. (2010). Rictor forms a complex with Cullin-1 to promote SGK1 ubiquitination and destruction. *Molecular cell* **39**, 797-808.

Gao, T., Furnari, F. and Newton, A. C. (2005). PHLPP: a phosphatase that directly dephosphorylates Akt, promotes apoptosis, and suppresses tumor growth. *Molecular cell* **18**, 13-24.

Gibson, P., Tong, Y., Robinson, G., Thompson, M. C., Currle, D. S., Eden, C., Kranenburg, T. A., Hogg, T., Poppleton, H., Martin, J., et al. (2010). Subtypes of medulloblastoma have distinct developmental origins. *Nature* **468**, 1095-1099.

Gilbertson, R. J. and Ellison, D. W. (2008). The origins of medulloblastoma subtypes. *Annual review of pathology* **3**, 341-365.

Grammel, D., Warmuth-Metz, M., von Bueren, A. O., Kool, M., Pietsch, T., Kretzschmar, H. A., Rowitch, D. H., Rutkowski, S., Pfister, S. M. and Schuller, U. (2012). Sonic hedgehog-associated medulloblastoma arising from the cochlear nuclei of the brainstem. *Acta neuropathologica* **123**, 601-614.

Greaves, M. and Maley, C. C. (2012). Clonal evolution in cancer. *Nature* **481**, 306-313.

Guertin, D. A., Stevens, D. M., Saitoh, M., Kinkel, S., Crosby, K., Sheen, J. H., Mullholland, D. J., Magnuson, M. A., Wu, H. and Sabatini, D. M. (2009). mTOR complex 2 is required for the development of prostate cancer induced by Pten loss in mice. *Cancer cell* **15**, 148-159.

Guertin, D. A., Stevens, D. M., Thoreen, C. C., Burds, A. A., Kalaany, N. Y., Moffat, J., Brown, M., Fitzgerald, K. J. and Sabatini, D. M. (2006). Ablation in mice of the mTORC components raptor, rictor, or mLST8 reveals that mTORC2 is required for signaling to Akt-FOXO and PKCalpha, but not S6K1. *Developmental cell* **11**, 859-871.

Hahn, H., Wicking, C., Zaphiropoulous, P. G., Gailani, M. R., Shanley, S., Chidambaram, A., Vorechovsky, I., Holmberg, E., Unden, A. B., Gillies, S., et al. (1996). Mutations of the human homolog of Drosophila patched in the nevoid basal cell carcinoma syndrome. *Cell* **85**, 841-851.

Hajra, K. M. and Fearon, E. R. (2002). Cadherin and catenin alterations in human cancer. *Genes, chromosomes & cancer* **34**, 255-268.

Hatten, M. E. and Roussel, M. F. (2011). Development and cancer of the cerebellum. *Trends in neurosciences* **34**, 134-142.

Hatton, B. A., Villavicencio, E. H., Tsuchiya, K. D., Pritchard, J. I., Ditzler, S., Pullar, B., Hansen, S., Knoblaugh, S. E., Lee, D., Eberhart, C. G., et al. (2008). The Smo/Smo model: hedgehog-induced medulloblastoma with 90% incidence and leptomeningeal spread. *Cancer research* **68**, 1768-1776.

He, X., Zhang, L., Chen, Y., Remke, M., Shih, D., Lu, F., Wang, H., Deng, Y., Yu, Y., Xia, Y., et al. (2014). The G protein alpha subunit Galphas is a tumor suppressor in Sonic hedgehog-driven medulloblastoma. *Nature medicine* **20**, 1035-1042.

Hegi, M. E., Diserens, A. C., Gorlia, T., Hamou, M. F., de Tribolet, N., Weller, M., Kros, J. M., Hainfellner, J. A., Mason, W., Mariani, L., et al. (2005). MGMT gene silencing and benefit from temozolomide in glioblastoma. *The New England journal of medicine* **352**, 997-1003.

Hietakangas, V. and Cohen, S. M. (2008). TOR complex 2 is needed for cell cycle progression and anchorage-independent growth of MCF7 and PC3 tumor cells. *BMC cancer* **8**, 282.

Holland, E. C., Celestino, J., Dai, C., Schaefer, L., Sawaya, R. E. and Fuller, G. N. (2000). Combined activation of Ras and Akt in neural progenitors induces glioblastoma formation in mice. *Nature genetics* **25**, 55-57.

Hollander, M. C., Blumenthal, G. M. and Dennis, P. A. (2011). PTEN loss in the continuum of common cancers, rare syndromes and mouse models. *Nature reviews. Cancer* **11**, 289-301.

Hoshino, M., Nakamura, S., Mori, K., Kawauchi, T., Terao, M., Nishimura, Y. V., Fukuda, A., Fuse, T., Matsuo, N., Sone, M., et al. (2005). Ptf1a, a bHLH transcriptional gene, defines GABAergic neuronal fates in cerebellum. *Neuron* **47**, 201-213.

Huang, W., Zhu, P. J., Zhang, S., Zhou, H., Stoica, L., Galiano, M., Krnjevic, K., Roman, G. and Costa-Mattioli, M. (2013). mTORC2 controls actin polymerization required for consolidation of long-term memory. *Nature neuroscience* **16**, 441-448.

Huse, J. T., Brennan, C., Hambardzumyan, D., Wee, B., Pena, J., Rouhanifard, S. H., Sohn-Lee, C., le Sage, C., Agami, R., Tuschl, T., et al. (2009). The PTEN-regulating microRNA miR-26a is amplified in high-grade glioma and facilitates gliomagenesis in vivo. *Genes & development* **23**, 1327-1337.

Huse, J. T., Holland, E. and DeAngelis, L. M. (2013). Glioblastoma: molecular analysis and clinical implications. *Annual review of medicine* **64**, 59-70.

Huse, J. T. and Holland, E. C. (2010). Targeting brain cancer: advances in the molecular pathology of malignant glioma and medulloblastoma. *Nature reviews. Cancer* **10**, 319-331.

Ikenoue, T., Inoki, K., Yang, Q., Zhou, X. and Guan, K. L. (2008). Essential function of TORC2 in PKC and Akt turn motif phosphorylation, maturation and signalling. *The EMBO journal* **27**, 1919-1931.

Inda, M. M., Bonavia, R., Mukasa, A., Narita, Y., Sah, D. W., Vandenberg, S., Brennan, C., Johns, T. G., Bachoo, R., Hadwiger, P., et al. (2010). Tumor heterogeneity is an active process maintained by a mutant EGFR-induced cytokine circuit in glioblastoma. *Genes & development* **24**, 1731-1745.

Jacques, T. S., Swales, A., Brzozowski, M. J., Henriquez, N. V., Linehan, J. M., Mirzadeh, Z., C, O. M., Naumann, H., Alvarez-Buylla, A. and Brandner, S. (2010). Combinations of genetic mutations in the adult neural stem cell compartment determine brain tumour phenotypes. *The EMBO journal* **29**, 222-235.

Jones, D. T., Jager, N., Kool, M., Zichner, T., Hutter, B., Sultan, M., Cho, Y. J., Pugh, T. J., Hovestadt, V., Stutz, A. M., et al. (2012). Dissecting the genomic complexity underlying medulloblastoma. *Nature* **488**, 100-105.

Jones, M. J. and Jallepalli, P. V. (2012). Chromothripsis: chromosomes in crisis. *Developmental cell* **23**, 908-917.

Katso, R., Okkenhaug, K., Ahmadi, K., White, S., Timms, J. and Waterfield, M. D. (2001). Cellular function of phosphoinositide 3-kinases: implications for development, homeostasis, and cancer. *Annual review of cell and developmental biology* **17**, 615-675.

Kawauchi, D., Robinson, G., Uziel, T., Gibson, P., Rehg, J., Gao, C., Finkelstein, D., Qu, C., Pounds, S., Ellison, D. W., et al. (2012). A mouse model of the most aggressive subgroup of human medulloblastoma. *Cancer cell* **21**, 168-180.

Kool, M., Jones, D. T., Jager, N., Northcott, P. A., Pugh, T. J., Hovestadt, V., Piro, R. M., Esparza, L. A., Markant, S. L., Remke, M., et al. (2014). Genome sequencing of SHH medulloblastoma predicts genotype-related response to smoothened inhibition. *Cancer cell* **25**, 393-405.

Kool, M., Korshunov, A., Remke, M., Jones, D. T., Schlanstein, M., Northcott, P. A., Cho, Y. J., Koster, J., Schouten-van Meeteren, A., van Vuurden, D., et al. (2012). Molecular subgroups of medulloblastoma: an international meta-analysis of transcriptome, genetic aberrations, and clinical data of WNT, SHH, Group 3, and Group 4 medulloblastomas. *Acta neuropathologica* **123**, 473-484.

Kool, M., Koster, J., Bunt, J., Hasselt, N. E., Lakeman, A., van Sluis, P., Troost, D., Meeteren, N. S., Caron, H. N., Cloos, J., et al. (2008). Integrated genomics identifies five medulloblastoma subtypes with distinct genetic profiles, pathway signatures and clinicopathological features. *PloS one* **3**, e3088.

Koul, D., Shen, R., Bergh, S., Sheng, X., Shishodia, S., Lafortune, T. A., Lu, Y., de Groot, J. F., Mills, G. B. and Yung, W. K. (2006). Inhibition of Akt survival pathway by a small-molecule inhibitor in human glioblastoma. *Molecular cancer therapeutics* **5**, 637-644.

Kwon, C. H., Zhao, D., Chen, J., Alcantara, S., Li, Y., Burns, D. K., Mason, R. P., Lee, E. Y., Wu, H. and Parada, L. F. (2008). Pten haploinsufficiency accelerates formation of high-grade astrocytomas. *Cancer research* **68**, 3286-3294.

Laplante, M. and Sabatini, D. M. (2012). mTOR signaling in growth control and disease. *Cell* **149**, 274-293.

Lee, A., Kessler, J. D., Read, T. A., Kaiser, C., Corbeil, D., Huttner, W. B., Johnson, J. E. and Wechsler-Reya, R. J. (2005). Isolation of neural stem cells from the postnatal cerebellum. *Nature neuroscience* **8**, 723-729.

Leto, K., Rolando, C. and Rossi, F. (2012). The genesis of cerebellar GABAergic neurons: fate potential and specification mechanisms. *Frontiers in neuroanatomy* **6**, 6.

Li, D. M. and Sun, H. (1997). TEP1, encoded by a candidate tumor suppressor locus, is a novel protein tyrosine phosphatase regulated by transforming growth factor beta. *Cancer research* **57**, 2124-2129.

Li, J., Yen, C., Liaw, D., Podsypanina, K., Bose, S., Wang, S. I., Puc, J., Miliaresis, C., Rodgers, L., McCombie, R., et al. (1997). PTEN, a putative protein tyrosine phosphatase gene mutated in human brain, breast, and prostate cancer. *Science* **275**, 1943-1947.

Lino, M. M. and Merlo, A. (2011). PI3Kinase signaling in glioblastoma. *Journal of neuro-oncology* **103**, 417-427.

Little, S. E., Popov, S., Jury, A., Bax, D. A., Doey, L., Al-Sarraj, S., Jurgensmeier, J. M. and Jones, C. (2012). Receptor tyrosine kinase genes amplified in glioblastoma exhibit a mutual exclusivity in variable proportions reflective of individual tumor heterogeneity. *Cancer research* **72**, 1614-1620.

Liu, C., Sage, J. C., Miller, M. R., Verhaak, R. G., Hippenmeyer, S., Vogel, H., Foreman, O., Bronson, R. T., Nishiyama, A., Luo, L., et al. (2011). Mosaic analysis with double markers reveals tumor cell of origin in glioma. *Cell* **146**, 209-221.

Lorenz, A., Deutschmann, M., Ahlfeld, J., Prix, C., Koch, A., Smits, R., Fodde, R., Kretzschmar, H. A. and Schuller, U. (2011). Severe alterations of cerebellar cortical development after constitutive activation of Wnt signaling in granule neuron precursors. *Molecular and cellular biology* **31**, 3326-3338.

Louis, D. N. (2006). Molecular pathology of malignant gliomas. *Annual review of pathology* **1**, 97-117.

Louis, D. N., Ohgaki, H., Wiestler, O. D., Cavenee, W. K., Burger, P. C., Jouvet, A., Scheithauer, B. W. and Kleihues, P. (2007). The 2007 WHO classification of tumours of the central nervous system. *Acta neuropathologica* **114**, 97-109.

Machold, R. and Fishell, G. (2005). Math1 is expressed in temporally discrete pools of cerebellar rhombic-lip neural progenitors. *Neuron* **48**, 17-24.

Maehama, T. and Dixon, J. E. (1998). The tumor suppressor, PTEN/MMAC1, dephosphorylates the lipid second messenger, phosphatidylinositol 3,4,5-trisphosphate. *The Journal of biological chemistry* **273**, 13375-13378.

Magee, J. A., Ikenoue, T., Nakada, D., Lee, J. Y., Guan, K. L. and Morrison, S. J. (2012). Temporal changes in PTEN and mTORC2 regulation of hematopoietic stem cell self-renewal and leukemia suppression. *Cell stem cell* **11**, 415-428.

Manning, B. D. and Cantley, L. C. (2007). AKT/PKB signaling: navigating downstream. *Cell* **129**, 1261-1274.

Marzban, H., Del Bigio, M. R., Alizadeh, J., Ghavami, S., Zachariah, R. M. and Rastegar, M. (2014). Cellular commitment in the developing cerebellum. *Frontiers in cellular neuroscience* **8**, 450.

Masri, J., Bernath, A., Martin, J., Jo, O. D., Vartanian, R., Funk, A. and Gera, J. (2007). mTORC2 activity is elevated in gliomas and promotes growth and cell motility via overexpression of rictor. *Cancer research* **67**, 11712-11720.

Masui, K., Tanaka, K., Akhavan, D., Babic, I., Gini, B., Matsutani, T., Iwanami, A., Liu, F., Villa, G. R., Gu, Y., et al. (2013). mTOR complex 2 controls glycolytic metabolism in glioblastoma through FoxO acetylation and upregulation of c-Myc. *Cell metabolism* **18**, 726-739.

Mellinghoff, I. K., Wang, M. Y., Vivanco, I., Haas-Kogan, D. A., Zhu, S., Dia, E. Q., Lu, K. V., Yoshimoto, K., Huang, J. H., Chute, D. J., et al. (2005). Molecular determinants of the response of glioblastomas to EGFR kinase inhibitors. *The New England journal of medicine* **353**, 2012-2024.

Meng, F., Henson, R., Wehbe-Janek, H., Ghoshal, K., Jacob, S. T. and Patel, T. (2007). MicroRNA-21 regulates expression of the PTEN tumor suppressor gene in human hepatocellular cancer. *Gastroenterology* **133**, 647-658.

Meyer, M., Reimand, J., Lan, X., Head, R., Zhu, X., Kushida, M., Bayani, J., Pressey, J. C., Lionel, A. C., Clarke, I. D., et al. (2015). Single cell-derived clonal analysis of human glioblastoma links functional and genomic heterogeneity. *Proceedings of the National Academy of Sciences of the United States of America* **112**, 851-856.

Miao, B., Skidan, I., Yang, J., Lugovskoy, A., Reibarkh, M., Long, K., Brazell, T., Durugkar, K. A., Maki, J., Ramana, C. V., et al. (2010). Small molecule inhibition of phosphatidylinositol-3,4,5-triphosphate (PIP3) binding to pleckstrin homology

domains. *Proceedings of the National Academy of Sciences of the United States of America* **107**, 20126-20131.

Millen, K. J. and Gleeson, J. G. (2008). Cerebellar development and disease. *Current opinion in neurobiology* **18**, 12-19.

Momota, H., Nerio, E. and Holland, E. C. (2005). Perifosine inhibits multiple signaling pathways in glial progenitors and cooperates with temozolomide to arrest cell proliferation in gliomas in vivo. *Cancer research* **65**, 7429-7435.

Moniz, L. S. and Vanhaesebroeck, B. (2013). AKT-ing out: SGK kinases come to the fore. *The Biochemical journal* **452**, e11-13.

Munoz, D. M., Tung, T., Agnihotri, S., Singh, S., Guha, A., Zadeh, G. and Hawkins, C. (2013). Loss of p53 cooperates with K-ras activation to induce glioma formation in a region-independent manner. *Glia* **61**, 1862-1872.

Newton, A. C. (2003). Regulation of the ABC kinases by phosphorylation: protein kinase C as a paradigm. *The Biochemical journal* **370**, 361-371.

Nobusawa, S., Watanabe, T., Kleihues, P. and Ohgaki, H. (2009). IDH1 mutations as molecular signature and predictive factor of secondary glioblastomas. *Clinical cancer research : an official journal of the American Association for Cancer Research* **15**, 6002-6007.

Northcott, P. A., Jones, D. T., Kool, M., Robinson, G. W., Gilbertson, R. J., Cho, Y. J., Pomeroy, S. L., Korshunov, A., Lichter, P., Taylor, M. D., et al. (2012a). Medulloblastomics: the end of the beginning. *Nature reviews. Cancer* **12**, 818-834.

Northcott, P. A., Korshunov, A., Witt, H., Hielscher, T., Eberhart, C. G., Mack, S., Bouffet, E., Clifford, S. C., Hawkins, C. E., French, P., et al. (2011). Medulloblastoma comprises four distinct molecular variants. *Journal of clinical oncology : official journal of the American Society of Clinical Oncology* **29**, 1408-1414.

Northcott, P. A., Lee, C., Zichner, T., Stutz, A. M., Erkek, S., Kawauchi, D., Shih, D. J., Hovestadt, V., Zapatka, M., Sturm, D., et al. (2014). Enhancer hijacking activates GFI1 family oncogenes in medulloblastoma. *Nature* **511**, 428-434.

Northcott, P. A., Shih, D. J., Peacock, J., Garzia, L., Morrissy, A. S., Zichner, T., Stutz, A. M., Korshunov, A., Reimand, J., Schumacher, S. E., et al. (2012b). Subgroup-specific structural variation across 1,000 medulloblastoma genomes. *Nature* **488**, 49-56.

Noushmehr, H., Weisenberger, D. J., Diefes, K., Phillips, H. S., Pujara, K., Berman, B. P., Pan, F., Pelloski, C. E., Sulman, E. P., Bhat, K. P., et al. (2010). Identification of a CpG island methylator phenotype that defines a distinct subgroup of glioma. *Cancer cell* **17**, 510-522.

Oh, W. J. and Jacinto, E. (2011). mTOR complex 2 signaling and functions. *Cell cycle* **10**, 2305-2316.

Ohgaki, H. and Kleihues, P. (2013). The definition of primary and secondary glioblastoma. *Clinical cancer research : an official journal of the American Association for Cancer Research* **19**, 764-772.

Oliver, T. G., Read, T. A., Kessler, J. D., Mehmeti, A., Wells, J. F., Huynh, T. T., Lin, S. M. and Wechsler-Reya, R. J. (2005). Loss of patched and disruption of

granule cell development in a pre-neoplastic stage of medulloblastoma. *Development* **132**, 2425-2439.

Ozawa, T., Riester, M., Cheng, Y. K., Huse, J. T., Squatrito, M., Helmy, K., Charles, N., Michor, F. and Holland, E. C. (2014). Most human non-GCIMP glioblastoma subtypes evolve from a common proneural-like precursor glioma. *Cancer cell* **26**, 288-300.

Park, W. S., Heo, W. D., Whalen, J. H., O'Rourke, N. A., Bryan, H. M., Meyer, T. and Teruel, M. N. (2008). Comprehensive identification of PIP3-regulated PH domains from C. elegans to H. sapiens by model prediction and live imaging. *Molecular cell* **30**, 381-392.

Parsons, D. W., Jones, S., Zhang, X., Lin, J. C., Leary, R. J., Angenendt, P., Mankoo, P., Carter, H., Siu, I. M., Gallia, G. L., et al. (2008). An integrated genomic analysis of human glioblastoma multiforme. *Science* **321**, 1807-1812.

Pascual, M., Abasolo, I., Mingorance-Le Meur, A., Martinez, A., Del Rio, J. A., Wright, C. V., Real, F. X. and Soriano, E. (2007). Cerebellar GABAergic progenitors adopt an external granule cell-like phenotype in the absence of Ptf1a transcription factor expression. *Proceedings of the National Academy of Sciences of the United States of America* **104**, 5193-5198.

Patel, A. P., Tirosh, I., Trombetta, J. J., Shalek, A. K., Gillespie, S. M., Wakimoto, H., Cahill, D. P., Nahed, B. V., Curry, W. T., Martuza, R. L., et al. (2014). Single-cell RNA-seq highlights intratumoral heterogeneity in primary glioblastoma. *Science* **344**, 1396-1401.

Pei, Y., Moore, C. E., Wang, J., Tewari, A. K., Eroshkin, A., Cho, Y. J., Witt, H., Korshunov, A., Read, T. A., Sun, J. L., et al. (2012). An animal model of MYC-driven medulloblastoma. *Cancer cell* **21**, 155-167.

Pfister, S., Remke, M., Benner, A., Mendrzyk, F., Toedt, G., Felsberg, J., Wittmann, A., Devens, F., Gerber, N. U., Joos, S., et al. (2009). Outcome prediction in pediatric medulloblastoma based on DNA copy-number aberrations of chromosomes 6q and 17q and the MYC and MYCN loci. *Journal of clinical oncology : official journal of the American Society of Clinical Oncology* **27**, 1627-1636.

Phillips, H. S., Kharbanda, S., Chen, R., Forrest, W. F., Soriano, R. H., Wu, T. D., Misra, A., Nigro, J. M., Colman, H., Soroceanu, L., et al. (2006). Molecular subclasses of high-grade glioma predict prognosis, delineate a pattern of disease progression, and resemble stages in neurogenesis. *Cancer cell* **9**, 157-173.

Pugh, T. J., Weeraratne, S. D., Archer, T. C., Pomeranz Krummel, D. A., Auclair, D., Bochicchio, J., Carneiro, M. O., Carter, S. L., Cibulskis, K., Erlich, R. L., et al. (2012). Medulloblastoma exome sequencing uncovers subtype-specific somatic mutations. *Nature* **488**, 106-110.

Rausch, T., Jones, D. T., Zapatka, M., Stutz, A. M., Zichner, T., Weischenfeldt, J., Jager, N., Remke, M., Shih, D., Northcott, P. A., et al. (2012). Genome sequencing of pediatric medulloblastoma links catastrophic DNA rearrangements with TP53 mutations. *Cell* **148**, 59-71.

Robinson, G., Parker, M., Kranenburg, T. A., Lu, C., Chen, X., Ding, L., Phoenix, T. N., Hedlund, E., Wei, L., Zhu, X., et al. (2012). Novel mutations target distinct subgroups of medulloblastoma. *Nature* **488**, 43-48.

Roussel, M. F. and Hatten, M. E. (2011). Cerebellum development and medulloblastoma. *Current topics in developmental biology* **94**, 235-282.

Salmena, L., Carracedo, A. and Pandolfi, P. P. (2008). Tenets of PTEN tumor suppression. *Cell* **133**, 403-414.

Sarbassov, D. D., Guertin, D. A., Ali, S. M. and Sabatini, D. M. (2005). Phosphorylation and regulation of Akt/PKB by the rictor-mTOR complex. *Science* **307**, 1098-1101.

Schonbrun, M., Laor, D., Lopez-Maury, L., Bahler, J., Kupiec, M. and Weisman, R. (2009). TOR complex 2 controls gene silencing, telomere length maintenance, and survival under DNA-damaging conditions. *Molecular and cellular biology* **29**, 4584-4594.

Schwartzentruber, J., Korshunov, A., Liu, X. Y., Jones, D. T., Pfaff, E., Jacob, K., Sturm, D., Fontebasso, A. M., Quang, D. A., Tonjes, M., et al. (2012). Driver mutations in histone H3.3 and chromatin remodelling genes in paediatric glioblastoma. *Nature* **482**, 226-231.

Sharma, S. V. and Settleman, J. (2007). Oncogene addiction: setting the stage for molecularly targeted cancer therapy. *Genes & development* **21**, 3214-3231.

Shi, Q., Qin, L., Wei, W., Geng, F., Fan, R., Shin, Y. S., Guo, D., Hood, L., Mischel, P. S. and Heath, J. R. (2012). Single-cell proteomic chip for profiling intracellular signaling pathways in single tumor cells. *Proceedings of the National Academy of Sciences of the United States of America* **109**, 419-424.

Shimada, K., Filipuzzi, I., Stahl, M., Helliwell, S. B., Studer, C., Hoepfner, D., Seeber, A., Loewith, R., Movva, N. R. and Gasser, S. M. (2013). TORC2 signaling pathway guarantees genome stability in the face of DNA strand breaks. *Molecular cell* **51**, 829-839.

Singh, S. K., Hawkins, C., Clarke, I. D., Squire, J. A., Bayani, J., Hide, T., Henkelman, R. M., Cusimano, M. D. and Dirks, P. B. (2004). Identification of human brain tumour initiating cells. *Nature* **432**, 396-401.

Snuderl, M., Fazlollahi, L., Le, L. P., Nitta, M., Zhelyazkova, B. H., Davidson, C. J., Akhavanfard, S., Cahill, D. P., Aldape, K. D., Betensky, R. A., et al. (2011). Mosaic amplification of multiple receptor tyrosine kinase genes in glioblastoma. *Cancer cell* **20**, 810-817.

Sommer, E. M., Dry, H., Cross, D., Guichard, S., Davies, B. R. and Alessi, D. R. (2013). Elevated SGK1 predicts resistance of breast cancer cells to Akt inhibitors. *The Biochemical journal* **452**, 499-508.

Song, M. S., Salmena, L. and Pandolfi, P. P. (2012). The functions and regulation of the PTEN tumour suppressor. *Nature reviews. Molecular cell biology* **13**, 283-296.

Sottoriva, A., Spiteri, I., Piccirillo, S. G., Touloumis, A., Collins, V. P., Marioni, J. C., Curtis, C., Watts, C. and Tavare, S. (2013). Intratumor heterogeneity in human glioblastoma reflects cancer evolutionary dynamics. *Proceedings of the National Academy of Sciences of the United States of America* **110**, 4009-4014.

Sparks, C. A. and Guertin, D. A. (2010). Targeting mTOR: prospects for mTOR complex 2 inhibitors in cancer therapy. *Oncogene* **29**, 3733-3744.

Stambolic, V., Suzuki, A., de la Pompa, J. L., Brothers, G. M., Mirtsos, C., Sasaki, T., Ruland, J., Penninger, J. M., Siderovski, D. P. and Mak, T. W. (1998).

Negative regulation of PKB/Akt-dependent cell survival by the tumor suppressor PTEN. *Cell* **95**, 29-39.

Steck, P. A., Pershouse, M. A., Jasser, S. A., Yung, W. K., Lin, H., Ligon, A. H., Langford, L. A., Baumgard, M. L., Hattier, T., Davis, T., et al. (1997). Identification of a candidate tumour suppressor gene, MMAC1, at chromosome 10q23.3 that is mutated in multiple advanced cancers. *Nature genetics* **15**, 356-362.

Stiles, C. D. and Rowitch, D. H. (2008). Glioma stem cells: a midterm exam. *Neuron* **58**, 832-846.

Sturm, D., Witt, H., Hovestadt, V., Khuong-Quang, D. A., Jones, D. T., Konermann, C., Pfaff, E., Tonjes, M., Sill, M., Bender, S., et al. (2012). Hotspot mutations in H3F3A and IDH1 define distinct epigenetic and biological subgroups of glioblastoma. *Cancer cell* **22**, 425-437.

Sulis, M. L. and Parsons, R. (2003). PTEN: from pathology to biology. *Trends in cell biology* **13**, 478-483.

Swartling, F. J., Grimmer, M. R., Hackett, C. S., Northcott, P. A., Fan, Q. W., Goldenberg, D. D., Lau, J., Masic, S., Nguyen, K., Yakovenko, S., et al. (2010). Pleiotropic role for MYCN in medulloblastoma. *Genes & development* **24**, 1059-1072.

Swartling, F. J., Savov, V., Persson, A. I., Chen, J., Hackett, C. S., Northcott, P. A., Grimmer, M. R., Lau, J., Chesler, L., Perry, A., et al. (2012). Distinct neural stem cell populations give rise to disparate brain tumors in response to N-MYC. *Cancer cell* **21**, 601-613.

Szerlip, N. J., Pedraza, A., Chakravarty, D., Azim, M., McGuire, J., Fang, Y., Ozawa, T., Holland, E. C., Huse, J. T., Jhanwar, S., et al. (2012). Intratumoral heterogeneity of receptor tyrosine kinases EGFR and PDGFRA amplification in glioblastoma defines subpopulations with distinct growth factor response. *Proceedings of the National Academy of Sciences of the United States of America* **109**, 3041-3046.

Tabori, U., Baskin, B., Shago, M., Alon, N., Taylor, M. D., Ray, P. N., Bouffet, E., Malkin, D. and Hawkins, C. (2010). Universal poor survival in children with medulloblastoma harboring somatic TP53 mutations. *Journal of clinical oncology : official journal of the American Society of Clinical Oncology* **28**, 1345-1350.

Taipale, J. and Beachy, P. A. (2001). The Hedgehog and Wnt signalling pathways in cancer. *Nature* **411**, 349-354.

Tanaka, K., Babic, I., Nathanson, D., Akhavan, D., Guo, D., Gini, B., Dang, J., Zhu, S., Yang, H., De Jesus, J., et al. (2011). Oncogenic EGFR signaling activates an mTORC2-NF-kappaB pathway that promotes chemotherapy resistance. *Cancer discovery* **1**, 524-538.

Taylor, M. D., Northcott, P. A., Korshunov, A., Remke, M., Cho, Y. J., Clifford, S. C., Eberhart, C. G., Parsons, D. W., Rutkowski, S., Gajjar, A., et al. (2012). Molecular subgroups of medulloblastoma: the current consensus. *Acta neuropathologica* **123**, 465-472.

Testa, J. R. and Bellacosa, A. (2001). AKT plays a central role in tumorigenesis. *Proceedings of the National Academy of Sciences of the United States of America* **98**, 10983-10985.

Thomanetz, V., Angliker, N., Cloetta, D., Lustenberger, R. M., Schweighauser, M., Oliveri, F., Suzuki, N. and Ruegg, M. A. (2013). Ablation of the mTORC2 component rictor in brain or Purkinje cells affects size and neuron morphology. *The Journal of cell biology* **201**, 293-308.

Thompson, M. C., Fuller, C., Hogg, T. L., Dalton, J., Finkelstein, D., Lau, C. C., Chintagumpala, M., Adesina, A., Ashley, D. M., Kellie, S. J., et al. (2006). Genomics identifies medulloblastoma subgroups that are enriched for specific genetic alterations. *Journal of clinical oncology : official journal of the American Society of Clinical Oncology* **24**, 1924-1931.

Thorpe, L. M., Yuzugullu, H. and Zhao, J. J. (2015). PI3K in cancer: divergent roles of isoforms, modes of activation and therapeutic targeting. *Nature reviews. Cancer* **15**, 7-24.

Vanhaesebroeck, B., Guillermet-Guibert, J., Graupera, M. and Bilanges, B. (2010). The emerging mechanisms of isoform-specific PI3K signalling. *Nature reviews. Molecular cell biology* **11**, 329-341.

Vanner, R. J., Remke, M., Gallo, M., Selvadurai, H. J., Coutinho, F., Lee, L., Kushida, M., Head, R., Morrissy, S., Zhu, X., et al. (2014). Quiescent sox2(+) cells drive hierarchical growth and relapse in sonic hedgehog subgroup medulloblastoma. *Cancer cell* **26**, 33-47.

Verhaak, R. G., Hoadley, K. A., Purdom, E., Wang, V., Qi, Y., Wilkerson, M. D., Miller, C. R., Ding, L., Golub, T., Mesirov, J. P., et al. (2010). Integrated genomic analysis identifies clinically relevant subtypes of glioblastoma characterized by abnormalities in PDGFRA, IDH1, EGFR, and NF1. *Cancer cell* **17**, 98-110.

Wang, Y., Yang, J., Zheng, H., Tomasek, G. J., Zhang, P., McKeever, P. E., Lee, E. Y. and Zhu, Y. (2009). Expression of mutant p53 proteins implicates a lineage relationship between neural stem cells and malignant astrocytic glioma in a murine model. *Cancer cell* **15**, 514-526.

Watkins, S. and Sontheimer, H. (2012). Unique biology of gliomas: challenges and opportunities. *Trends in neurosciences* **35**, 546-556.

Weiler, M., Blaes, J., Pusch, S., Sahm, F., Czabanka, M., Luger, S., Bunse, L., Solecki, G., Eichwald, V., Jugold, M., et al. (2014). mTOR target NDRG1 confers MGMT-dependent resistance to alkylating chemotherapy. *Proceedings of the National Academy of Sciences of the United States of America* **111**, 409-414.

Weinstein, I. B. (2002). Cancer. Addiction to oncogenes--the Achilles heal of cancer. *Science* **297**, 63-64.

Weinstein, I. B. and Joe, A. K. (2006). Mechanisms of disease: Oncogene addiction--a rationale for molecular targeting in cancer therapy. *Nature clinical practice. Oncology* **3**, 448-457.

Wen, P. Y. and Kesari, S. (2008). Malignant gliomas in adults. *The New England journal of medicine* **359**, 492-507.

Wetmore, C., Eberhart, D. E. and Curran, T. (2001). Loss of p53 but not ARF accelerates medulloblastoma in mice heterozygous for patched. *Cancer research* **61**, 513-516.

White, J. J. and Sillitoe, R. V. (2013). Development of the cerebellum: from gene expression patterns to circuit maps. *Wiley interdisciplinary reviews. Developmental biology* **2**, 149-164.

Yang, Z. J., Ellis, T., Markant, S. L., Read, T. A., Kessler, J. D., Bourboulas, M., Schuller, U., Machold, R., Fishell, G., Rowitch, D. H., et al. (2008). Medulloblastoma can be initiated by deletion of Patched in lineage-restricted progenitors or stem cells. *Cancer cell* **14**, 135-145.

Zheng, H., Ying, H., Yan, H., Kimmelman, A. C., Hiller, D. J., Chen, A. J., Perry, S. R., Tonon, G., Chu, G. C., Ding, Z., et al. (2008). p53 and Pten control neural and glioma stem/progenitor cell renewal and differentiation. *Nature* **455**, 1129-1133.

Zhu, Y., Guignard, F., Zhao, D., Liu, L., Burns, D. K., Mason, R. P., Messing, A. and Parada, L. F. (2005). Early inactivation of p53 tumor suppressor gene cooperating with NF1 loss induces malignant astrocytoma. *Cancer cell* **8**, 119-130.

Zhukova, N., Ramaswamy, V., Remke, M., Pfaff, E., Shih, D. J., Martin, D. C., Castelo-Branco, P., Baskin, B., Ray, P. N., Bouffet, E., et al. (2013). Subgroup-specific prognostic implications of TP53 mutation in medulloblastoma. *Journal of clinical oncology : official journal of the American Society of Clinical Oncology* **31**, 2927-2935.

Zong, H., Parada, L. F. and Baker, S. J. (2015). Cell of Origin for Malignant Gliomas and Its Implication in Therapeutic Development. *Cold Spring Harbor perspectives in biology*.

Chapter II: Mutant-*p53* driven gliomagenesis is blocked and/or delayed by inhibition of Rictor/mTORC2 signaling

2.1 Introduction

Glioblastoma is the most common malignant neoplasm of the central nervous system in adults with an annual incidence of 5 cases per 100,000 people (Furnari et al., 2007; Louis, 2006; Wen and Kesari, 2008). The median survival rate remains approximately 12-15 months in spite of supportive care and intense treatment plans, which includes surgery, chemotherapy and radiotherapy (Huse et al., 2013; Stupp et al., 2009). Complications associated with tumor debulking, poor drug delivery, and tumor heterogeneity are considered to be the main factors that limit the effectiveness of these treatment strategies (Sottoriva et al., 2013). The presence of intratumor and intertumor heterogeneity, in particular, suggests that molecularly distinct tumors might exhibit differences in progression, prognosis, and clinical implications (Phillips et al., 2006; Verhaak et al., 2010). In order to better understand this complexity, glioblastomas have been extensively studied in terms of their genome-wide DNA copy number events, sequence-based mutations, and DNA methylation profiles, and categorized into multiple subgroups (Classic, Proneural, Neural, Mesenchymal) based on their gene expression profiles (Brennan et al., 2013; Noushmehr et al., 2010; Parsons et al., 2008; Phillips et al., 2006; Sturm et al., 2012; Verhaak et al., 2010). Nevertheless, it remains a challenge as to whether and how the identification of subgroups can improve the current treatment options, especially as recent studies have suggested that tumor cells associated with

different subgroups or with different molecular characteristics could be found within a single tumor mass (Patel et al., 2014; Sottoriva et al., 2013). Furthermore, some tumors have shown the ability to switch their profile upon the occurrence of certain molecular events such as *NF1* loss (Ozawa et al., 2014) or NF-κB activation (Bhat et al., 2013), suggesting a tumor evolution.

Even in the presence of generally unpredictable tumor dynamics and molecular heterogeneity, a gain of several chr7 copies and a loss of at least one chr10q copy remain the most common molecular events in a majority of glioblastoma tumors and tumor cells (86% and 90%, respectively) (Ozawa et al., 2014; Patel et al., 2014). These two chromosomal abnormalities are specifically associated with the amplification of *EGFR* and *PDGFA*, and the loss of *PTEN*, respectively (Ozawa et al., 2014; Verhaak et al., 2010), consistent with the previous findings that PI3K/RTK pathway is altered in 90% of human glioblastomas, leading to highly active AKT signaling (Brennan et al., 2013; Cancer Genome Atlas Research, 2008; Furnari et al., 2007). Furthermore, the finding showing that frequency of AKT activation significantly correlates with the histologic grade of gliomas underlines the important roles of this pathway in disease progression (Wang et al., 2004). Hence, the inhibition of PI3K and/or AKT signaling has been of particular interest in many cancer studies, including glioblastoma (Altomare and Testa, 2005; Bellacosa et al., 2005; Cully et al., 2006; Momota et al., 2005; Testa and Bellacosa, 2001; Wen and Kesari, 2008).

mTORC2 is a major kinase that activates AKT through its phosphorylation at Serine-473 (Ser^{473}), along with PDK1, which phosphorylates AKT at Threonine-308 (Thr^{308}) (Alessi et al., 1997; Guertin et al., 2006; Ikenoue et al., 2008; Sarbassov et al., 2005). It has been shown that functional loss of *Rictor*, a critical subunit of mTORC2, is sufficient to block Akt activation and tumor growth in various cancer models (Guertin et al., 2009; Magee et al., 2012; Masui et al., 2013). These findings indicate that tumor cells characterized by elevated Akt signaling are dependent on this molecule for survival, and are thus vulnerable to Akt inhibition (Bellacosa et al., 2005; Koul et al., 2006). Similarly, mouse

models containing tissue specific mutations in critical tumor suppressor genes such as *p53*, *Pten*, *Nf1* and *Rb,* as well as models with combined activation of Ras and Akt in neural progenitors, lead to high grade gliomas characterized by elevated PI3K/Akt pathway (Chow et al., 2011; Holland et al., 2000; Kwon et al., 2008; Zheng et al., 2008; Zhu et al., 2005). It is not well established, however, as to whether these mouse tumors undergo the spontaneous genomic events that are frequently observed in human glioblastomas. Furthermore, the introduction of multiple genetic modifications, especially in key tumor suppressor genes, might change the cascades of genomic alterations required for tumor initiation and/or progression. It is, therefore, critical to test whether the inhibition of Rictor/mTORC2 has an impact on tumorigenesis using *de novo* glioma models that carry minimal genetic modifications and allow the occurrence of sporadic genomic alterations characteristic to human glioblastomas.

Consistent with the fact that p53 signaling is altered in 86% of human glioblastomas (Brennan et al., 2013; Cancer Genome Atlas Research, 2008), mouse models with *p53*-deficiency alone are capable of giving rise to high-grade gliomas with elevated PI3K/Akt signaling (Wang et al., 2009), As this model carried relatively minimal genetic modifications, allowing for occurrence of the spontaneous molecular events observed during the natural progression of human glioblastomas, it provided us with a unique tool to test the therapeutic potential of targeting Rictor/mTORC2 signaling *in vivo*. More specifically, we used genetically engineered mouse (GEM) models to investigate the effects of loss of Akt signaling in the development of glioblastomas by deleting Rictor/mTORC2. We show that during mutant *p53*-driven gliomagenesis, loss of chr19 and chr7, syntenic to human chr10q, spontaneously occurs in many *p53*-mutant high-grade gliomas, which is accompanied by loss of *Pten* and activation of PI3K/Akt signaling. Moreover, we show that the inhibition of Rictor/mTORC2, and by extension PI3K/Akt signaling pathway, exerts significant tumor suppressive activity, but not absolutely required for mutant *p53*-driven glioma development. These results underline the therapeutic potential of Rictor/mTORC2 inhibitors, and also underline the necessity

to prescreen and classify glioblastoma patients based on their plausible response to these inhibitors.

2.2 Results

2.2.1 *p53*-mutant GEM gliomas undergo key genomic alterations observed In human Glioblastoma

We previously developed three GEM glioma models driven by (1) a conditional in-frame deletion of exons 5 and 6 of the *p53* gene alone (hGFAP-cre;$p53^{E5\text{-}6/E5\text{-}6}$) or (2) in combination with a germline heterozygous *Nf1* mutation (hGFAP-cre;$p53^{E5\text{-}6/E5\text{-}6}$;$Nf1^{+/-}$), and (3) a conditional cis-*p53*/*Nf1* mutation (hGFAP-cre;cis-$p53^{+/-}$;$Nf1^{+/flox}$) (Wang et al., 2009; Zhu et al., 2005). Based on the status of *p53* and *Nf1* in these gliomas, we hereafter referred these three GEM gliomas as $p53^{\Delta5\text{-}6/\Delta5\text{-}6}$, $p53^{\Delta5\text{-}6/\Delta5\text{-}6}Nf1^{-/-}$ and $p53^{-/-}Nf1^{-/-}$, respectively. These GEM gliomas exhibited critical histopathological characteristics of human high-grade gliomas, approximately 40% of which showed necrosis and/or microvascular proliferation – the diagnostic features of glioblastoma (Zhu et al., 2005).

We further analyzed these tumors in collaboration with Dr. Roeland G.W. Verhaak and Dr. Siyuan Zheng at the University of Texas MD Anderson Cancer Center, Houston, TX. Our findings showed that the gene expression profiles of *p53*- and *p53*/*Nf1*-mutant GEM gliomas were most similar to the Proneural subgroup of glioblastoma with one exception that showed the Classical signature (Figure 1A). Consistent with human Proneural glioblastomas, these GEM gliomas exhibited high similarity to the gene expression profile of oligodendrocyte precursor cells (OPCs) characterized by high expression of *Olig2* and *Ascl1* (Figures 1B and 1C). However, high levels of *Nestin* expression observed in these GEM gliomas also suggest their similarity to a subset of Type C transit-amplifying progenitors with $Olig2^{+}Ascl1^{+}Nestin^{+}$ expression in the subventricular zone (SVZ) of the lateral ventricle – the neural stem niche of the adult brain (Figure 1C).

Based on our findings that GEM gliomas resemble the G-CIMP$^{(negative)}$ Proneural subgroup of human glioblastoma (Figure 1A), and the observations that no *Idh1/2* mutation was identified in these GEM gliomas (data not shown), we propose that the *p53*- and *p53*/*Nf1*-mutant GEM gliomas genetically resemble the Proneural subtype of primary, but not *IDH1*-mutated secondary, glioblastoma in humans.

To determine the cooperating oncogenic events following inactivation of *p53* or *p53* and *Nf1*, we analyzed the copy number alterations (CNA) in these 23 GEM gliomas ($p53^{\Delta 5\text{-}6/\Delta 5\text{-}6}$, n = 4; $p53^{\Delta 5\text{-}6/\Delta 5\text{-}6}Nf1^{-/-}$, n = 4; $p53^{-/-}Nf1^{-/-}$, n = 15). Although human chr10q is distributed in multiple chromosomes in the mouse genome, almost half of the human chr10q corresponds to the segments in mouse chr19 and chr7 (Figure 2A). Remarkably, we found that chr19 and chr7 underwent simultaneous and independent deletions in many of the *p53*- and *p53*/*Nf1*-mutant GEM gliomas (Figures 2B (lower segment) and 2C). Especially the deletion of chr19, which harbors the *Pten* gene, further demonstrates that these GEM gliomas recapitulate the critical genetic events during primary glioblastoma development in humans (Figure 2D). It is worth noting that the region in mouse chr7 corresponding to human chr19 was actually amplified in some of the *p53*-mutant GEM gliomas, which harbored the deletion of the chr7 segment syntenic to human chr10q (Figures 2B and 2C). These observations not only reveal the specificity of the focal deletion event in mouse chr7 that is syntenic to human chr10q during glioblastoma development, but also recapitulates the previously reported chr19 amplification in human glioblastomas (Brennan et al., 2013). Together, the co-deletion of two different chromosome segments in mouse chr19 and chr7, which both are syntenic to human chr10q, suggests that the whole chromosomal arm deletion of chr10q is critical to primary glioblastoma pathogenesis, but not merely a by-product of *PTEN* loss in humans. Moreover, these results provide the support for the hypothesis that a single genetic event of chr10q loss leads to the deletion of multiple tumor suppressor genes (besides *PTEN*), providing a greater growth advantage. In support, we also identified a simultaneous deletion of *Pten* and *Dmbt1*, a tumor suppressor gene located in mouse chr7 (in human

10q), of another group of mutant-*p53* GEM gliomas (Figures 2E and 2F) (see next section for details about these new mouse models).

When a conditional heterozygous *Pten* mutation with a floxed exon 5 ($Pten^{+/E5}$) was introduced to the $p53^{\Delta 5\text{-}6}$ model, the resultant $p53^{\Delta 5\text{-}6}$;$Pten^{+/\Delta}$ gliomas exhibited targeted loss of exon 5, but untargeted exon 9 was less affected. In contrast, both exons 5 and 9 were lost in the $p53^{\Delta 5\text{-}6}$ gliomas, an observation that is consistent with the CNA data - loss of the entire chr19 containing *Pten* (Figure 2E). Similarly, a previous study using conditional inactivation of *p53* and *Pten* with or without *Rb* induced malignant gliomas including glioblastomas, which exhibited no loss of chr19 or chr7 (Figure 2B (upper two segments)) (Chow et al., 2011). These results suggest that despite the existence of additional tumor suppressor genes in mouse chr19 and chr7 (human chr10q), the major tumor suppressor gene in chr10q is *Pten*, as the targeted loss of *Pten* can circumvent chr19/chr7 loss to promote mutant *p53*-driven gliomagenesis. Therefore, a strategy that targets downstream events of *PTEN*/*Pten* loss would be effective for primary glioblastoma.

2.2.2 *RICTOR* expression is upregulated in human Glioblastomas with *TP53* mutation

We next sought to further elucidate potential signaling pathways critical to the progression of human glioblastomas. *PTEN* is a negative regulator of the PI3K/AKT pathway and its deletion leads to increased phosphorylation of AKT (Li and Sun, 1997; Li et al., 1997; Stambolic et al., 1998; Steck et al., 1997) at Thr^{308} by PDK1 (Alessi et al., 1997) and at Ser^{473} by mTORC2 (Sarbassov et al., 2005). Previous studies suggest that both phosphorylation events are required in order for AKT to be fully activated (Alessi et al., 1996; Foster and Fingar, 2010; Laplante and Sabatini, 2009). Even though PI3K/AKT signaling is elevated in majority of the human glioblastomas (Brennan et al., 2013), we found that both $pAKT^{T308}$ and $pAKT^{S473}$ protein levels varied significantly, as some samples had higher expression levels than the others (Figure 3A). This finding suggests

that the degree at which the AKT signaling involves in glioma initiation/progression might differ between the tumors. As expected, glioblastomas with *TP53* mutations had higher p53 protein levels, consistent with previous studies (Figure 3A) (Anker et al., 1993; Brosh and Rotter, 2009; Louis et al., 1993). More interestingly, human glioblastomas with a *TP53* mutation had significantly higher expression of *RICTOR*, a critical subunit of mTORC2, compared to the tumors without a *TP53* mutation (Figure 3B), suggesting that mTORC2 signaling might have a crucial role especially in *TP53*-mutant glioblastomas. Thus, these results suggest that *RICTOR* expression, and by extension mTORC2 activity, is critical for glioblastomas with a *TP53* mutation.

2.2.3 *Rictor*-deficiency reduces forebrain tumor formation while increasing hindbrain tumor incidence

Our initial findings showing that *p53*-mutant GEM gliomas spontaneously undergo key genomic alterations (e.g. chr10q/*PTEN* deletion) typical in human glioblastomas, and that mTORC2 signaling may play a key oncogenic role led me to test whether the removal of mTORC2 can affect glioma initiation and/or progression. Thus, in addition to utilizing the previously established hGFAP-cre; $p53^{flox/flox}$ mice ($p53^{\Delta 5\text{-}6/\Delta 5\text{-}6}$, hereafter) (Wang et al., 2009), I generated hGFAP-cre; $p53^{flox/flox}$; $Rictor^{flox/+}$ ($p53^{\Delta 5\text{-}6/\Delta 5\text{-}6}$; $Rictor^{+/\Delta}$, hereafter) mice, which had an additional heterozygous *Rictor* mutation, as well as hGFAP-cre ; $p53^{flox/flox}$; $Rictor^{flox/flox}$ ($p53^{\Delta 5\text{-}6/\Delta 5\text{-}6}$; $Rictor^{\Delta/\Delta}$, hereafter) mice, which lacked both *Rictor* alleles (Figure 4A). Cre-mediated recombination occurs at around embryonic stage 12.5 (E12.5) and it targets multipotent radial glial cells in the brain. Consequently, nearly all neurons, glia and neural stem cells in the dorsal forebrain, as well as the majority of the cerebellar population except for the Purkinje cells are targeted by this strategy (Wang et al., 2009; Zhuo et al., 2001).

Approximately 70% of the $p53^{\Delta 5\text{-}6/\Delta 5\text{-}6}$ and $p53^{\Delta 5\text{-}6/\Delta 5\text{-}6}$; $Rictor^{+/\Delta}$ mice and 55% of the $p53^{\Delta 5\text{-}6/\Delta 5\text{-}6}$; $Rictor^{\Delta/\Delta}$ mice were sacrificed due to observable neurological symptoms including enlarged head, tremor, seizure, ataxia, or lack of balance indicating the

presence of an end-stage brain tumor (Figure 4B). These symptoms were encountered between 4-24 months of age, representing a wide time window for tumor formation and/or progression (Figure 4D). Remaining mice were sacrificed due to other health problems including dermatitis, old age leading to poor health conditions, rectal or penile prolapse, GI tract obstruction, rarely observed eye injuries likely due to fighting, spinal cord problems including paralysis, hyperplasia in the brain, and enlarged and/or ulcerated soft tissue sarcomas outside the central nervous system (CNS) (Figure 4B) due to hGFAP-cre expression in cells outside of the CNS. Interestingly, $p53^{\Delta 5\text{-}6/\Delta 5\text{-}6}$; $Rictor^{\Delta/\Delta}$ mice with these non-brain-tumor problems lived significantly longer than both $p53^{\Delta 5\text{-}6/\Delta 5\text{-}6}$ and $p53^{\Delta 5\text{-}6/\Delta 5\text{-}6}$; $Rictor^{+/\Delta}$ mice (Figure 4C), implying that *Rictor* deficiency reduces the overall brain tumor formation even when mice are aged. More interestingly, though there was no significant survival difference between $p53^{\Delta 5\text{-}6/\Delta 5\text{-}6}$ (n = 38) and $p53^{\Delta 5\text{-}6/\Delta 5\text{-}6}$; $Rictor^{+/\Delta}$ (n = 72) mice with brain tumors, $p53^{\Delta 5\text{-}6/\Delta 5\text{-}6}$; $Rictor^{\Delta/\Delta}$ (n = 52) mice with brain tumors lived significantly longer than both $p53^{\Delta 5\text{-}6/\Delta 5\text{-}6}$ and $p53^{\Delta 5\text{-}6/\Delta 5\text{-}6}$; $Rictor^{+/\Delta}$ mice (median = 254 days, 268 days, 308 days; respectively) (Figure 4D). Furthermore, $p53^{\Delta 5\text{-}6/\Delta 5\text{-}6}$ and $p53^{\Delta 5\text{-}6/\Delta 5\text{-}6}$; $Rictor^{+/\Delta}$ mice were characterized by brain tumors positioned predominantly in the forebrain (i.e. supratentorial or prosencephalon) while $p53^{\Delta 5\text{-}6/\Delta 5\text{-}6}$; $Rictor^{\Delta/\Delta}$ mice had a lower incidence of this type of tumor (forebrain tumor incidence: 84%, 72% and 46%, respectively) (Figure 4E). On the other hand, tumor formation in the hindbrain (i.e. infratentorial or rhombencephalon), especially in the cerebellum, was significantly increased in $p53^{\Delta 5\text{-}6/\Delta 5\text{-}6}$; $Rictor^{\Delta/\Delta}$ mice compared to $p53^{\Delta 5\text{-}6/\Delta 5\text{-}6}$ and $p53^{\Delta 5\text{-}6/\Delta 5\text{-}6}$; $Rictor^{+/\Delta}$ (hindbrain tumor incidence: 16%, 28%, 54%) (Figure 4E). These results suggest that *Rictor* loss extends the survival of the mice with brain tumors, and shifts the tumor location from forebrain to hindbrain.

2.2.4 *p53*-mutant GEM gliomas are inhibited and/or delayed by Rictor/mTORC2 loss

After characterizing these mouse models based on their brain tumor location, I further examined the tumors based on their pathology on the basis of WHO (World Health

Organization) criteria with the help of Sandra Dr. Camelo-Piragua, a neuropathologist at the University of Michigan Medical School (Louis et al., 2007). Consistent with previous studies, the majority of the forebrain tumors and some of the hindbrain tumors in all models were high-grade gliomas characterized by a significant number of mitotic figures, necrotic tissue, pleomorphic nuclei, multi-nucleated giant tumor cells, abnormal mitoses, neuronal satellitosis and microvascularization (Figure 5A). These tumor cells were also immunoreactive to GFAP and Olig2, as observed in human glioblastomas (Figures 5B and 5C) (Furnari et al., 2007). Notably, Olig2 expression was observed in all GEM gliomas, making it a reliable glioma marker, while Pax6 was virtually absent (Figures 5B, 5C, 9D and 9E). Furthermore, many tumor cells expressed mutant-p53 protein (Figures 5B, and 5C), as previously reported (Wang et al., 2009) - a phenomenon also observed in many other human tumors (Brosh and Rotter, 2009). When quantified, I did not observe a significant difference between $p53^{\Delta 5\text{-}6}$ and $p53^{\Delta 5\text{-}6/\Delta 5\text{-}6}$; $Rictor^{+/\Delta}$ mice in terms of glioma penetrance as both models predominantly formed high-grade gliomas and rarely MBs (Figure 5D). However, overall glioma formation in $p53^{\Delta 5\text{-}6/\Delta 5\text{-}6}$; $Rictor^{\Delta/\Delta}$ mice (49%) reduced significantly compared to $p53^{\Delta 5\text{-}6/\Delta 5\text{-}6}$ (95%) and $p53^{\Delta 5\text{-}6/\Delta 5\text{-}6}$; $Rictor^{+/\Delta}$ (81%) mice (Figure 5D). Even more strikingly, glioma bearing $p53^{\Delta 5\text{-}6/\Delta 5\text{-}6}$; $Rictor^{\Delta/\Delta}$ mice lived significantly longer than their counterparts in both $p53^{\Delta 5\text{-}6/\Delta 5\text{-}6}$ and $p53^{\Delta 5\text{-}6/\Delta 5\text{-}6}$; $Rictor^{+/\Delta}$ with an up to 48% increase in life span (median = 380 days, 257 days and 284 days, respectively) (Figure 5E). These results suggest that mutant-*p53* mediated glioma formation is inhibited and/or delayed by *Rictor* loss and *Rictor*-deficiency provides a survival advantage to glioma-bearing mice.

2.2.5 *Rictor* deficiency impairs mTORC2 and mTORC1 signaling in mutant-*p53* GEM gliomas accompanied by a reduction in tumor cell proliferation

The reduction in glioma penetrance and increase in the overall survival of glioma bearing mice upon *Rictor* deficiency raised the question of how *Rictor* deletion alone can lead to such significant tumor suppression. I first confirmed that end-stage tumors came from the recombined cells that had undergone cre-mediated recombination by examining the

floxed, wild type, and deleted alleles of *p53*, *Rictor*, and *cre* genes (Figure 6A). In order to identify the molecular consequences of *Rictor*-deficiency, I analyzed the key components of the mTORC2 pathway. As expected, all of the $p53^{\Delta 5\text{-}6/\Delta 5\text{-}6}$; $Rictor^{\Delta/\Delta}$ mice had very low levels of $pAkt^{S473}$ compared to $p53^{\Delta 5\text{-}6/\Delta 5\text{-}6}$ and $p53^{\Delta 5\text{-}6/\Delta 5\text{-}6}$; $Rictor^{+/\Delta}$ gliomas, which were characterized by very high levels of $pAkt^{S473}$ (Figure 6B), consistent with human glioblastoma samples (Altomare and Testa, 2005; Wang et al., 2004). Surprisingly, $pAkt^{T308}$ was also very low in *Rictor*-deficient gliomas even though this site is phosphorylated by PDK1 (Figure 6B), consistent with previous studies suggesting that AKT/Akt phosphorylation at Ser^{473} is required for phosphorylation at Thr^{308} (Guertin et al., 2009; Scheid et al., 2002). Another downstream target of mTORC2, Ndrg1, also showed reduced phosphorylation in many $p53^{\Delta 5\text{-}6/\Delta 5\text{-}6}$; $Rictor^{\Delta/\Delta}$ gliomas even though this reduction was not as robust as pAkt (Figure 6B). Consistent with our copy number analyses, Pten expression was reduced in gliomas of all three models including $p53^{\Delta 5\text{-}6/\Delta 5\text{-}6}$; $Rictor^{\Delta/\Delta}$ tumors, which lack $pAkt^{S473}$ and $pAkt^{T308}$ (Figures 6B and 2E). We did not observe any difference between the mouse models in terms of pErk1/2, and pGSK3-β and c-Myc levels, which served as readouts for MAPK and Wnt signaling pathways (Figure 6C). These findings suggest that *Rictor* is required for an intact mTORC2 activity, including the phosphorylation of Akt, and impediment of the mTORC2 signaling may cause reduction in glioma formation and/or progression.

Since active Akt positively regulates mTORC1 signaling (Laplante and Sabatini, 2009), I determined whether loss of pAkt in *Rictor*-deficient gliomas had an impact on mTORC1 activity. TSC2 forms a dimer with TSC1 and upon dimerization, the TSC1/TSC2 complex functions as a GTPase-activating protein that inactivates mTORC1 by hydrolyzing Rheb-GTP. Active Akt, on the other hand, releases this inhibition by directly phosphorylating TSC2 and preventing the dimerization (Inoki et al., 2002; Potter et al., 2002). I first analyzed the two components of the mTORC1 pathway, S6K and 4E-BP1, which are phosphorylated by mTORC1 itself (Figure 6D) (Inoki et al., 2002). Our results showed that only 1/8 of the $p53^{\Delta 5\text{-}6/\Delta 5\text{-}6}$; $Rictor^{\Delta/\Delta}$ gliomas had $pS6K^{T389}$ while 4/4 of the $p53^{\Delta 5\text{-}6/\Delta 5\text{-}6}$ and 6/8 of the $p53^{\Delta 5\text{-}6/\Delta 5\text{-}6}$; $Rictor^{+/\Delta}$ gliomas had prominent levels of $pS6K^{T389}$

(Figure 6D). Similarly, p4E-BP1$^{T37/46}$ was detected in only half of the *p53*$^{\Delta5\text{-}6/\Delta5\text{-}6}$; *Rictor*$^{+/\Delta}$ and *p53*$^{\Delta5\text{-}6/\Delta5\text{-}6}$; *Rictor*$^{\Delta/\Delta}$ gliomas whereas all of the *p53*$^{\Delta5\text{-}6/\Delta5\text{-}6}$ gliomas were positive for this molecule (Figure 6D). I then examined pTSC2^{T1462} levels in order to determine whether the reduction in mTORC1 activity was mediated by TSC1/TSC2 complex (Figure 6D). The reduced levels of pTSC2^{T1462} in *p53*$^{\Delta5\text{-}6/\Delta5\text{-}6}$; *Rictor*$^{\Delta/\Delta}$ gliomas indicated that *Rictor* loss could modulate mTORC1 activity by releasing the inhibition on TSC1/TSC2 complex, which is otherwise phosphorylated and inhibited by the active Akt. These results suggest that removal of *Rictor* can inhibit glioma initiation and/or progression by impairing mTORC2 and mTORC1 activity, which are the two important signaling pathways in malignant gliomas.

Lastly, I examined the proliferation rate of the end-stage GEM gliomas by quantifying the Ki-67^{+} tumor cells. Interestingly, *Rictor*-deficient gliomas had significantly lower Ki-67^{+} tumor cell percentage compared to both *p53*$^{\Delta5\text{-}6/\Delta5\text{-}6}$ and *p53*$^{\Delta5\text{-}6/\Delta5\text{-}6}$; *Rictor*$^{+/\Delta}$ gliomas (Figures 6E and 6F). I did not detect a significant difference between *p53*$^{\Delta5\text{-}6}$ vs *p53*$^{\Delta5\text{-}6/\Delta5\text{-}6}$; *Rictor*$^{+/\Delta}$ gliomas consistent with their comparable glioma incidence and survival rate (Figures 6E and 6F). These results indicate that *Rictor* deficiency can reduce the tumor cell proliferation, which may explain the 48% life span increase in the glioma bearing *p53*$^{\Delta5\text{-}6/\Delta5\text{-}6}$; *Rictor*$^{\Delta/\Delta}$ mice.

2.2.6 Expansion of the plausible early glioma-forming cells are inhibited by *Rictor* loss

Our previous studies have showed that mutant-*p53* expressing (p53^{+}, thereafter) precursor-like cells were easily detectable in the vicinity of the subventricular zone (SVZ) around 4-7 months of age and were suggested as the early tumor forming cells (Wang et al., 2009). These p53^{+} glioma precursor cells typically form clusters with high levels of proliferation in the vicinity of the SVZ areas such as the corpus callosum (CC), (RMS), cerebral cortex (Ctx), hippocampus, and olfactory bulb (OB) (Wang et al., 2009). Given this finding, I aimed to determine whether and how the early tumor forming cells

are affected by the *Rictor* loss. I examined the $p53^{+}$ cells residing in two main locations: inside the germinal zone defined by the cells in the SVZ and rostral migratory stream (RMS) and outside the germinal zone, which are all of the remaining $p53^{+}$ cells scattered throughout the brain. $p53^{\Delta 5\text{-}6/\Delta 5\text{-}6}$; $Rictor^{+/\Delta}$ mice were excluded from this investigation since end-stage tumor analyses demonstrated a very similar phenotype between $p53^{\Delta 5\text{-}6}$ and $p53^{\Delta 5\text{-}6/\Delta 5\text{-}6}$; $Rictor^{+/\Delta}$ mice. Consistent with the previous studies (Wang et al., 2009), I detected an expansion of the $p53^{+}Olig2^{+}$ cells outside the germinal zone in 5/9 of the $p53^{\Delta 5\text{-}6/\Delta 5\text{-}6}$ mice (Figures 7B-7D). These tumor incipient cells were found in various places of the brain, including the corpus callosum, hippocampus, olfactory bulb, striatum, and the vicinity of the anterior RMS (Figure 7A). Interestingly, only 1/9 of the $p53^{\Delta 5\text{-}6/\Delta 5\text{-}6}$; $Rictor^{\Delta/\Delta}$ mice had a similar expansion outside of the germinal zone, while most of the mice had $p53^{+}$ cells restricted in the SVZ/RMS region (Figures 7C and 7D). Furthermore, the proliferation of the $p53^{+}$ cells was also different between these two models: while the average proliferation rate of the scattered $p53^{+}$ cells in $p53^{\Delta 5\text{-}6/\Delta 5\text{-}6}$ was about 30-35%, the same ratio was only 10% in $p53^{\Delta 5\text{-}6/\Delta 5\text{-}6}$; $Rictor^{\Delta/\Delta}$ brain (Figure 7E). On the other hand, the number and the proliferation of the $p53^{+}$ cells within the germinal zone (i.e. SVZ/RMS) were comparable between $p53^{\Delta 5\text{-}6/\Delta 5\text{-}6}$ and $p53^{\Delta 5\text{-}6/\Delta 5\text{-}6}$; $Rictor^{\Delta/\Delta}$ mice (Figure 7F). These results suggest that even though the generation of tumor forming cells within the germinal zone is almost identical between $p53^{\Delta 5\text{-}6/\Delta 5\text{-}6}$ and $p53^{\Delta 5\text{-}6/\Delta 5\text{-}6}$; $Rictor^{\Delta/\Delta}$ mice, their expansion and cluster formation outside the germinal zone requires functional Rictor/mTORC2 and, more specifically, an intact Akt pathway, underlining one of the mechanisms by which *Rictor* deficiency reduced gliomagenesis.

2.2.7 *Rictor* loss has minimal effects in the developing Subventricular zone

Since the expanding $p53^{+}$ population in $p53^{\Delta 5\text{-}6/\Delta 5\text{-}6}$ brains reduced dramatically upon *Rictor* loss, I assessed whether the *Rictor*-deficient developing brain, especially in SVZ, had any abnormality in overall structure or major cell populations. In these analyses, I used an additional mouse model - $hGFAP^{Cre}$; $p53^{flox/+}$; $Rictor^{flox/flox}$ ($Rictor^{\Delta/\Delta}$, hereafter) - to better understand the mutant-*Rictor* phenotype in the absence of complete *p53*-loss.

Based on our previous studies and experience, hGFAP^{Cre} ; *p53*$^{flox/+}$ mice do not have any noticeable abnormalities and they do not form tumors (data not shown), thus the *Rictor*$^{\Delta/\Delta}$ phenotype can be attributed only to *Rictor* deficiency. I compared *Rictor*$^{\Delta/\Delta}$ and *p53*$^{\Delta5\text{-}6/\Delta5\text{-}6}$; *Rictor*$^{\Delta/\Delta}$ mice to wild-type controls and noted that both *Rictor*-deficient brains were significantly smaller and weighed less than controls in various stages of the lifespan including P8, P16, P22, and 4-months even though the body weights were very similar (Figures 8A-8C). Furthermore, the total number of proliferating Ki-67^{+} cells in the SVZ was comparable between P16 controls and mutants even though there was a slight but statistically significant reduction in the Ki-67^{+}/DAPI^{+} percentage within the mutant SVZ population, especially *p53*$^{\Delta5\text{-}6/\Delta5\text{-}6}$; *Rictor*$^{\Delta/\Delta}$ (Figures 8D-8F). Similarly, the number of the stem cells in the P16 SVZ labeled by GFAP and Nestin did not change significantly between controls and *Rictor* mutants (Figures 8G-8I). I, thus, concluded that *Rictor* loss does not have a dramatic effect on the overall structure of the neonatal brain and the developing SVZ in relation to the tumorigenesis, consistent with a recent study showing that *Rictor* deletion has only modest effects on hematopoietic stem cell frequency and function (Magee et al., 2012). As the glioma cells are more fragile to the loss of Rictor/mTORC2 signaling pathway, these findings are inline with a phenomenon called "oncogene addiction", which describes a dependence of cancer cells on a single oncogenic pathway for malignancy, proliferation and/or survival, while the normal cells rely on multiple redundant signals and/or molecules (Sharma and Settleman, 2007).

2.3 Discussion

Herein, we demonstrated that mutant-*p53* driven high-grade gliomas recapitulate the key genomic alterations of human glioblastomas, and that genetic deletion of *Rictor* has significant tumor suppressive activity in these tumors. More specifically, our data suggest that *Rictor* loss reduces gliomagenesis approximately by half, as well as provides a substantial survival advantage to the remaining mice with high-grade gliomas. Despite of this anti-glioma activity, formation of gliomas in a subset of *Rictor*-deficient mice

accentuates the essential need to reveal the major oncogenic signals in Rictor/mTORC2-independent gliomagenesis.

2.3.1 *p53*-mutant GEM gliomas undergo genomic alterations described in human glioblastomas

Mouse models provide a unique platform to delineate the complexity of glioblastoma formation and perform preclinical studies by designing and applying novel therapies. There are, though, some aspects of the disease that have not been well recapitulated in genetically engineered models, including its intratumoral cellular and molecular heterogeneity (Huse et al., 2013). The introduction of specific genetic modifications into these models has the potential to direct tumor cells to acquire only selected oncogenic features, rather than representing this diversity. Thus, generating models that allow the tumor forming cells to gain sporadic molecular alterations that are heterogenic and - more importantly - comparable to human counterparts is essential to achieve both scientific and clinical goals. We have, both here and previously, shown that *p53* deficiency alone gives rise to highly anaplastic cells that are capable of accumulating various oncogenic features leading to malignant glioma formation (Wang et al., 2009). Our current study, additionally, demonstrates that GEM gliomas carry key genomic alterations frequently seen in human glioblastomas. In particular, co-deletion of genomic loci in mouse chr7 and chr19 corresponding to human chr10q suggested that, in addition to having similar gene expression profiles, mouse tumors recapitulate human glioblastomas at the genomic level. Several studies have proposed that deletion of multiple tumor suppressor genes located in chr10q, including *DMBT1*, *WDR11*, *and LGI1*, was involved in glioma initiation and/or progression. (Chernova et al., 2001; Ichimura et al., 1998). Homozygous deletion of *DMBT1*, especially, was associated with unfavorable clinical outcomes (Motomura et al., 2012). Thus, the independent but simultaneous deletion of *Pten* (chr19) and *Dmbt1* (chr7) in our GEM gliomas was in line with this hypothesis, and suggested an additive oncogenic effect for the loss of at least two tumor suppressor genes located in human chr10q. However, the absence of such chromosomal deletions, especially deletion

of chr7, in mouse models that are prepared by genetic deletion of *Pten* suggests that the major target of chr19 (chr10q in humans) loss in high-grade gliomas is *Pten/PTEN* gene. This observation also implies that additional mutations introduced to mouse models might eliminate the necessity to undergo critical genomic alterations observed during the natural progression of human glioblastomas. In addition to deletion, we detected significant amplification in a different locus of mouse chr7 that corresponds to human chr19. Interestingly, this region found to be amplified in human glioblastomas as well, and contained several cancer-associated genes, including *AKT2*, *MAP3K10*, *PLD3*, and *MAP4K1*.

2.3.2 Rictor/mTORC2 is important for both the initiation and progression of mutant-*p53* GEM gliomas

Many human cancers manifest themselves with multiple genomic, epigenetic and chromosomal alterations accumulating in a complex sequence of events. Consequently, regulation of numerous genes and networks is disrupted, mostly leading to more malignant tumors. It is, therefore, remarkable that reversal of only one or a couple altered signaling pathways, which promote tumor initiation and growth, can lead to such dramatic benefits in terms of controlling the tumor progression, if not totally eliminating it (Weinstein and Joe, 2006). Various experimental systems and successful clinical investigations, including *chronic myelogenous leukemia*, melanoma, and non-small-cell lung cancer (Huse et al., 2013) provided profound evidences for identifying the "Achilles' heel" of the tumor cells to attack the diseases efficiently (Weinstein, 2002). These studies described this phenomenon as 'oncogene addiction', which explains the dependence of cancer cells on a single oncogenic pathway for their malignancy, proliferation and/or survival (Sharma and Settleman, 2007; Weinstein, 2002). Accordingly, our study here indicated that Rictor/mTORC2 is a critical molecule for high-grade gliomas as its absence significantly reduces glioma penetrance as well as extends the survival of glioma-bearing mice. Our early stage analyses suggested that functional loss of *Rictor* does not affect the formation of the tumor incipient cells within

the germinal zone but rather blocks the spreading of these cells to surrounding areas. Since cellular expansion is a central event for tumor growth, this finding implies that intact *Rictor*, and by extension PI3K/Akt signaling, is essential for glioma initiation. Consistently, it has been shown that *PTEN* loss and *EGFR* amplification are two driver events in human glioblastomas (Brennan et al., 2013; Ozawa et al., 2014). Furthermore, we found that *Rictor*-deficient end-stage GEM gliomas had a lower proliferation percentage compared to *Rictor* wild type or heterozygous models, suggesting that Rictor/mTORC2 provides a growth advantage to glioma cells in addition to its impact on early tumorigenesis. We, therefore, strongly advocate that combinatory treatment plans involving Rictor/mTORC2 inhibition will benefit patients during both the early and late stages of glioblastomas (Figure 22). However, the fact that a group of *Rictor*-deficient mice still form mutant-*p53* driven gliomas, Rictor/mTORC2 signaling is not absolutely required for every glioma case (see next section).

2.3.3 Rictor/mTORC2-independent gliomagenesis underscores the necessity of additional molecular stratification of Glioblastomas

Targeted therapies that include novel agents have made only a small impact on the clinical outcome of glioblastoma patients. For instance, PI3K/AKT pathway inhibitors, including monotherapies and combinatory strategies with other agents and/or radiation, produced mostly inconsistent and short-lived responses (Wen et al., 2012). This could be partly because of an imperfection in patient selection. Consequently, many glioblastoma patients succumb from recurring tumors that acquire resistance to current therapies, a phenomenon that has not been well recapitulated and established in mouse models (Hambardzumyan et al., 2011). Our study here showed that while *Rictor* deficiency reduced mutant-*p53* driven glioma penetrance by half, the remaining mice still maintained the deadly tumor, in spite of a 50% increase in their overall survival. This finding implies the presence of *Rictor*-deficient early transforming cells or malignant tumor cells that are capable of escaping from “an oncogene addiction” (Sharma and Settleman, 2007). More specifically, although Rictor/mTORC2/Akt signaling exerts an

essential role in the development of high-grade gliomas, it is not absolutely required for every tumor case. It is, therefore, critical to identify the prominent oncogenic pathways in *Rictor*-deficient gliomas, and determine whether these tumors correspond to a novel molecular subgroup within human glioblastomas. Subsequent classification of human tumors based on their plausible response to the inhibition of Rictor/mTORC2 pathway will not only increase the potential of novel Rictor/mTORC2 inhibitors, but also improve the success rate of the existing treatment plans utilizing PI3K/AKT inhibitors.

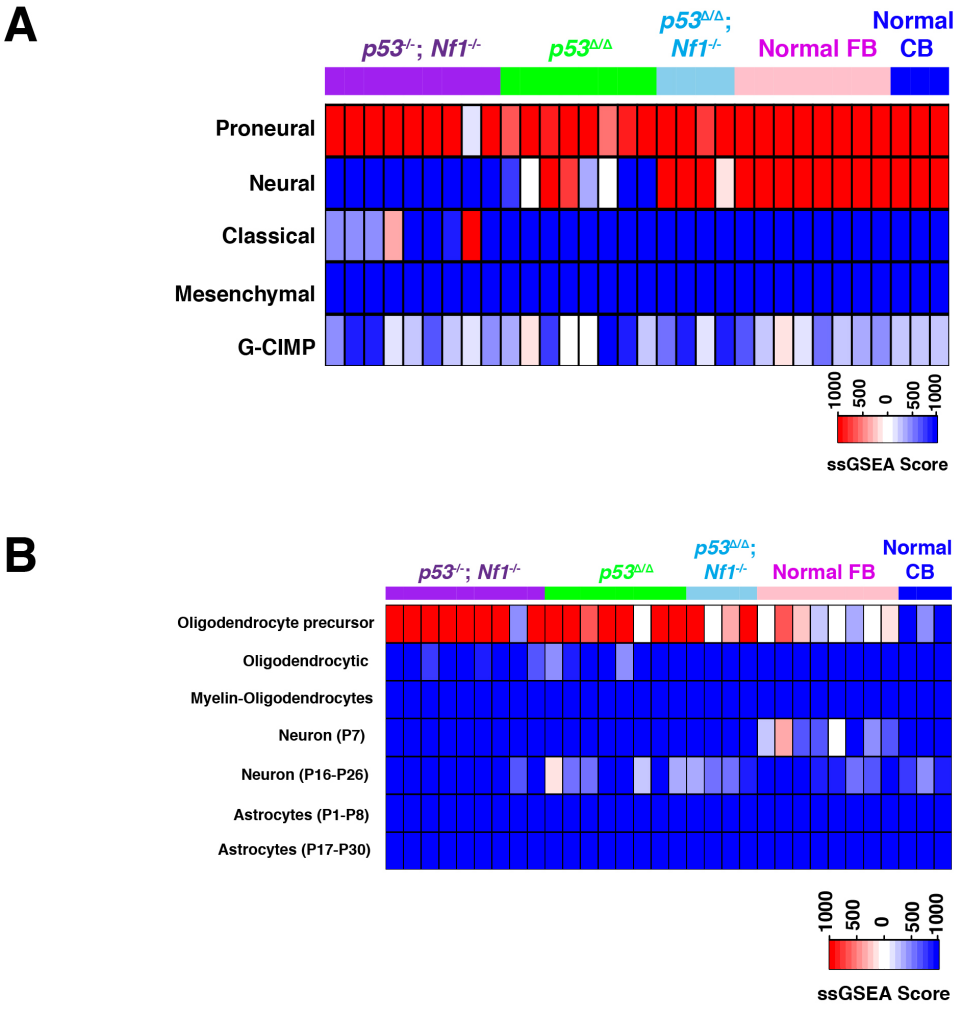
A
p53-/-; Nf1-/-
p53Δ/Δ
p53Δ/Δ; Nf1-/-
Normal FB
Normal CB
Proneural
Neural
Classical
Mesenchymal
G-CIMP
1000
500
0
500
1000
ssGSEA Score
B
p53-/-; Nf1-/-
p53Δ/Δ
p53Δ/Δ; Nf1-/-
Normal FB
Normal CB
Oligodendrocyte precursor
Oligodendrocytic
Myelin-Oligodendrocytes
Neuron (P7)
Neuron (P16-P26)
Astrocytes (P1-P8)
Astrocytes (P17-P30)
1000
500
0
500
1000
ssGSEA Score
C
Ascl1
Olig2
Nestin
Expression levels
p53-/-; Nf1-/-
Normal
p53Δ/Δ
p53Δ/Δ; Nf1-/-

Figure 1. High-grade gliomas induced by mutant-*p53* (with or without *Nf1* mutations) resemble proneural subgroup of human glioblastomas.

(A) Subgroup analysis of genetically engineered mouse (GEM) gliomas based on gene expression profiles. Each tumor is compared to Proneural, Neural, Classical and Mesenchymal subgroups of human glioblastomas. High similarity is indicated by red, low similarity is indicated by blue. G-CIMP signature is also analyzed. Note that none of the GEM gliomas are found to be G-CIMP^{+}.

(B) Gene expression profile of GEM gliomas in comparison with different cell populations. High ssGSEA Score (red) indicates strong resemblance; low scores (blue) indicate difference. The expression profile of GEM gliomas resemble to that of oligodendrocyte precursors.

(C) Detailed analyses of the expression levels of *Ascl1*, *Olig2* and *Nestin* genes in GEM gliomas in comparison to normal brain tissue.

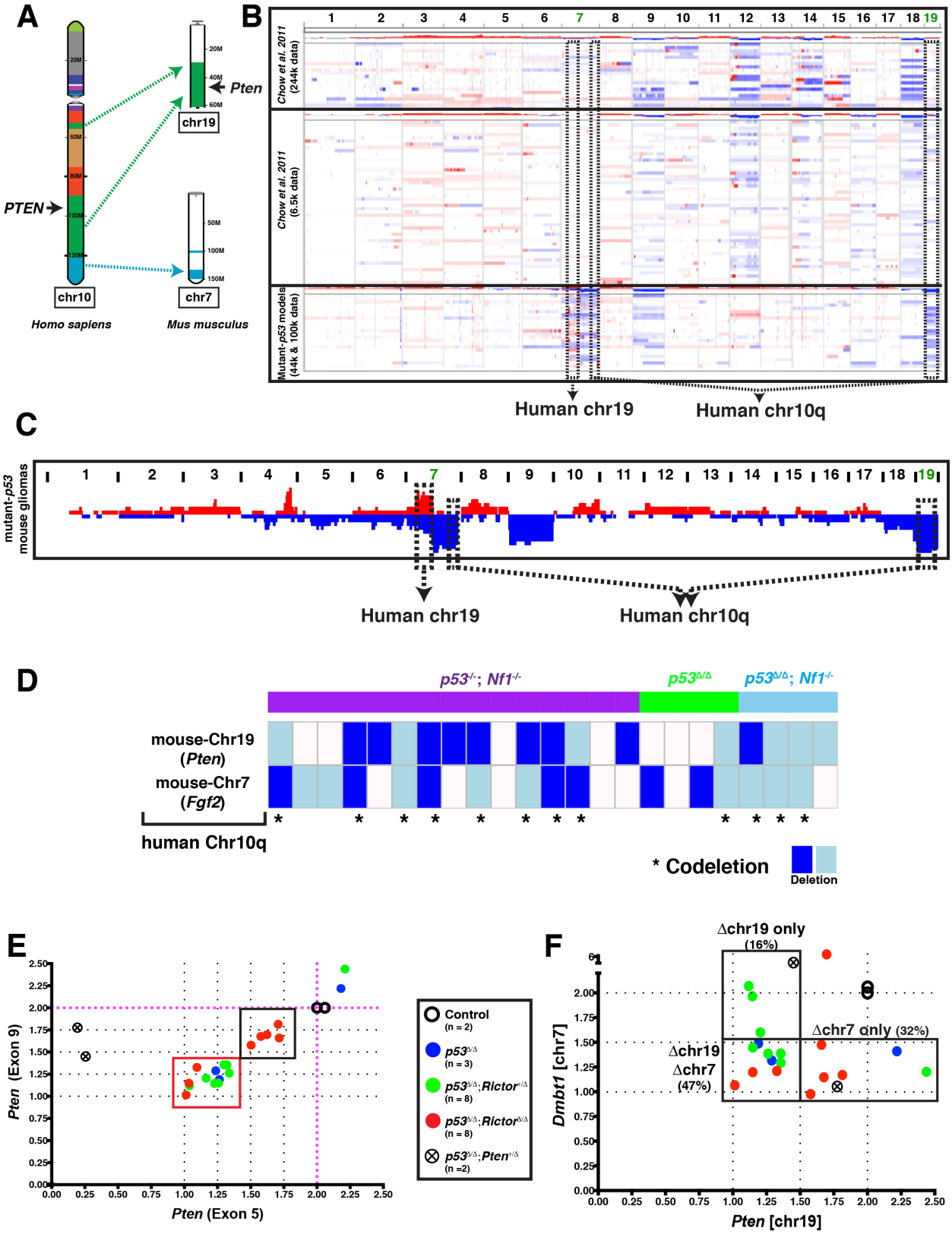
A
PTEN
Pten
chr10
chr19
chr7
Homo sapiens
Mus musculus
B
Chow et al. 2011 (244k data)
Chow et al. 2011 (6.5k data)
Mutant-p53 models (44k & 100k data)
Human chr19
Human chr10q
C
mutant-p53 mouse gliomas
Human chr19
Human chr10q
D
p53-/-; Nf1-/-
p53Δ/Δ
p53Δ/Δ; Nf1-/-
mouse-Chr19 (Pten)
mouse-Chr7 (Fgf2)
human Chr10q
* Codeletion
Deletion
E
Pten (Exon 9)
Pten (Exon 5)
Control (n = 2)
p53Δ/Δ (n = 3)
p53Δ/Δ;Rictor+/Δ (n = 8)
p53Δ/Δ;Rictor Δ/Δ (n = 8)
p53Δ/Δ;Pten+/Δ (n =2)
F
Δchr19 only (16%)
Δchr7 only (32%)
Δchr19 Δchr7 (47%)
Dmbt1 [chr7]
Pten [chr19]

Figure 2. Mutant-*p53* mediated GEM gliomas share key genomic alterations with human glioblastomas.

(A) Synteny map illustrating the equivalents of human (*Homo sapiens*) chr10q in mouse (*Mus musculus*) chr19 and chr7. The location of the *PTEN*/*Pten* gene is indicated in both human and mouse chromosomes.
(B) Heatmap representation of the copy number changes (blue for deletion, red for amplification) across the entire genome of the GEM gliomas. Upper two segments include the samples from a previous study (Chow *et. al*, 2011) that used conditional inactivation of *p53* and *Pten* with or without *Rb* genes. Lower segment includes our samples from 23 GEM gliomas carrying mutant-*p53* with or without mutant-*Nf1* alleles. Mouse chromosomes (chr19 and chr7) corresponding to human chr10q and chr19 are indicated.
(C) Genome plot displaying the frequencies of the copy number gains (red) and copy number losses (blue) in the genome of 23 GEM gliomas carrying mutant-*p53* with or without mutant-*Nf1* alleles. Two loci in mouse chromosomes (i.e. chr19 and chr7) corresponding to human chr10q and chr19 are boxed.
(D) Deletion analysis of *Pten* (chr19) and *Fgf2* (chr7) genes in GEM gliomas carrying mutant-*p53* with or without mutant-*Nf1* alleles. Light blue implicates heterozygous deletions while dark blue indicates homozygous deletions. Co-deletions of *Pten* and *Fgf2* genes are pointed with asterisks.
(E) Copy number estimates of the *Pten* gene in GEM gliomas based on readings on exon-5 and exon-9.
(F) Copy number estimates of *Dmbt1* (chr7) gene in comparison with *Pten* (chr19) gene in GEM gliomas.
Estimates were calculated by RT-PCR using the genomic DNA as template and the readings were normalized to *β-Actin* (mouse chr5), which served as an internal reference gene for each sample. The average of readings from wild-type controls was set to "2" and all of the samples were calculated accordingly.

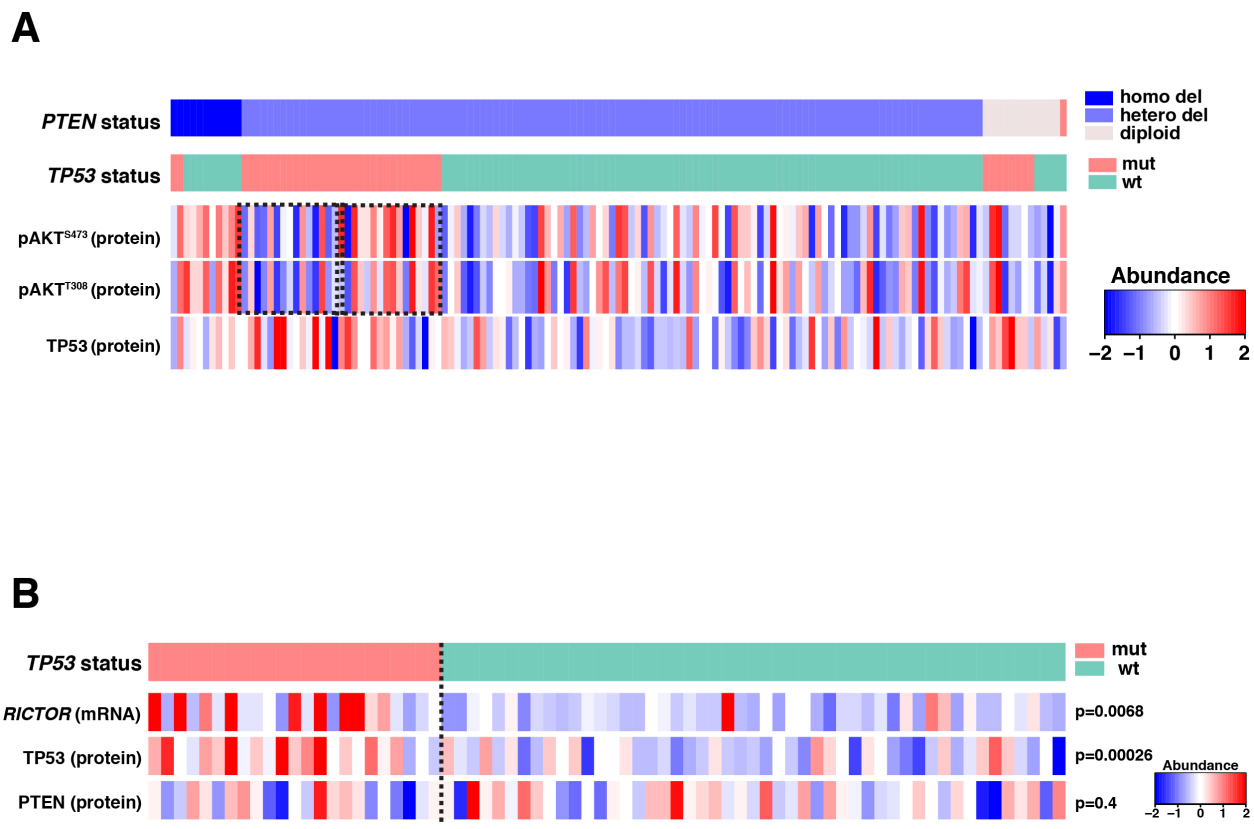

Figure 3. RICTOR expression and AKT signaling across the human glioblastoma samples.

(A) Protein level analyses of pAKT^{S473}, pAKT^{T308} and TP53 in relation to *PTEN* and *TP53* status in human glioblastoma samples. The level of protein abundance is represented with a color scale as depicted. *PTEN* deletions or *TP53* mutations are colored as indicated.

(B) The expression levels of *RICTOR* (mRNA), TP53 (protein) and PTEN (protein) among the human glioblastoma samples with or without *TP53* mutation. The level of abundance is represented with a color scale as depicted.

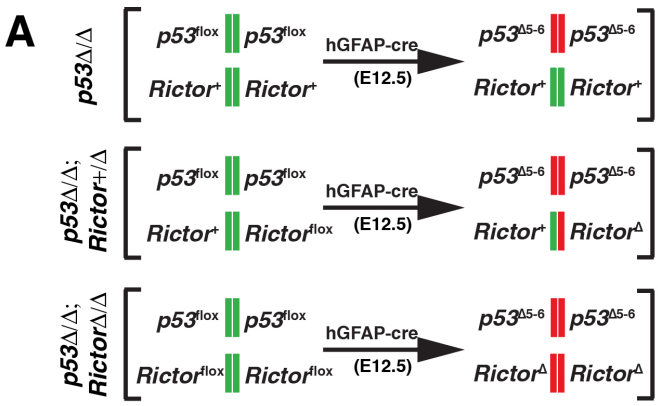
A
p53Δ/Δ
p53flox p53flox
Rictor+ Rictor+
hGFAP-cre
(E12.5)
p53Δ5-6 p53Δ5-6
Rictor+ Rictor+
p53Δ/Δ; Rictor+/Δ
p53flox p53flox
Rictor+ Rictorflox
hGFAP-cre
(E12.5)
p53Δ5-6 p53Δ5-6
Rictor+ RictorΔ
p53Δ/Δ; RictorΔ/Δ
p53flox p53flox
Rictorflox Rictorflox
hGFAP-cre
(E12.5)
p53Δ5-6 p53Δ5-6
RictorΔ RictorΔ

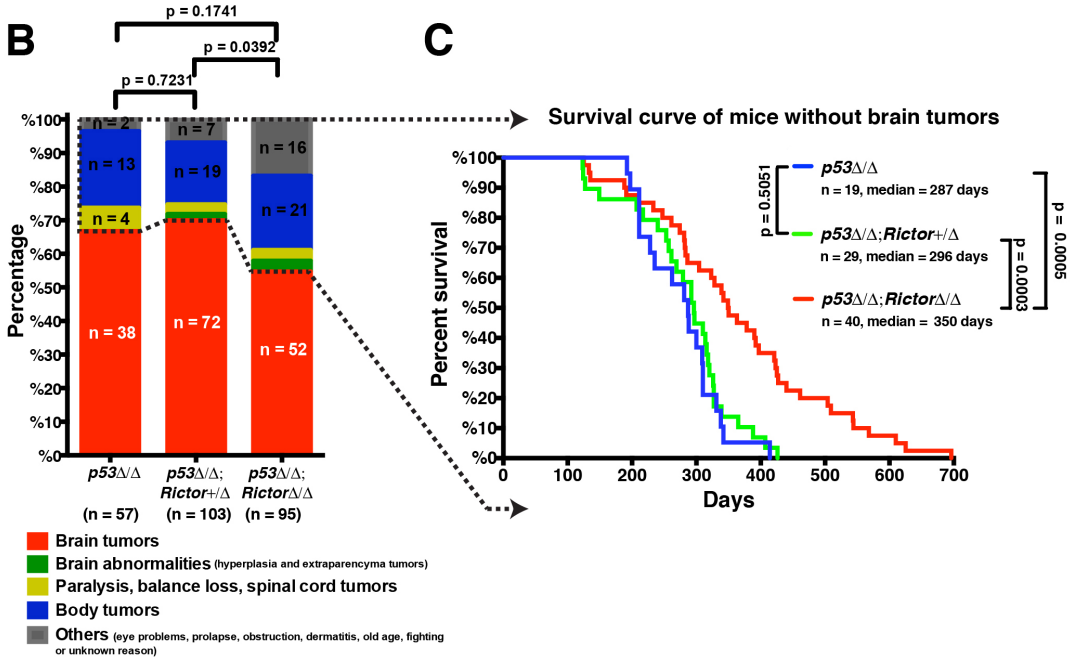
B
p = 0.1741
p = 0.0392
p = 0.7231
Percentage
n = 2
n = 13
n = 4
n = 38
n = 7
n = 19
n = 72
n = 16
n = 21
n = 52
p53Δ/Δ (n = 57)
p53Δ/Δ; Rictor+/Δ (n = 103)
p53Δ/Δ; RictorΔ/Δ (n = 95)
Brain tumors
Brain abnormalities (hyperplasia and extraparencyma tumors)
Paralysis, balance loss, spinal cord tumors
Body tumors
Others (eye problems, prolapse, obstruction, dermatitis, old age, fighting or unknown reason)
C
Survival curve of mice without brain tumors
Percent survival
Days
p = 0.5051
p53Δ/Δ
n = 19, median = 287 days
p53Δ/Δ;Rictor+/Δ
n = 29, median = 296 days
p = 0.0003
p53Δ/Δ;RictorΔ/Δ
n = 40, median = 350 days
p = 0.0005

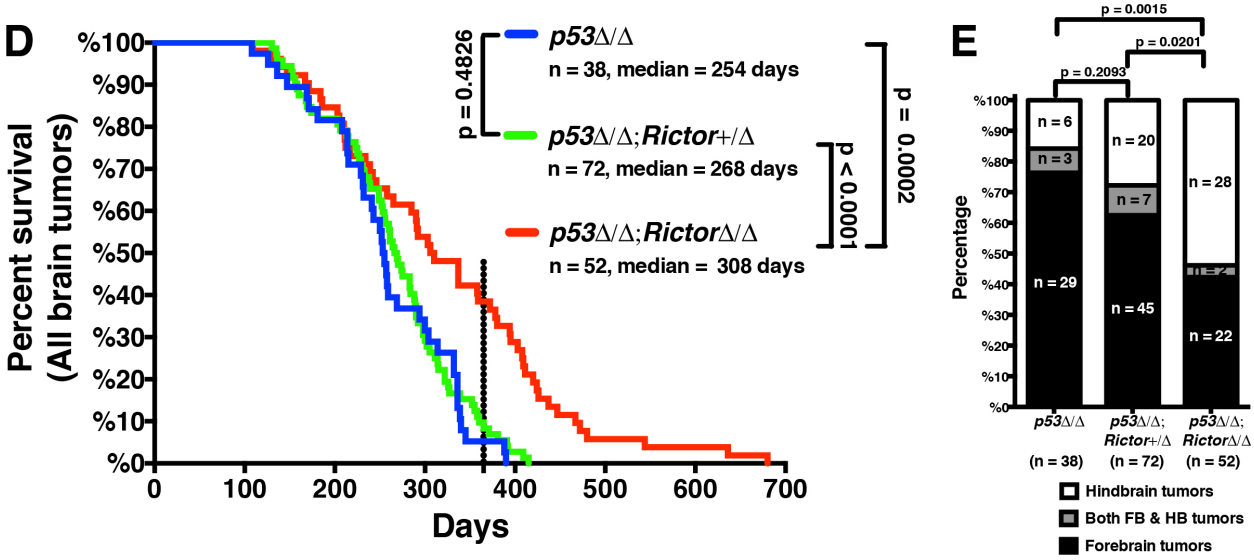
D
Percent survival (All brain tumors)
Days
p = 0.4826
p53Δ/Δ
n = 38, median = 254 days
p53Δ/Δ;Rictor+/Δ
n = 72, median = 268 days
p < 0.0001
p53Δ/Δ;RictorΔ/Δ
n = 52, median = 308 days
p = 0.0002
E
p = 0.0015
p = 0.0201
p = 0.2093
Percentage
n = 6
n = 3
n = 29
n = 20
n = 7
n = 45
n = 28
n = 22
p53Δ/Δ (n = 38)
p53Δ/Δ; Rictor+/Δ (n = 72)
p53Δ/Δ; RictorΔ/Δ (n = 52)
Hindbrain tumors
Both FB & HB tumors
Forebrain tumors

Figure 4. Mutant-*p53* mediated GEM brain tumors display distinct brain locations based on *Rictor* status.

(A) Schematic representation of the genetic configurations in $p53^{\Delta 5\text{-}6/\Delta 5\text{-}6}$, $p53^{\Delta 5\text{-}6/\Delta 5\text{-}6}$; $Rictor^{+/\Delta}$, and $p53^{\Delta 5\text{-}6/\Delta 5\text{-}6}$; $Rictor^{\Delta/\Delta}$ mice. Floxed genes undergo hGFAP-cre-mediated recombination at around E12.5, therefore the mice are named after the genotype of the recombined cells.

(B) Phenotypic classification of the entire cohort of mice used in this study. The mice that represented brain tumors at the time of euthanasia are shown in red bars. Other bars show the phenotypes of the mice that did not generate brain tumors. These mice without brain tumors represented other health-concerning reasons, including large and/or ulcerated soft tissue sarcomas, dermatitis, eye problems, prolapse, GI tract obstruction, old age, fighting and poor health conditions.

(C) Kaplan-Meier survival curves of all the mice used in this study including the ones with or without brain tumors. Brain tumor cases are entered as uncensored events (i.e. "1") while others are entered as censored events (i.e. "0"). The Mantel-Cox (Log-rank) test was used to compare the curves statistically.

(D) Kaplan-Meier survival curves of the in $p53^{\Delta 5\text{-}6/\Delta 5\text{-}6}$, $p53^{\Delta 5\text{-}6/\Delta 5\text{-}6}$; $Rictor^{+/\Delta}$, and $p53^{\Delta 5\text{-}6/\Delta 5\text{-}6}$; $Rictor^{\Delta/\Delta}$ mice euthanized due to end-stage brain tumor(s). 1 year of time is indicated with a vertical dashed line on the graph. The Mantel-Cox (Log-rank) test is used to compare the curves statistically.

(E) The brain tumors from in $p53^{\Delta 5\text{-}6/\Delta 5\text{-}6}$, $p53^{\Delta 5\text{-}6/\Delta 5\text{-}6}$; $Rictor^{+/\Delta}$, and $p53^{\Delta 5\text{-}6/\Delta 5\text{-}6}$; $Rictor^{\Delta/\Delta}$ mice were grouped based on their location within the brain. Two-tailed Fisher's exact test is used to compare the groups.

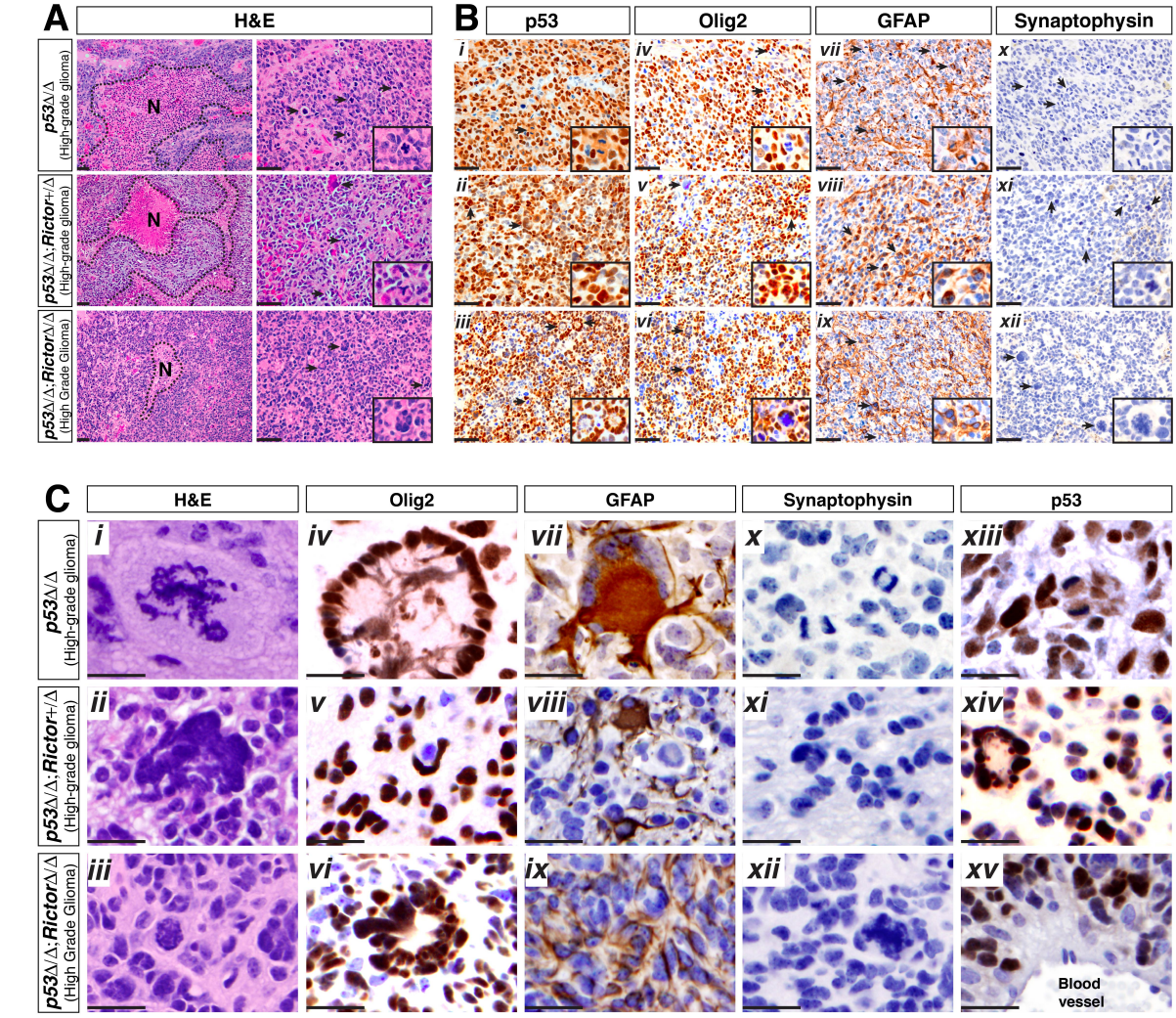
A
H&E
p53Δ/Δ (High-grade glioma)
p53Δ/Δ;Rictor+/Δ (High-grade glioma)
p53Δ/Δ;RictorΔ/Δ (High Grade Glioma)
N
B
p53
Olig2
GFAP
Synaptophysin
i
ii
iii
iv
v
vi
vii
viii
ix
x
xi
xii
C
H&E
Olig2
GFAP
Synaptophysin
p53
i
ii
iii
iv
v
vi
vii
viii
ix
x
xi
xii
xiii
xiv
xv
Blood vessel

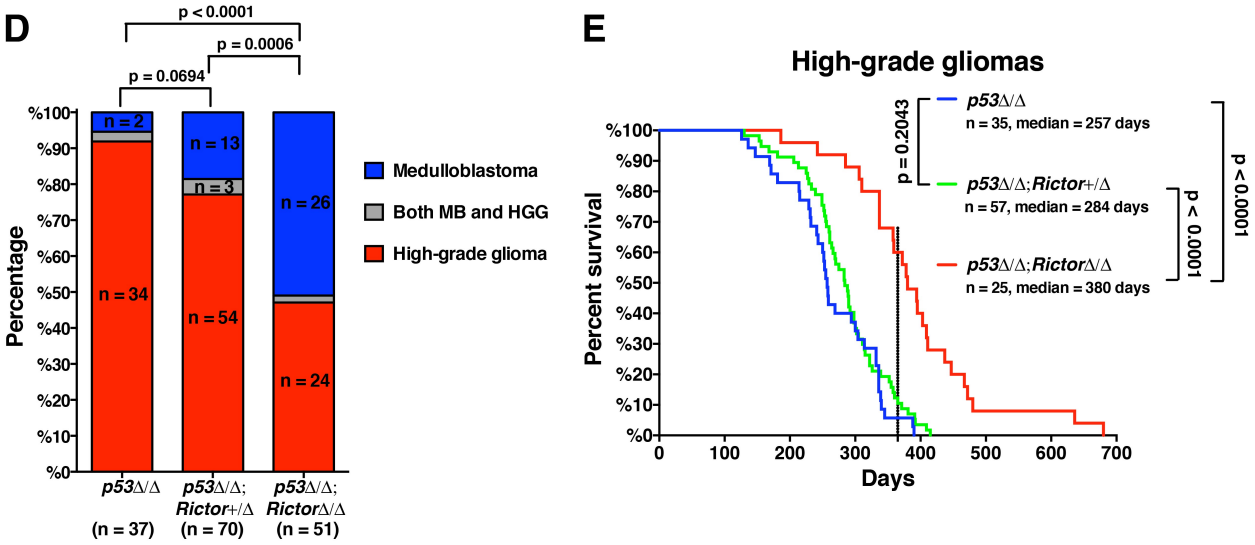
D
p < 0.0001
p = 0.0006
p = 0.0694
Percentage
%100
%90
%80
%70
%60
%50
%40
%30
%20
%10
%0
n = 2
n = 34
n = 13
n = 3
n = 54
n = 26
n = 24
Medulloblastoma
Both MB and HGG
High-grade glioma
p53Δ/Δ (n = 37)
p53Δ/Δ; Rictor+/Δ (n = 70)
p53Δ/Δ; RictorΔ/Δ (n = 51)
E
High-grade gliomas
Percent survival
p53Δ/Δ
n = 35, median = 257 days
p53Δ/Δ;Rictor+/Δ
n = 57, median = 284 days
p53Δ/Δ;RictorΔ/Δ
n = 25, median = 380 days
p = 0.2043
p < 0.0001
p < 0.0001
0
100
200
300
400
500
600
700
Days

Figure 5. Mutant-*p53* driven GEM gliomas are inhibited and/or delayed by concurrent deletion of *Rictor* gene.

(A) H&E staining of the high-grade gliomas (HGG) in three mouse models. Necrotic areas are indicated with "N". Characteristic features of the GEM gliomas are shown with arrowheads. The insets show abnormal mitotic figures (in $p53^{\Delta 5\text{-}6/\Delta 5\text{-}6}$ and $p53^{\Delta 5\text{-}6/\Delta 5\text{-}6}$; $Rictor^{+/\Delta}$) and a multinucleated giant cell (in $p53^{\Delta 5\text{-}6/\Delta 5\text{-}6}$; $Rictor^{\Delta/\Delta}$).

(B) Histopathology analyses of the GEM gliomas using p53, Olig2, GFAP and Synaptophysin antibodies. Insets illustrate the immunoreactivity at higher magnification, as well as some glioma features including the mitotic figures (*i, iv,* and *vii*), multinucleated giant cells (*iii* and *xii*), abnormal mitosis (*xi*) and a giant tumor nucleus (*vi*).

(C) In-depth histopathology analyses of the GEM gliomas. Multipolar or abnormal mitoses (*i, iii* and *xii*), multinucleated giant cells (*ii, iv, vi, vii* and *xiv*), mitotic figures (*x* and *xiii*) and vascular proliferation (*xv*) are noted.

(D) The frequency of the high-grade glioma and medulloblastoma formation in each mouse model. Two-tailed Fisher's exact test is used to compare the groups.

(E) Kaplan-Meier survival curves of the $p53^{\Delta 5\text{-}6/\Delta 5\text{-}6}$, $p53^{\Delta 5\text{-}6/\Delta 5\text{-}6}$; $Rictor^{+/\Delta}$, and $p53^{\Delta 5\text{-}6/\Delta 5\text{-}6}$; $Rictor^{\Delta/\Delta}$ mice euthanized due to end-stage high-grade gliomas. 1 year of time is indicated with a vertical dashed line on the graph. The Mantel-Cox (Log-rank) test is used to compare the curves statistically. Scale bars, 50 μm (A-B), 25 μm (C).

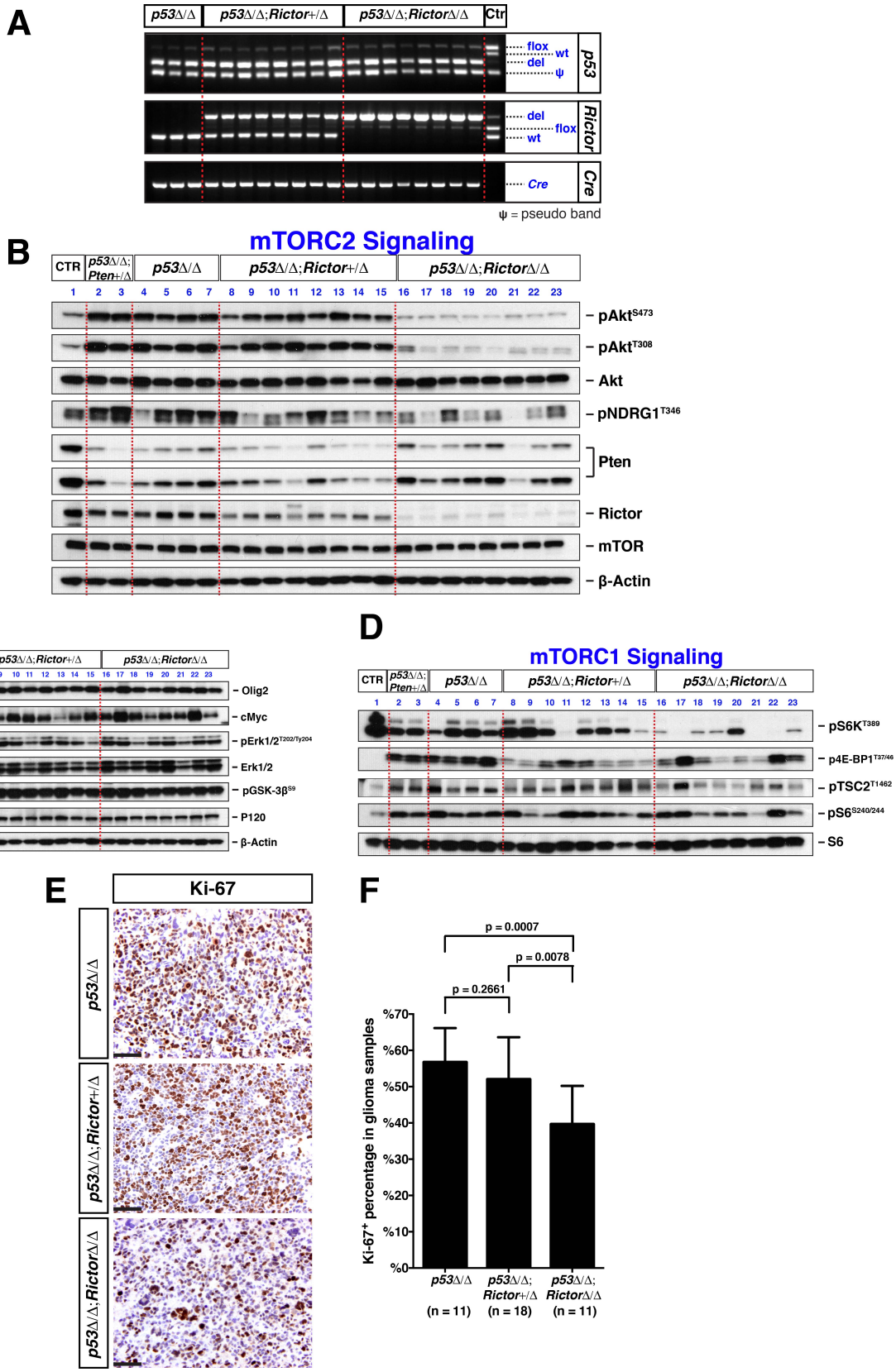
A
p53Δ/Δ
p53Δ/Δ;Rictor+/Δ
p53Δ/Δ;RictorΔ/Δ
Ctr
flox
wt
del
ψ
p53
del
flox
wt
Rictor
Cre
Cre
ψ = pseudo band
B
mTORC2 Signaling
CTR
p53Δ/Δ; Pten+/Δ
p53Δ/Δ
p53Δ/Δ;Rictor+/Δ
p53Δ/Δ;RictorΔ/Δ
1 2 3 4 5 6 7 8 9 10 11 12 13 14 15 16 17 18 19 20 21 22 23
– pAktS473
– pAktT308
– Akt
– pNDRG1T346
Pten
– Rictor
– mTOR
– β-Actin
C
CTR
p53Δ/Δ; Pten+/Δ
p53Δ/Δ
p53Δ/Δ;Rictor+/Δ
p53Δ/Δ;RictorΔ/Δ
1 2 3 4 5 6 7 8 9 10 11 12 13 14 15 16 17 18 19 20 21 22 23
– Olig2
– cMyc
– pErk1/2T202/Ty204
– Erk1/2
– pGSK-3βS9
– P120
– β-Actin
D
mTORC1 Signaling
CTR
p53Δ/Δ; Pten+/Δ
p53Δ/Δ
p53Δ/Δ;Rictor+/Δ
p53Δ/Δ;RictorΔ/Δ
1 2 3 4 5 6 7 8 9 10 11 12 13 14 15 16 17 18 19 20 21 22 23
– pS6KT389
– p4E-BP1T37/46
– pTSC2T1462
– pS6S240/244
– S6
E
Ki-67
p53Δ/Δ
p53Δ/Δ;Rictor+/Δ
p53Δ/Δ;RictorΔ/Δ
F
p = 0.0007
p = 0.0078
p = 0.2661
Ki-67+ percentage in glioma samples
%70
%60
%50
%40
%30
%20
%10
%0
p53Δ/Δ (n = 11)
p53Δ/Δ; Rictor+/Δ (n = 18)
p53Δ/Δ; RictorΔ/Δ (n = 11)

Figure 6. *Rictor*-deficient GEM gliomas display reduced tumor proliferation accompanied by impaired mTORC1 and mTORC2 signaling pathways.

(A) Genotyping of the glioma samples from $p53^{\Delta 5\text{-}6/\Delta 5\text{-}6}$, $p53^{\Delta 5\text{-}6/\Delta 5\text{-}6}$; $Rictor^{+/\Delta}$, and $p53^{\Delta 5\text{-}6/\Delta 5\text{-}6}$; $Rictor^{\Delta/\Delta}$ mice. hGFAP-cre; $p53^{flox/+}$; $Rictor^{flox/+}$ normal brain tissue is used as a positive control (CTR) for *p53* and *Rictor* genes, while cre-negative normal brain tissue is used as a negative control (CTR) for Cre band.

(B-D) Western blotting analyses of the mTORC2 signaling pathway (B), Olig2, Erk, GSK-3β and c-Myc signaling (C), and mTORC1 signaling pathway (D) in GEM gliomas. Tissue samples include a normal cerebral cortex tissue (CTR) and high-grade gliomas from two $p53^{\Delta 5\text{-}6/\Delta 5\text{-}6}$; $Pten^{+/\Delta}$, four $p53^{\Delta 5\text{-}6/\Delta 5\text{-}6}$, eight $p53^{\Delta 5\text{-}6/\Delta 5\text{-}6}$; $Rictor^{+/\Delta}$, and eight $p53^{\Delta 5\text{-}6/\Delta 5\text{-}6}$; $Rictor^{\Delta/\Delta}$ mice. Gliomas from $p53^{\Delta 5\text{-}6/\Delta 5\text{-}6}$; $Pten^{+/\Delta}$ mice are used as positive controls and the details about this mouse model is described in detail in the next sections of Chapter III.

(E-F) Analyses of the cellular proliferation in GEM gliomas based on Ki-67 immunoreactivity (E) and the Ki-67$^+$ cell percentage (F), which is calculated by the ratio of Ki-67$^+$ cell number to the total cell number in 40X images. The images from each sample are taken from the regions that displayed the highest Ki-67 immunoreactivity. The images shown in the figure are picked from samples that have approximately average Ki-67$^+$ percentage for each group. Scale bars, 50 μm.

A

Early tumor forming cells

6-7 months old		
Mutant	**Location**	**Structure**
*p53*Δ/Δ	On top of SVZ/RMS	Scattered/cluster
	Corpus collasum	Scattered/cluster
	Hippocampus vicinity	Individual cells
*p53*Δ/Δ	Hippocampus vicinity	Scattered/cluster
*p53*Δ/Δ	Olfactory bulb	Scattered/cluster
*p53*Δ/Δ	Corpus collasum	Small cluster
	Hippocampus vicinity	Small cluster
	RMS extantion into Olfactory bulb	Scattered/cluster
	Anterior striatum	Scattered/cluster
	Posterior striatum	Small clusters
*p53*Δ/Δ	Brain stem	Small cluster
	Hippocampus	Small cluster
*p53*Δ/Δ; *Rictor*Δ/Δ	Hippocampus vicinity	Small cluster

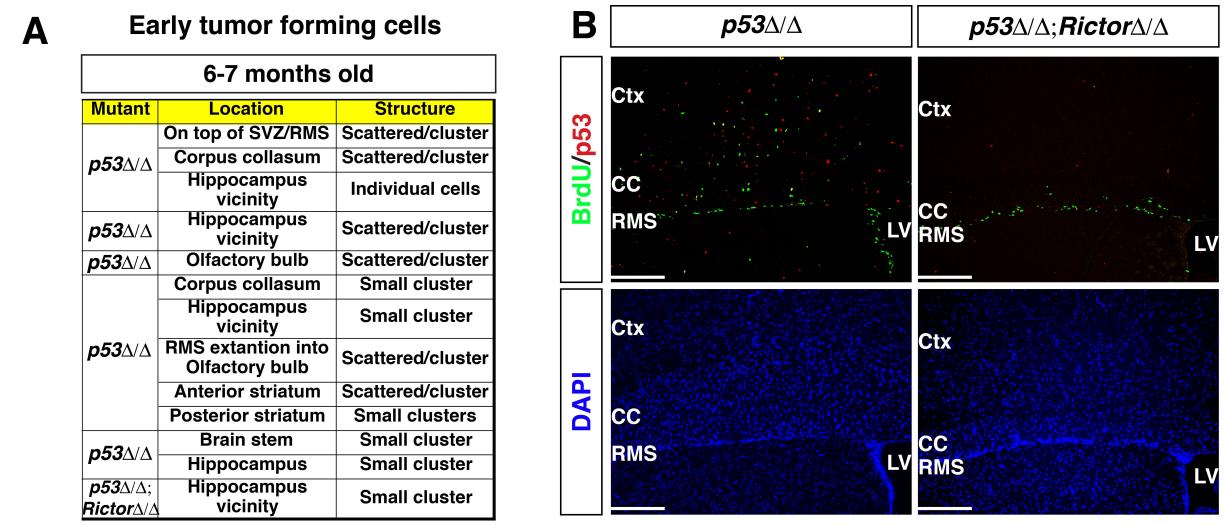

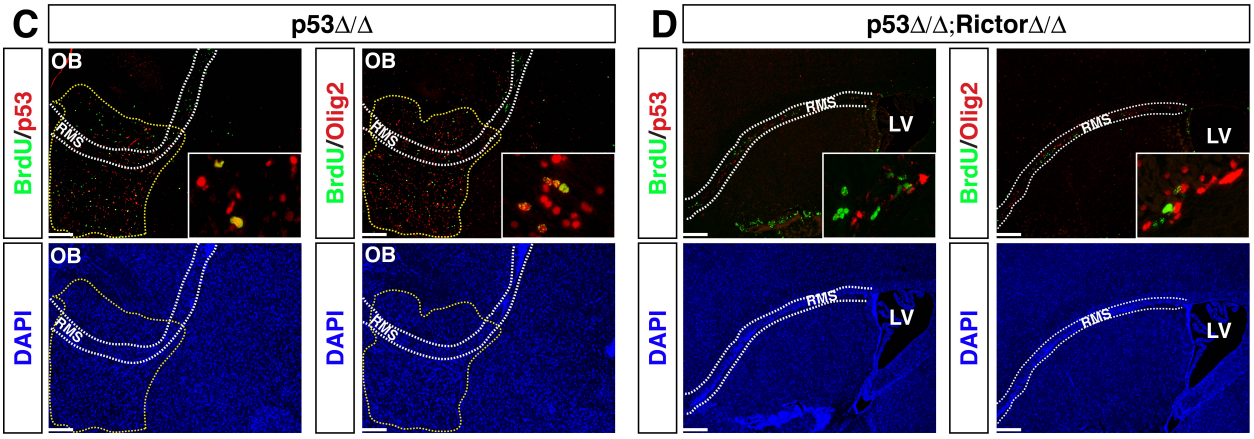

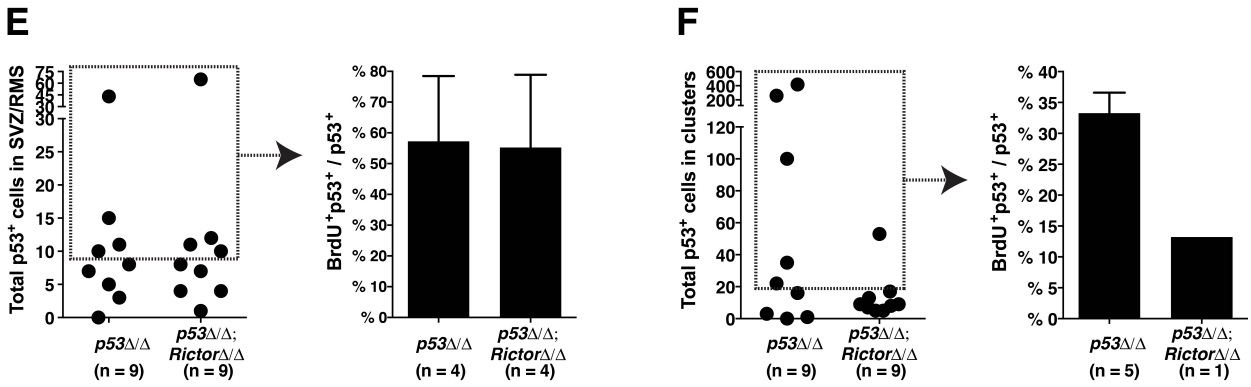

Figure 7. Expansion of the plausible early glioma-forming cells are inhibited by *Rictor* loss.

(A-F) 6-7 months old control and mutant mice are injected with BrdU (10 mg/kg) five times every two hours. All the mice are sacrificed two hours after the last injection.

(A) Various locations where $p53^{+}$ cells are detected in the forebrain of 6-7 months old $p53^{\Delta 5\text{-}6/\Delta 5\text{-}6}$ and $p53^{\Delta 5\text{-}6/\Delta 5\text{-}6}$; $Rictor^{\Delta/\Delta}$ mice are listed.

(B) The cells that might carry tumor-forming ability are detected by p53 and BrdU staining in 6-7 months old $p53^{\Delta 5\text{-}6/\Delta 5\text{-}6}$ and $p53^{\Delta 5\text{-}6/\Delta 5\text{-}6}$; $Rictor^{\Delta/\Delta}$ brains.

(C-D) $p53^{+}$ cells expanding outside of the germinal zone in $p53^{\Delta 5\text{-}6/\Delta 5\text{-}6}$ brains (C) or restricted within the germinal zone in $p53^{\Delta 5\text{-}6/\Delta 5\text{-}6}$; $Rictor^{\Delta/\Delta}$ brains (D) are illustrated by p53, Olig2 and BrdU staining in 6-7 months old mice. White line indicates the RMS, yellow line indicates the $p53^{+}$ and $Olig2^{+}$ proliferating cell clusters.

(E-F) The number of the total $p53^{+}$ cells that remain in the germinal zone (i.e. SVZ/RMS) (E) or scattered and/or clustered outside the germinal zone (F) are quantified in 6-7 months old $p53^{\Delta 5\text{-}6/\Delta 5\text{-}6}$ and $p53^{\Delta 5\text{-}6/\Delta 5\text{-}6}$; $Rictor^{\Delta/\Delta}$ mice. The proliferation percentages of the $p53^{+}$ cells (i.e. $BrdU^{+}p53^{+}$ / $p53^{+}$) are also calculated using the samples that have at least 20 or more $p53^{+}$ cells (scattered and/or clustered group) or at least 10 or more $p53^{+}$ cells (SVZ/RMS group). Unpaired t-test is used to compare the groups.

All the quantification data are presented as mean ± SD.

Scale bars 250 μm. Ctx: Cerebral cortex, CC: Corpus callosum, RMS: Rostral migratory stream, LV: Lateral ventricle, OB: Olfactory bulb.

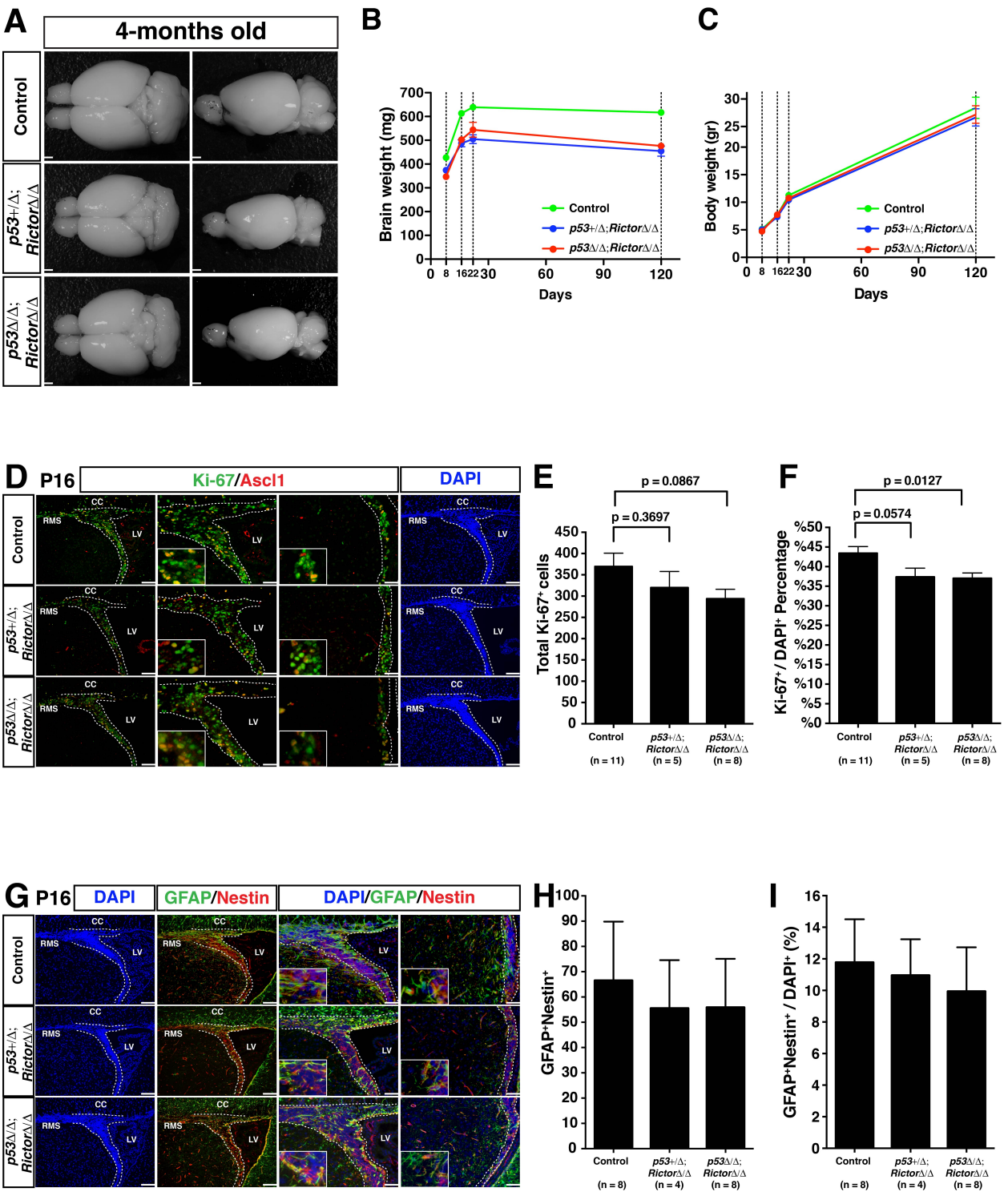
A
4-months old
Control
p53+/Δ; RictorΔ/Δ
p53Δ/Δ; RictorΔ/Δ
B
Brain weight (mg)
Days
Control
p53+/Δ;RictorΔ/Δ
p53Δ/Δ;RictorΔ/Δ
C
Body weight (gr)
Days
Control
p53+/Δ;RictorΔ/Δ
p53Δ/Δ;RictorΔ/Δ
D
P16
Ki-67/Ascl1
DAPI
CC
RMS
LV
E
p = 0.0867
p = 0.3697
Total Ki-67+ cells
Control (n = 11)
p53+/Δ; RictorΔ/Δ (n = 5)
p53Δ/Δ; RictorΔ/Δ (n = 8)
F
p = 0.0127
p = 0.0574
Ki-67+ / DAPI+ Percentage
Control (n = 11)
p53+/Δ; RictorΔ/Δ (n = 5)
p53Δ/Δ; RictorΔ/Δ (n = 8)
G
P16
DAPI
GFAP/Nestin
DAPI/GFAP/Nestin
H
GFAP+Nestin+
Control (n = 8)
p53+/Δ; RictorΔ/Δ (n = 4)
p53Δ/Δ; RictorΔ/Δ (n = 8)
I
GFAP+Nestin+ / DAPI+ (%)
Control (n = 8)
p53+/Δ; RictorΔ/Δ (n = 4)
p53Δ/Δ; RictorΔ/Δ (n = 8)

Figure 8. *Rictor* loss is mostly tolerated in the developing subventricular zone.

(A) Whole-mount images of the PFA-fixed, 4-months old wild-type control, *Rictor*$^{\Delta/\Delta}$ and *p53*$^{\Delta5\text{-}6/\Delta5\text{-}6}$; *Rictor*$^{\Delta/\Delta}$ mice.

(B-C) Brain (B) and body (C) weights of the wild-type control, *Rictor*$^{\Delta/\Delta}$ and *p53*$^{\Delta5\text{-}6/\Delta5\text{-}6}$; *Rictor*$^{\Delta/\Delta}$ mice at P8, P16, P22 and 4-months (P120).

(D) Proliferating cells and the overall structure of the P16 SVZ were compared between the control and mutant brains using Ki-67 and Ascl1 antibodies. Insets show higher magnification images.

(E-F) Total Ki-67^{+} proliferating cells (E) and the Ki-67^{+}/DAPI^{+} percentage (F) were examined in the SVZ of P16 brains.

(G-I) Stem cells in the SVZ of P16 mice were examined using GFAP and Nestin antibodies (G). Total stem cell number (H) and their representation within the SVZ population was also measured (I).

All the quantification data are presented as mean ± SD. Unpaired t-test is used for statistical comparison. Scale bars, 1 mm (A) and 100 μm (B and G). CC: Corpus callosum, RMS: Rostral migratory stream, LV: Lateral ventricle.

2.4 References

Alessi, D. R., Andjelkovic, M., Caudwell, B., Cron, P., Morrice, N., Cohen, P. and Hemmings, B. A. (1996). Mechanism of activation of protein kinase B by insulin and IGF-1. *The EMBO journal* **15**, 6541-6551.

Alessi, D. R., James, S. R., Downes, C. P., Holmes, A. B., Gaffney, P. R., Reese, C. B. and Cohen, P. (1997). Characterization of a 3-phosphoinositide-dependent protein kinase which phosphorylates and activates protein kinase Balpha. *Current biology : CB* **7**, 261-269.

Altomare, D. A. and Testa, J. R. (2005). Perturbations of the AKT signaling pathway in human cancer. *Oncogene* **24**, 7455-7464.

Anker, L., Ohgaki, H., Ludeke, B. I., Herrmann, H. D., Kleihues, P. and Westphal, M. (1993). p53 protein accumulation and gene mutations in human glioma cell lines. *International journal of cancer. Journal international du cancer* **55**, 982-987.

Bellacosa, A., Kumar, C. C., Di Cristofano, A. and Testa, J. R. (2005). Activation of AKT kinases in cancer: implications for therapeutic targeting. *Advances in cancer research* **94**, 29-86.

Bhat, K. P., Balasubramaniyan, V., Vaillant, B., Ezhilarasan, R., Hummelink, K., Hollingsworth, F., Wani, K., Heathcock, L., James, J. D., Goodman, L. D., et al. (2013). Mesenchymal differentiation mediated by NF-kappaB promotes radiation resistance in glioblastoma. *Cancer cell* **24**, 331-346.

Brennan, C. W., Verhaak, R. G., McKenna, A., Campos, B., Noushmehr, H., Salama, S. R., Zheng, S., Chakravarty, D., Sanborn, J. Z., Berman, S. H., et al. (2013). The somatic genomic landscape of glioblastoma. *Cell* **155**, 462-477.

Brosh, R. and Rotter, V. (2009). When mutants gain new powers: news from the mutant p53 field. *Nature reviews. Cancer* **9**, 701-713.

Cancer Genome Atlas Research, N. (2008). Comprehensive genomic characterization defines human glioblastoma genes and core pathways. *Nature* **455**, 1061-1068.

Chernova, O. B., Hunyadi, A., Malaj, E., Pan, H., Crooks, C., Roe, B. and Cowell, J. K. (2001). A novel member of the WD-repeat gene family, WDR11, maps to the 10q26 region and is disrupted by a chromosome translocation in human glioblastoma cells. *Oncogene* **20**, 5378-5392.

Chow, L. M., Endersby, R., Zhu, X., Rankin, S., Qu, C., Zhang, J., Broniscer, A., Ellison, D. W. and Baker, S. J. (2011). Cooperativity within and among Pten, p53, and Rb pathways induces high-grade astrocytoma in adult brain. *Cancer cell* **19**, 305-316.

Cully, M., You, H., Levine, A. J. and Mak, T. W. (2006). Beyond PTEN mutations: the PI3K pathway as an integrator of multiple inputs during tumorigenesis. *Nature reviews. Cancer* **6**, 184-192.

Foster, K. G. and Fingar, D. C. (2010). Mammalian target of rapamycin (mTOR): conducting the cellular signaling symphony. *The Journal of biological chemistry* **285**, 14071-14077.

Furnari, F. B., Fenton, T., Bachoo, R. M., Mukasa, A., Stommel, J. M., Stegh, A., Hahn, W. C., Ligon, K. L., Louis, D. N., Brennan, C., et al. (2007). Malignant

astrocytic glioma: genetics, biology, and paths to treatment. *Genes & development* **21**, 2683-2710.

Guertin, D. A., Stevens, D. M., Saitoh, M., Kinkel, S., Crosby, K., Sheen, J. H., Mullholland, D. J., Magnuson, M. A., Wu, H. and Sabatini, D. M. (2009). mTOR complex 2 is required for the development of prostate cancer induced by Pten loss in mice. *Cancer cell* **15**, 148-159.

Guertin, D. A., Stevens, D. M., Thoreen, C. C., Burds, A. A., Kalaany, N. Y., Moffat, J., Brown, M., Fitzgerald, K. J. and Sabatini, D. M. (2006). Ablation in mice of the mTORC components raptor, rictor, or mLST8 reveals that mTORC2 is required for signaling to Akt-FOXO and PKCalpha, but not S6K1. *Developmental cell* **11**, 859-871.

Hambardzumyan, D., Parada, L. F., Holland, E. C. and Charest, A. (2011). Genetic modeling of gliomas in mice: new tools to tackle old problems. *Glia* **59**, 1155-1168.

Holland, E. C., Celestino, J., Dai, C., Schaefer, L., Sawaya, R. E. and Fuller, G. N. (2000). Combined activation of Ras and Akt in neural progenitors induces glioblastoma formation in mice. *Nature genetics* **25**, 55-57.

Huse, J. T., Holland, E. and DeAngelis, L. M. (2013). Glioblastoma: molecular analysis and clinical implications. *Annual review of medicine* **64**, 59-70.

Ichimura, K., Schmidt, E. E., Miyakawa, A., Goike, H. M. and Collins, V. P. (1998). Distinct patterns of deletion on 10p and 10q suggest involvement of multiple tumor suppressor genes in the development of astrocytic gliomas of different malignancy grades. *Genes, chromosomes & cancer* **22**, 9-15.

Ikenoue, T., Inoki, K., Yang, Q., Zhou, X. and Guan, K. L. (2008). Essential function of TORC2 in PKC and Akt turn motif phosphorylation, maturation and signalling. *The EMBO journal* **27**, 1919-1931.

Inoki, K., Li, Y., Zhu, T., Wu, J. and Guan, K. L. (2002). TSC2 is phosphorylated and inhibited by Akt and suppresses mTOR signalling. *Nature cell biology* **4**, 648-657.

Koul, D., Shen, R., Bergh, S., Sheng, X., Shishodia, S., Lafortune, T. A., Lu, Y., de Groot, J. F., Mills, G. B. and Yung, W. K. (2006). Inhibition of Akt survival pathway by a small-molecule inhibitor in human glioblastoma. *Molecular cancer therapeutics* **5**, 637-644.

Kwon, C. H., Zhao, D., Chen, J., Alcantara, S., Li, Y., Burns, D. K., Mason, R. P., Lee, E. Y., Wu, H. and Parada, L. F. (2008). Pten haploinsufficiency accelerates formation of high-grade astrocytomas. *Cancer research* **68**, 3286-3294.

Laplante, M. and Sabatini, D. M. (2009). mTOR signaling at a glance. *Journal of cell science* **122**, 3589-3594.

Li, D. M. and Sun, H. (1997). TEP1, encoded by a candidate tumor suppressor locus, is a novel protein tyrosine phosphatase regulated by transforming growth factor beta. *Cancer research* **57**, 2124-2129.

Li, J., Yen, C., Liaw, D., Podsypanina, K., Bose, S., Wang, S. I., Puc, J., Miliaresis, C., Rodgers, L., McCombie, R., et al. (1997). PTEN, a putative protein tyrosine phosphatase gene mutated in human brain, breast, and prostate cancer. *Science* **275**, 1943-1947.

Louis, D. N. (2006). Molecular pathology of malignant gliomas. *Annual review of pathology* **1**, 97-117.

Louis, D. N., Ohgaki, H., Wiestler, O. D., Cavenee, W. K., Burger, P. C., Jouvet, A., Scheithauer, B. W. and Kleihues, P. (2007). The 2007 WHO classification of tumours of the central nervous system. *Acta neuropathologica* **114**, 97-109.

Louis, D. N., von Deimling, A., Chung, R. Y., Rubio, M. P., Whaley, J. M., Eibl, R. H., Ohgaki, H., Wiestler, O. D., Thor, A. D. and Seizinger, B. R. (1993). Comparative study of p53 gene and protein alterations in human astrocytic tumors. *Journal of neuropathology and experimental neurology* **52**, 31-38.

Magee, J. A., Ikenoue, T., Nakada, D., Lee, J. Y., Guan, K. L. and Morrison, S. J. (2012). Temporal changes in PTEN and mTORC2 regulation of hematopoietic stem cell self-renewal and leukemia suppression. *Cell stem cell* **11**, 415-428.

Masui, K., Tanaka, K., Akhavan, D., Babic, I., Gini, B., Matsutani, T., Iwanami, A., Liu, F., Villa, G. R., Gu, Y., et al. (2013). mTOR complex 2 controls glycolytic metabolism in glioblastoma through FoxO acetylation and upregulation of c-Myc. *Cell metabolism* **18**, 726-739.

Momota, H., Nerio, E. and Holland, E. C. (2005). Perifosine inhibits multiple signaling pathways in glial progenitors and cooperates with temozolomide to arrest cell proliferation in gliomas in vivo. *Cancer research* **65**, 7429-7435.

Motomura, K., Mittelbronn, M., Paulus, W., Brokinkel, B., Keyvani, K., Sure, U., Wrede, K., Nakazato, Y., Tanaka, Y., Pierscianek, D., et al. (2012). DMBT1 homozygous deletion in diffuse astrocytomas is associated with unfavorable clinical outcome. *Journal of neuropathology and experimental neurology* **71**, 702-707.

Noushmehr, H., Weisenberger, D. J., Diefes, K., Phillips, H. S., Pujara, K., Berman, B. P., Pan, F., Pelloski, C. E., Sulman, E. P., Bhat, K. P., et al. (2010). Identification of a CpG island methylator phenotype that defines a distinct subgroup of glioma. *Cancer cell* **17**, 510-522.

Ozawa, T., Riester, M., Cheng, Y. K., Huse, J. T., Squatrito, M., Helmy, K., Charles, N., Michor, F. and Holland, E. C. (2014). Most human non-GCIMP glioblastoma subtypes evolve from a common proneural-like precursor glioma. *Cancer cell* **26**, 288-300.

Parsons, D. W., Jones, S., Zhang, X., Lin, J. C., Leary, R. J., Angenendt, P., Mankoo, P., Carter, H., Siu, I. M., Gallia, G. L., et al. (2008). An integrated genomic analysis of human glioblastoma multiforme. *Science* **321**, 1807-1812.

Patel, A. P., Tirosh, I., Trombetta, J. J., Shalek, A. K., Gillespie, S. M., Wakimoto, H., Cahill, D. P., Nahed, B. V., Curry, W. T., Martuza, R. L., et al. (2014). Single-cell RNA-seq highlights intratumoral heterogeneity in primary glioblastoma. *Science* **344**, 1396-1401.

Phillips, H. S., Kharbanda, S., Chen, R., Forrest, W. F., Soriano, R. H., Wu, T. D., Misra, A., Nigro, J. M., Colman, H., Soroceanu, L., et al. (2006). Molecular subclasses of high-grade glioma predict prognosis, delineate a pattern of disease progression, and resemble stages in neurogenesis. *Cancer cell* **9**, 157-173.

Potter, C. J., Pedraza, L. G. and Xu, T. (2002). Akt regulates growth by directly phosphorylating Tsc2. *Nature cell biology* **4**, 658-665.

Sarbassov, D. D., Guertin, D. A., Ali, S. M. and Sabatini, D. M. (2005). Phosphorylation and regulation of Akt/PKB by the rictor-mTOR complex. *Science* **307**, 1098-1101.

Scheid, M. P., Marignani, P. A. and Woodgett, J. R. (2002). Multiple phosphoinositide 3-kinase-dependent steps in activation of protein kinase B. *Molecular and cellular biology* **22**, 6247-6260.

Sharma, S. V. and Settleman, J. (2007). Oncogene addiction: setting the stage for molecularly targeted cancer therapy. *Genes & development* **21**, 3214-3231.

Sottoriva, A., Spiteri, I., Piccirillo, S. G., Touloumis, A., Collins, V. P., Marioni, J. C., Curtis, C., Watts, C. and Tavare, S. (2013). Intratumor heterogeneity in human glioblastoma reflects cancer evolutionary dynamics. *Proceedings of the National Academy of Sciences of the United States of America* **110**, 4009-4014.

Stambolic, V., Suzuki, A., de la Pompa, J. L., Brothers, G. M., Mirtsos, C., Sasaki, T., Ruland, J., Penninger, J. M., Siderovski, D. P. and Mak, T. W. (1998). Negative regulation of PKB/Akt-dependent cell survival by the tumor suppressor PTEN. *Cell* **95**, 29-39.

Steck, P. A., Pershouse, M. A., Jasser, S. A., Yung, W. K., Lin, H., Ligon, A. H., Langford, L. A., Baumgard, M. L., Hattier, T., Davis, T., et al. (1997). Identification of a candidate tumour suppressor gene, MMAC1, at chromosome 10q23.3 that is mutated in multiple advanced cancers. *Nature genetics* **15**, 356-362.

Stupp, R., Hegi, M. E., Mason, W. P., van den Bent, M. J., Taphoorn, M. J., Janzer, R. C., Ludwin, S. K., Allgeier, A., Fisher, B., Belanger, K., et al. (2009). Effects of radiotherapy with concomitant and adjuvant temozolomide versus radiotherapy alone on survival in glioblastoma in a randomised phase III study: 5-year analysis of the EORTC-NCIC trial. *The Lancet. Oncology* **10**, 459-466.

Sturm, D., Witt, H., Hovestadt, V., Khuong-Quang, D. A., Jones, D. T., Konermann, C., Pfaff, E., Tonjes, M., Sill, M., Bender, S., et al. (2012). Hotspot mutations in H3F3A and IDH1 define distinct epigenetic and biological subgroups of glioblastoma. *Cancer cell* **22**, 425-437.

Testa, J. R. and Bellacosa, A. (2001). AKT plays a central role in tumorigenesis. *Proceedings of the National Academy of Sciences of the United States of America* **98**, 10983-10985.

Verhaak, R. G., Hoadley, K. A., Purdom, E., Wang, V., Qi, Y., Wilkerson, M. D., Miller, C. R., Ding, L., Golub, T., Mesirov, J. P., et al. (2010). Integrated genomic analysis identifies clinically relevant subtypes of glioblastoma characterized by abnormalities in PDGFRA, IDH1, EGFR, and NF1. *Cancer cell* **17**, 98-110.

Wang, H., Wang, H., Zhang, W., Huang, H. J., Liao, W. S. and Fuller, G. N. (2004). Analysis of the activation status of Akt, NFkappaB, and Stat3 in human diffuse gliomas. *Laboratory investigation; a journal of technical methods and pathology* **84**, 941-951.

Wang, Y., Yang, J., Zheng, H., Tomasek, G. J., Zhang, P., McKeever, P. E., Lee, E. Y. and Zhu, Y. (2009). Expression of mutant p53 proteins implicates a lineage relationship between neural stem cells and malignant astrocytic glioma in a murine model. *Cancer cell* **15**, 514-526.

Weinstein, I. B. (2002). Cancer. Addiction to oncogenes--the Achilles heal of cancer. *Science* **297**, 63-64.

Weinstein, I. B. and Joe, A. K. (2006). Mechanisms of disease: Oncogene addiction--a rationale for molecular targeting in cancer therapy. *Nature clinical practice. Oncology* **3**, 448-457.

Wen, P. Y. and Kesari, S. (2008). Malignant gliomas in adults. *The New England journal of medicine* **359**, 492-507.

Wen, P. Y., Lee, E. Q., Reardon, D. A., Ligon, K. L. and Alfred Yung, W. K. (2012). Current clinical development of PI3K pathway inhibitors in glioblastoma. *Neuro-oncology* **14**, 819-829.

Zheng, H., Ying, H., Yan, H., Kimmelman, A. C., Hiller, D. J., Chen, A. J., Perry, S. R., Tonon, G., Chu, G. C., Ding, Z., et al. (2008). p53 and Pten control neural and glioma stem/progenitor cell renewal and differentiation. *Nature* **455**, 1129-1133.

Zhu, Y., Guignard, F., Zhao, D., Liu, L., Burns, D. K., Mason, R. P., Messing, A. and Parada, L. F. (2005). Early inactivation of p53 tumor suppressor gene cooperating with NF1 loss induces malignant astrocytoma. *Cancer cell* **8**, 119-130.

Zhuo, L., Theis, M., Alvarez-Maya, I., Brenner, M., Willecke, K. and Messing, A. (2001). hGFAP-cre transgenic mice for manipulation of glial and neuronal function in vivo. *Genesis* **31**, 85-94.

Chapter III: Rictor/mTORC2 deficiency facilitates mutant-*p53* mediated medulloblastoma formation

3.1 Introduction

In contrast to glioblastoma, which mainly occurs in adulthood, medulloblastoma is largely a childhood malignancy, as it predominantly occurs in infants (≤ 3 years old) and children (4-17 years old). Despite the increased survival rates, a significant portion of the treated patients suffers from long-term adverse sequelae, including neurological, neuroendocrine and psychosocial deficits, as well as various problems in fertility, cardiopulmonary fitness, hearing, and physical performance (Gajjar and Robinson, 2014; Northcott et al., 2012a). Similar to glioblastomas, molecular stratification of medulloblastomas is critical in the comprehension of the disease and implementation of targeted therapies based on the genetic makeup that defines individual cases (Northcott et al., 2012a; Taylor et al., 2012). The current consensus of molecular classification predicts four subgroups with specific mutations and genetic alterations, each of which are associated with different survival rates (Jones et al., 2012; Northcott et al., 2011; Northcott et al., 2012b; Pugh et al., 2012; Robinson et al., 2012; Thompson et al., 2006). WNT medulloblastomas (10%) have the best outcome with 5-year overall survival (OS) of 95% followed by SHH (30%) and Group-4 (35%) medulloblastomas with approximately 75% OS. The worst outcome was seen in Group-3 or MYC (25%) patients with approximately 50% OS (Gajjar and Robinson, 2014; Kool et al., 2012; Northcott et al., 2012a).

The role of PI3K/AKT signaling in medulloblastoma formation, however, is relatively less understood. Previous research has revealed that mutations and copy number alterations in key pathway components, including *PTEN*, *PIK3CA*, *IGF1R* and *IRS2* are mostly enriched in SHH medulloblastomas (Northcott et al., 2012a; Northcott et al., 2012b; Robinson et al., 2012). Nevertheless, these alterations are still rare compared to glioblastomas, as only 10% of the SHH medulloblastomas have copy number changes associated with PI3K/RTK signaling (Northcott et al., 2012b). Especially SHH medulloblastomas in children between the ages of 3-18 (childhood SHH medulloblastomas, thereafter) exhibited a virtually absence of mutations in *PIK3CA*, *PTEN* and *PIK3C2G* genes, making these alterations restricted to adults (≥ 18 years old) and infants (< 3 years old) (Kool et al., 2014). Consistently, only less than 10% of the childhood SHH medulloblastomas are found to be immunoreactive to $pAKT^{S473}$, while majority of the positive cases are found in the adult tumors (Kool et al., 2014). These findings underline the essential roles of AKT signaling in adult tumors (e.g. glioblastoma), while raise questions about its roles in pediatric tumors.

Interestingly, almost 50% of the childhood SHH medulloblastomas had *TP53* alterations in contrast to their relatively normal PI3K/AKT signaling. Similar alterations in *TP53* gene are virtually absent in the remaining SHH medulloblastoma patients, as well as Group-3 and Group-4 tumors (Kool et al., 2014; Zhukova et al., 2013). This finding has particular clinical importance, as *TP53*-mutated medulloblastomas observed specifically in SHH children have an early recurrence and extremely poor outcome, making *TP53* status the most decisive adverse prognostic factor (Tabori et al., 2010; Zhukova et al., 2013). Subsequent studies have revealed that *TP53*-mutant SHH medulloblastomas undergo a chromosomal phenomenon called “chromothripsis”, which results in catastrophic DNA rearrangements (Jones and Jallepalli, 2012; Rausch et al., 2012; Stephens et al., 2011), as well as amplifications in *GLI2* and *N-MYC* genes (Jones and Jallepalli, 2012; Rausch et al., 2012). These genomic events have also been associated with poor clinical outcome and resistance to SMO-inhibitors (Kool et al., 2014; Northcott et al., 2012a; Northcott et al., 2012b; Pfister et al., 2009).

In the present study, I aimed to understand the role of *TP53* alterations in the context of PI3K/AKT signaling during the medulloblastoma formation. To this end, I utilized the same mouse models that are described in Chapter II. As discussed earlier, genetic deletion of *Rictor*, leading to an alleviated PI3K/Akt signaling, was sufficient to inhibit and/or delay mutant-*p53* driven gliomagenesis. However, removal of this well-known oncogenic signal at embryonic stages significantly increased medulloblastoma frequency, suggesting that Rictor/mTORC2, and thus PI3K/Akt signaling, has opposite roles in glioblastoma and medulloblastoma formation. Our further analyses in this chapter have revealed that *Rictor* loss increases a pool of cerebellar granule neuron precursor cells with a longer susceptible window, leading to an increased incidence of mutant-*p53* driven medulloblastoma formation. Subsequently, we showed that these medulloblastomas were characterized by their unique genomic and chromosomal alterations that resemble a subgroup of human medulloblastomas with poor clinical outcome. This study, combined with the previous chapter, underscores the differential functions of an important signaling pathway in adult and pediatric brain tumors, emphasizing the context-dependent roles of molecular alterations.

3.2 Results

3.2.1 Mutant-*p53* mediated medulloblastoma formation is increased upon *Rictor* loss

As described in Chapter II, *Rictor* loss had a robust suppressive effect on mutant-*p53* driven gliomagenesis. However, more than half of the $p53^{\Delta 5\text{-}6/\Delta 5\text{-}6}$; $Rictor^{\Delta/\Delta}$ mice still succumbed to death due to severe medulloblastomas as there was a significant increase in the medulloblastoma formation from 8% and 23% observed in $p53^{\Delta 5\text{-}6/\Delta 5\text{-}6}$ and $p53^{\Delta 5\text{-}6/\Delta 5\text{-}6}$; $Rictor^{+/\Delta}$ mice to 53% in $p53^{\Delta 5\text{-}6/\Delta 5\text{-}6}$; $Rictor^{\Delta/\Delta}$ (Figures 5D and 5E). Though the survival rate of medulloblastoma-bearing $p53^{\Delta 5\text{-}6/\Delta 5\text{-}6}$ and $p53^{\Delta 5\text{-}6/\Delta 5\text{-}6}$; $Rictor^{+/\Delta}$ mice were similar, there was a marginal increase in $p53^{\Delta 5\text{-}6/\Delta 5\text{-}6}$; $Rictor^{\Delta/\Delta}$ mice (Figure 9A). Almost

all of the $p53^{\Delta 5\text{-}6/\Delta 5\text{-}6}$; $Rictor^{\Delta/\Delta}$ medulloblastomas had either large cell/anaplastic or classic pathology characterized by a high density of tumor cells with dark nuclei making them look like "blue tumors", nuclear moldings, pseudo-palisading tumor cells, Rosette structures, small round or ellipsoid cells, carrot-shaped nuclei, and apoptotic cells (Figures 9B and 9C) (Gilbertson and Ellison, 2008; Louis et al., 2007). These tumors were sometimes immunoreactive to Synaptophysin, indicative of their neuronal differentiation, and sometimes to GFAP, indicating glial differentiation (Figures 9B and 9C). Similar to high-grade gliomas, GEM medulloblastomas were also characterized by the overexpression of the mutant-p53 protein (Figures 9B and 9C). More interestingly, as opposed to gliomas, all of the medulloblastomas notably expressed Pax6, while Olig2 expression was either absent or very minimal (Figures 9D-9F). Thus, Pax6 and Olig2 expression in brain tumors were mutually exclusive and Pax6 specifically labeled medulloblastomas while Olig2 was a distinguishing marker for high-grade gliomas regardless of their localization within the brain (Figures 9E and 9F).

My further analyses of $p53^{\Delta 5\text{-}6/\Delta 5\text{-}6}$; $Rictor^{\Delta/\Delta}$ medulloblastomas revealed a minor population of $Sox2^{+}$ cells within the tumor mass, which were recently described as tumor propagating cells and are resistant to current treatments (Figures 10A-10C) (Vanner et al., 2014). While some of the $Sox2^{+}$ cells coexpressed Pax6 protein at high levels, some of them had lower or no Pax6 expression (i.e. $Sox2^{+}Pax6^{high}$ and $Sox2^{+}Pax6^{low}$ or $Sox2^{+}Pax6^{-}$), suggesting heterogeneity and possibly a complex hierarchy within a single tumor (Figures 10A and 10D). Indicative of their quiescent nature, $Sox2^{+}$ cells were comparatively less proliferative and they rarely expressed mutant-p53 proteins (Figures 10B-10D). Interestingly, I detected a significant correlation between mutant-p53 expression and the proliferation in medulloblastomas. More specifically, the mutant-p53 expressing $Sox2^{+}$ cell percentage ($Sox2^{+}p53^{+}$ / $Sox2^{+}$) was significantly correlated with the proliferating $Sox2^{+}$ cell percentage ($Sox2^{+}Ki\text{-}67^{+}$ / $Sox2^{+}$) within the whole $Sox2^{+}$ cell population (Figure 10E). One possible explanation is that quiescent $Sox2^{+}$ cells trigger p53-signaling pathway upon induction of cellular proliferation mechanisms. These results overall suggest that even though *Rictor* deficiency plays an anti-glioma role in adulthood,

its loss at the embryonic stages may facilitate the formation of the mutant-*p53* driven medulloblastoma with distinctive histopathologic and clinical characteristics.

3.2.2 *Pten* mutation cooperates with *Rictor*-deficiency in facilitating mutant-*p53* induced medulloblastoma formation

Next, I wanted to further test my findings utilizing additional mouse models where I introduced a heterozygous *Pten* mutation into each $p53^{\Delta 5\text{-}6/\Delta 5\text{-}6}$, $p53^{\Delta 5\text{-}6/\Delta 5\text{-}6}$; $Rictor^{+/\Delta}$, and $p53^{\Delta 5\text{-}6/\Delta 5\text{-}6}$; $Rictor^{\Delta/\Delta}$ mouse model, and the new mouse models were called $p53^{\Delta 5\text{-}6/\Delta 5\text{-}6}$; $Pten^{+/\Delta}$, $p53^{\Delta 5\text{-}6/\Delta 5\text{-}6}$; $Pten^{+/\Delta}$; $Rictor^{+/\Delta}$, and $p53^{\Delta 5\text{-}6/\Delta 5\text{-}6}$; $Pten^{+/\Delta}$; $Rictor^{\Delta/\Delta}$, respectively (Figure 11A). All three new models with brain tumors showed comparable survival rates (Figure 11B), though they did live significantly shorter than their counterparts lacking the heterozygous *Pten* mutation (compare with Figure 4D). This finding suggests that the heterozygous *Pten* mutation itself may be an oncogenic signal, regardless of the *Rictor* or Akt status. Similar to $p53^{\Delta 5\text{-}6/\Delta 5\text{-}6}$ mice, $p53^{\Delta 5\text{-}6/\Delta 5\text{-}6}$; $Pten^{+/\Delta}$ tumors were primarily high-grade gliomas (83%), even though there was a slight increase in the hindbrain tumorigenesis (Figures 11C and 11D, compare with Figures 4E and 5D). Interestingly, $p53^{\Delta 5\text{-}6/\Delta 5\text{-}6}$; $Pten^{+/\Delta}$ tumors were enriched in the hindbrain, and medulloblastoma incidence increased up to 50%, which is slightly different than our observations in $p53^{\Delta 5\text{-}6/\Delta 5\text{-}6}$; $Rictor^{+/\Delta}$ mice (Figures 11C, 11D, compare with Figures 4E and 5D). Remarkably, and consistent with the differential role of *Rictor*-deficiency in brain tumorigenesis, $p53^{\Delta 5\text{-}6/\Delta 5\text{-}6}$; $Pten^{+/\Delta}$; $Rictor^{\Delta/\Delta}$ mice predominantly formed hindbrain tumors that were mostly medulloblastomas (86% and 79%, respectively), and only 26% of the mice formed high-grade gliomas (Figures 11C and 11D). Similar to the first group of mice that we studied, all of the $p53^{\Delta 5\text{-}6/\Delta 5\text{-}6}$; $Pten^{+/\Delta}$, $p53^{\Delta 5\text{-}6/\Delta 5\text{-}6}$; $Pten^{+/\Delta}$; $Rictor^{+/\Delta}$, and $p53^{\Delta 5\text{-}6/\Delta 5\text{-}6}$; $Pten^{+/\Delta}$; $Rictor^{\Delta/\Delta}$ GEM gliomas exhibited distinctive histology, including multinucleated tumor cells, increased mitotic activity, nuclear atypia, horseshoe-like structures and immunoreactivity to Olig2, GFAP and p53 (Figure 11E). medulloblastomas displayed classic or L/A type features including dense nuclei, nuclear molding, Rosette structure, apoptotic cells, carrot-shaped nuclei and immunoreactivity to Synaptophysin and p53

(Figure 11E). While these tumors were mainly Olig2^{-}, GFAP immunoreactivity was observed occasionally (Figure 11E). As expected, Akt signaling was elevated in both *p53*$^{\Delta 5\text{-}6/\Delta 5\text{-}6}$; *Pten*$^{+/\Delta}$ and *p53*$^{\Delta 5\text{-}6/\Delta 5\text{-}6}$; *Pten*$^{+/\Delta}$; *Rictor*$^{+/\Delta}$, however virtually inhibited in *p53*$^{\Delta 5\text{-}6/\Delta 5\text{-}6}$; *Pten*$^{+/\Delta}$; *Rictor*$^{\Delta/\Delta}$ gliomas. Pten expression was significantly reduced in all glioma models (Figure 11F). These results confirm my previous findings and suggest that *Pten* mutation is a key oncogenic event for both gliomas and medulloblastomas, however additional *Rictor* deficiency can inhibit/delay high-grade glioma formation while facilitating the medulloblastoma formation.

3.2.3 Proliferating granule neuron precursors are maintained in *Rictor*-deficient cerebella

Oncogenic activation, but not inhibition, of mTORC2 signaling has been previously associated with many cancer types including glioblastoma, prostate cancer, and leukemia, therefore, it was surprising to see that deletion of *Rictor* gene facilitated medulloblastoma formation. Thus, I investigated potential mechanisms by which *Rictor* loss promotes medulloblastoma development. Given that medulloblastoma arises from the developing cerebellum, I determined the consequences of *Rictor* loss during the cerebellar development. At postnatal day 16 (P16), granule neuron precursors (GNPs) in the external granular layer (EGL) – a cell-of-origin of medulloblastoma, ceased proliferation, became differentiated and migrated out of the EGL in all but two folia of the control cerebellum (Folium-6 and -10, F6 and F10) (Figure 12A) (White and Sillitoe, 2013). Remarkably, in addition to the actively proliferating BrdU^{+} cells seen in control F6 and F10, both *Rictor*$^{\Delta/\Delta}$ and *p53*$^{\Delta 5\text{-}6\ \Delta 5\text{-}6}$; *Rictor*$^{\Delta/\Delta}$ mutants had ectopically proliferating BrdU^{+} cells at the superficial surface of the EGL in virtually all of the cerebellar folia (Figures 12A and 12B). Overall, we observed a 2-fold increase in the total number of BrdU^{+} cells and 3-fold increase in the number per unit area in *Rictor* mutants compared to the control cerebella (Figures 12D and 12E). Ectopically proliferating BrdU^{+} cells were also observed in *p53*$^{\Delta 5\text{-}6}$ cerebella, despite that both the total number and the number per unit area were not as high as the *Rictor*-deficient cerebella (Figures 12A, 12B, 12D and 12E).

Thus, I concluded that the increase in the $p53^{\Delta5\text{-}6/\Delta5\text{-}6}Rictor^{\Delta/\Delta}$ cerebellum was mainly caused by *Rictor* loss. Of note, compared to control and $p53^{\Delta5\text{-}6/\Delta5\text{-}6}$ cerebella, *Rictor*-deficient cerebella, including both $Rictor^{\Delta/\Delta}$ and $p53^{\Delta5\text{-}6/\Delta5\text{-}6}$; $Rictor^{\Delta/\Delta}$, were significantly smaller accompanied by a reduction in brain weight by *Rictor* loss during the postnatal stages (Figures 12C, 8A and 8B). In all of the mutant cerebella, the ectopically proliferating cells expressed high levels of neural lineage marker Pax6 (Engelkamp et al., 1999; Yamasaki et al., 2001), suggesting that these cells are GNPs that failed to exit cell cycle and, remained in the EGL (Figure 12A)**.**

Subsequently, I analyzed three individual folia (F-5/6, F-9/10a and F-10b) in order to confirm my findings. I found that EGL-associated $Pax6^{+}$ cell number was notably increased in all three folia of both $Rictor^{\Delta/\Delta}$ and $p53^{\Delta5\text{-}6/\Delta5\text{-}6}$; $Rictor^{\Delta/\Delta}$ cerebella compared to wild type controls. Though, $p53^{\Delta5\text{-}6/\Delta5\text{-}6}$; $Rictor^{\Delta/\Delta}$ cerebella had slightly higher $Pax6^{+}$ cells especially in F-9/10a and F-10b than $Rictor^{\Delta/\Delta}$ cerebella (Figures 13A-13D). Similar increase was also observed in $p53^{\Delta5\text{-}6/\Delta5\text{-}6}$ cerebella, although it was mostly pronounced in F-10b (Figure 13D). I also detected proliferating $Pax6^{+}BrdU^{+}$ cells in all three folia of both *Rictor*-deficient cerebella, while there was already a reduction in F-5/6 of $p53^{\Delta5\text{-}6/\Delta5\text{-}6}$ cerebellum (Figures 13A-13D). Together, these results suggest that *Rictor* deficiency alone can lead to the formation of ectopically proliferating GNPs when control cells have already differentiated.

3.2.4 A minor population of GNPs requires intact mTORC2 signaling for proper differentiation

In order to better understand how *Rictor* deficiency led to ectopically proliferating GNPs in the cerebellum, I performed a BrdU pulse-chase experiment where mice were injected with BrdU at P15 and sacrificed at P17. I then determined whether the proliferating cells at P15 (i.e. $BrdU^{+}$) exited ($BrdU^{+}Ki\text{-}67^{-}$) or remained in ($BrdU^{+}Ki\text{-}67^{+}$) cell cycle after two days (Figure 14A). As I aimed to specifically determine the role of *Rictor* deficiency in ectopic GNPs, I excluded $p53^{\Delta5\text{-}6/\Delta5\text{-}6}$ mice from this analysis. At P17, there were

almost no proliferating cells ($Ki67^{+}$) in the control cerebellum except in the most posterior folium (F-10b), whereas a considerable number of proliferating cells were observed in *Rictor*-deficient cerebella regardless of the presence or absence of *p53* (Figure 14B). Moreover, many of the proliferating cells in *Rictor*-deficient cerebella were labeled by BrdU, indicating that the proliferating GNPs in *Rictor*-deficient cerebella at P15 failed to exit the cell cycle two days later at P17, as did the wild type control GNPs (Figure 14C). Consistently, the ratio of the cells exiting the cell cycle to the cells remaining in the cell cycle was significantly reduced in $Rictor^{\Delta/\Delta}$ cerebella and also noticeably smaller in the $p53^{\Delta 5\text{-}6\ \Delta 5\text{-}6}$; $Rictor^{\Delta/\Delta}$ compared to controls (Figure 14D). These results suggest that *Rictor* is required for a subset of GNPs to undergo timely cell-cycle exit and become differentiated during postnatal cerebellar development.

Consistent with the role of Rictor/mTORC2 in the normal differentiation of GNPs, $pAkt^{S473}$ levels were largely absent in the highly proliferative EGL at P8, and reached a very high level in newly differentiated neurons located in the Molecular Layer (ML) (Figures 14E and 14G). Once these neurons were fully differentiated and migrated to the IGL, $pAkt^{S473}$ levels were kept at an intermediate level (Figures 14E and 14G). In contrast, Pten had an opposite expression pattern: while it had an intermediate level in the ML, it reached a very high level in the IGL (Figures 14E and 14G). As expected, $pAkt^{S473}$ levels in the $Rictor^{\Delta/\Delta}$ was not detectable in any part of the cerebellum except for the Purkinje cells, which were not targeted by the cre-flox system (Figures S5E and S5F) (Zhuo et al., 2001). These results suggest that Rictor/mTORC2-dependent Akt activation is required for a subset of GCPs to undergo timely cell-cycle exit and become differentiated in the postnatal developing cerebellum.

3.2.5 Ectopically proliferating GNPs transform into early-tumor forming cells in the absence of Rictor/mTORC2 and *p53*

I next analyzed cerebella at later stages to determine whether the ectopically proliferating cells in the EGL provided any indication of early tumor initiation process. I first

examined the mice at P22 when the wild type control cerebellum was completely formed, and there were virtually no proliferating cells in the EGL (Figures 15A-15D) (White and Sillitoe, 2013). Remarkably, $p53^{\Delta 5\text{-}6/\Delta 5\text{-}6}$; $Rictor^{\Delta/\Delta}$ mice were the only mutants that still had $BrdU^{+}Pax6^{+}$ proliferating cells in all three analyzed folia, while only half of the $p53^{\Delta 5\text{-}6/\Delta 5\text{-}6}$ mice had a similar population and they were restricted to F-10b (Figures 15A-15D). I also observed $BrdU^{+}Pax6^{+}$ cells in the $Rictor^{\Delta/\Delta}$ cerebella, however the total number was noticeably smaller than the $p53^{\Delta 5\text{-}6/\Delta 5\text{-}6}$; $Rictor^{\Delta/\Delta}$ cerebella (Figures 15A-15D). Importantly, $Pax6^{+}$ cells were abnormally accumulated in the EGL and ML of both *Rictor*-deficient cerebella, of which the $p53^{\Delta 5\text{-}6/\Delta 5\text{-}6}Rictor^{\Delta/\Delta}$ cerebellum exhibited a greater increase (Figures 15D and 15E). Given no abnormal accumulation of $Pax6^{+}$ cells in the EGL and ML of the $p53^{\Delta 5\text{-}6/\Delta 5\text{-}6}$ cerebellum, these results are most consistent with a model wherein *Rictor* loss delayed the timely differentiation of a subset of GNPs, triggering a p53-dependent cell-cycle arrest/differentiation response that leads to accumulation of differentiated $Pax6^{+}$ cells in the EGL and ML of the $Rictor^{\Delta/\Delta}$ cerebellum. However, upon loss of both *Rictor* and *p53*, a subset of proliferating $BrdU^{+}Pax6^{+}$ cells were maintained in the EGL and ML of the $p53^{\Delta 5\text{-}6/\Delta 5\text{-}6}Rictor^{\Delta/\Delta}$ cerebellum. It is worth noting that even in the $p53^{\Delta 5\text{-}6/\Delta 5\text{-}6}$; $Rictor^{\Delta/\Delta}$ mice, the total number of the proliferating cells reduced dramatically from P16 to P22, indicating the presence of p53-independent pathways that induce cell cycle exit/differentiation response in $p53^{\Delta 5\text{-}6/\Delta 5\text{-}6}$; $Rictor^{\Delta/\Delta}$ cerebella (Figure 16F).

To provide additional support for this model, I examined the expression of mutant p53 protein that was shown to accumulate at a high level upon oncogenic stress (Wang et al., 2009). I analyzed P16, P22 and P60 cerebella, and did not detect p53 expression in the control and $Rictor^{\Delta/\Delta}$ cerebella, as none of these mice formed brain tumors throughout their life (Figure 16D). However, $p53^{+}$ GNPs were readily detected in $p53^{\Delta 5\text{-}6/\Delta 5\text{-}6}$ and $p53^{\Delta 5\text{-}6/\Delta 5\text{-}6}Rictor^{\Delta/\Delta}$ cerebella as early as P16 (Figures 16A and 16E). Remarkably, with the maturation of the cerebellum from P16 to P22, 4/5 of the $p53^{\Delta 5\text{-}6/\Delta 5\text{-}6}Rictor^{\Delta/\Delta}$ mice maintained a significant number of $p53^{+}$ cells in their cerebella, however these cells disappeared in 3/4 of the $p53^{\Delta 5\text{-}6/\Delta 5\text{-}6}$ cerebella (Figures 16B, 16C and 16E) (images are

provided for only $p53^{\Delta 5\text{-}6/\Delta 5\text{-}6}Rictor^{\Delta/\Delta}$ cerebella). Importantly, when the mice reached P60, I still detected $p53^{+}$ cells in 4/7 $p53^{\Delta 5\text{-}6/\Delta 5\text{-}6}Rictor^{\Delta/\Delta}$ mice (Figures 16D and 16E). As most of the $p53^{+}$ cells already disappeared in P22 $p53^{\Delta 5\text{-}6/\Delta 5\text{-}6}$ cerebella, I did not further analyze $p53^{\Delta 5\text{-}6/\Delta 5\text{-}6}$ mice at P60. These results were, interestingly, in contrast to my earlier findings where $p53^{\Delta 5\text{-}6/\Delta 5\text{-}6}$ mice were characterized with the $p53^{+}$ cells scattered around various places of the forebrain, while only one $p53^{\Delta 5\text{-}6/\Delta 5\text{-}6}Rictor^{\Delta/\Delta}$ mouse displayed a comparable phenotype, underlining the opposite roles of Rictor in glioma forming cells versus medulloblastoma forming cells (Figure 7A).

While the proliferating $BrdU^{+}$ cells in the EGL of the $p53^{\Delta 5\text{-}6/\Delta 5\text{-}6}$; $Rictor^{\Delta/\Delta}$ mice reduced over time (Figure 16F), the percentage of $p53^{+}$ cells within this population increased to 90%, suggesting that there was a clonal expansion of the $p53^{+}$ cells from P16 to P60, while the remaining proliferating cells disappeared through various mechanisms such as differentiation (Figure 16G). It is worth noting that 4/7 of the $p53^{\Delta 5\text{-}6/\Delta 5\text{-}6}$; $Rictor^{\Delta/\Delta}$ mice maintained $p53^{+}$ cells in the EGL - a ratio similar to the medulloblastoma penetrance observed in this mouse model (Figures 16G and 5D). Together, these results suggest that the delay in timely differentiation of GNPs caused by *Rictor* loss increases a pool of targeted cells with a longer susceptible window, leading to an increased incidence of mutant-*p53* driven medulloblastoma development (Figure 17).

As described above, distinct regulation of the tumor-initiating cell pools by Rictor/mTORC2 signaling elucidates the opposing effects of *Rictor* on gliomagenesis versus medulloblastoma formation. We found that Rictor/mTORC2 deficiency reduces the number and proliferation of the glioma-initiating progenitor cells in the forebrain, while it prolongs the ectopic presence of the proliferating progenitor cells in the cerebellum. Thus, our study here demonstrates a recently identified correlation between the total number of divisions in various stem cell pools and the lifetime risk of cancers in respective organs (Tomasetti and Vogelstein, 2015).

3.2.6 Mutant-*p53* induced medulloblastomas share molecular events with *Ptch1*$^{+/-}$ tumors

Having shown that Rictor/mTORC2 deficiency can facilitate mutant-*p53* induced medulloblastoma formation, I then aimed to characterize the molecular signatures of the tumors in this novel model. Since *TP53* mutation has been mostly associated with the Sonic Hedgehog-group medulloblastomas (SHH medulloblastomas) (Jones et al., 2012; Kool et al., 2014; Zhukova et al., 2013), I included *Ptch1*$^{+/-}$ medulloblastoma samples (i.e. *Ptch1*$^{+/-}$, *p53*$^{\Delta 5\text{-}6/\Delta 5\text{-}6}$; *Ptch1*$^{+/-}$, and *p53*$^{\Delta 5\text{-}6/R172P}$; *Ptch1*$^{+/-}$) into my analyses. My laboratory colleague Daniel M. Triesman generously provided these *Ptch1*$^{+/-}$ medulloblastoma samples. As predicted, all of the *p53*$^{\Delta 5\text{-}6/\Delta 5\text{-}6}$; *Rictor*$^{\Delta/\Delta}$ medulloblastomas lacked pAkt^{S473} and also pAkt^{T308} (Figure 18A). As opposed to GEM high-grade gliomas, pAkt levels were very low in the majority of the *p53*$^{\Delta 5\text{-}6/\Delta 5\text{-}6}$ and *p53*$^{\Delta 5\text{-}6/\Delta 5\text{-}6}$; *Rictor*$^{+/\Delta}$ medulloblastomas, and more importantly, all of the *Ptch1*$^{+/-}$ medulloblastomas (Figure 18A). This finding is particularly interesting because neither *p53*$^{\Delta 5\text{-}6/\Delta 5\text{-}6}$ nor *Ptch1*$^{+/-}$ medulloblastomas had any reduction in Rictor expression, and *p53*$^{\Delta 5\text{-}6/\Delta 5\text{-}6}$; *Rictor*$^{+/\Delta}$ medulloblastomas had only about 50% decrease (Figure 18A). These results support the model that low levels of Akt activity promote medulloblastoma development.

While Olig2 expression was uniformly absent in medulloblastoma samples as we noted earlier (Figures 9C-9F), Gli1 expression was easily detectable in many samples (Figure 18A). I, therefore, extended my analyses to other genes associated with Shh-signaling, and found that all of the medulloblastoma samples had significant *Gli1*, *Gli2*, *N-Myc* and *Atoh1* expression - very similar to the Ptch1$^{+/-}$ samples (Figure 18B). Surprisingly, *Ptch1* expression was elevated in many *p53*$^{\Delta 5\text{-}6/\Delta 5\text{-}6}$; *Rictor*$^{\Delta/\Delta}$ medulloblastomas raising the question of whether they carried loss-of-function mutations in this gene (Figure 18C). Of note, c-Myc expression in the *p53*$^{\Delta 5\text{-}6/\Delta 5\text{-}6}$*Rictor*$^{\Delta/\Delta}$ medulloblastomas was not as consistently high as *Ptch1*$^{+/-}$ medulloblastomas, though both groups exhibited elevated levels of Ezh2 expression. I did not observe a consistent pattern across the

medulloblastoma samples in terms of pErk1/2 levels, however its expression was mostly lower than the glioma samples (Figure 18D). Together, these results suggest that mutant-*p53* induced medulloblastomas are characterized by Shh-signature gene expression similar to the *Ptch1*$^{+/-}$ tumors, and that the absence of pAkt is a characteristic feature of this group of tumors regardless of the *Rictor* and *p53* status.

3.2.7 *Rictor* deficiency facilitates mutant-*p53* mediated medulloblastomas that resemble human SHH medulloblastomas

Previous studies identified distinct molecular variants of medulloblastomas named after the important signaling pathways associated with them and current consensus categorizes the medulloblastomas into four: WNT, SHH, Group C (or MYC) and Group D (Kool et al., 2008; Northcott et al., 2011; Taylor et al., 2012; Thompson et al., 2006). Expression of the Shh-related genes in mutant-*p53* mediated medulloblastomas raised the question of whether these tumors belonged to the SHH medulloblastomas. In order to answer this question, we analyzed the gene expression prolife of our samples in comparison with previously determined mouse SHH medulloblastomas, Group C medulloblastomas, GNPs, and normal brain tissue. This part of the project was carried out as collaboration with the scientists at the German Cancer Research Center (DKFZ), Heidelberg, Germany. More specifically, I collaborated with Dr. Stefan M. Pfister, Dr. Marcel Kool, Dr. Sebastian Stark and Susanne Gröbner.

Our results showed that 16/22 of the analyzed medulloblastoma samples were strongly associated with SHH medulloblastomas, and also shared similarity with the GNP expression profile (Figure 19A), consistent with the previous findings showing that SHH-medulloblastomas arise from neural lineage committed GNPs (Gibson et al., 2010; Schuller et al., 2008; Yang et al., 2008). We did not observe such significant resemblance between our samples and the Group C tumors, and the normal tissue samples had a significantly distinct profile. (Figure 19A). The remaining 6/22 of our medulloblastoma samples shared similarity with the normal tissues, yet were still characterized by the

expression of Shh-specific genes including *Otx1*, *Pdlim3*, *Boc*, *Atoh1*, *Sfrp1* and *Gli1*, suggesting that these samples may have been contaminated with the normal tissue during the dissection procedures (Figures 19A and 19B). When we focused on the expression of *Gli1*, *Gli2*, *Atoh1* and *Sfrp1* - four of the most characteristic genes in SHH medulloblastomas -, we found that all of our samples were intermixed with the previously identified SHH medulloblastomas with significant expression of these Shh-marker genes (Figure 19C). Of note, there was no difference between the mutant-*p53* mediated medulloblastomas in terms of *Rictor* status, as they all had similar levels of Shh-signature gene expression (Figures 19A and 19D). These results overall suggest that *Rictor* loss facilitates mutant-*p53* driven medulloblastomas that are most similar to SHH medulloblastomas in humans.

3.2.8 *Rictor*-deficient medulloblastomas are characterized by distinctive genomic and chromosomal abnormalities associated with poor clinical outcomes

Approximately 21% of the human SHH medulloblastomas carry *TP53* mutations, and almost all of these patients are children between the ages of 5 and 18 years (Zhukova et al., 2013). It has been reported that childhood medulloblastomas with *TP53* mutations also harbored *N-MYC* and/or *GLI2* amplifications rendering them resistant to Smoothened inhibitors (Kool et al., 2014). A recent study also underlined the combined effects of *TP53* mutation and *N-MYC* amplification in relapse medulloblastomas that correlated with rapid disease progression (Hill et al., 2015). I, therefore, tested whether our GEM medulloblastomas carried such genomic abnormalities. I first performed a series of RT-PCR experiments using tumor genomic DNA as template. I calculated the copy numbers of *N-Myc* and *Gli2* genes in comparison to two internal reference genes (*β-Actin* in chr5 and *Gapdh* in chr7), and I included $Ptch1^{+/-}$ mediated medulloblastoma samples into my analyses. My results showed that the copy number readings based on the two reference genes are significantly similar to each other, supporting the accuracy of my copy number estimates (Figures 20A and 20B). Remarkably, 7/9 of the $p53^{\Delta 5\text{-}6/\Delta 5\text{-}6}$; $Rictor^{\Delta/\Delta}$ tumors had notable *N-Myc* amplifications, while only 1/7 of the $Ptch1^{+/-}$, and

none of the $p53^{\Delta 5\text{-}6}$ (n = 2) and $p53^{\Delta 5\text{-}6/\Delta 5\text{-}6}$; $Rictor^{+/\Delta}$ (n = 3) medulloblastomas had a similar amplification (Figure 20C). The *N-Myc* amplification clearly distinguished $p53^{\Delta 5\text{-}6/\Delta 5\text{-}6}$; $Rictor^{\Delta/\Delta}$ medulloblastomas from the rest of the mutant-*p53* mediated medulloblastomas. In terms of the *Gli2* gene, I observed that 3/9 of the $p53^{\Delta 5\text{-}6/\Delta 5\text{-}6}$; $Rictor^{\Delta/\Delta}$, 2/7 of the $Ptch1^{+/-}$, and 1/3 of the $p53^{\Delta 5\text{-}6/\Delta 5\text{-}6}$; $Rictor^{+/\Delta}$ tumors had slight to intermediate level of amplifications (Figure 20C). We confirmed these results with a low-coverage copy number analysis using another set of tumor samples. We detected similar amplifications in *Gli1*, *Gli2* and *N-Myc* genes, though *Gli2* amplification was much noticeable in this set of samples (Figure 20D). Interestingly, we also noticed chr13/*Ptch1* deletions in 10/15 samples (Figure 20D), suggesting that multiple alterations occurring simultaneously contribute to the Shh-signatures observed in these mutant-*p53* driven medulloblastomas

One critical genomic abnormality that has been strongly linked to SHH medulloblastomas with *p53* mutations is tetraploidy - harboring four times the haploid number of chromosomes (Jones et al., 2012). Having shown that $p53^{\Delta 5\text{-}6/\Delta 5\text{-}6}$; $Rictor^{\Delta/\Delta}$ tumors are SHH medulloblastomas with important gene amplifications, I aimed to test whether there were any chromosomal aneuploidies within these tumors that might also be relevant to the observed gene alterations. For this purpose, I established primary tumor cell lines using fresh tumor tissue samples, and examined the structure and number of the chromosomes at very early passages (passages 0-2). I detected characteristic chromosomal abnormalities including head-to-head and head-to-tail chromosome fusions, breaks, translocations, centromere losses and double minute chromosomes in $p53^{\Delta 5\text{-}6/\Delta 5\text{-}6}$; $Rictor^{\Delta/\Delta}$ cell lines (Figures 21A, 21C and data not shown). 1/1 of the $p53^{\Delta 5\text{-}6/\Delta 5\text{-}6}$; $Rictor^{+/\Delta}$ and 6/9 of the $p53^{\Delta 5\text{-}6/\Delta 5\text{-}6}$; $Rictor^{\Delta/\Delta}$ medulloblastoma cell lines had increased number of the chromosomes ranging between 45-85 reminiscent of triploidy or tetraploidy (Figure 21B). Interestingly, 2/5 of the $p53^{\Delta 5\text{-}6/\Delta 5\text{-}6}$; $Rictor^{\Delta/\Delta}$ cell lines gained aneuploidy, and 1/5 had increased its chromosome number at later passages (passages $\geq$ 3), suggesting that passaging might introduce further abnormalities or allow the expansion of particular clones (Figures 21C and 21D). These distinctive genomic and

chromosomal events, which mimic childhood medulloblastomas with *TP53* mutations, led us to investigate whether RICTOR/mTORC2 signaling is altered in human tumors too. We interestingly found that childhood medulloblastomas with *TP53* mutations had notably lower *RICTOR* expression compared to the tumors with wt-*TP53* (Figure 21E). As previously noted, we observed somewhat the opposite results in human GBMs (Figure 3B), where *RICTOR* expression was higher in tumors with *TP53* mutation compared to tumors with wt-*TP53*, underlining the opposite roles of *RICTOR/Rictor* in adult and pediatric brain tumors. Overall, these results suggest that *Rictor* deficiency facilitates the formation of medulloblastomas that undergo specific genomic and chromosomal abnormalities that have been associated with resistance to current treatments and poor clinical outcomes in childhood SHH medulloblastomas.

3.3 Discussion

In combination with the previous chapter, here we demonstrated that Rictor/mTORC2 signaling has opposite roles in gliomagenesis and medulloblastoma formation. Our data suggest that despite the significant tumor suppressive activity of *Rictor* loss in glioma development, its embryonic deletion increases the frequency of medulloblastoma formation. This phenomenon occurs mainly through a temporary delay in differentiation of a subset of *p53*-deficient cerebellar granule neuron precursors (Figure 22). This study, therefore, identifies a molecular signaling pathway - Rictor/mTORC2 - with distinct functions in adult and pediatric brain tumors.

3.3.1 Abnormal presence of a cerebellar progenitor cell population in *Rictor*-deficient brains underlies increased medulloblastoma formation

Li-Fraumeni syndrome patients carrying germline *TP53* mutations have increased risks of developing malignant gliomas and medulloblastoma, however medulloblastoma formation in these patients is still a rare event. Similarly, medulloblastoma development

in mutant-*p53* mice is also a rare event (5-10%), as shown here and previously (Wang et al., 2009). One likely explanation for this fact is that the rapid stem/progenitor cell depletion in the cerebellum leads to a relatively quiescent organ that prevents the emergence and/or accumulation of the mutant-*p53* induced sporadic molecular alterations. Furthermore, this biological phenomenon may be responsible for the largely pediatric nature of medulloblastoma. Here, we have shown that alterations in a critical molecular pathway, such as Rictor/mTORC2 and possibly PI3K/Akt, can interfere with the natural differentiation of the cerebellar progenitor cells, providing a short but essential window for the mutant-*p53* cells to undergo sufficient molecular abnormalities required for medulloblastoma formation. More specifically, *Rictor* loss increases a pool of GNPs with a longer period of predisposition, causing an increased frequency of mutant-*p53* driven medulloblastoma formation (Figure 17).

It is worth noting that *Rictor*-deficiency alone is not capable of initiating medulloblastoma formation, which suggests that *p53* mutation is the main driver of the tumorigenesis, while *Rictor*-deficiency is a facilitator of this process. It also indicates that abnormally proliferating *Rictor*-deficient GNPs exit cell cycle and differentiate into mature cells by p53-dependent mechanisms. Consistent with these findings, we found that $pAkt^{S473}$ was virtually absent in actively proliferating GNPs, while the newly differentiating cells in ML and mature neurons in IGL had prominent Akt activation. Therefore, PI3K/Akt signaling functions as an essential pathway that regulates the lineage progress from cerebellar progenitor cells to fully differentiated neurons. As $Rictor^{\Delta/\Delta}$ GNPs eventually differentiate into mature neurons, there might be other redundant pathways that allow this transition. Lastly, we cannot dispute the possibility that other downstream components of Rictor/mTORC2 signaling (e.g. PKC-α and SGK1) are responsible for the phenotypes that we observed.

3.3.2 *Rictor* loss facilitates the formation of mutant-*p53* driven medulloblastomas with SHH signature

The comprehensive analyses performed in our laboratory and also in collaboration with scientists in DKFZ indicated that all of our mutant-*p53* driven medulloblastoma samples had Shh gene expression profile. Accordingly, these tumors were categorized along with the previously generated GEM models of SHH medulloblastoma. It is worth noting that we did not detect a difference among our mutant-*p53* driven medulloblastomas with regards to *Rictor* status, as they all had similar histopathologic features and Shh activation. Therefore, the major role of *Rictor* loss in medulloblastoma formation seems to prolong the time of susceptibility of cerebellar progenitor cells to transform into tumor cells by mechanisms described in previous section.

Almost all of the previous SHH medulloblastoma mouse models were generated by introducing a mutation in *Ptch1* or *Smo* gene, which results in elevated Shh signaling (Northcott et al., 2012a). Our mutant-*p53* models, however, represented a spontaneous activation of Shh signaling pathway that drives tumorigenesis from cerebellar progenitor cells. Of note, same *p53* mutation in the forebrain led to glioma formation accompanied by Akt activation. Thus, the same gene mutation allowed different stem/progenitor cell populations to acquire distinct oncogenic pathways for the development of different tumors.

3.3.3 *Rictor*-deficient medulloblastomas display unique genomic and chromosomal alterations

Aberrant activation of Shh signaling in medulloblastomas, often due to inactivating mutations in *PTCH1*, led researchers to develop drugs that target this oncogenic pathway (Ng and Curran, 2011). Virtually all of the current Shh antagonists target the transmembrane protein *Smoothened* (*SMO*) itself with promising results seen in both mouse model studies (Berman et al., 2002; Romer et al., 2004) and clinical trials (Amakye et al., 2013). However, inhibiting the Shh pathway in medulloblastomas is more challenging and complicated than it seems, as several strategies for pathway activation have been identified (Amakye et al., 2013). Consistently, only 50% of medulloblastoma

cases with Shh activation are associated with mutations in *PTCH1*, *SUFU* or *SMO* (Ng and Curran, 2011), implying the presence of other molecular alterations, including the downstream components, leading to pathway activation. Furthermore, acquired drug resistance plays an important role in disease complexity, as evidenced by a case study reporting the emergence of a novel mutation in *SMO* gene, resulting in irresponsiveness to SMO-inhibitors (Rudin et al., 2009; Yauch et al., 2009). Similarly, amplifications in key Shh downstream target genes such as *GLI1*, *GLI2* and *N-MYC*, detected especially in patients with *TP53* mutations, are thought to render the tumors inherently resistant to SMO-inhibitors (Gajjar and Robinson, 2014; Northcott et al., 2012a). It is, therefore, critical to 1) distinguish between SMO-dependent and SMO-independent pathway activation (Amakye et al., 2013), 2) identify unique genetic alterations, and subsequently tailor precise treatment plans for each patient, 3) develop novel drugs that are able to target Shh pathway downstream components (Hyman et al., 2009; Kool et al., 2014), and finally 4) generate mouse models that recapitulate various genomic alterations observed in human medulloblastomas to test these newly designed drugs and study drug resistance. Although insightful, the majority of the current mouse models for SHH medulloblastoma do not represent the complete genetic diversity observed in human tumors (Ng and Curran, 2011), especially those that have a natural resistance to SMO-inhibitors. This might be partly because many models are engineered to have a *Ptch1* mutation, making them inherently vulnerable to SMO-inhibitors. Mutant-*p53*-*Rictor* medulloblastomas, then, are unique in that they are easily distinguished from other models by their prominent amplifications in *N-Myc* and *Gli2* genes, as well as increased chromosome numbers reminiscent of tetraploidy. These tumors resemble the childhood SHH medulloblastomas, which show a limited or no response to SMO-inhibitors (Kool et al., 2014) and associated with poor prognosis (Northcott et al., 2012b). Thus, we strongly advocate the utilization of *Rictor*-deficient medulloblastomas, with or without a *Pten* mutation, as unique tools to test novel drugs targeting Shh pathway downstream components such as Gli1, Gli2, and N-Myc (Figure 22).

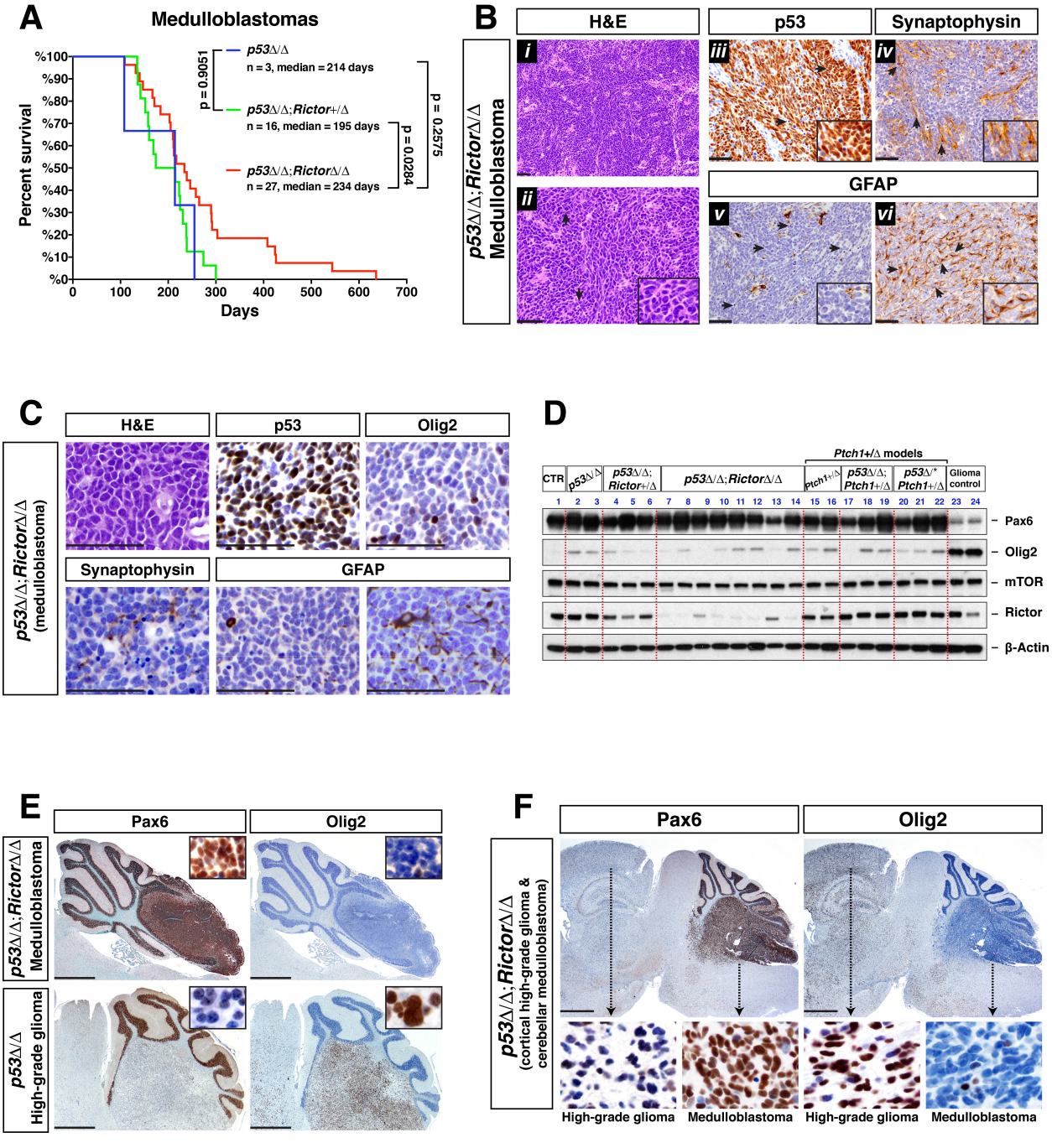
A
Medulloblastomas
Percent survival
%100
%90
%80
%70
%60
%50
%40
%30
%20
%10
%0
0
100
200
300
400
500
600
700
Days
p53Δ/Δ
n = 3, median = 214 days
p53Δ/Δ;Rictor+/Δ
n = 16, median = 195 days
p53Δ/Δ;RictorΔ/Δ
n = 27, median = 234 days
p = 0.9051
p = 0.0284
p = 0.2575
B
H&E
p53
Synaptophysin
GFAP
i
ii
iii
iv
v
vi
p53Δ/Δ;RictorΔ/Δ
Medulloblastoma
C
H&E
p53
Olig2
Synaptophysin
GFAP
p53Δ/Δ;RictorΔ/Δ
(medulloblastoma)
D
Ptch1+/Δ models
CTR
p53Δ/Δ
p53Δ/Δ; Rictor+/Δ
p53Δ/Δ;RictorΔ/Δ
Ptch1+/Δ
p53Δ/Δ; Ptch1+/Δ
p53Δ/* Ptch1+/Δ
Glioma control
1 2 3 4 5 6 7 8 9 10 11 12 13 14 15 16 17 18 19 20 21 22 23 24
Pax6
Olig2
mTOR
Rictor
β-Actin
E
Pax6
Olig2
p53Δ/Δ;RictorΔ/Δ
Medulloblastoma
p53Δ/Δ
High-grade glioma
F
Pax6
Olig2
p53Δ/Δ;RictorΔ/Δ
(cortical high-grade glioma & cerebellar medulloblastoma)
High-grade glioma
Medulloblastoma
High-grade glioma
Medulloblastoma

Figure 9. *Rictor*-deficient medulloblastomas have distinctive histopathologic features.

(A) Kaplan-Meier survival curves of $p53^{\Delta 5\text{-}6/\Delta 5\text{-}6}$, $p53^{\Delta 5\text{-}6/\Delta 5\text{-}6}$; $Rictor^{+/\Delta}$, and $p53^{\Delta 5\text{-}6/\Delta 5\text{-}6}$; $Rictor^{\Delta/\Delta}$ mice that developed end-stage medulloblastoma. The Mantel-Cox (Log-rank) test is used to compare the curves statistically.

(B) Histopathologic features of the $p53^{\Delta 5\text{-}6/\Delta 5\text{-}6}$; $Rictor^{\Delta/\Delta}$ medulloblastomas. H&E staining illustrates the dense tumor (*i*) with carrot-shaped nuclei, apoptotic cells and nuclear moldings (*ii*). Tumors were immunoreactive to p53 (*iii*) and Synaptophysin (*iv*). Some areas of the tumors are $GFAP^{+}$ (*vi*) while others were $GFAP^{-}$ (*v*). Insets show the immunoreactivity to each antibody at a higher magnification.

(C) In-depth analyses of the histopathologic features of the medulloblastomas in $p53^{\Delta 5\text{-}6/\Delta 5\text{-}6}$; $Rictor^{\Delta/\Delta}$ mice. Tumors were characterized by dense nuclei with nuclear moldings (illustrated in H&E staining), p53 immunoreactivity, occasional Synaptophysin and GFAP staining, and very minimal $Olig2^{+}$ cells.

(D) Western blotting analysis of the $p53^{\Delta 5\text{-}6/\Delta 5\text{-}6}$, $p53^{\Delta 5\text{-}6/\Delta 5\text{-}6}$; $Rictor^{+/\Delta}$, and $p53^{\Delta 5\text{-}6/\Delta 5\text{-}6}$; $Rictor^{\Delta/\Delta}$ medulloblastoma samples along with the various $Ptch1^{+/-}$ (i.e. $Ptch1^{+/-}$, $p53^{\Delta 5\text{-}6/\Delta 5\text{-}6}$; $Ptch1^{+/-}$, and $p53^{\Delta 5\text{-}6/R172P}$; $Ptch1^{+/-}$) SHH medulloblastoma models. Wild type cerebellar tissue is used as a control (CTR), and two glioma samples from $p53^{\Delta 5\text{-}6/\Delta 5\text{-}6}$; $Rictor^{+/\Delta}$ and $p53^{\Delta 5\text{-}6/\Delta 5\text{-}6}$; $Pten^{+/\Delta}$ (last two lanes) are also included into the analysis. Expression levels of glioma marker Olig2 and medulloblastoma marker Pax6 are analyzed along with mTOR and Rictor.

(E) Immunohistochemical analysis of Pax6 and Olig2 in and $p53^{\Delta 5\text{-}6/\Delta 5\text{-}6}$; $Rictor^{\Delta/\Delta}$ medulloblastoma and $p53^{\Delta 5\text{-}6/\Delta 5\text{-}6}$ cerebellar high-grade glioma. Note the mutually exclusive staining of the Pax6 and Olig2 in both medulloblastoma and glioma.

(F) Pax6 and Olig2 staining in two consecutive sections of a $p53^{\Delta 5\text{-}6/\Delta 5\text{-}6}$; $Rictor^{\Delta/\Delta}$ brain with a forebrain glioma and a cerebellar medulloblastoma. Note the $Pax6^{-}Olig2^{+}$ glioma and the $Pax6^{+}Olig2^{-}$ medulloblastoma.

Scale bars, 50 μm (B and C), 1 mm (E and F).

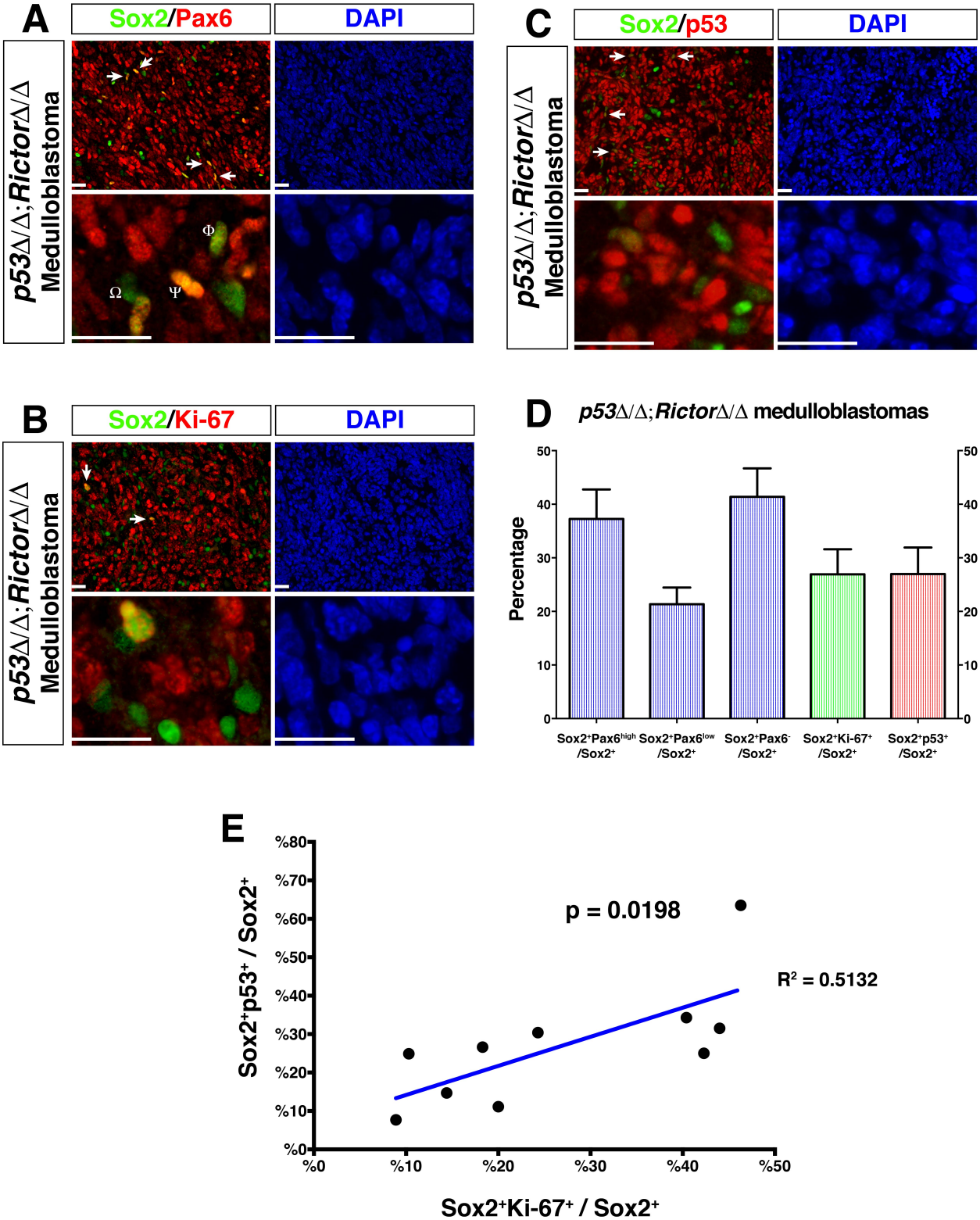
A
Sox2/Pax6
DAPI
p53Δ/Δ;RictorΔ/Δ Medulloblastoma
Φ
Ω
Ψ
C
Sox2/p53
DAPI
p53Δ/Δ;RictorΔ/Δ Medulloblastoma
B
Sox2/Ki-67
DAPI
p53Δ/Δ;RictorΔ/Δ Medulloblastoma
D
p53Δ/Δ;RictorΔ/Δ medulloblastomas
Percentage
0
10
20
30
40
50
Sox2+Pax6high /Sox2+
Sox2+Pax6low /Sox2+
Sox2+Pax6- /Sox2+
Sox2+Ki-67+ /Sox2+
Sox2+p53+ /Sox2+
E
p = 0.0198
R2 = 0.5132
Sox2+p53+ / Sox2+
%0
%10
%20
%30
%40
%50
%60
%70
%80
Sox2+Ki-67+ / Sox2+

Figure 10. A minor population of Sox2^{+} stem-like cells is detected within *Rictor*-deficient medulloblastomas.

(A-C) Expression patterns of Sox2 in relation to Pax6 (A), Ki-67 (B) and p53 (C) in *p53*$^{\Delta 5\text{-}6/\Delta 5\text{-}6}$; *Rictor*$^{\Delta/\Delta}$ medulloblastomas are examined. Arrows show the colocalized expressions.

(D) Pax6 expression, proliferation rate and mutant-p53 expression of Sox2^{+} cells in *p53*$^{\Delta 5\text{-}6/\Delta 5\text{-}6}$; *Rictor*$^{\Delta/\Delta}$ medulloblastomas are quantified. Three different populations of Sox2^{+} cells in relation to Pax6 expression levels are identified: Sox2^{+}Pax6^{high} (marked with Ψ), Sox2^{+}Pax6^{low} (marked with Φ) and Sox2^{+}Pax6^{-} (marked with Ω). Proliferation rate of Sox2^{+} cells is calculated by the ratio of the total number of Sox2^{+}Ki-67^{+} cells to the total number of the Sox2^{+} cells. Percentage of the mutant-p53 expressing Sox2^{+} cells is calculated by the total number of Sox2^{+}p53^{+} cells to the total number of the Sox2^{+} cells. Quantifications are done using 40X images of the two different regions in each tumor and the average percentage of the two are taken for each sample (n = 10). The data are presented as mean ± SEM.

Scale bars, 25 μm.

(E) The correlation between the mutant-p53 expression (Sox2^{+}p53^{+}) and the proliferation (Sox2^{+}Ki-67^{+}) within the Sox2^{+} cells is determined by a linear regression analysis. Goodness of fit (R^2), and the significance of the slope are calculated (p-value). Note the significant correlation between the mutant-p53 expression and the increased proliferation within the Sox2^{+} cell population in mutant-*p53* mediated medulloblastomas.

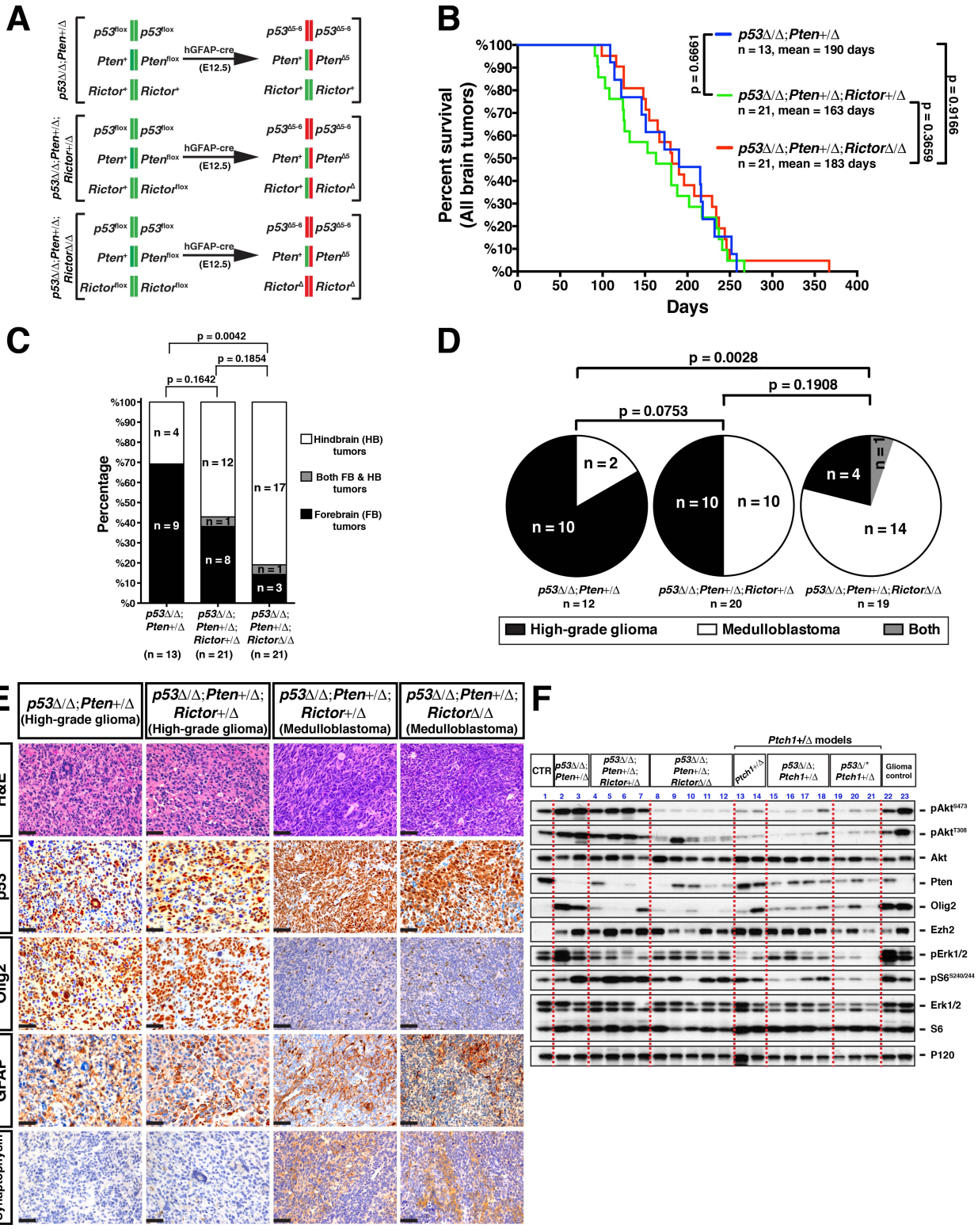
A
p53Δ/Δ;Pten+/Δ
p53flox p53flox
Pten+ Ptenflox
Rictor+ Rictor+
hGFAP-cre
(E12.5)
p53Δ5-6 p53Δ5-6
Pten+ PtenΔ5
Rictor+ Rictor+
p53Δ/Δ;Pten+/Δ;Rictor+/Δ
Rictor+ Rictorflox
Rictor+ RictorΔ
p53Δ/Δ;Pten+/Δ;RictorΔ/Δ
Rictorflox Rictorflox
RictorΔ RictorΔ
B
Percent survival (All brain tumors)
Days
p53Δ/Δ;Pten+/Δ
n = 13, mean = 190 days
p53Δ/Δ;Pten+/Δ;Rictor+/Δ
n = 21, mean = 163 days
p53Δ/Δ;Pten+/Δ;RictorΔ/Δ
n = 21, mean = 183 days
p = 0.6661
p = 0.3659
p = 0.9169
C
p = 0.0042
p = 0.1854
p = 0.1642
Percentage
Hindbrain (HB) tumors
Both FB & HB tumors
Forebrain (FB) tumors
n = 4
n = 9
n = 12
n = 1
n = 8
n = 17
n = 1
n = 3
p53Δ/Δ; Pten+/Δ (n = 13)
p53Δ/Δ; Pten+/Δ; Rictor+/Δ (n = 21)
p53Δ/Δ; Pten+/Δ; RictorΔ/Δ (n = 21)
D
p = 0.0028
p = 0.1908
p = 0.0753
n = 2
n = 10
n = 10
n = 10
n = 4
n = 1
n = 14
p53Δ/Δ;Pten+/Δ n = 12
p53Δ/Δ;Pten+/Δ;Rictor+/Δ n = 20
p53Δ/Δ;Pten+/Δ;RictorΔ/Δ n = 19
High-grade glioma
Medulloblastoma
Both
E
p53Δ/Δ;Pten+/Δ (High-grade glioma)
p53Δ/Δ;Pten+/Δ; Rictor+/Δ (High-grade glioma)
p53Δ/Δ;Pten+/Δ; Rictor+/Δ (Medulloblastoma)
p53Δ/Δ;Pten+/Δ; RictorΔ/Δ (Medulloblastoma)
H&E
p53
Olig2
GFAP
Synaptophysin
F
Ptch1+/Δ models
CTR
p53Δ/Δ; Pten+/Δ
p53Δ/Δ; Pten+/Δ; Rictor+/Δ
p53Δ/Δ; Pten+/Δ; RictorΔ/Δ
Ptch1+/Δ
p53Δ/Δ; Ptch1+/Δ
p53Δ/* Ptch1+/Δ
Glioma control
1 2 3 4 5 6 7 8 9 10 11 12 13 14 15 16 17 18 19 20 21 22 23
pAktS473
pAktT308
Akt
Pten
Olig2
Ezh2
pErk1/2
pS6S240/244
Erk1/2
S6
P120

Figure 11. *Pten* mutation cooperates with *Rictor*-deficiency in facilitating mutant-*p53* induced medulloblastoma formation.

(A) Schematic representation of the genetic configurations in $p53^{\Delta 5\text{-}6/\Delta 5\text{-}6}$; $Pten^{+/\Delta}$, $p53^{\Delta 5\text{-}6/\Delta 5\text{-}6}$; $Pten^{+/\Delta}$; $Rictor^{+/\Delta}$, and $p53^{\Delta 5\text{-}6/\Delta 5\text{-}6}$; $Pten^{+/\Delta}$; $Rictor^{\Delta/\Delta}$ mice. Floxed genes undergo hGFAP-cre-mediated recombination at around E12.5, therefore the mice are named after the genotype of the recombined cells.

(B) Kaplan-Meier survival curves of the $p53^{\Delta 5\text{-}6/\Delta 5\text{-}6}$; $Pten^{+/\Delta}$, $p53^{\Delta 5\text{-}6/\Delta 5\text{-}6}$; $Pten^{+/\Delta}$; $Rictor^{+/\Delta}$, and $p53^{\Delta 5\text{-}6/\Delta 5\text{-}6}$; $Pten^{+/\Delta}$; $Rictor^{\Delta/\Delta}$ mice sacrificed due to end-stage brain tumor(s). The Mantel-Cox (Log-rank) test is used to compare the curves statistically.

(C) The tumors from $p53^{\Delta 5\text{-}6/\Delta 5\text{-}6}$; $Pten^{+/\Delta}$, $p53^{\Delta 5\text{-}6/\Delta 5\text{-}6}$; $Pten^{+/\Delta}$; $Rictor^{+/\Delta}$, and $p53^{\Delta 5\text{-}6/\Delta 5\text{-}6}$; $Pten^{+/\Delta}$; $Rictor^{\Delta/\Delta}$ are grouped based on their location within the brain. Two-tailed Fisher's exact test is used to compare the groups.

(D) Pie-chart representation of the high-grade glioma and medulloblastoma frequency in each mouse model. Two-tailed Fisher's exact test is used to compare the groups.

(E) Histopathologic analyses of the high-grade gliomas from $p53^{\Delta 5\text{-}6/\Delta 5\text{-}6}$; $Pten^{+/\Delta}$ and $p53^{\Delta 5\text{-}6/\Delta 5\text{-}6}$; $Pten^{+/\Delta}$; $Rictor^{+/\Delta}$ mice, and medulloblastomas from $p53^{\Delta 5\text{-}6/\Delta 5\text{-}6}$; $Pten^{+/\Delta}$; $Rictor^{+/\Delta}$, and $p53^{\Delta 5\text{-}6/\Delta 5\text{-}6}$; $Pten^{+/\Delta}$; $Rictor^{\Delta/\Delta}$ mice. High-grade gliomas were relatively less dense with more cytoplasmic material making them appear as "pink" tumors in H&E staining while medulloblastomas had very crowded nuclei with minimal amount of cytoplasm making them "blue" tumors. Note the differential Olig2 immunoreactivity between the gliomas and medulloblastomas.

(F) Western blotting analyses of the tissue samples from two $p53^{\Delta 5\text{-}6/\Delta 5\text{-}6}$; $Pten^{+/\Delta}$, four $p53^{\Delta 5\text{-}6/\Delta 5\text{-}6}$; $Pten^{+/\Delta}$; $Rictor^{+/\Delta}$, five $p53^{\Delta 5\text{-}6/\Delta 5\text{-}6}$; $Pten^{+/\Delta}$; $Rictor^{\Delta/\Delta}$ medulloblastomas along with the various $Ptch1^{+/-}$ (i.e. $Ptch1^{+/-}$, $p53^{\Delta 5\text{-}6/\Delta 5\text{-}6}$; $Ptch1^{+/-}$, and $p53^{\Delta 5\text{-}6/R172P}$; $Ptch1^{+/-}$) SHH medulloblastoma models. Analysis also includes a normal cerebral cortex tissue (CTR), and two glioma control samples from $p53^{\Delta 5\text{-}6/\Delta 5\text{-}6}$; $Rictor^{+/\Delta}$ and $p53^{\Delta 5\text{-}6/\Delta 5\text{-}6}$; $Pten^{+/\Delta}$ mice (last two lanes).

Scale bars, 50 μm.

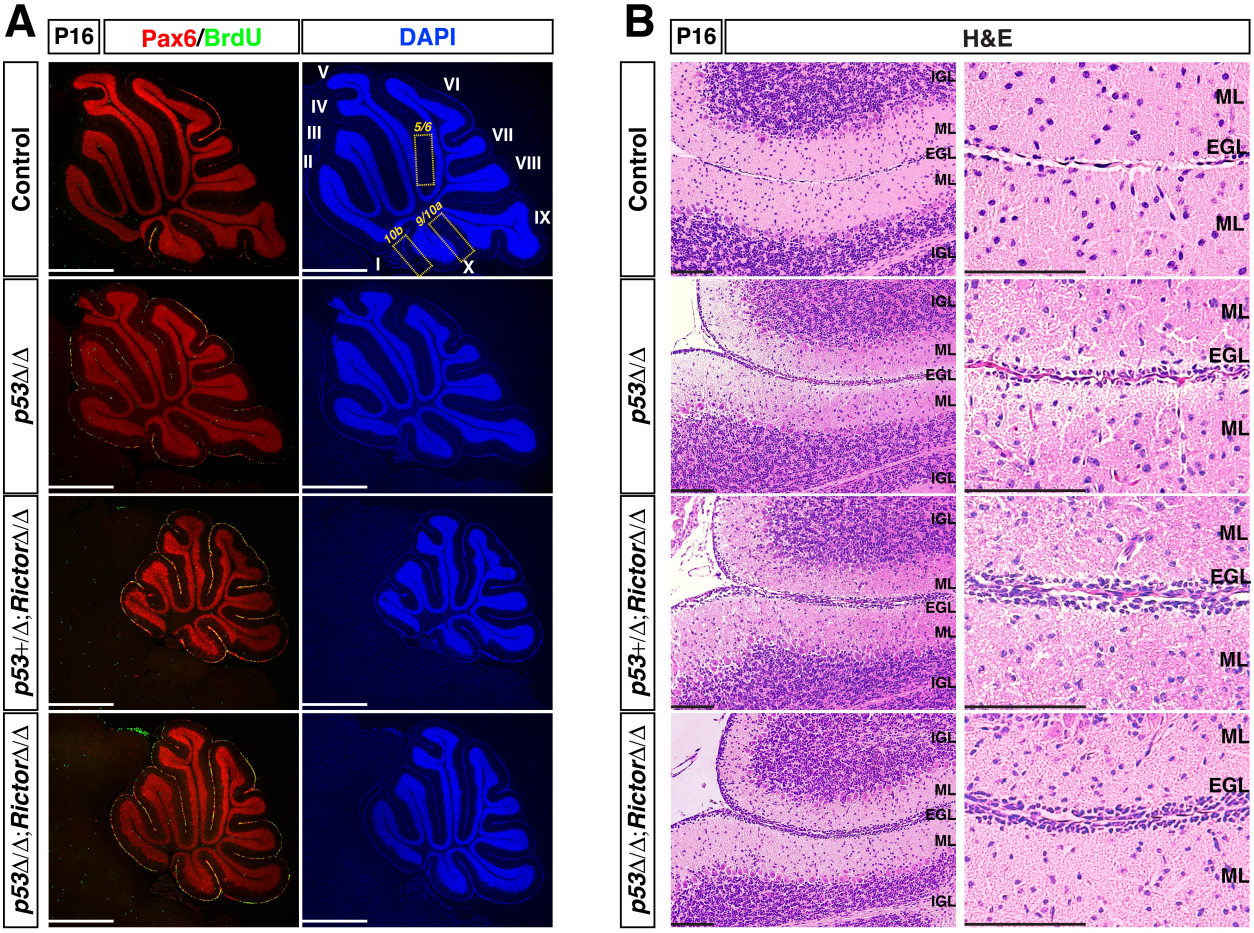
A
P16
Pax6/BrdU
DAPI
Control
p53Δ/Δ
p53+/Δ;RictorΔ/Δ
p53Δ/Δ;RictorΔ/Δ
V
VI
IV
III
II
VII
VIII
IX
I
X
5/6
9/10a
10b
B
P16
H&E
IGL
ML
EGL

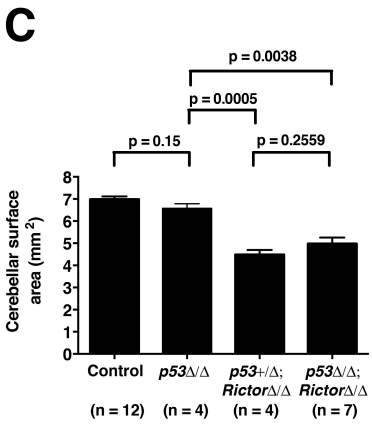
C
p = 0.0038
p = 0.0005
p = 0.15
p = 0.2559
Cerebellar surface area (mm2)
Control (n = 12)
p53Δ/Δ (n = 4)
p53+/Δ; RictorΔ/Δ (n = 4)
p53Δ/Δ; RictorΔ/Δ (n = 7)

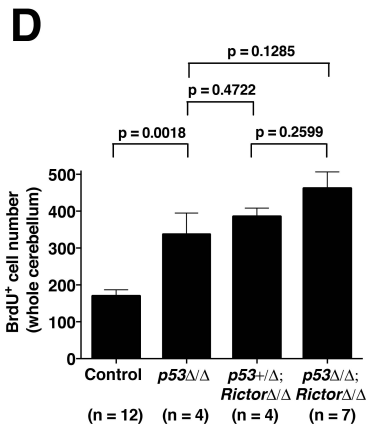
D
p = 0.1285
p = 0.4722
p = 0.0018
p = 0.2599
BrdU+ cell number (whole cerebellum)
Control (n = 12)
p53Δ/Δ (n = 4)
p53+/Δ; RictorΔ/Δ (n = 4)
p53Δ/Δ; RictorΔ/Δ (n = 7)

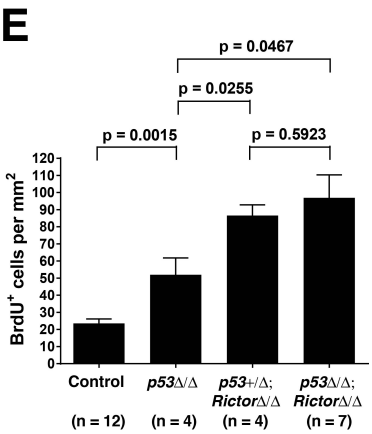
E
p = 0.0467
p = 0.0255
p = 0.0015
p = 0.5923
BrdU+ cells per mm2
Control (n = 12)
p53Δ/Δ (n = 4)
p53+/Δ; RictorΔ/Δ (n = 4)
p53Δ/Δ; RictorΔ/Δ (n = 7)

Figure 12. *Rictor*-deficient cerebella are characterized by ectopically proliferating granule neuron precursors (part-I).

(A-D) The control and mutant mice at P16 are injected with BrdU (10 mg/kg) twice every two hours. All the mice are sacrificed two hours after the last injection, followed by analyses of cellular proliferation.

(A) The overall cerebellar structure along with the $Pax6^{+}$ neural lineage cells and $BrdU^{+}$ proliferating cells are examined in P16 mice. Each folium is labeled with Roman numbers. Yellow frames indicate the three areas that are further analyzed.

(B) H&E staining showing Folium 9/10a (F-9/10a) of the cerebella from P16 control and mutant mice.

(C-D) The cerebellar surface area (mm^2) (C), total number of the $BrdU^{+}$ cells in the whole cerebella (D), and the total number of the cerebellar $BrdU^{+}$ proliferating cells per unit area (mm^2) (E) is calculated.

The data are presented as mean ± SD. Unpaired t-test is used to compare the groups statistically. Scale bars, 1 mm (A) and 100 μm (B). ML: Molecular layer, EGL: External granular layer.

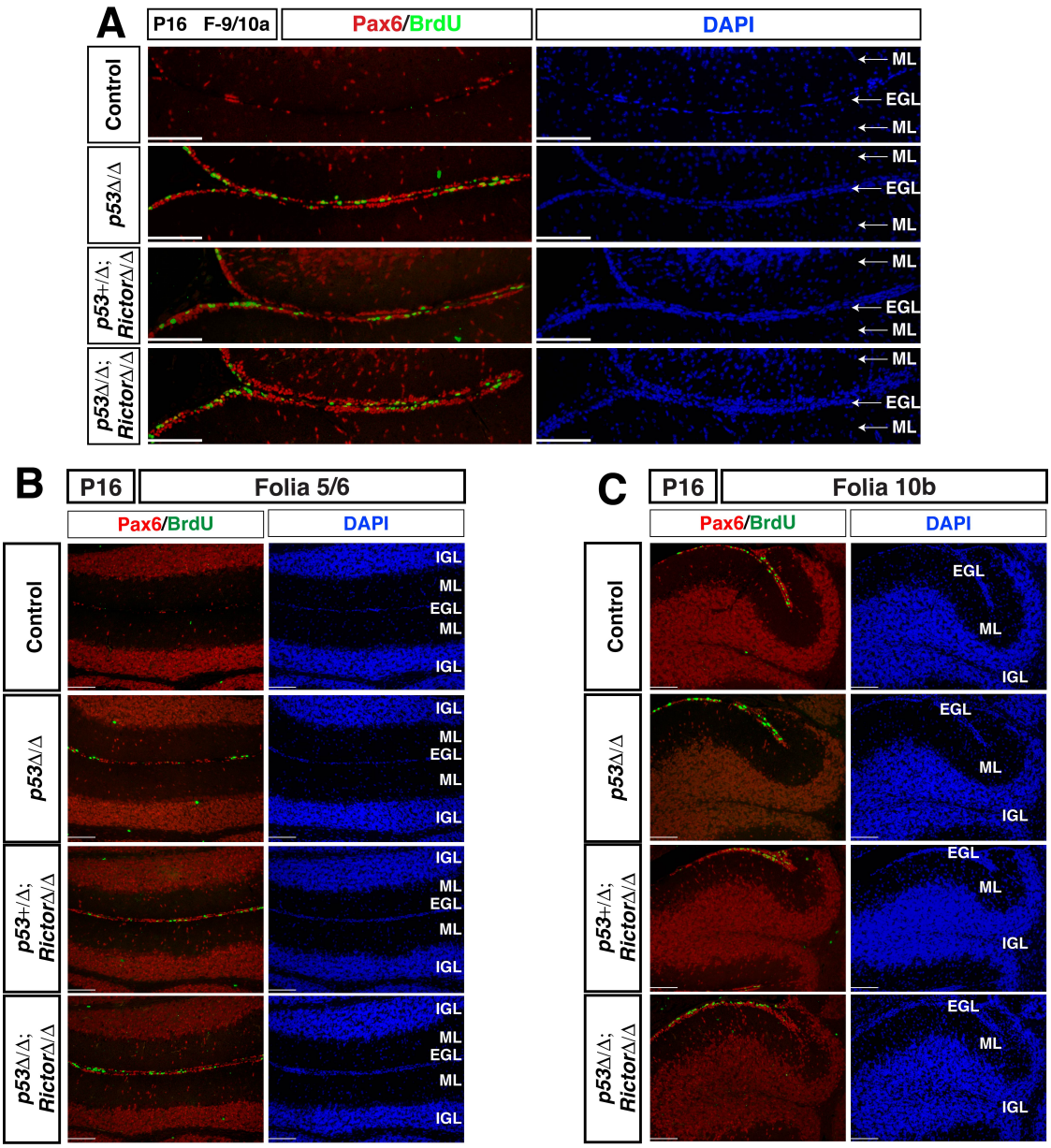
A
P16 F-9/10a
Pax6/BrdU
DAPI
Control
p53Δ/Δ
p53+/Δ; RictorΔ/Δ
p53Δ/Δ; RictorΔ/Δ
ML
EGL
B
P16
Folia 5/6
C
P16
Folia 10b
IGL
D
Control
p53Δ/Δ
p53+/Δ; RictorΔ/Δ
p53Δ/Δ; RictorΔ/Δ
Cell number (EGL-associated)
F-5/6
F-9/10a
F-10b
Pax6+BrdU-
Pax6+BrdU+

Figure 13. *Rictor*-deficient cerebella are characterized by ectopically proliferating granule neuron precursors (part-II).

(A-D) The control and mutant mice at P16 were injected with BrdU (10 mg/kg) twice every two hours. All the mice were sacrificed two hours after the last injection, followed by analyses of cellular proliferation.

(A-C) High magnification images of F-9/10a (A), F-5/6 (B) and F-10b (C) of P16 wild type control and mutant cerebella illustrating the $BrdU^{+}$ proliferating cells and $Pax6^{+}$ cells.

(D) EGL-associated $Pax6^{+}$ cells are quantified in relation to their BrdU content in F-5/6, F-9/10a and F-10b of the control and mutant cerebella.

All the quantification data are presented as mean ± SEM. Scale bars, 100 μm. IGL: Internal granular layer, ML: Molecular layer, EGL: External granular layer.

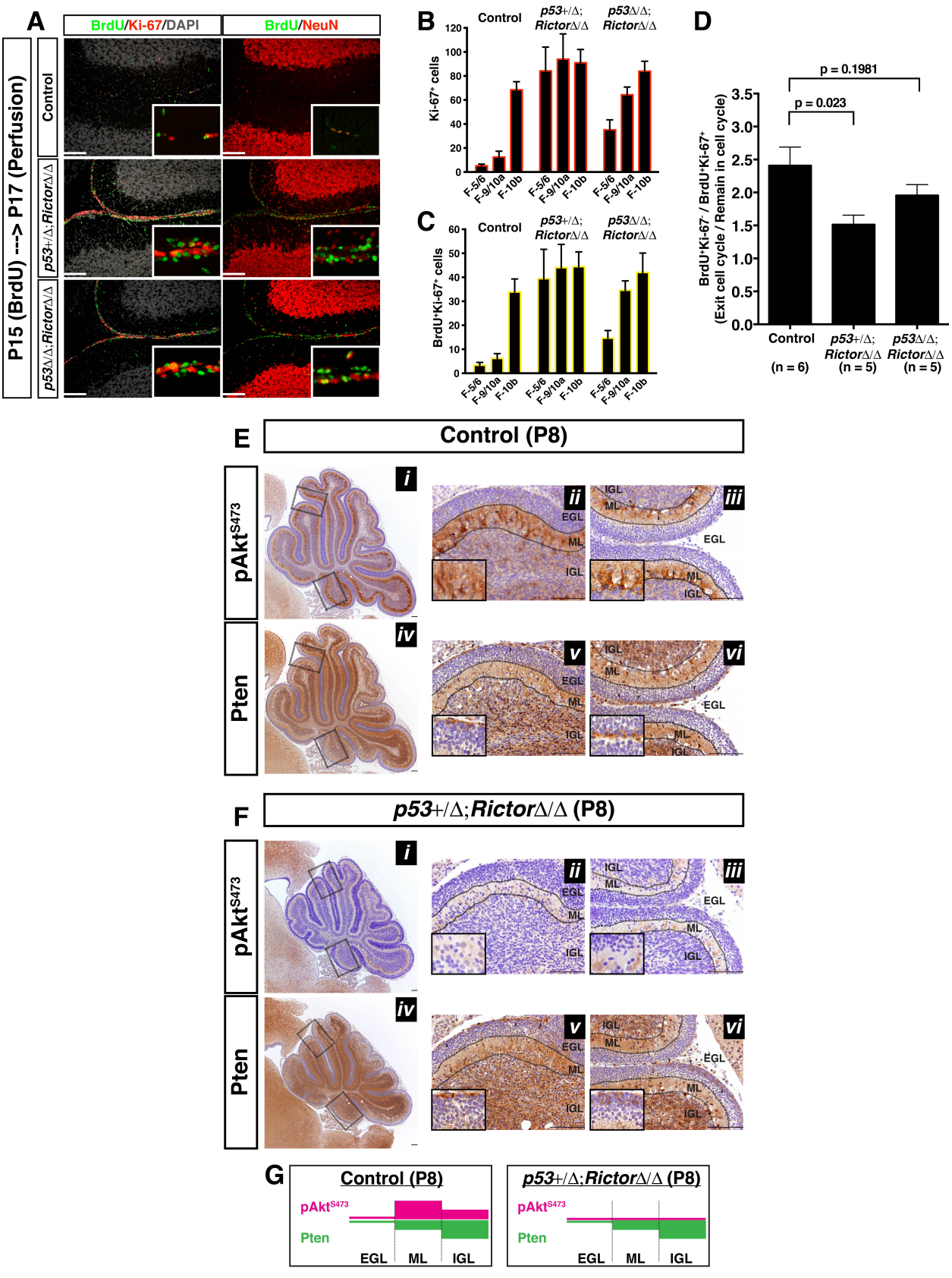
A
P15 (BrdU) ---> P17 (Perfusion)
Control
p53+/Δ;RictorΔ/Δ
p53Δ/Δ;RictorΔ/Δ
BrdU/Ki-67/DAPI
BrdU/NeuN
B
Control
p53+/Δ; RictorΔ/Δ
p53Δ/Δ; RictorΔ/Δ
Ki-67+ cells
F-5/6
F-9/10a
F-10b
C
BrdU+Ki-67+ cells
D
p = 0.1981
p = 0.023
BrdU+Ki-67+ / BrdU+Ki-67+
(Exit cell cycle / Remain in cell cycle)
Control
(n = 6)
p53+/Δ; RictorΔ/Δ
(n = 5)
p53Δ/Δ; RictorΔ/Δ
(n = 5)
E
Control (P8)
pAktS473
Pten
i
ii
iii
iv
v
vi
EGL
ML
IGL
F
p53+/Δ;RictorΔ/Δ (P8)
G
Control (P8)
p53+/Δ;RictorΔ/Δ (P8)
pAktS473
Pten
EGL
ML
IGL

Figure 14. A minor population of GNPs requires intact mTORC2/Akt signaling for proper differentiation.

(A-D) Cell cycle analysis is performed by injecting the mice with BrdU (10 mg/kg) once at P15 and analyzing at P17.

(A) The cells proliferating at P15 are labeled with BrdU (green), proliferating at P17 were labeled with Ki-67 (red), the cells that are in the cell cycle at both time points are $BrdU^{+}Ki\text{-}67^{+}$ (yellow). Fully differentiated neurons are labeled with NeuN (red). $BrdU^{+}NeuN^{+}$ cells indicate the mature neurons that are generated from progenitor cells proliferating between P15-P17. Insets show higher magnification view of the EGL cells. Images are taken from F-9/10a.

(B-C) Quantification of the cells from the experiment described above. Total $Ki\text{-}67^{+}$ cells (B) and $BrdU^{+}Ki\text{-}67^{+}$ cells (C) are counted.

(D) The cell cycle exit index is calculated by the ratio of $BrdU^{+}Ki\text{-}67^{-}/BrdU^{+}Ki\text{-}67^{+}$.

(E-F) Immunohistochemistry analysis of $pAkt^{S473}$ and Pten expression in P8 control (E) and $Rictor^{\Delta/\Delta}$ (F) cerebella. Boxed regions in the whole cerebella are depicted at higher magnification. Insets show higher magnification at ML (*ii* and *iii*) or EGL (*v* and *vi*).

(G) Illustration of the differential expression of $pAkt^{S473}$ and Pten in the P8 control and $Rictor^{\Delta/\Delta}$ cerebella. Pten expression is shown in green and $pAkt^{S473}$ is shown in pink. The thickness of the bars depicts the relative expression levels.

The data are presented as mean ± SD. Unpaired t-test is used to compare the groups statistically. IGL: Internal granular layer, ML: Molecular layer, EGL: External granular layer. Scale bars, 100 μm.

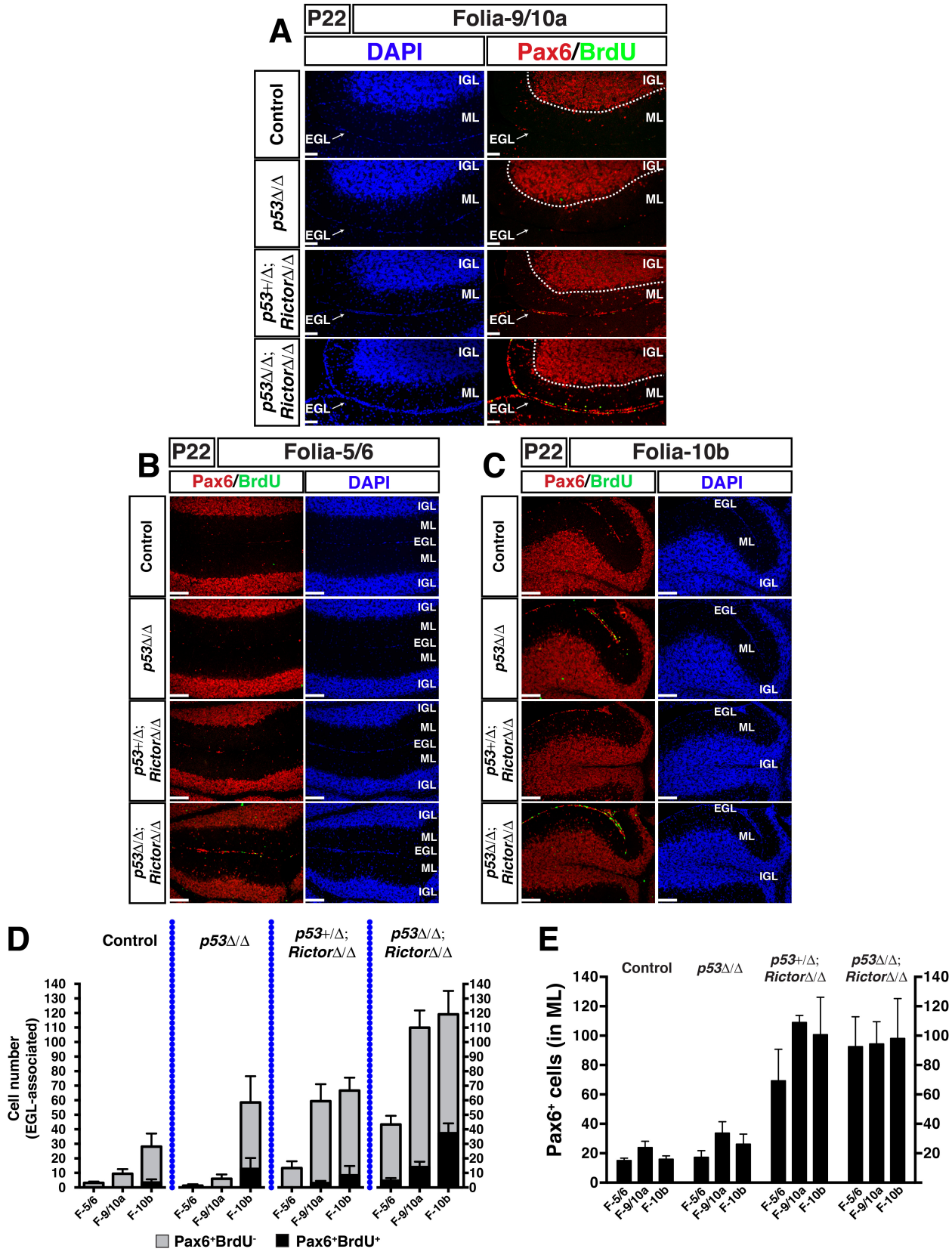
A
P22
Folia-9/10a
DAPI
Pax6/BrdU
Control
p53Δ/Δ
p53+/Δ; RictorΔ/Δ
p53Δ/Δ; RictorΔ/Δ
IGL
ML
EGL
B
P22
Folia-5/6
Pax6/BrdU
DAPI
C
P22
Folia-10b
Pax6/BrdU
DAPI
D
Control
p53Δ/Δ
p53+/Δ; RictorΔ/Δ
p53Δ/Δ; RictorΔ/Δ
Cell number (EGL-associated)
F-5/6
F-9/10a
F-10b
Pax6+BrdU-
Pax6+BrdU+
E
Pax6+ cells (in ML)

Figure 15. Ectopically proliferating GNPs are maintained in postnatal *Rictor*-deficient cerebella.

(A-D) The control and mutant mice at P22 are injected with BrdU (10 mg/kg) twice every two hours. All the mice are sacrificed two hours after the last injection.

(A-C) $Pax6^{+}$ cells and $BrdU^{+}$ proliferating cells are examined in P22 mice. The representative images are from F-9/10a (A), F-5/6 (B) and F-10b (C).

(D) EGL-associated $Pax6^{+}$ cells are quantified in relation to their BrdU content in F-5/6, F-9/10a and F-10b of the control and mutant cerebella.

(E) Total $Pax6^{+}$ cells located in ML are quantified in F-5/6, F-9/10a and F-10b of the control and mutant cerebella.

All the quantification data are presented as mean ± SEM. Scale bars, 100 μm. IGL: Internal granular layer, ML: Molecular layer, EGL: External granular layer. Arrows in (A) point the EGL layers.

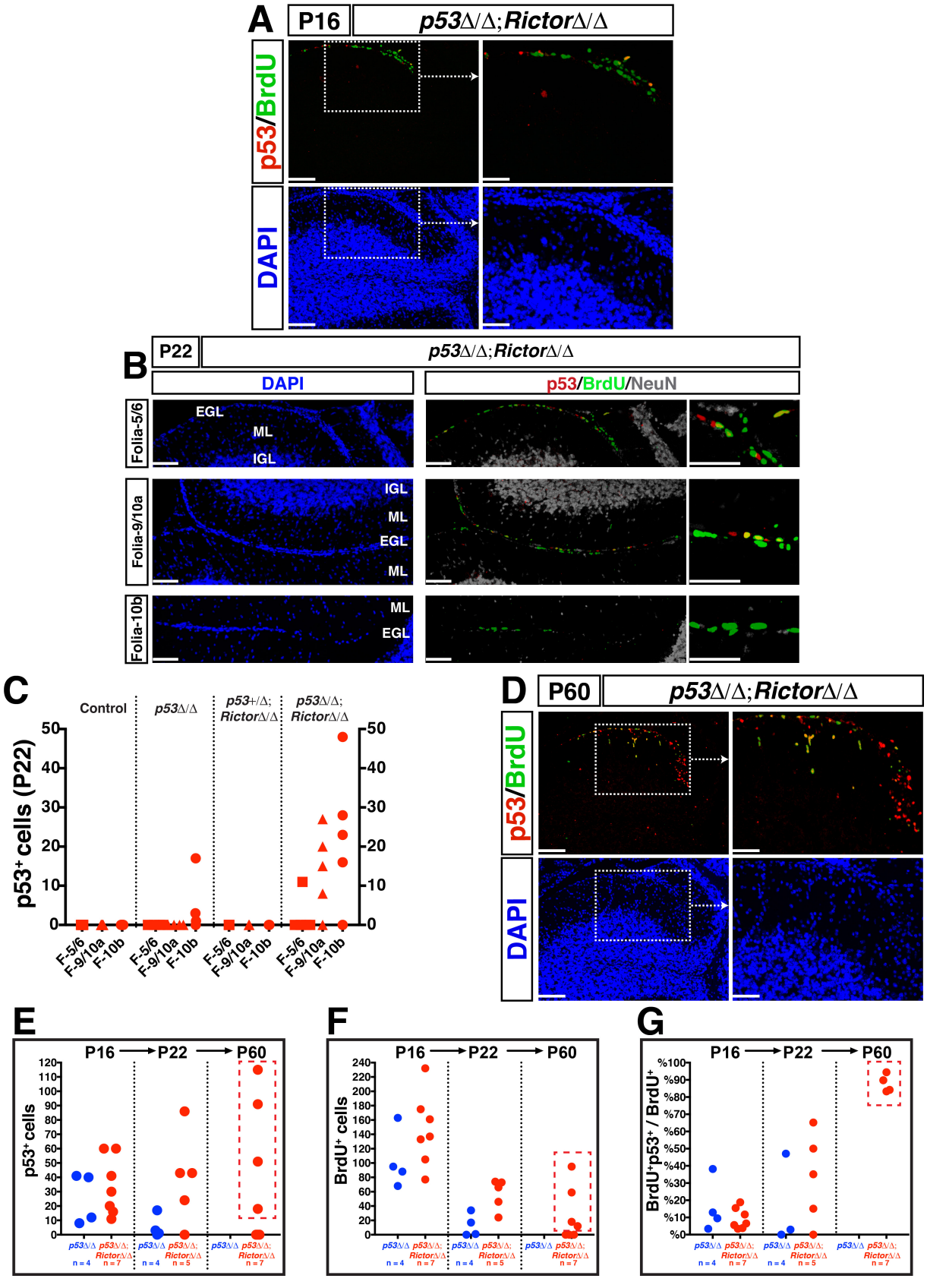
A
P16
p53Δ/Δ;RictorΔ/Δ
p53/BrdU
DAPI
B
P22
p53Δ/Δ;RictorΔ/Δ
DAPI
p53/BrdU/NeuN
Folia-5/6
Folia-9/10a
Folia-10b
EGL
ML
IGL
C
Control
p53Δ/Δ
p53+/Δ; RictorΔ/Δ
p53Δ/Δ; RictorΔ/Δ
p53+ cells (P22)
F-5/6
F-9/10a
F-10b
D
P60
p53Δ/Δ;RictorΔ/Δ
p53/BrdU
DAPI
E
P16 → P22 → P60
p53+ cells
F
P16 → P22 → P60
BrdU+ cells
G
P16 → P22 → P60
BrdU+p53+ / BrdU+
p53Δ/Δ
p53Δ/Δ; RictorΔ/Δ
n = 4
n = 7
n = 5

Figure 16. *Rictor*-deficient ectopically proliferating GNPs transform into early-tumor forming cells in the absence of *p53*.

(A-G) The control and mutant mice at P16 and P22 are injected with BrdU (10 mg/kg) twice, while P60 mice are injected three times every two hours. All the mice are sacrificed two hours after the last injection, followed by analyses of cellular proliferation.

(A, B and D) Proliferating $p53^{+}$ cells in $p53^{\Delta 5\text{-}6/\Delta 5\text{-}6}$; $Rictor^{\Delta/\Delta}$ cerebella are examined at P16 (A), P22 (B) and P60 (D) using p53 and BrdU antibodies. Neuronal populations ($NeuN^{+}$) are also shown for P22 brains in (B). Boxed areas indicate the regions where higher magnification images are taken.

(C) The total number of the $p53^{+}$ cells in F-5/6, F-9/10a, and F-10b of P22 control and mutant cerebella is quantified.

(E-G) Quantification of the cells from the experiments described above.

The number of the $p53^{+}$ cells (E) and $BrdU^{+}$ cells (F) in $p53^{\Delta 5\text{-}6/\Delta 5\text{-}6}$ and $p53^{\Delta 5\text{-}6/\Delta 5\text{-}6}$; $Rictor^{\Delta/\Delta}$ cerebella is calculated over three time points – P16, P22 and P60. The frequency of the proliferating $p53^{+}$ cells among the entire proliferating population is calculated by the ratio of $BrdU^{+}p53^{+}/BrdU^{+}$ (G).

Scale bars, 50 μm. IGL: Internal granular layer, ML: Molecular layer, EGL: External granular layer. Arrows point the EGL layers.

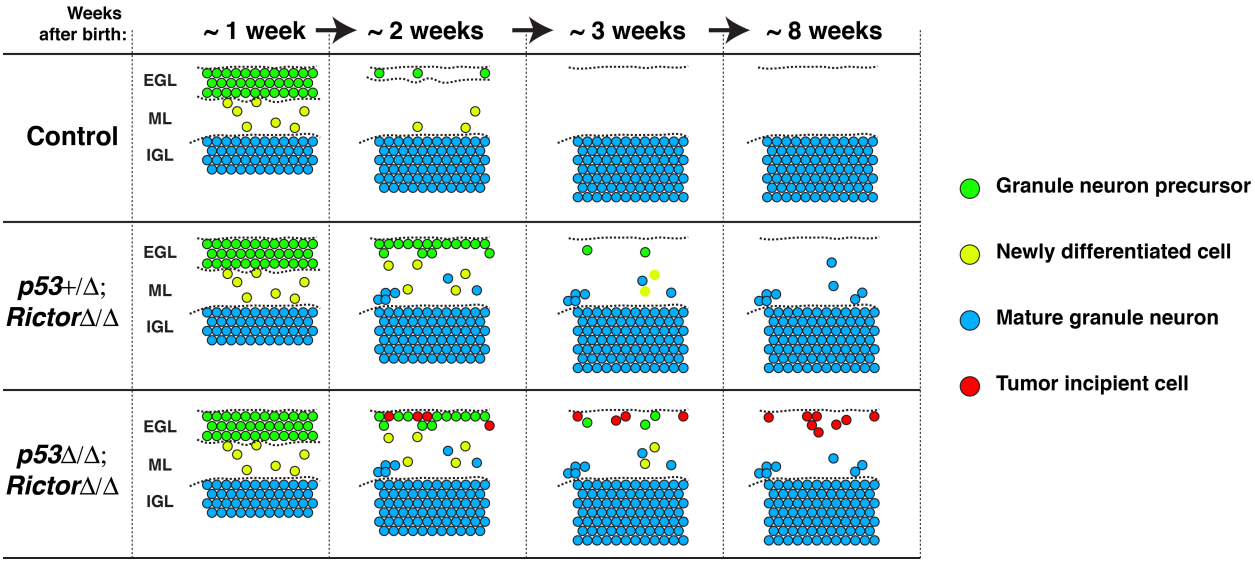

Figure 17. Schematic representation of the different cell populations in wild type control and mutant cerebella during the development.

Wild type control cerebellum completes its maturation around P16, and virtually lacks proliferating GNPs after then. *p53*+/Δ; *Rictor*Δ/Δ cerebellum, on the other hand, temporarily maintains a subpopulation of proliferating GNPs past P16. Despite of a delay, these cells abnormally differentiate in different regions of the cerebellum, including the ML, by possibly p53-dependent mechanisms. Evidenced by their mutant-p53 expression, a subset of ectopically proliferating GNPs acquires cellular stress and possibly transform into early tumor-forming cells in the absence of *p53* (e.g. *p53*Δ/Δ; *Rictor*Δ/Δ).

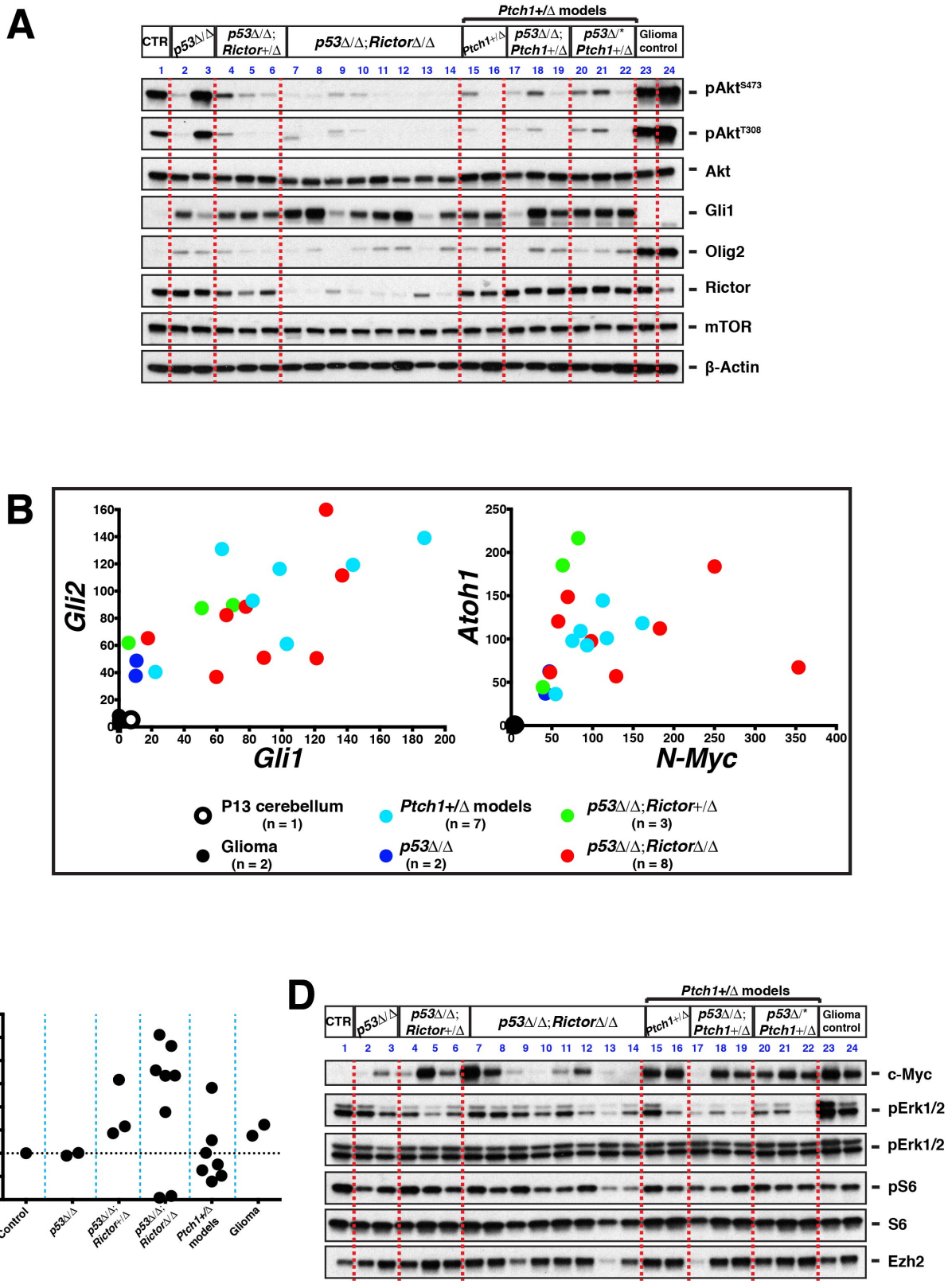
A
Ptch1+/Δ models
CTR
p53Δ/Δ
p53Δ/Δ; Rictor+/Δ
p53Δ/Δ;RictorΔ/Δ
Ptch1+/Δ
p53Δ/Δ; Ptch1+/Δ
p53Δ/* Ptch1+/Δ
Glioma control
1 2 3 4 5 6 7 8 9 10 11 12 13 14 15 16 17 18 19 20 21 22 23 24
pAktS473
pAktT308
Akt
Gli1
Olig2
Rictor
mTOR
β-Actin
B
Gli2
Gli1
Atoh1
N-Myc
P13 cerebellum (n = 1)
Glioma (n = 2)
Ptch1+/Δ models (n = 7)
p53Δ/Δ (n = 2)
p53Δ/Δ;Rictor+/Δ (n = 3)
p53Δ/Δ;RictorΔ/Δ (n = 8)
C
Ptch1 Expression
Control
p53Δ/Δ
p53Δ/Δ; Rictor+/Δ
p53Δ/Δ; RictorΔ/Δ
Ptch1+/Δ models
Glioma
D
Ptch1+/Δ models
CTR
p53Δ/Δ
p53Δ/Δ; Rictor+/Δ
p53Δ/Δ;RictorΔ/Δ
Ptch1+/Δ
p53Δ/Δ; Ptch1+/Δ
p53Δ/* Ptch1+/Δ
Glioma control
1 2 3 4 5 6 7 8 9 10 11 12 13 14 15 16 17 18 19 20 21 22 23 24
c-Myc
pErk1/2
pErk1/2
pS6
S6
Ezh2

Figure 18. Mutant-*p53*-*Rictor* induced medulloblastomas share molecular events with *Ptch1*$^{+/-}$ tumors.

(A and D) Western blotting analysis of the *p53*$^{\Delta 5\text{-}6/\Delta 5\text{-}6}$, *p53*$^{\Delta 5\text{-}6/\Delta 5\text{-}6}$; *Rictor*$^{+/\Delta}$, and *p53*$^{\Delta 5\text{-}6/\Delta 5\text{-}6}$; *Rictor*$^{\Delta/\Delta}$ medulloblastoma samples along with the various *Ptch1*$^{+/-}$ (i.e. *Ptch1*$^{+/-}$, *p53*$^{\Delta 5\text{-}6/\Delta 5\text{-}6}$; *Ptch1*$^{+/-}$, and *p53*$^{\Delta 5\text{-}6/R172P}$; *Ptch1*$^{+/-}$) models. Wild type cerebellar tissue is used as a control (CTR), and two glioma samples from *p53*$^{\Delta 5\text{-}6/\Delta 5\text{-}6}$; *Rictor*$^{+/\Delta}$ and *p53*$^{\Delta 5\text{-}6/\Delta 5\text{-}6}$; *Pten*$^{+/\Delta}$ (last two lanes) are also included into the analysis.

(B-C) RT-PCR experiments were performed using cDNAs from the mutant-*p53* medulloblastomas in comparison with the *Ptch1*$^{+/-}$ models.

The average expression levels of each *Gli1*, *Gli2*, *N-Myc* and *Atoh1* (B) and *Ptch1* (C) genes for the *Ptch1*$^{+/-}$ tumors are set to 100 and all of the samples are calculated accordingly. Two glioma samples and a P13 normal cerebellar tissue are used as negative controls.

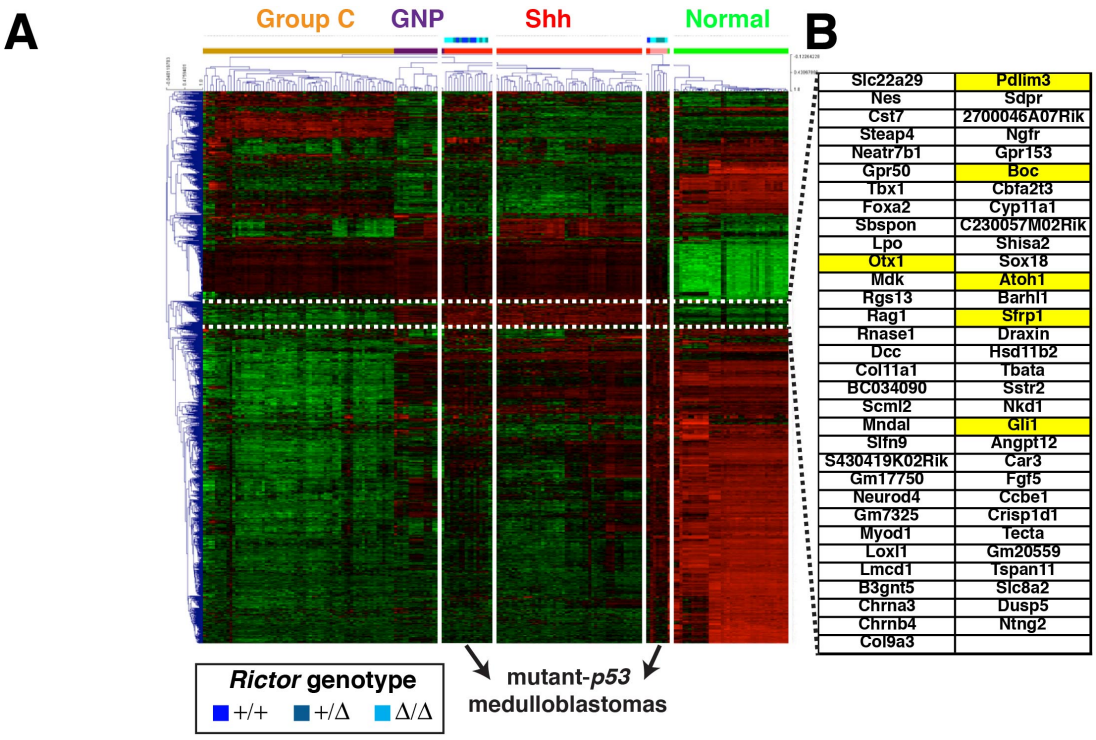
A
Group C
GNP
Shh
Normal
B
Slc22a29 Pdlim3
Nes Sdpr
Cst7 2700046A07Rik
Steap4 Ngfr
Neatr7b1 Gpr153
Gpr50 Boc
Tbx1 Cbfa2t3
Foxa2 Cyp11a1
Sbspon C230057M02Rik
Lpo Shisa2
Otx1 Sox18
Mdk Atoh1
Rgs13 Barhl1
Rag1 Sfrp1
Rnase1 Draxin
Dcc Hsd11b2
Col11a1 Tbata
BC034090 Sstr2
Scml2 Nkd1
Mndal Gli1
Slfn9 Angpt12
S430419K02Rik Car3
Gm17750 Fgf5
Neurod4 Ccbe1
Gm7325 Crisp1d1
Myod1 Tecta
Loxl1 Gm20559
Lmcd1 Tspan11
B3gnt5 Slc8a2
Chrna3 Dusp5
Chrnb4 Ntng2
Col9a3
Rictor genotype
+/+ +/Δ Δ/Δ
mutant-p53
medulloblastomas

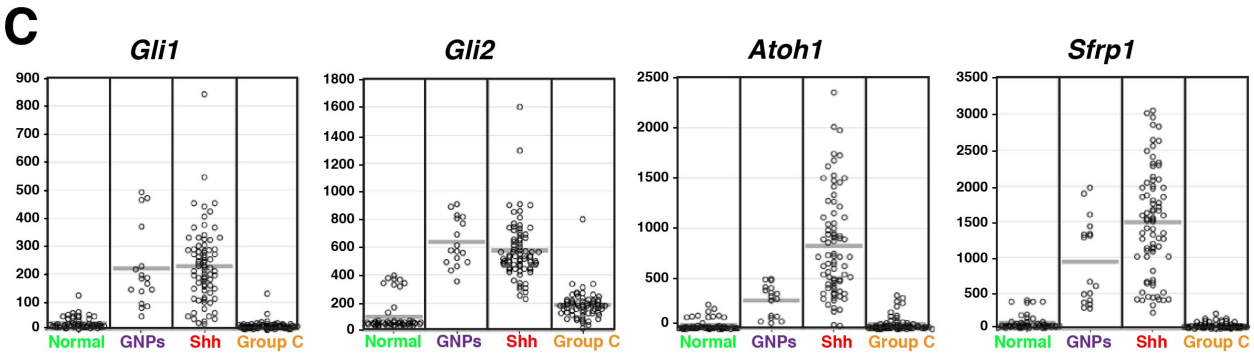
C
Gli1
Gli2
Atoh1
Sfrp1
Normal GNPs Shh Group C

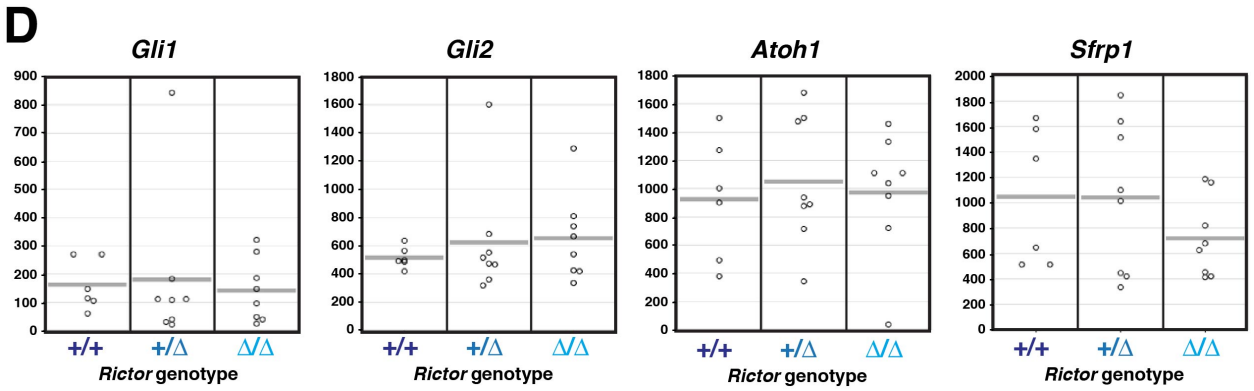
D
Gli1
Gli2
Atoh1
Sfrp1
+/+ +/Δ Δ/Δ
Rictor genotype

Figure 19. *Rictor* deficiency facilitates mutant-*p53* driven medulloblastomas that resemble human SHH medulloblastomas.

(A-B) Heatmap representation of the microarray analysis illustrating the gene expression prolife of the mutant-*p53* medulloblastomas in comparison with the previously established SHH GEM medulloblastomas.

The expression profiles of the Group C medulloblastomas, GNPs and normal tissues are also included into the array. An area containing the genes that are specifically upregulated in the SHH tumors is highlighted with a dashed white box (A). The genes that are found in the white-dashed area are listed, and the important ones are highlighted in yellow (B).

Samples used in this analysis: three $p53^{-/-}$, two $p53^{\Delta 5\text{-}6/\Delta 5\text{-}6}$; $Rictor^{+/\Delta}$, five $p53^{\Delta 5\text{-}6/\Delta 5\text{-}6}$; $Rictor^{\Delta/\Delta}$, three $p53^{\Delta 5\text{-}6/\Delta 5\text{-}6}$; $Pten^{+/\Delta}$, six $p53^{\Delta 5\text{-}6/\Delta 5\text{-}6}$; $Pten^{+/\Delta}$; $Rictor^{+/\Delta}$ (three of which had germline *Rictor* mutation) and three $p53^{\Delta 5\text{-}6/\Delta 5\text{-}6}$; $Pten^{+/\Delta}$; $Rictor^{\Delta/\Delta}$.

(C) Detailed gene expression analyses of *Gli1*, *Gli2*, *Atoh1*, and *Sfrp1* (SHH medulloblastoma signature genes).

(D) Microarray gene expression levels of *Gli1*, *Gli2*, *Atoh1* and *Sfrp1* are examined in relation to *Rictor* status of mutant-*p53* mediated GEM medulloblastomas.

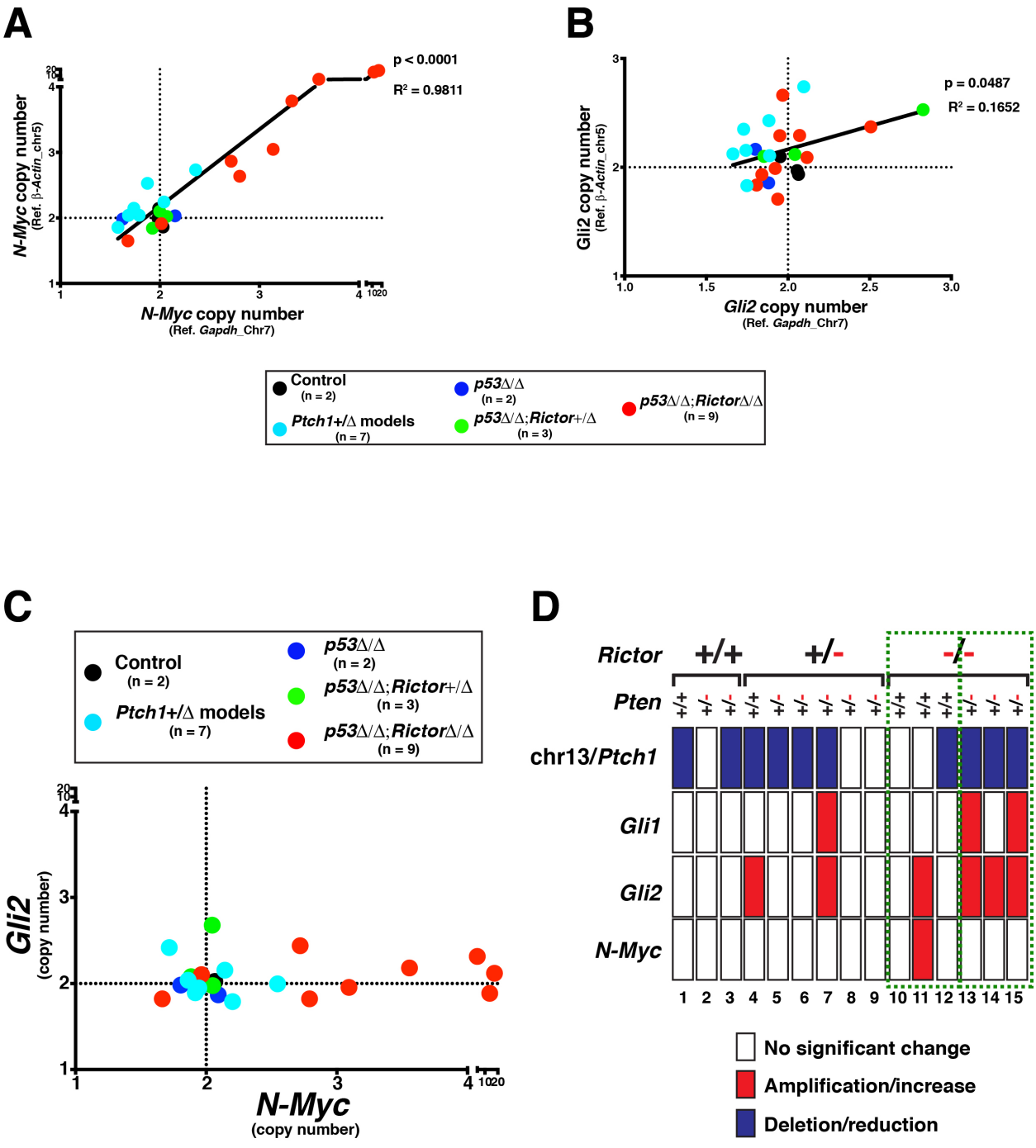
A
p < 0.0001
R² = 0.9811
N-Myc copy number
(Ref. β-Actin_chr5)
N-Myc copy number
(Ref. Gapdh_Chr7)
B
p = 0.0487
R² = 0.1652
Gli2 copy number
(Ref. β-Actin_chr5)
Gli2 copy number
(Ref. Gapdh_Chr7)
Control
(n = 2)
Ptch1+/Δ models
(n = 7)
p53Δ/Δ
(n = 2)
p53Δ/Δ;Rictor+/Δ
(n = 3)
p53Δ/Δ;RictorΔ/Δ
(n = 9)
C
Control
(n = 2)
Ptch1+/Δ models
(n = 7)
p53Δ/Δ
(n = 2)
p53Δ/Δ;Rictor+/Δ
(n = 3)
p53Δ/Δ;RictorΔ/Δ
(n = 9)
Gli2
(copy number)
N-Myc
(copy number)
D
Rictor
+/+
+/-
-/-
Pten
chr13/Ptch1
Gli1
Gli2
N-Myc
1 2 3 4 5 6 7 8 9 10 11 12 13 14 15
No significant change
Amplification/increase
Deletion/reduction

Figure 20. *Rictor*-deficient medulloblastomas are distinguished from other SHH GEM medulloblastomas by their gene amplification events.

(A-B) Copy number estimates of each *N-Myc* (A) and *Gli2* (B) genes based on two different reference genes (*β-Actin* on chr5 and *Gapdh* on chr7) are compared. The readings of both *N-Myc* and *Gli2* in relation to *β-Actin* showed highly similar results to those in relation to *Gapdh,* indicating the accuracy of the analysis.

(C) Copy number estimates of the *N-Myc* and *Gli2* genes in $p53^{\Delta 5\text{-}6/\Delta 5\text{-}6}$, $p53^{\Delta 5\text{-}6/\Delta 5\text{-}6}$; $Rictor^{+/\Delta}$, and $p53^{\Delta 5\text{-}6/\Delta 5\text{-}6}$; $Rictor^{\Delta/\Delta}$ medulloblastomas in comparison to $Ptch1^{+/-}$ tumors. Copy numbers were calculated by a series of RT-PCR experiments using the tumor genomic DNA as template. *β-Actin* in chr5 and *Gapdh* in chr7 were used as internal reference genes for each sample. Wild-type controls were set to "2" and all of the samples were calculated accordingly.

(D) Low-coverage copy number analysis of chr13/*Ptch1*, *Gli1*, *Gli2* and *N-Myc* was performed using various mutant-*p53* mediated medulloblastomas. All the tumors had mutant *p53* genes, and the status of *Rictor* and *Pten* is indicated.

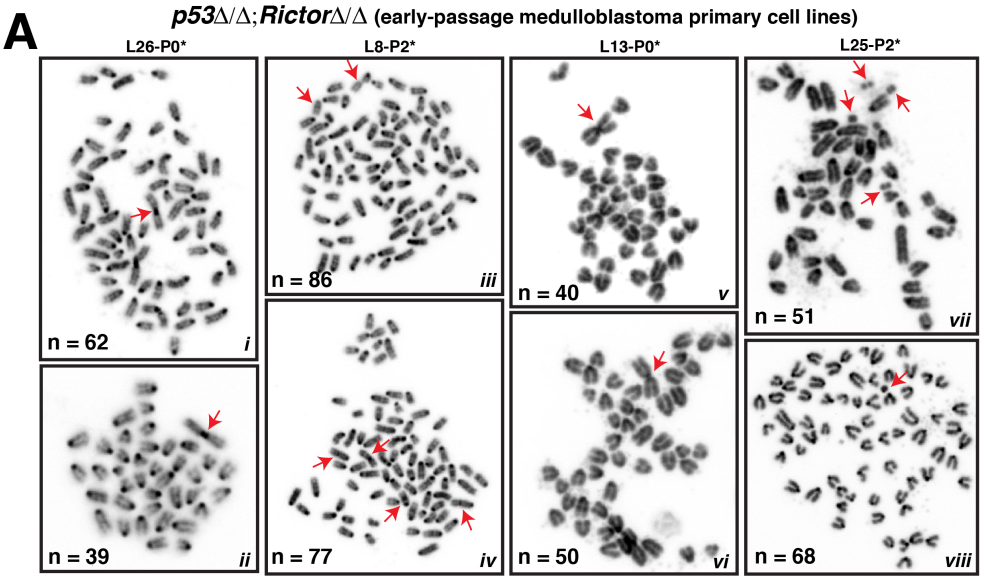
A
p53Δ/Δ;RictorΔ/Δ (early-passage medulloblastoma primary cell lines)
L26-P0*
L8-P2*
L13-P0*
L25-P2*
n = 62
i
n = 86
iii
n = 40
v
n = 51
vii
n = 39
ii
n = 77
iv
n = 50
vi
n = 68
viii

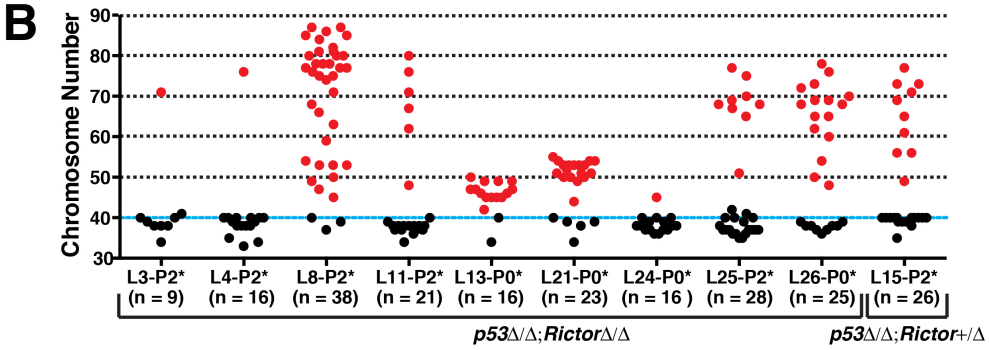
B
Chromosome Number
90
80
70
60
50
40
30
L3-P2* (n = 9)
L4-P2* (n = 16)
L8-P2* (n = 38)
L11-P2* (n = 21)
L13-P0* (n = 16)
L21-P0* (n = 23)
L24-P0* (n = 16)
L25-P2* (n = 28)
L26-P0* (n = 25)
L15-P2* (n = 26)
p53Δ/Δ;RictorΔ/Δ
p53Δ/Δ;Rictor+/Δ

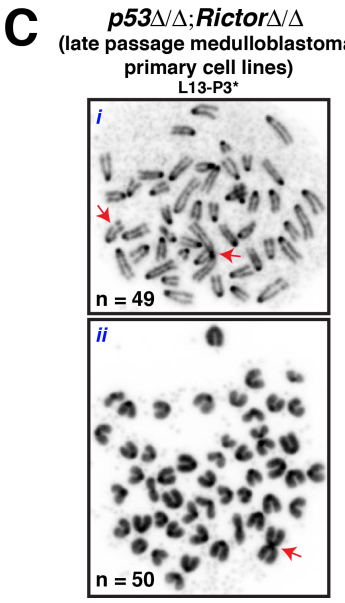
C
p53Δ/Δ;RictorΔ/Δ
(late passage medulloblastoma primary cell lines)
L13-P3*
i
n = 49
ii
n = 50

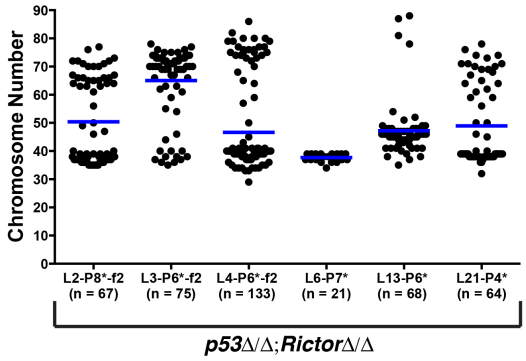
D
Chromosome Number
90
80
70
60
50
40
30
20
10
0
L2-P8*-f2 (n = 67)
L3-P6*-f2 (n = 75)
L4-P6*-f2 (n = 133)
L6-P7* (n = 21)
L13-P6* (n = 68)
L21-P4* (n = 64)
p53Δ/Δ;RictorΔ/Δ

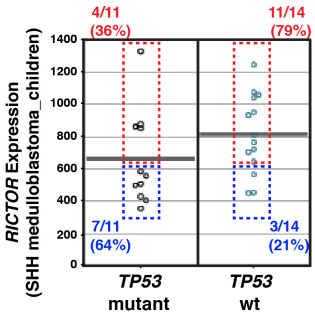
E
RICTOR Expression (SHH medulloblastoma_children)
4/11 (36%)
11/14 (79%)
7/11 (64%)
3/14 (21%)
1400
1200
1000
800
600
400
200
0
TP53 mutant
TP53 wt

Figure 21. Chromosomal abnormalities are readily detectable in *Rictor*-deficient medulloblastomas.

(A) Chromosome metaphase assay is performed in order to examine the structure and number of the chromosomes in $p53^{\Delta 5\text{-}6/\Delta 5\text{-}6}$; $Rictor^{\Delta/\Delta}$ early-passage (passage number ≤ 2) cell lines. Head-to-head fusions (*i*, *ii*, *iv*, *v* and *vi*), head-to-tail fusions or translocations (*iv*) and centrosome loss (*iii*), double minute chromosomes (*vii*), and centrosome pieces (*viii*) are pointed with red arrows.
(B) The chromosome numbers were quantified in nine $p53^{\Delta 5\text{-}6/\Delta 5\text{-}6}$; $Rictor^{\Delta/\Delta}$ and one $p53^{\Delta 5\text{-}6/\Delta 5\text{-}6}$; $Rictor^{+/\Delta}$ early passage cell lines. The cells with clear aneuploidy are shown with red dots while others are black.
(C) Chromosomes from late-passage (passage number ≥ 3) $p53^{\Delta 5\text{-}6/\Delta 5\text{-}6}$; $Rictor^{\Delta/\Delta}$ cell lines are examined. Chromosome break (*i*) and chromosome fusion (*i* and *ii*) are pointed with red arrows.
(D) The chromosome numbers are quantified in late-passage (passage number ≥ 3) $p53^{\Delta 5\text{-}6/\Delta 5\text{-}6}$; $Rictor^{\Delta/\Delta}$ cell lines. Mean value is indicated.
(E) *RICTOR* expression within SHH childhood medulloblastomas with or without *TP53* mutation. Samples in blue frames have expression levels ≤ 600, samples in red frames have expression levels > 600.

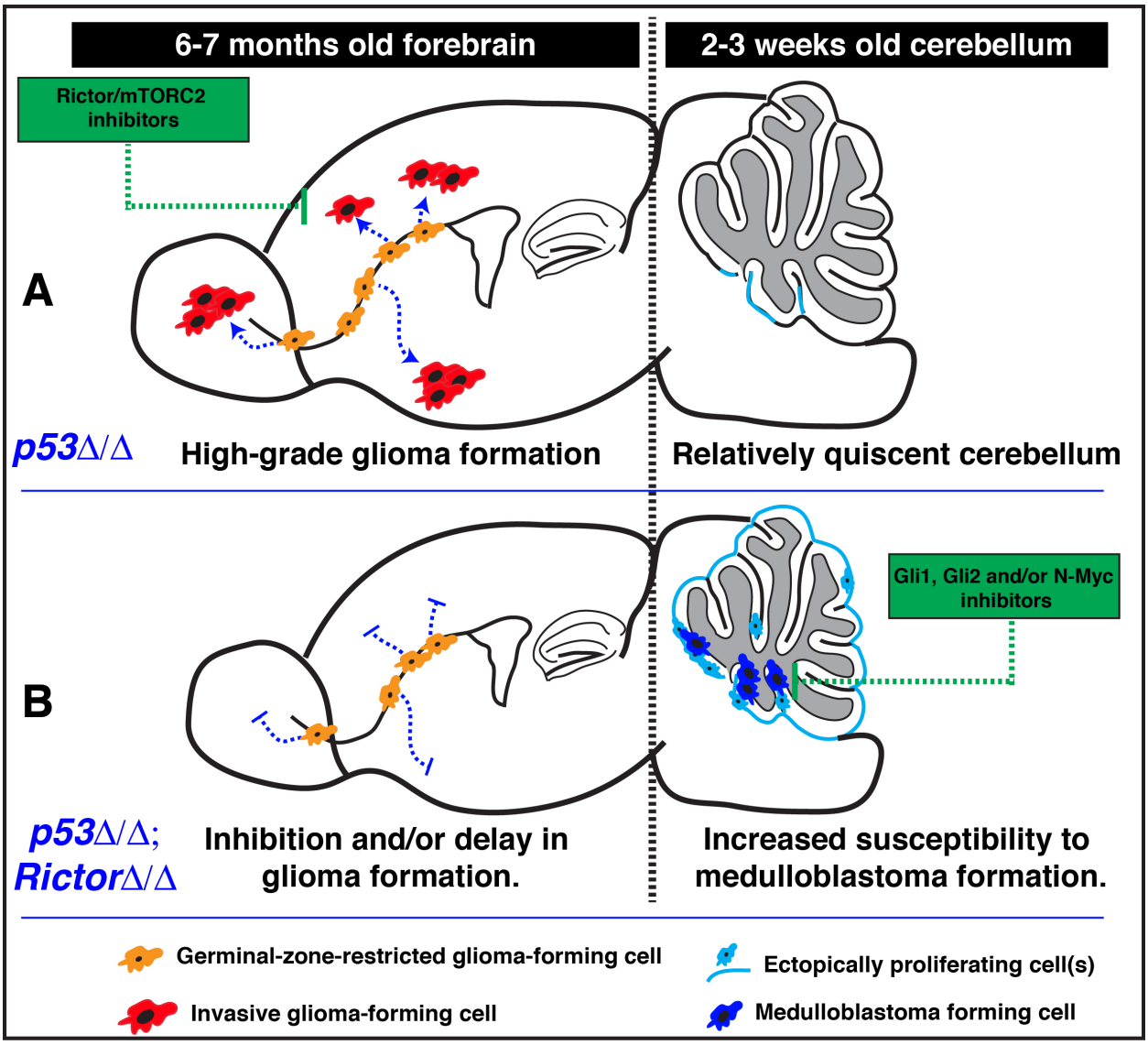
6-7 months old forebrain
2-3 weeks old cerebellum
Rictor/mTORC2 inhibitors
A
p53Δ/Δ
High-grade glioma formation
Relatively quiscent cerebellum
B
Gli1, Gli2 and/or N-Myc inhibitors
p53Δ/Δ; Rictor Δ/Δ
Inhibition and/or delay in glioma formation.
Increased susceptibility to medulloblastoma formation.
Germinal-zone-restricted glioma-forming cell
Invasive glioma-forming cell
Ectopically proliferating cell(s)
Medulloblastoma forming cell

Figure 22. Schematic representation of the brain tumorigenesis distinctively regulated by Rictor/mTORC2 signaling pathway.

(A) Early glioma cells or glioma-forming cells (orange cells) in an adult *p53*Δ/Δ forebrain require intact Rictor/mTORC2 signaling in order to expand outside the germinal zones, and invade the surrounding tissue. These cells may migrate several remote locations of the brain to form clusters (red cells) leading to glioma development. *p53*-mutant cerebellum, on the other hand, mostly develops properly, and becomes a quiescent organ throughout the organism's life span. Only in rare cases mutations in *p53* gene can lead to medulloblastoma development.
(B) *Rictor* deficiency inhibits the initial expansion of the early glioma cells or glioma-forming cells (orange cells) in an adult *p53*Δ/Δ; *Rictor*Δ/Δ forebrain. These cells remain restricted to the germinal zones, and do not display an expansion to the surrounding areas. It should be noted that some of those cells may eventually escape from this restriction and form high-grade gliomas at very late stages. *Rictor*-deficient neonatal cerebellum is characterized by the ectopically proliferating cerebellar progenitor cells (light blue cells or lines), some of which might have already acquired tumorigenic potential driven by *p53* mutation (dark blue cells). *Rictor* deficiency facilitates the formation of mutant-*p53* driven medulloblastomas that carry gene amplifications in downstream components of the Shh signaling pathway.
Based on these two major findings, inhibition of Rictor/mTORC2 signaling in malignant gliomas may have therapeutic potential in a group of adult patients, but not pediatric cases. Medulloblastomas that are driven by mutant-*p53* and carry gene amplifications in Shh signaling pathway components will likely need novel therapies, including Gli1, Gli2 and N-Myc inhibitors.

3.4 References

Amakye, D., Jagani, Z. and Dorsch, M. (2013). Unraveling the therapeutic potential of the Hedgehog pathway in cancer. *Nature medicine* **19**, 1410-1422.

Berman, D. M., Karhadkar, S. S., Hallahan, A. R., Pritchard, J. I., Eberhart, C. G., Watkins, D. N., Chen, J. K., Cooper, M. K., Taipale, J., Olson, J. M., et al. (2002). Medulloblastoma growth inhibition by hedgehog pathway blockade. *Science* **297**, 1559-1561.

Engelkamp, D., Rashbass, P., Seawright, A. and van Heyningen, V. (1999). Role of Pax6 in development of the cerebellar system. *Development* **126**, 3585-3596.

Gajjar, A. J. and Robinson, G. W. (2014). Medulloblastoma-translating discoveries from the bench to the bedside. *Nature reviews. Clinical oncology* **11**, 714-722.

Gibson, P., Tong, Y., Robinson, G., Thompson, M. C., Currle, D. S., Eden, C., Kranenburg, T. A., Hogg, T., Poppleton, H., Martin, J., et al. (2010). Subtypes of medulloblastoma have distinct developmental origins. *Nature* **468**, 1095-1099.

Gilbertson, R. J. and Ellison, D. W. (2008). The origins of medulloblastoma subtypes. *Annual review of pathology* **3**, 341-365.

Hill, R. M., Kuijper, S., Lindsey, J. C., Petrie, K., Schwalbe, E. C., Barker, K., Boult, J. K., Williamson, D., Ahmad, Z., Hallsworth, A., et al. (2015). Combined MYC and P53 Defects Emerge at Medulloblastoma Relapse and Define Rapidly Progressive, Therapeutically Targetable Disease. *Cancer cell* **27**, 72-84.

Hyman, J. M., Firestone, A. J., Heine, V. M., Zhao, Y., Ocasio, C. A., Han, K., Sun, M., Rack, P. G., Sinha, S., Wu, J. J., et al. (2009). Small-molecule inhibitors reveal multiple strategies for Hedgehog pathway blockade. *Proceedings of the National Academy of Sciences of the United States of America* **106**, 14132-14137.

Jones, D. T., Jager, N., Kool, M., Zichner, T., Hutter, B., Sultan, M., Cho, Y. J., Pugh, T. J., Hovestadt, V., Stutz, A. M., et al. (2012). Dissecting the genomic complexity underlying medulloblastoma. *Nature* **488**, 100-105.

Jones, M. J. and Jallepalli, P. V. (2012). Chromothripsis: chromosomes in crisis. *Developmental cell* **23**, 908-917.

Kool, M., Jones, D. T., Jager, N., Northcott, P. A., Pugh, T. J., Hovestadt, V., Piro, R. M., Esparza, L. A., Markant, S. L., Remke, M., et al. (2014). Genome sequencing of SHH medulloblastoma predicts genotype-related response to smoothened inhibition. *Cancer cell* **25**, 393-405.

Kool, M., Korshunov, A., Remke, M., Jones, D. T., Schlanstein, M., Northcott, P. A., Cho, Y. J., Koster, J., Schouten-van Meeteren, A., van Vuurden, D., et al. (2012). Molecular subgroups of medulloblastoma: an international meta-analysis of transcriptome, genetic aberrations, and clinical data of WNT, SHH, Group 3, and Group 4 medulloblastomas. *Acta neuropathologica* **123**, 473-484.

Kool, M., Koster, J., Bunt, J., Hasselt, N. E., Lakeman, A., van Sluis, P., Troost, D., Meeteren, N. S., Caron, H. N., Cloos, J., et al. (2008). Integrated genomics identifies five medulloblastoma subtypes with distinct genetic profiles, pathway signatures and clinicopathological features. *PloS one* **3**, e3088.

Louis, D. N., Ohgaki, H., Wiestler, O. D., Cavenee, W. K., Burger, P. C., Jouvet, A., Scheithauer, B. W. and Kleihues, P. (2007). The 2007 WHO classification of tumours of the central nervous system. *Acta neuropathologica* **114**, 97-109.

Ng, J. M. and Curran, T. (2011). The Hedgehog's tale: developing strategies for targeting cancer. *Nature reviews. Cancer* **11**, 493-501.

Northcott, P. A., Jones, D. T., Kool, M., Robinson, G. W., Gilbertson, R. J., Cho, Y. J., Pomeroy, S. L., Korshunov, A., Lichter, P., Taylor, M. D., et al. (2012a). Medulloblastomics: the end of the beginning. *Nature reviews. Cancer* **12**, 818-834.

Northcott, P. A., Korshunov, A., Witt, H., Hielscher, T., Eberhart, C. G., Mack, S., Bouffet, E., Clifford, S. C., Hawkins, C. E., French, P., et al. (2011). Medulloblastoma comprises four distinct molecular variants. *Journal of clinical oncology : official journal of the American Society of Clinical Oncology* **29**, 1408-1414.

Northcott, P. A., Shih, D. J., Peacock, J., Garzia, L., Morrissy, A. S., Zichner, T., Stutz, A. M., Korshunov, A., Reimand, J., Schumacher, S. E., et al. (2012b). Subgroup-specific structural variation across 1,000 medulloblastoma genomes. *Nature* **488**, 49-56.

Pfister, S., Remke, M., Benner, A., Mendrzyk, F., Toedt, G., Felsberg, J., Wittmann, A., Devens, F., Gerber, N. U., Joos, S., et al. (2009). Outcome prediction in pediatric medulloblastoma based on DNA copy-number aberrations of chromosomes 6q and 17q and the MYC and MYCN loci. *Journal of clinical oncology : official journal of the American Society of Clinical Oncology* **27**, 1627-1636.

Pugh, T. J., Weeraratne, S. D., Archer, T. C., Pomeranz Krummel, D. A., Auclair, D., Bochicchio, J., Carneiro, M. O., Carter, S. L., Cibulskis, K., Erlich, R. L., et al. (2012). Medulloblastoma exome sequencing uncovers subtype-specific somatic mutations. *Nature* **488**, 106-110.

Rausch, T., Jones, D. T., Zapatka, M., Stutz, A. M., Zichner, T., Weischenfeldt, J., Jager, N., Remke, M., Shih, D., Northcott, P. A., et al. (2012). Genome sequencing of pediatric medulloblastoma links catastrophic DNA rearrangements with TP53 mutations. *Cell* **148**, 59-71.

Robinson, G., Parker, M., Kranenburg, T. A., Lu, C., Chen, X., Ding, L., Phoenix, T. N., Hedlund, E., Wei, L., Zhu, X., et al. (2012). Novel mutations target distinct subgroups of medulloblastoma. *Nature* **488**, 43-48.

Romer, J. T., Kimura, H., Magdaleno, S., Sasai, K., Fuller, C., Baines, H., Connelly, M., Stewart, C. F., Gould, S., Rubin, L. L., et al. (2004). Suppression of the Shh pathway using a small molecule inhibitor eliminates medulloblastoma in Ptc1(+/-)p53(-/-) mice. *Cancer cell* **6**, 229-240.

Rudin, C. M., Hann, C. L., Laterra, J., Yauch, R. L., Callahan, C. A., Fu, L., Holcomb, T., Stinson, J., Gould, S. E., Coleman, B., et al. (2009). Treatment of medulloblastoma with hedgehog pathway inhibitor GDC-0449. *The New England journal of medicine* **361**, 1173-1178.

Schuller, U., Heine, V. M., Mao, J., Kho, A. T., Dillon, A. K., Han, Y. G., Huillard, E., Sun, T., Ligon, A. H., Qian, Y., et al. (2008). Acquisition of granule neuron precursor identity is a critical determinant of progenitor cell competence to form Shh-induced medulloblastoma. *Cancer cell* **14**, 123-134.

Stephens, P. J., Greenman, C. D., Fu, B., Yang, F., Bignell, G. R., Mudie, L. J., Pleasance, E. D., Lau, K. W., Beare, D., Stebbings, L. A., et al. (2011). Massive genomic rearrangement acquired in a single catastrophic event during cancer development. *Cell* **144**, 27-40.

Tabori, U., Baskin, B., Shago, M., Alon, N., Taylor, M. D., Ray, P. N., Bouffet, E., Malkin, D. and Hawkins, C. (2010). Universal poor survival in children with medulloblastoma harboring somatic TP53 mutations. *Journal of clinical oncology : official journal of the American Society of Clinical Oncology* **28**, 1345-1350.

Taylor, M. D., Northcott, P. A., Korshunov, A., Remke, M., Cho, Y. J., Clifford, S. C., Eberhart, C. G., Parsons, D. W., Rutkowski, S., Gajjar, A., et al. (2012). Molecular subgroups of medulloblastoma: the current consensus. *Acta neuropathologica* **123**, 465-472.

Thompson, M. C., Fuller, C., Hogg, T. L., Dalton, J., Finkelstein, D., Lau, C. C., Chintagumpala, M., Adesina, A., Ashley, D. M., Kellie, S. J., et al. (2006). Genomics identifies medulloblastoma subgroups that are enriched for specific genetic alterations. *Journal of clinical oncology : official journal of the American Society of Clinical Oncology* **24**, 1924-1931.

Tomasetti, C. and Vogelstein, B. (2015). Cancer etiology. Variation in cancer risk among tissues can be explained by the number of stem cell divisions. *Science* **347**, 78-81.

Vanner, R. J., Remke, M., Gallo, M., Selvadurai, H. J., Coutinho, F., Lee, L., Kushida, M., Head, R., Morrissy, S., Zhu, X., et al. (2014). Quiescent sox2(+) cells drive hierarchical growth and relapse in sonic hedgehog subgroup medulloblastoma. *Cancer cell* **26**, 33-47.

Wang, Y., Yang, J., Zheng, H., Tomasek, G. J., Zhang, P., McKeever, P. E., Lee, E. Y. and Zhu, Y. (2009). Expression of mutant p53 proteins implicates a lineage relationship between neural stem cells and malignant astrocytic glioma in a murine model. *Cancer cell* **15**, 514-526.

White, J. J. and Sillitoe, R. V. (2013). Development of the cerebellum: from gene expression patterns to circuit maps. *Wiley interdisciplinary reviews. Developmental biology* **2**, 149-164.

Yamasaki, T., Kawaji, K., Ono, K., Bito, H., Hirano, T., Osumi, N. and Kengaku, M. (2001). Pax6 regulates granule cell polarization during parallel fiber formation in the developing cerebellum. *Development* **128**, 3133-3144.

Yang, Z. J., Ellis, T., Markant, S. L., Read, T. A., Kessler, J. D., Bourboulas, M., Schuller, U., Machold, R., Fishell, G., Rowitch, D. H., et al. (2008). Medulloblastoma can be initiated by deletion of Patched in lineage-restricted progenitors or stem cells. *Cancer cell* **14**, 135-145.

Yauch, R. L., Dijkgraaf, G. J., Alicke, B., Januario, T., Ahn, C. P., Holcomb, T., Pujara, K., Stinson, J., Callahan, C. A., Tang, T., et al. (2009). Smoothened mutation confers resistance to a Hedgehog pathway inhibitor in medulloblastoma. *Science* **326**, 572-574.

Zhukova, N., Ramaswamy, V., Remke, M., Pfaff, E., Shih, D. J., Martin, D. C., Castelo-Branco, P., Baskin, B., Ray, P. N., Bouffet, E., et al. (2013). Subgroup-specific prognostic implications of TP53 mutation in medulloblastoma. *Journal of*

clinical oncology : official journal of the American Society of Clinical Oncology **31**, 2927-2935.

Zhuo, L., Theis, M., Alvarez-Maya, I., Brenner, M., Willecke, K. and Messing, A. (2001). hGFAP-cre transgenic mice for manipulation of glial and neuronal function in vivo. *Genesis* **31**, 85-94.

Chapter IV: Pten and mTORC2 signaling pathways orchestrate cortical neurons and neuronal layering during the embryonic development

4.1 Introduction

4.1.1 Neuroepithelium and radial glial cells are the earliest stem cells in the developing brain

Neuroepithelium of ectodermal origin constitutes the earliest stem cells during the embryonic brain development. These neuroepithelial cells divide extensively in a symmetric manner to populate the pseudo-lining of the early cerebral ventricles - the ventricular zone (VZ). Upon this hyperproliferation of the neuroepithelia, VZ becomes a thick and dense layer of stem cells, which remain tightly anchored to the pial and ventricular surfaces. Even though it is thought that neuroepithelial cells might directly give rise to mature neurons, cortical neurogenesis in mouse brain does not start until approximately E10 (Gotz and Huttner, 2005; Kriegstein and Alvarez-Buylla, 2009). One of the key events that initiate the cortical neurogenesis, however, is the transformation of neuroepithelium to radial glial cells (RGCs), which serve as the major neural stem cells (NSCs) in an embryonic brain (Martynoga et al., 2012).

Different from neuroepithelial cells, RGCs elongate and extend their radial filament to the meninges at the basal surface of the cortex while remain attached to the ventricle at the apical surface (Kriegstein and Alvarez-Buylla, 2009; Mori et al., 2005). This tight

apico-basal network of fibers accompanies the gradual thickening of the cortex, and they convert to comparatively looser and shorter processes only after birth. RGCs are also attached to each other, and together with their apico-basal polarity, these tight junctions maintain the delicate architecture of VZ. Several studies have shown that mutations that disrupt these firm connections and basal contact of RGCs lead to disorganized cortical layering and severely altered cortical structure (Kriegstein and Alvarez-Buylla, 2009). In addition to morphologic changes during the transition from the epithelium, RGCs also starts expressing intermediate filament proteins, including nestin, glial fibrillary acidic protein (GFAP), and vimentin, and astrocyte-specific proteins, including L-glutamate/L-aspartate transporter (GLAST), brain lipid-binding protein (BLBP) and the β subunit of calcium-binding protein S100 (S100β) (Hartfuss et al., 2001; Mori et al., 2005). Self-renewal and lineage progression of RGCs occurs through asymmetric cell divisions, where the daughter cells can be a neuron, an intermediate progenitor cell (IPC) or a new RGC. It is important to note that, IPCs form a second layer called subventricular zone (SVZ) basal to the VZ at around E13.5, and they further divide to generate neurons (from nIPC) or oligodendrocytes (from oIGC). As the RGC progeny is continuously generated during the development, they migrate tangentially or radially into the mantel, causing an increase in cortical thickness. As a response, RGCs elongate further, and their fibers can extend to the apical surface as long as a millimeter in mammalian cortices (Kriegstein and Alvarez-Buylla, 2009; Rakic, 2009). At the end of the embryonic development, a portion of RGCs starts detaching from the VZ surface and converts into mature astrocytes. The remaining RGC population, on the other hand, maintains its tight attachment with the VZ, serving as NSCs that continue to generate neurons, oligodendrocytes (through specific IPCs), and ependymal cells lining the ventricle. In later stages after birth, VZ shrinks to a single layer of ependymal cells, and RGCs convert into type B cells, which function as a central NSC pool in adult brains thereafter (Doetsch et al., 1999; Noctor et al., 2007).

4.1.2 Cortical neurogenesis and pyramidal projection neurons

The majority of the cortical neurogenesis takes place between E12-E17 (Hartfuss et al., 2001), and neurons can be produced in three different ways based on their origin 1) In early development, asymmetric divisions of neuroepithelial cells and RGCs can generate mature neurons (direct neurogenesis, aka radial unit hypothesis). This type of neurogenesis mostly takes place in VZ. 2) More restricted nIPCs that are generated from RGCs can divide symmetrically and produce two neurons (indirect neurogenesis aka intermediate progenitor hypothesis). 3) Additionally, nIPCs can undergo extra rounds of symmetric cell divisions giving rise to new IPCs, and subsequently produce mature neurons (indirect neurogenesis) (Kriegstein et al., 2006; Molyneaux et al., 2007; Noctor et al., 2008). The latter two events occur mainly in SVZ and recent studies have suggested that SVZ is actually the major site for cortical neurogenesis. As opposed to neuroepithelia and RGCs, nIPCs do not form tight connections with pial or ventricular surfaces. (Noctor et al., 2007).

Once the cortical neurogenesis is completed, pyramidal neurons, which are glutamatergic projection neurons, are arranged into morphologically distinguishable six layers (I-VI) in a postnatal mouse brain. Except for layer-I neurons, which are located at the most superficial portion of the cortex, all layers are formed in an inside-out manner. Accordingly, formation of initial deeper layers is followed by subsequent addition of more superficial layers, which migrate through preformed neuronal layers (deep layers first, upper layers last gradient) (Britanova et al., 2006; Tarabykin et al., 2001). Late-born superficial cortical layers (II-IV) constitute “upper layer neurons” (ULNs), and early-born more apical layers (V-VI) consist of “deeper layer neurons” (DLNs). Upper layer neurons are mostly corticocortical projection neurons, which form a complex connection between different cortical areas in an ipsilateral and contralateral manner. While deeper layer-IV neurons provide the major neuronal input, the majority of the deeper layer-V and –VI neurons send their axons to more distant areas, including spinal cord, pons, tectum, and thalamus. Therefore, the majority of the DLNs are considered as subcortical projections neurons (Britanova et al., 2008; Leone et al., 2008). Cux1 and Cux2 are

expressed in all ULNs, while Ctip2 and Fezf5 are used as a DLN marker (Leone et al., 2008; Nieto et al., 2004).

4.1.3 Embryonic neurogenesis is regulated by various signaling pathways, including PTEN signaling

A complex interaction of several signaling pathways regulates the cortical neurogenesis, starting with the early transition of neuroepithelium to RGCs, and ending with the completion of cortical development (reviewed in (Martynoga et al., 2012)). Notch, ErB and Fgfr2 signals facilitate the transformation of neuroepithelial cells into RGCs at around E10. Meanwhile, Wnt and Myc signaling pathways promote the self-renewal of RGCs. While Wnt, Bmp, Pax6, and Prc signaling pathways control the direct neurogenesis, a complex network of Ezh2, Tbr2, N-Myc, Foxg1 and Wnt signals provide indirect neurogenesis by inducing the IPC generation from RGCs (Martynoga et al., 2012). These signaling pathways are essential for accurate lineage progression from multipotent stem cells to fully differentiated and functional neurons, and by extension, for proper neural network. Therefore, abnormalities in any of the signaling pathways may be pathological, as evidenced by cognitive problems resulting from an absence of connectivity in callosal projection neurons (CPN), which are enriched in cortical layers II and III, and to a lesser extent in V and VI. Unfortunately, the patients suffering from CPN dysgenesis exhibit autism spectrum disorders (ASD), defects in abstract reasoning, problem solving and generalization (Fame et al., 2011; Paul et al., 2007). Similarly, germline mutations in *PTEN* gene can lead to several autosomal dominant syndromes that manifest themselves with neurological and cognitive deficits. These disorders altogether are called "PTEN hamartoma tumor syndromes (PHTS)", which include Cowden syndrome, Bannayan-Riley-Ruvalcaba syndrome, Lhermitte-Duclos disease and Proteus and Proteus-like syndromes (Salmena et al., 2008; Sulis and Parsons, 2003). Numerous studies have identified strong correlation between germline *PTEN* mutations and ASD, developmental delay, and mental retardation. These patients, in general, are characterized by impaired cognitive functioning, low IQ, deficits in adaptive behaviors, compromised

social, emotional and verbal skills, and unusually large head (macrocephaly). Remarkably, virtually all of the patients with germline *PTEN* mutations exhibited macrocephaly, and approximately 20-50% of those patients were diagnosed with ASD (Butler et al., 2005; Lynch et al., 2009; McBride et al., 2010; Orrico et al., 2009; Varga et al., 2009).

4.1.4 *PTEN* deficiency leads to aberrations in neural stem cells, mature neurons and glia

Since the identification of *PTEN* gene in 1997 (Li and Sun, 1997; Li et al., 1997; Steck et al., 1997), several studies have made a significant effort to understand the essential functions of PTEN and downstream AKT signaling pathway at the cellular, tissue, and organ level. The initial findings suggested that Pten has essential roles in cell cycle progress and cell survival, as *Pten*-deficient embryonic stem cells exhibited rapid entry to S-phase, accompanied by increased growth and proliferation (Sun et al., 1999). Consistently, tissue specific deletion of *Pten* in CNS stem/progenitor cells *in vivo* resulted in increased cellular proliferation, decreased cell death, and enlarged cell size, all of which contributed significantly to enlarged cranium and neonatal lethality (Groszer et al., 2001). It was then reported that *Pten* deletion promotes self-renewal of neural stem/progenitor cells without changing their multipotential differentiation ability, as opposed to the wild type stem/progenitor cells which have a limited self-renewal capacity and gradually lose their ability to generate subsequent progeny, including neurons (Groszer et al., 2006). Less restricted deletion of *Pten* in cerebellar and dentate gyrus granule neurons caused seizures, ataxia and increased soma size in neurons, reminiscent of Lhermitte-Duclos disease (Backman et al., 2001; Kwon et al., 2001). Subsequent studies have identified the deregulated signaling pathways that lead to the observed phenotypes upon *Pten* deletion. Akt and mTOR signaling, particularly, have been shown to be hyperactivated in *Pten*-deficient mice, and inhibition of mTOR decreases the seizure frequency, lethality, and neuronal hypertrophy (Kwon et al., 2003). Functions of Pten in glial populations have been also studied. Similar to the phenotypes in neural

stem/progenitor cells and neurons, increased proliferation and hypertrophy was observed in *Pten*-deficient astrocytes, which was thought underlie the enlarged brains in mutant mice (Fraser et al., 2004). More importantly, *Pten* deficiency in Bergmann glia of cerebellum caused premature differentiation and abnormal anchorage of glia leading to a failure in granule neuron migration. Consequently, *Pten*-mutant cerebellum exhibited severely disorganized foliation and lamination (Yue et al., 2005).

The successful studies summarized above documented the major molecular and cellular consequences of *Pten* mutations that may underlie the deformities in brain tissue and architecture. However, more definitive findings reflecting the neurological dysfunctions represented by PTEN syndrome patients only came with the behavioral studies and more comprehensive neural network analyses. Accordingly, deletion of mouse *Pten* gene specifically in cortical neurons, and in a subpopulation of hippocampal neurons caused notable phenotypes similar to ASD, including macrocephaly, abnormal social behaviors, and exaggerated responses to sensory stimuli (Kwon et al., 2006). More rigorous studies have uncovered that *Pten*-deficient neurons exhibit abnormal neuronal structure, including enlarged caliber of neuronal projections and increased dendritic spine density. *Pten* deletion also led to defects in synaptic structures as evidenced by weakened synaptic transmission and synaptic plasticity in pyramidal neurons of hippocampus. Lastly, mutant brains displayed severe myelination defects, including thickening and unraveling of the myelin sheath surrounding the hypertrophic axons in the corpus callosum (Fraser et al., 2008).

4.1.5 Neuronal diversity and PTEN signaling

It should be considered that mammalian cerebral cortex accommodates several types of neurons with different functions, morphology and origin. It is, however, still not well known about how different neuronal populations respond to *PTEN* mutations in the cortex, which functions as the main cognition site. Therefore, identifying the major cell types that are severely affected by *PTEN* mutations will contribute significantly to my

understanding of mechanisms leading to the observed disease manifestations. In the present study, I specifically analyzed pyramidal neurons, including corticocortical upper layer neurons and subcortical deeper layer neurons in *Pten*-mutant mice. My results showed that these two types of projection neurons are affected in distinctive ways in the absence of *Pten* gene. More specifically, 1) Even though I did not detect any defects in the production of upper layer neurons, they failed to migrate radially to more superficial cortical layers. Instead, they remained in the lower layers (V and VI) mixed with deeper layer neurons. Glial collapse seemed to be the major mechanisms that caused their ectopic localization. 2) On the other hand, deeper layer neurons were properly located, however their number was significantly reduced, suggesting a defect in their production or maintenance. This study, therefore, uncovers the distinct roles of Pten in different neuronal subpopulations of cerebral cortex, and further stresses the necessity to clarify the cellular defects in neurodevelopmental and cognitive disorders.

4.2 Results

4.2.1 *Pten* deficiency leads to neonatal lethality that can be rescued by *Rictor* loss

In order to understand the functions of *Pten* and *Rictor* genes in cortical neurogenesis during the embryonic stages, I generated three types of mutant mice. Upon cre-mediated recombination under the control of hGFAP promoter at around E12.5 (Wang et al., 2009), the genotypes of the mutant mice that I utilized were *Pten*Δ/Δ; *Rictor*+/Δ (*Pten*-deficient), *Pten*+/Δ; *Rictor*Δ/Δ (*Rictor*-deficient), and *Pten*Δ/Δ; *Rictor*Δ/Δ (*Pten*-*Rictor* double-deficient) (Figure 23A). It is worth nothing that *Pten*Δ/Δ; *Rictor*+/Δ and *Pten*+/Δ; *Rictor*Δ/Δ brains were indistinguishable from *Pten*Δ/Δ and *Rictor*Δ/Δ brains, respectively (data not shown), suggesting that *Rictor*-heterozygosity in *Pten*-deficient mice or *Pten*-heterozygosity in *Rictor*-deficient mice is inconsequential.

When I examined the overall phenotypes of the mutant mice, I noted that *Rictor*-deficient mice were indistinguishable from their wild type littermates in many aspects, including survival, social behaviors, breeding, body weight and health conditions (data not shown and Figure 23B). All of the *Pten*-deficient mice, however, had severely enlarged cranium and significantly reduced body weight. These mice were lethargic, scruffy and presented secondary abnormalities such as GI track obstruction. Since they were not even able to feed themselves after a certain stage, I humanely euthanized them within approximately 2-weeks of age based on the established protocols (data not shown and Figure 23B). Interestingly, most of the double-deficient mice had markedly improved health conditions, including increased body weight, ability to feed, and socializing behaviors with the littermates (data not shown). The median survival rate also increased from 15 days seen in *Pten*-deficient mice to 53 days in double-deficient mice. Furthermore, 20% of the double-deficient mice survived beyond 4-months (Figure 23B), though there was still a noticeable cranial enlargement (Figure 23C).

4.2.2 Brain enlargement and tissue degeneration caused by *Pten* deficiency is alleviated by concurrent *Rictor* loss

In order to identify the abnormalities that might led to early lethality in *Pten*-deficient mice, I analyzed the mutant brains in comparison to their littermate or aged-matched controls at birth (P0.5). I observed approximately 30% increase in brain weight compared to the wild type controls (Figures 23C and 23D), consistent with the previous findings (Groszer et al., 2001). Curiously, *Pten*-deficient brains also displayed red spots with varying sizes enriched at their pial surface of the cortices (Figure 23C). These spots were reminiscent of necrotic and bloody areas frequently observed in brain tumors. Remarkably, none of these red spots were detected upon concurrent *Rictor*-loss in double-deficient brains. Even though the brain weight of the double-deficient brains was 15-17% more than that of control brains, it was still significantly reduced compared to *Pten*-deficient brains (Figures 23C and 23D. *Rictor*-deficient brains, on the contrary,

were smaller and weighed marginally but significantly less than the controls (Figures 23C and 23D).

I then aimed to characterize whether there was a cellular damage in *Pten*-deficient brains, especially at the red blood-spots on the dorsal cortices. To this end, I analyzed the expression of an apoptotic marker, cleaved caspase-3, in parallel with Pten (Figure 23E). While control brains did not exhibit any signs of cell death indicated by the absence of cleaved caspase-3, I detected large apoptotic areas, which are accompanied by tissue degeneration in *Pten*-deficient brains. These areas of "dead-tissue" displayed diminished tissue integrity and enrichment of cells with small rounded apoptotic nuclei. On the other hand, I did not detect an obvious cell death in double-deficient brains, even though Pten expression was completely lost (Figure 23E). These results, altogether, suggest that *Pten* deficiency causes brain enlargement accompanied by cortical bleeding, apoptosis and tissue degeneration, which are significantly reversed by simultaneous *Rictor* loss.

4.2.3 *Pten* deficiency causes cortical layering defects

I further analyzed the dorsal neocortices of the mutant brains with regards to neural populations, more specifically, cortical pyramidal projection neurons to determine whether brain enlargement or tissue degeneration has any effects on specific cells. Among these neurons, Cux1 (Cutl1) is expressed by all upper layer neurons (ULNs), while Ctip2 is a deeper layer neuron (DLN) marker (Leone et al., 2008; Nieto et al., 2004). I firstly analyzed *Pten*-deficient brains in comparison to littermate controls to determine how/whether the extensive tissue degeneration and cellular death affect these cortical neurons. Control P0.5 brains displayed organized layering of ULNs at the upper parts of the cortex, and another layer of DLNs below this region (Figures 24A-24C). Between DLNs and the subventricular zone (SVZ), a well-defined intermediate progenitor cell (IPC) layer, which is also $Cux1^{+}$, was observed. *Pten*-deficient brains, however, were characterized by three easily noticeable layering defects: 1) As opposed to their normal location at the upper cortex close to pia matter, majority of the upper layer

neurons were found right above the IPC layer, and below or mixed with the deeper layer neurons (Figures 24A-24C). Since this area normally contains newly generated and radially migrating ULNs, I termed these cells as "migrating $Cux1^+$" cells. While approximately 42% of the total $Cux1^+$ cells were in a migrating position in control brains, this ratio increased up to 72% in *Pten*-deficient cortices (Figures 23D-23F). Consequently, there was a reduction in the percentage of ULNs properly located at the more superficial parts of the cortex (58% in control versus 28% in *Pten*-deficient brains). Total number of the $Cux1^+$ cells, however, changed only slightly between *Pten*-deficient versus control brains. 2) Deeper layer neurons were abnormally located on top of or mixed with the upper layer neurons as a result of this layering defect observed in ULNs (Figures 24A-24C). 3) There was a substantial (~70%) loss in deeper layer neuron number in the neocortices of *Pten*-deficient brains (Figure 24G). This might have partially happened due to the extensive apoptosis that I observed in *Pten*-deficient brains. Despite of this reduction in DLN, cortical thickness of the *Pten*-deficient brains was significantly increased, consistent with my previous findings and other studies showing that *Pten* loss causes an increase in brain size and brain weight (Figures 24A, 24C, 23C, 23D) (Backman et al., 2001; Groszer et al., 2001; Kwon et al., 2001).

My additional analyses using double-deficient brains have indicated that some, but not all, of these abnormalities can be reversed by simultaneous *Rictor* loss. More specifically, the percentage of the migrating $Cux1^+$ cells reduced to 50%, and the percentage of the $Cux1^+$ ULNs properly located at the upper cortex increased to 50% from 28% seen in *Pten*-deficient brains (Figures 24D-24F). This reduction in migrating $Cux1^+$ cells and improvement in the proper ULN localization resulted in a better layering of the cortical neurons (Figures 24B and 24C). However, the total number of the $Cux1^+$ cells, surprisingly, reduced by approximately 30% compared to control brains (Figure 24F). I also observed an increase in DLN number compared to *Pten*-deficient brains, however it was still less than the wild type control brains (Figure 24G). Increased cortical thickness was also alleviated, as I observed a thinner cortex in double-deficient brains compared to *Pten*-deficient brains (Figure 24C). *Rictor*-deficient brains, on the other hand, were

mostly normal except for a decrease in the cortical thickness, and a reduction in the total number of ULN (Figures 24B, 24C and 24F). These results altogether suggest that *Pten* loss causes major neuronal layering defects in the cortices, which are mainly contributed by misplaced ULNs, and that DLNs require functional *Pten* gene to form and/or survive. Additional *Rictor* loss, however, can partially alleviate brain abnormalities associated with the *Pten*-deficiency.

4.2.4 *Pten* deficiency causes a collapse in glial fibers in the cortex

My findings presenting the neuronal layering defects observed in *Pten*-deficient cortex necessitated the understanding of the cellular mechanisms leading to this noteworthy phenotype. Upon their formation, $Cux1^+$ cells climb up against the glial fibers, pass through the already formed DLNs, and ultimately terminate their migration at the dorsal side of the cortex (Britanova et al., 2006; Tarabykin et al., 2001). As the *Pten*-deficient $Cux1^+$ cells seem to accumulate below the DLNs, I hypothesized that there was a failure in proper migration leading to misplacement of the ULNs. I, therefore, examined the glial fibers labeled with Nestin. Control brains were characterized with a network of thin glial fibers stretching from the lateral ventricle (LV) to the very dorsal surface of the cortex, and forming a tight passage between the apical and basal surface of the cortex (Figure 25A). Many newly generated and migrating $Cux1^+$ cells were attached to or at the close proximity these fibers, suggesting that there is a physical interaction between the migrating neurons and the glial fibers facilitating the cellular movement. In stark contrast, this delicate network was severely damaged in *Pten*-deficient cortex, as the glial fibers were but short protrusions from the LV, which were disconnected from the rest of the cortex (Figure 25A). Interestingly, $Cux1^+$ cell accumulation was mostly observed right at the cortical end of the short glial fibers, suggesting that these cells could migrate only until the region where the defective glial tracks extend (Figure 25A). As evidenced by the altered glial fibers around the corpus callosum, the regional disconnections in *Pten*-deficient brains might not be limited to the cortex, but may even extend to the two hemispheres (Figure 25B). Since double-deficient brains had comparatively better ULN

migration, I asked whether the glial fibers were more intact compared to *Pten*-deficient cortices. I indeed observed an improvement in the formation of glial tracks, which were now able to better extend from the LV to the apical surface of the cortex (Figure 25A). These results suggest that an interruption in glial fibers as a result of *Pten* loss causes a disconnection between the LV, where many neurons are generated, and the superficial regions of the cortex, where the ULNs are ultimately located. As a result, the newly generated ULNs fail to migrate to their terminal destination, which can be partially rescued by simultaneous *Rictor* deficiency.

4.2.5 Intact Pten signaling is required for the generation and/or maintenance of deeper layer neurons

Having shown that migration defects, as a result of collapsed glial fibers, cause misplaced ULNs and layering abnormalities, I wanted to investigate the mechanisms leading to the significant loss in DLN population. hGFAP-cre is activated mainly at the dorsal regions of the brain, and only the cells located in or generated from this area undergo cre-mediated recombination (Wang et al., 2012). As a result, virtually entire ventral brain is wild type, whereas dorsal regions are mutant in a cre-positive mouse (Figure 26C). I initially tested this system in immunohistochemistry analyses, and showed that Pten was expressed in almost every part of the wild type brain, however its expression was indeed limited to the ventral parts of the *Pten*-deficient brains (Figure 26A). As a consequence of *Pten* deletion in the dorsal regions, including the neocortex, $pAkt^{S473}$ level was significantly elevated in *Pten*-deficient cortices, which was reversed upon simultaneous *Rictor* loss in double-deficient brains (Figure 26A).

I subsequently examined an area where cre-positive and cre-negative regions are adjacent to each other in order to test whether DLN loss was due to an intrinsic mechanism rather than a secondary phenotype of other abnormalities, including enlarged brain, cortical bleeding, and layering defects, (Figure 26C). In control brains, these two regions are not distinguishable, as both sides are wild type. In *Pten*-deficient brains, however, Pten

expression clearly delineates two different regions, as dorsal region (mutant) lacks Pten expression while the neighboring ventral part (wild type) has intact Pten expression (Figure 26B). Remarkably, DLNs were significantly reduced at the dorsal region of the *Pten*-deficient brains, where Pten was virtually absent (Figure 26B). On the contrary, ULNs of the ventral part in the same Pten-deficient brain was as normal as a control brain, since Pten expression was still intact at this region. Interestingly, both dorsal and ventral region of the double-deficient brains exhibited a normal layering of DLNs, even though only ventral region had intact Pten while the dorsal region lacked Pten expression (Figure 26B). These results suggest that Pten has critical roles for the generation and/or maintenance of DLNs, and that DLN loss was not due to a simple tissue degeneration I observed in *Pten*-deficient brains. Furthermore, even though Akt signaling is the major pathway that is regulated by Pten, other downstream components might have roles in the altered neuronal processes, underlining the findings that concurrent *Rictor* loss could rescue a portion of the *Pten* deficiency driven abnormalities, but not all.

4.2.6 *Pten* deficiency causes increased gliogenesis and cellular proliferation

The lethargic phenotypes that are gradually increasing in *Pten*-deficient mice led us to investigate how the brain abnormalities change over time. Due to the short life span of *Pten*-deficient mice, the latest time point that I could analyze was P16. However, as there was only one *Pten*-deficient mouse survived up to this period, I included P9 mutant mice into my analyses in comparison with the littermate or aged-matched wild type controls. *Pten*-deficient brain at P16 displayed significant enlargement in both dorsoventral and anteroposterior axes, though cerebellum was notably smaller than the controls (Figures 27A and 27B). Accordingly, cortical thickness was also drastically increased (Figure 27C). As these mice were perfused with 4% PFA, the red blood spots that we observed at *Pten*-deficient P0.5 cortices disappeared at P9 and P16. I then examined the glial populations to see whether they contributed to the increased brain size. Remarkably, both P9 and P16 *Pten*-deficient brains were occupied with $GFAP^+$ reactive astrocytes that spread to many areas in cortex and corpus callosum (Figures 28A and 28D). These cells

were also highly proliferative, indicative of their aggressive expansion (Figures 28B and 28C). Double-deficient brains and cortices, on the other hand, were markedly smaller than that of *Pten*-deficient brains, and more importantly, reactive astrocyte expansion was mostly limited to corpus callosum (Figure 28A and 28D). The total and the proliferating $GFAP^+$ reactive astrocytes were also reduced in double-deficient brains compared to *Pten*-deficient brain (Figures 28B and 28C). Even though some regions exhibited enrichment of $Olig2^+$ cells, I did not observe a consistent abnormality in $Olig2^+$ population in both *Pten*-deficient and double-deficient brains, even though further analyses are still required (Figures 28B and 28D). Interestingly, *Rictor*-deficient brains had a slight reduction in $GFAP^+$ population, consistent with the finding that these mutant brains are smaller than the control littermates (Figures 28C, 23C, 23D, 27A and 27B). These results indicate that *Pten* deficiency driven abnormal gliogenesis contribute significantly to enlarged cortex. Though, there might be other mechanisms leading to this enlargement, as double-deficient brains were still bigger that the wild type brains despite the alleviated gliogenesis.

4.2.7 Neuronal layering defects in *Pten*-deficient brains persist during the postnatal stages

Similar to my findings at P0.5, *Pten*-deficient brains had severe neuronal layering defects at P9 and P16 (Figures 29A and 29B). More specifically, the majority of the *Pten*-deficient $Cux1^+$ cells were accumulated and mixed with the $Ctip2^+$ DLN population right above the LV, causing an absence of neuronal delineation. Consequently, there was a significant reduction in ULN population properly located at the upper surface of the *Pten*-deficient cortex (Figures 29A and 29B). The persistent loss in DLN population displayed a regional variation, as some areas were more severe that the others. In double-deficient cortices, I observed an improved neuronal layering, as the ULN and DLN populations were more distinctly separated, though some double-deficient brains still exhibited the presence of ectopic ULNs below the DLN populations (Figure 29B). Furthermore, there was still a reduction in superficially located ULN and overall DLN populations in some

double-deficient brains (Figures 29A and 29B). These results suggest that, neuronal layering defects and reduction in DLN population persist in postnatal stages of *Pten*-deficient brains. Concurrent *Rictor* loss can only partially rescue these neuronal defects with an additional improvement in glial phenotype. Lastly, Akt-independent functions of Pten might also be involved in cortical deficits that I reported.

4.2.8 Pten regulates the formation of cerebellum via its Akt-dependent and – independent functions

Previous studies have shown that Pten is essential for the glial scaffold formation and granule neuron migration during the laminar formation in the cerebellum (Yue et al., 2005). Consistently, *Pten*-deficient cerebellum exhibited a failure in structural integrity with the absence of proper foliation. I, thus, aimed to test whether *Rictor* loss could reverse these phenotypes by inhibiting abnormally elevated Akt signaling. I first confirmed *Pten*-deficient cerebellum phenotype by examining the P9 cerebella (Figure 30A). While wild type control cerebellum had ten lobes with clear foliation patterns, the architecture of the *Pten*-deficient cerebellum was severely altered, as the foliation and lobular delineation was virtually absent. Cerebellar granule cell precursors and mature granule neurons were mostly randomly located, and failed to form distinct EGL and IGL, respectively. Cerebellar size was also reduced compared to the control (Figure 30A). Having established that *Pten* deficiency causes severe malformations in the cerebellum, I analyzed aged matched double-deficient mice. My preliminary results showed that there was only a slight improvement in the overall structure of the double-deficient cerebellum. Even though distinct cerebellar folia started to appear, the laminar formation was still drastically damaged (Figure 30A). I then decided to analyze the cerebella of the double-deficient mice that survived significantly longer than the *Pten*-deficient mice. I evaluated the cerebellar improvement by several criteria, including 1) Presence of an enhancement in overall architecture or structural integrity 2) Increased cerebellar size 3) Formation of IGL-like granule neuron clusters 4) Presence of distinct lamination 5) Absence/reduction of cell clusters in ML. Based on these criteria, only 2/8 double-deficient cerebella

displayed notable improvement, while another 2/8 had partial improvement, which mostly included an increase in granule neurons or granule neuron precursors. The remaining 4/8 double-deficient cerebella did not show a noteworthy change compared to the *Pten*-deficient cerebella (Figure 30B). I, therefore, concluded that both Akt-dependent and -independent functions of Pten regulate the cellular processes in a developing cerebellum, leading to a proper glial scaffold formation, granule neuron migration and ultimately cerebellar lamination.

4.3 Discussion

Herein I described the roles of Pten and Rictor in embryonic cortical development. Biallelic deletion of *Pten* in neural stem/progenitor cells during the early development of a mouse brain leads to previously characterized abnormalities, including enlarged brain, severe cerebellar malformations, and ultimately neonatal lethality. Additionally, I have uncovered novel and essential functions of Pten in cortical neuronal layering, maintenance of glial fibers facilitating the neural migration, and generation/maintenance of a population of cortical neurons. I further demonstrated that simultaneous deletion of *Rictor* reversed some, but not all, of the detected *Pten* deficiency phenotypes, suggesting that both Akt-dependent and -independent functions of Pten regulate the important stages of cortical neurogenesis.

4.3.1 Cortical tissue degeneration accompanies *Pten*-deficiency-associated macrocephaly

Megalencephaly is clinically categorized in "malformations of cortical development" (MCD), and it is a disorder of brain size. More specifically, megalencephaly refers to an abnormally large brain that is above the mean of the corresponding age and gender by 2 (or 3 in practice) standard deviations (SD). It is further classified as megalencephaly with normal cortex by imaging, megalencephaly with polymicrogyria, and dysplastic

megalencephaly (including hemimegalencephaly). These severe brain defects can all result from abnormalities in several components of PI3K/AKT signaling pathway, including *PTEN*, *PIK3R2*, *PIK3CA*, *MTOR*, *AKT*, *TSC1/2*, and *FGFR3* (Guerrini and Dobyns, 2014). Macrocephaly, a representation of megalencephaly, is the most common abnormality in PTEN syndrome patients (PHTS patients), 20-50% of whom are also diagnosed with ASD (Lynch et al., 2009; Varga et al., 2009). As previously shown, *Pten*-deficiency in mice causes enlarged cranium and bigger brain, suggestive of macrocephaly (Groszer et al., 2001). I additionally noted that *Pten*-deficient brains had "bleeding red spots" on their cortices, which subsequently correlated with extensive apoptotic regions and tissue degeneration. My following analyses suggested that a significant increase in the reactive astrocyte number occurs concomitantly with the progressive enlargement of the postnatal *Pten*-deficient brains. It is, therefore, possible that an initial enlargement in brain size due to *Pten* deficiency leads to an increased intracranial pressure. This stress may consequently initiate tissue bleeding in the cortex, which in turn triggers the expansion of reactive astrocytes. Thus, it is important to determine whether the brains of megalencephaly patients undergo this cascade of abnormalities leading to severe structural defects. Importantly, these abnormalities were significantly alleviated by simultaneous *Rictor* loss in double-deficient mouse brains, which exhibited a notable reduction in brain size, disappearance of cortical bleeding and improvement in glial response, as detected by a decline in reactive astrocytes. Given that PI3K/AKT signaling is one of the most altered pathways in megalencephaly syndromes in general, clinical strategies that target Rictor/mTORC2 signaling can benefit patients with megalencephaly.

4.3.2 Intact Pten signaling is essential for migration of upper layer neurons and neuronal lamination in cerebral cortex

Pyramidal neurons of the cerebral cortex form a six-layer structure in an inside out manner. According to this system, late-born neurons migrate and pass through the early-born neurons to be localized at more superficial levels. At the end of the cortical development, ULNs occupy upper layers (II-IV) below the pia mater, while deeper layer

neurons are located in lower layers (V-VI) despite that they are generated earlier than ULNs (Britanova et al., 2006). In order for this cellular process to work properly, an intact network of glial fibers stretching from the apical surface of the LV to the pial surface at the meninges is required. These long processes serve as a migratory scaffold and guide newborn neurons to their ultimate destinations in the cortical plate (Molyneaux et al., 2007). In *Pten*-deficient cortices, however, the majority of the ULNs were located right above the VZ/SVZ. Some of these ULNs were mixed with the DLNs, while some of them were even below the DLN layer. Consequently, neuronal layering was severely damaged, and I did not detect a proper neuronal lamination with distinct layers, even though total ULN number did not change. My later analyses underlined the essential roles of intact glial fibers, as *Pten*-deficient brains lacked an intact fibrous structure guiding the migrating neurons. Interestingly, ULNs could migrate only until a point where defective fibers were extending. It is, then, worth noting that one of the outcomes of MCD patients is a defect in cortical layer formation, which can occur when a large number of neurons do not reach the cortex, or to their proper position (Guerrini and Dobyns, 2014). My findings, therefore, uncover one of the cellular and molecular mechanisms triggering cortical layering defects. Extrapolations from this study to the human brains with abnormal neuronal migration (e.g. lissencephaly, pachygyria, cobblestone cortex) will help us better understand the underlying cause of cortical malformations.

4.3.3 Deeper layer neurons require Pten signaling to form and/or survive

During the embryonic development, neurons are generated by both direct and indirect modes of neurogenesis. While RGCs (and possibly neuroepithelia) can directly give rise to mature neurons through asymmetric divisions, neurogenesis from symmetric divisions of more restricted IPCs is considered as an indirect path (Kriegstein et al., 2006; Molyneaux et al., 2007; Noctor et al., 2008). Especially early-born neurons, such as DLNs, can be formed by both direct and indirect neurogenesis. My findings showed that, despite their proper localization right above the VZ/SVZ, DLN populations were severely reduced in *Pten*-deficient brains. This phenomenon was somewhat opposite of my

findings with regards to ULN populations, which were fully generated, however ectopically localized. These findings altogether suggest that pyramidal neurons of the cerebral cortex respond differently to *Pten* deficiency, and that it is critical to determine the specific neuronal defects in each PHTS patient before applying a broad-spectrum treatment plans. Furthermore, as concurrent *Rictor* loss rescues only a portion of DLNs, both Akt-dependent and -independent signals regulate the generation and/or maintenance of this neural population.

Future directions of this study will include identification of the specific roles of Pten in preserving the glial fibers and generating and/or maintaining the DLN populations. Furthermore, behavioral analyses will pinpoint the cognition-associated consequences of neuronal layering defects induced by *Pten* loss (future directions are discussed in detail in Chapter VI).

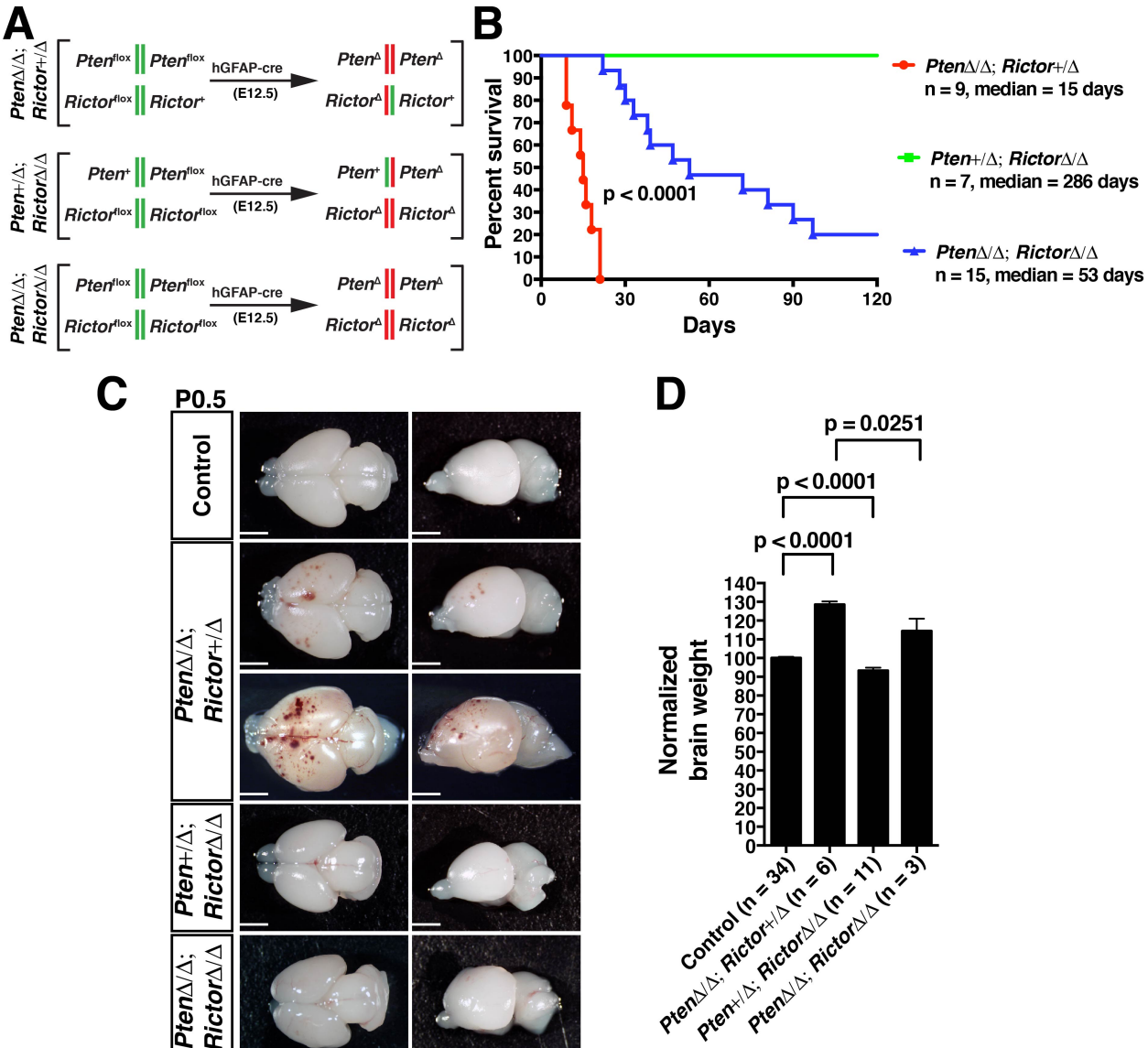
A
PtenΔ/Δ; RictorΔ/Δ
Ptenflox Ptenflox
Rictorflox Rictorflox
hGFAP-cre
(E12.5)
PtenΔ PtenΔ
RictorΔ RictorΔ
Pten+/Δ; RictorΔ/Δ
Pten+ Ptenflox
Rictorflox Rictorflox
Pten+ PtenΔ
RictorΔ RictorΔ
PtenΔ/Δ; Rictor+/Δ
Ptenflox Ptenflox
Rictorflox Rictor+
PtenΔ PtenΔ
RictorΔ Rictor+
B
Percent survival
Days
p < 0.0001
PtenΔ/Δ; Rictor+/Δ
n = 9, median = 15 days
Pten+/Δ; RictorΔ/Δ
n = 7, median = 286 days
PtenΔ/Δ; RictorΔ/Δ
n = 15, median = 53 days
C
P0.5
Control
PtenΔ/Δ; Rictor+/Δ
Pten+/Δ; RictorΔ/Δ
PtenΔ/Δ; RictorΔ/Δ
D
p = 0.0251
p < 0.0001
p < 0.0001
Normalized brain weight
Control (n = 34)
PtenΔ/Δ; Rictor+/Δ (n = 6)
Pten+/Δ; RictorΔ/Δ (n = 11)
PtenΔ/Δ; RictorΔ/Δ (n = 3)
E
P0.5
Cleaved Caspase-3
Pten
Control
PtenΔ/Δ; Rictor+/Δ
Pten+/Δ; RictorΔ/Δ
PtenΔ/Δ; RictorΔ/Δ
LV

Figure 23. *Pten* deficiency leads to various brain abnormalities and neonatal lethality that can be alleviated by *Rictor* loss.

(A) Schematic representation of the genetic configurations in *Pten*Δ/Δ; *Rictor*+/Δ (*Pten*-deficient), *Pten*+/Δ; *Rictor*Δ/Δ (*Rictor*-deficient), and *Pten*Δ/Δ; *Rictor*Δ/Δ (*Pten-Rictor* double-deficient) mice. Floxed genes undergo hGFAP-cre-mediated recombination at around E12.5.

(B) Kaplan-Meier survival curves of the mutant mice. The Mantel-Cox (Log-rank) test is used to compare the curves statistically.

(C) Whole-mount images of 4% PFA-fixed P0.5 brains from wild type control and mutant brains.

(D) Normalized brain weights of the P0.5 wild type control and mutant mice. The average brain weight of the control mice is set to 100, and each sample is calculated accordingly.

(E) Apoptotic marker (cleaved caspase-3) and Pten expression is detected using IHC techniques on P0.5 brains. Dashed areas indicate the apoptotic regions in *Pten*Δ/Δ; *Rictor*Δ/+ brain. Insets are higher magnification images from the spots indicated by asterisks.

Scale bars, 200 μm.

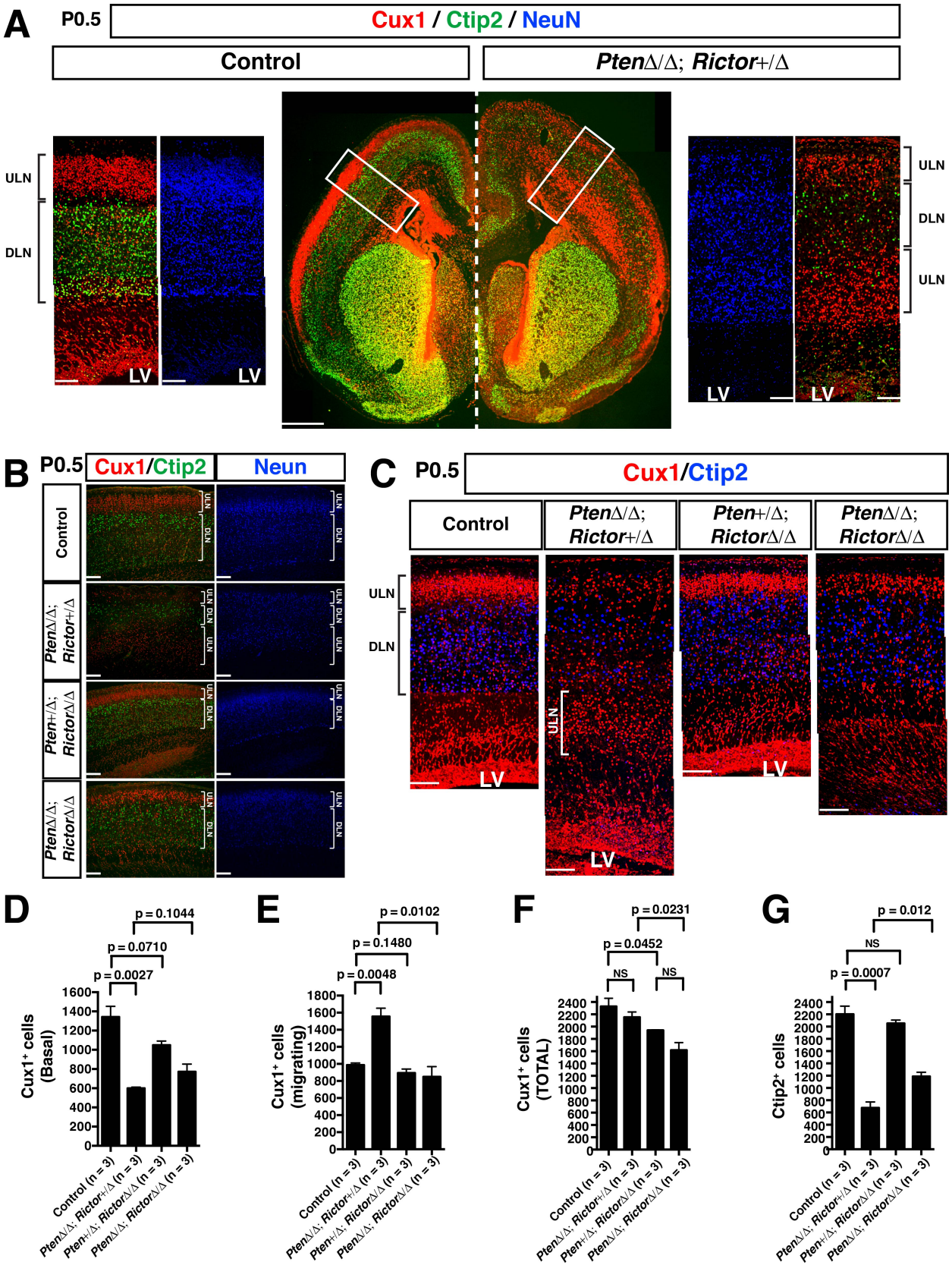
A
P0.5
Cux1 / Ctip2 / NeuN
Control
PtenΔ/Δ; Rictor+/Δ
ULN
DLN
LV
B
P0.5
Cux1/Ctip2
Neun
Control
PtenΔ/Δ; Rictor+/Δ
Pten+/Δ; RictorΔ/Δ
PtenΔ/Δ; RictorΔ/Δ
C
P0.5
Cux1/Ctip2
Control
PtenΔ/Δ; Rictor+/Δ
Pten+/Δ; RictorΔ/Δ
PtenΔ/Δ; RictorΔ/Δ
D
Cux1+ cells (Basal)
p = 0.1044
p = 0.0710
p = 0.0027
E
Cux1+ cells (migrating)
p = 0.0102
p = 0.1480
p = 0.0048
F
Cux1+ cells (TOTAL)
p = 0.0231
p = 0.0452
NS
NS
G
Ctip2+ cells
p = 0.012
NS
p = 0.0007
Control (n = 3)
PtenΔ/Δ; Rictor+/Δ (n = 3)
Pten+/Δ; RictorΔ/Δ (n = 3)
PtenΔ/Δ; RictorΔ/Δ (n = 3)

Figure 24. *Pten* deficiency causes defects in cortical neuronal layering.

(A-C) Upper layer neurons (ULNs) and deeper layer neurons (DLNs) of P0.5 wild type control, *Pten*-deficient, *Rictor*-deficient and double-deficient brains are labeled with Cux1 and Ctip2 antibodies, respectively. NeuN antibody is used as a general neuron marker.
Wild type control brain is shown on the left, *Pten*-deficient brain is shown on the right. White rectangles on the coronal brain sections indicate the areas that are shown in higher magnifications (A).
(D-G) Quantification of $Cux1^+$ cells (basal (D), migrating (E) and total (F)) and total $Ctip2^+$ cells (G)
Unpaired t-test is used to compare the groups. ULN: Upper layer neurons, DLN: Deeper layer neurons, LV: Lateral ventricle. Scale bars, 100 μm (except for the coronal whole brain image, which is 500 μm).

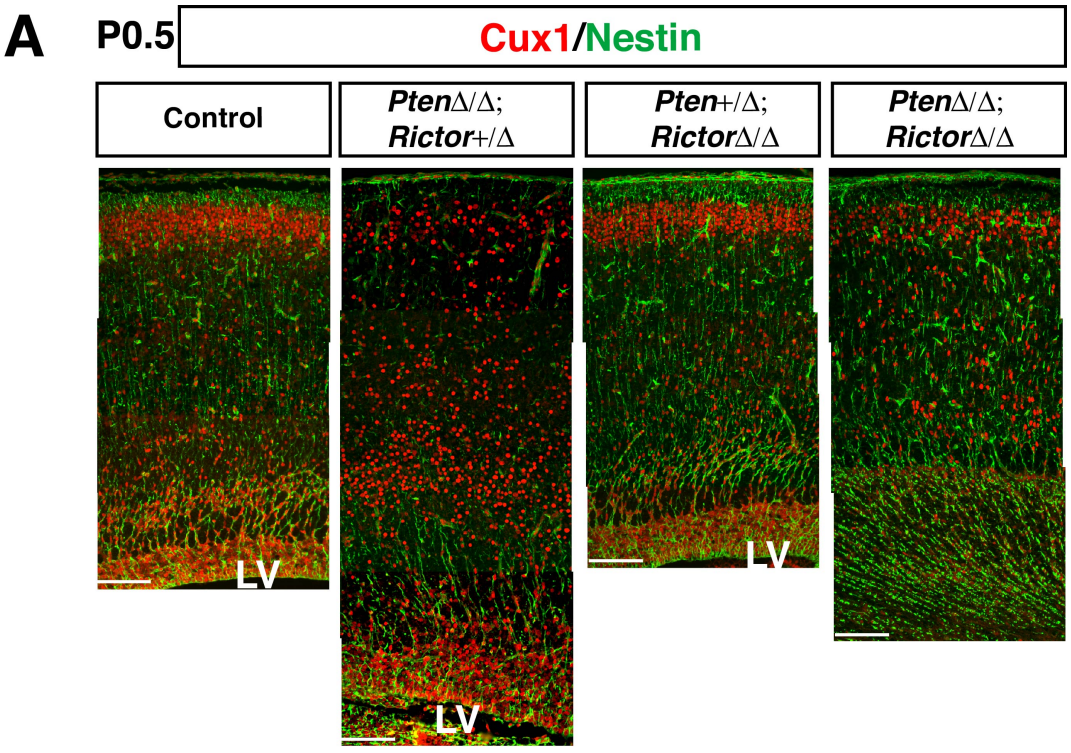
A
P0.5
Cux1/Nestin
Control
Pten Δ/Δ; Rictor +/Δ
Pten +/Δ; Rictor Δ/Δ
Pten Δ/Δ; Rictor Δ/Δ
LV
LV
LV

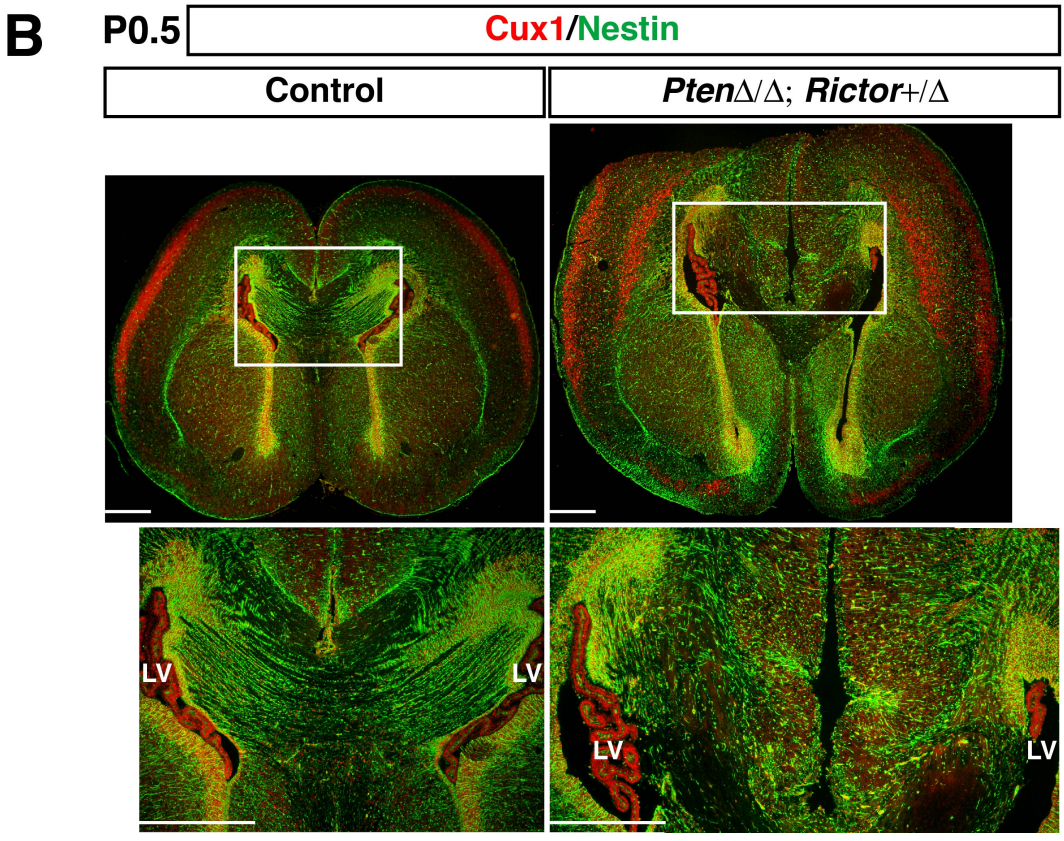
B
P0.5
Cux1/Nestin
Control
Pten Δ/Δ; Rictor +/Δ
LV
LV
LV
LV

Figure 25. *Pten* deficiency causes a collapse in the radial glial fibers of the cerebral cortex.

(A) $Cux1^+$ cells and $Nestin^+$ glial fibers are labeled in P0.5 wild type control brains along with the three mutants.

(B) A coronal view of the wild type control and *Pten*-deficient brain illustrating the glial abnormalities around the corpus callosum. White boxes indicate where the higher magnification images are taken.

LV: lateral ventricle. Scale bars, 100 μm (A), 500 μm (B).

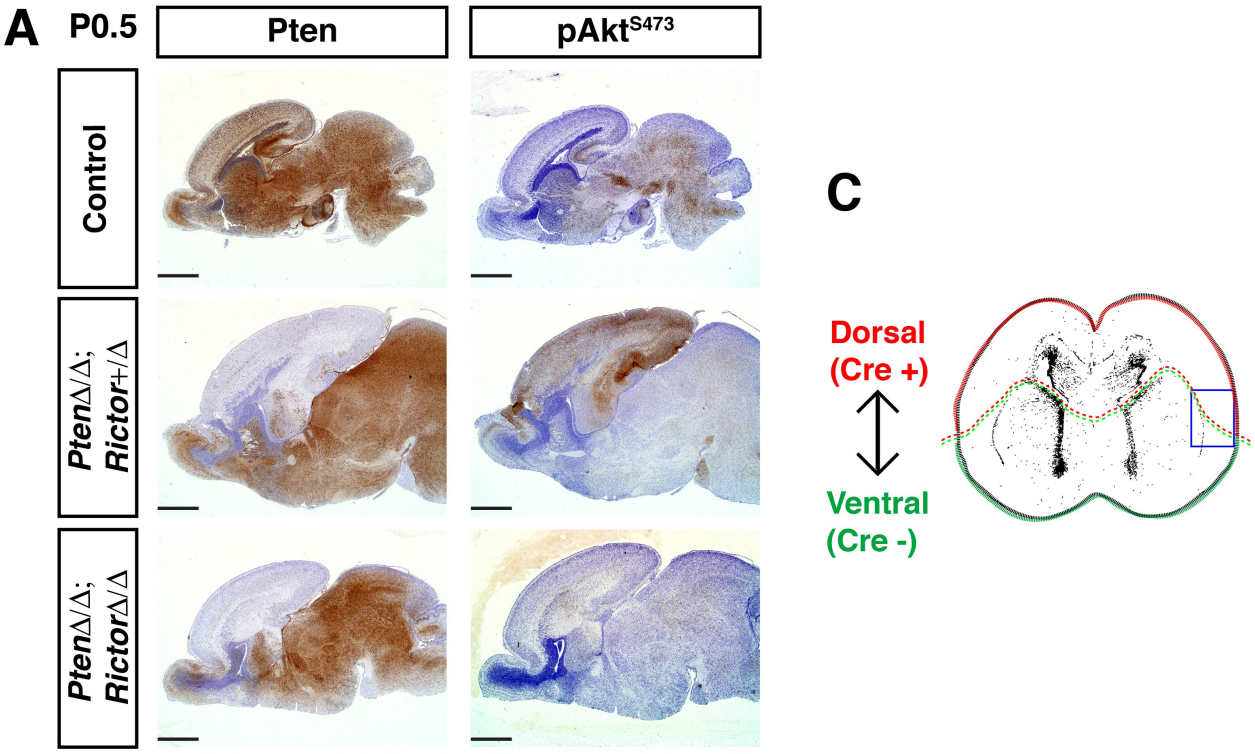
A
P0.5
Pten
pAktS473
Control
PtenΔ/Δ; RictorΔ/Δ
PtenΔ/Δ; RictorΔ/Δ
C
Dorsal
(Cre +)
Ventral
(Cre -)

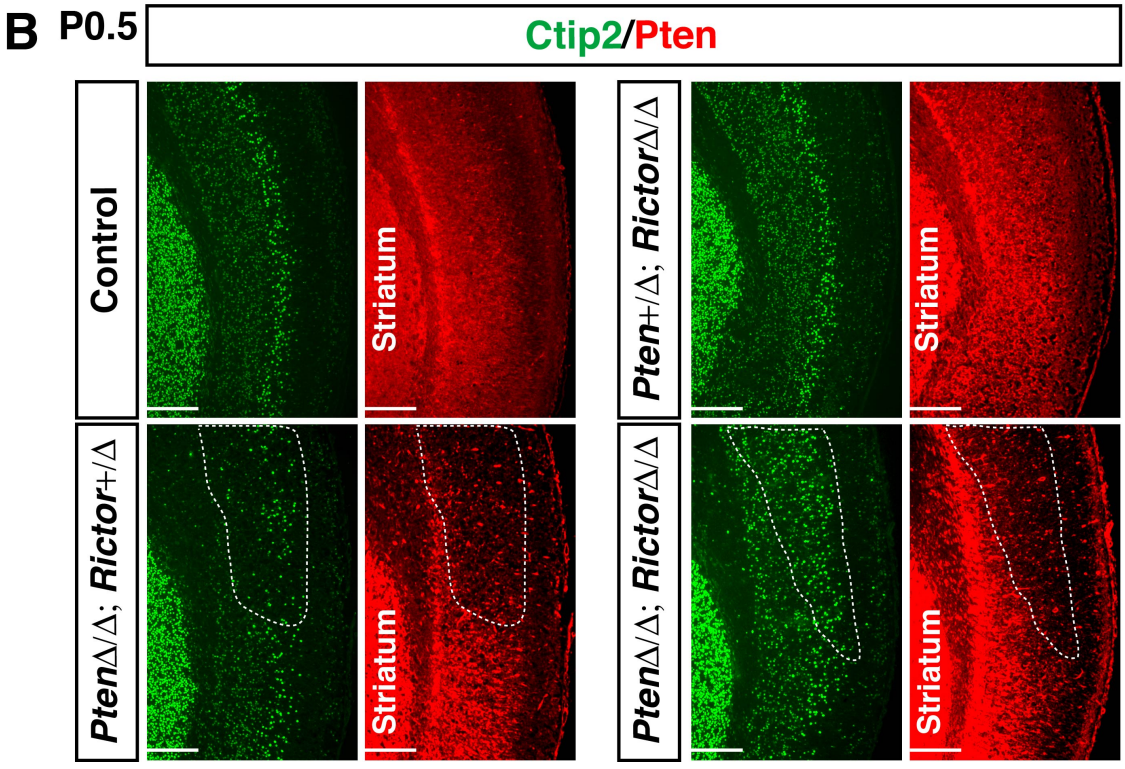
B
P0.5
Ctip2/Pten
Control
PtenΔ/Δ; RictorΔ/Δ
PtenΔ/Δ; RictorΔ/Δ
PtenΔ/Δ; RictorΔ/Δ
Striatum
Striatum
Striatum
Striatum

Figure 26. Intact Pten signaling is required for the generation and/or maintenance of the deeper layer neurons.

(A) Pten and $pAkt^{S473}$ expression is detected in P0.5 wild type control, *Pten*-deficient and double-deficient brains. Note the hGFAP-cre-mediated loss of Pten expression in the dorsal parts of the *Pten*-deficient and double deficient brains.
(B) $Ctip2^{+}$ DLNs and Pten expression is examined at a cross section that consists of adjacent cre-positive (dorsal) and cre-negative (ventral) parts. White dashed lines indicate the mutant regions that lack Pten expression.
(C) Cartoon representation of regional cre-activation in the brain. Dorsal brain undergoes cre-mediated recombination in a mutant brain, while ventral brain remains wild type.
Scale bars, 1 mm (A), 200 μm (B).

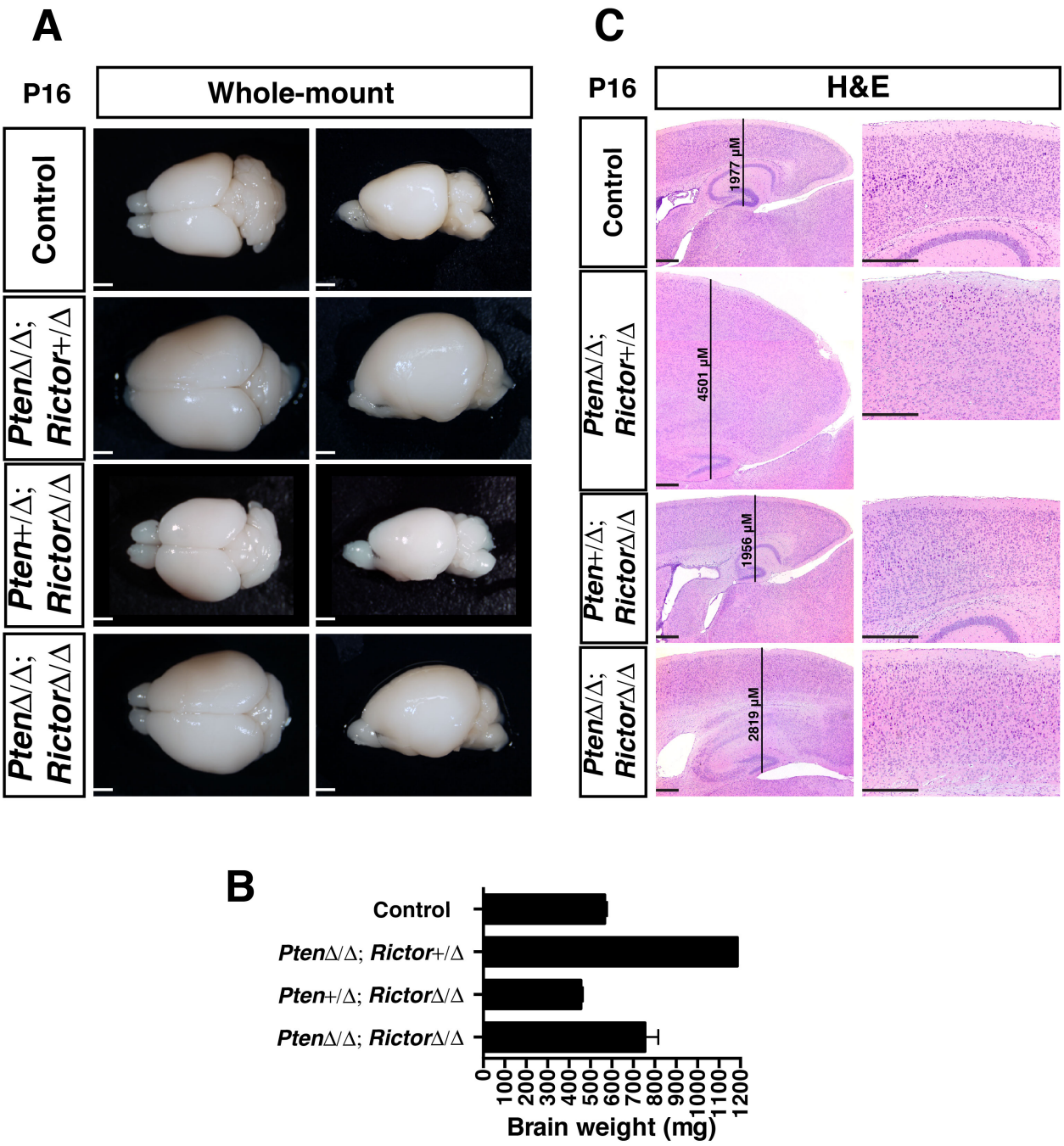
A
P16
Whole-mount
Control
Pten Δ/Δ; Rictor +/Δ
Pten +/Δ; Rictor Δ/Δ
Pten Δ/Δ; Rictor Δ/Δ
C
P16
H&E
Control
Pten Δ/Δ; Rictor +/Δ
Pten +/Δ; Rictor Δ/Δ
Pten Δ/Δ; Rictor Δ/Δ
1977 µM
4501 µM
1956 µM
2819 µM
B
Control
Pten Δ/Δ; Rictor +/Δ
Pten +/Δ; Rictor Δ/Δ
Pten Δ/Δ; Rictor Δ/Δ
0
100
200
300
400
500
600
700
800
900
1000
1100
1200
Brain weight (mg)

Figure 27. *Pten* deficiency associated abnormalities persist in postnatal brains.

(A) Whole-mount images of 4% PFA-fixed P16 brains from wild type control and mutant brains.
(B) Weights (mg) of the 4% PFA-fixed brains. Note that only one *Pten*-deficient brain is used in this analysis, as only one mouse from this mutant group survived until P16.
(C) H&E staining of P16 wild type control and mutant brains. The thickness of the cortices is indicated. Lower portion of the hippocampus is taken as reference point.
Scale bars, 200 μm (A), 500 μm (C).

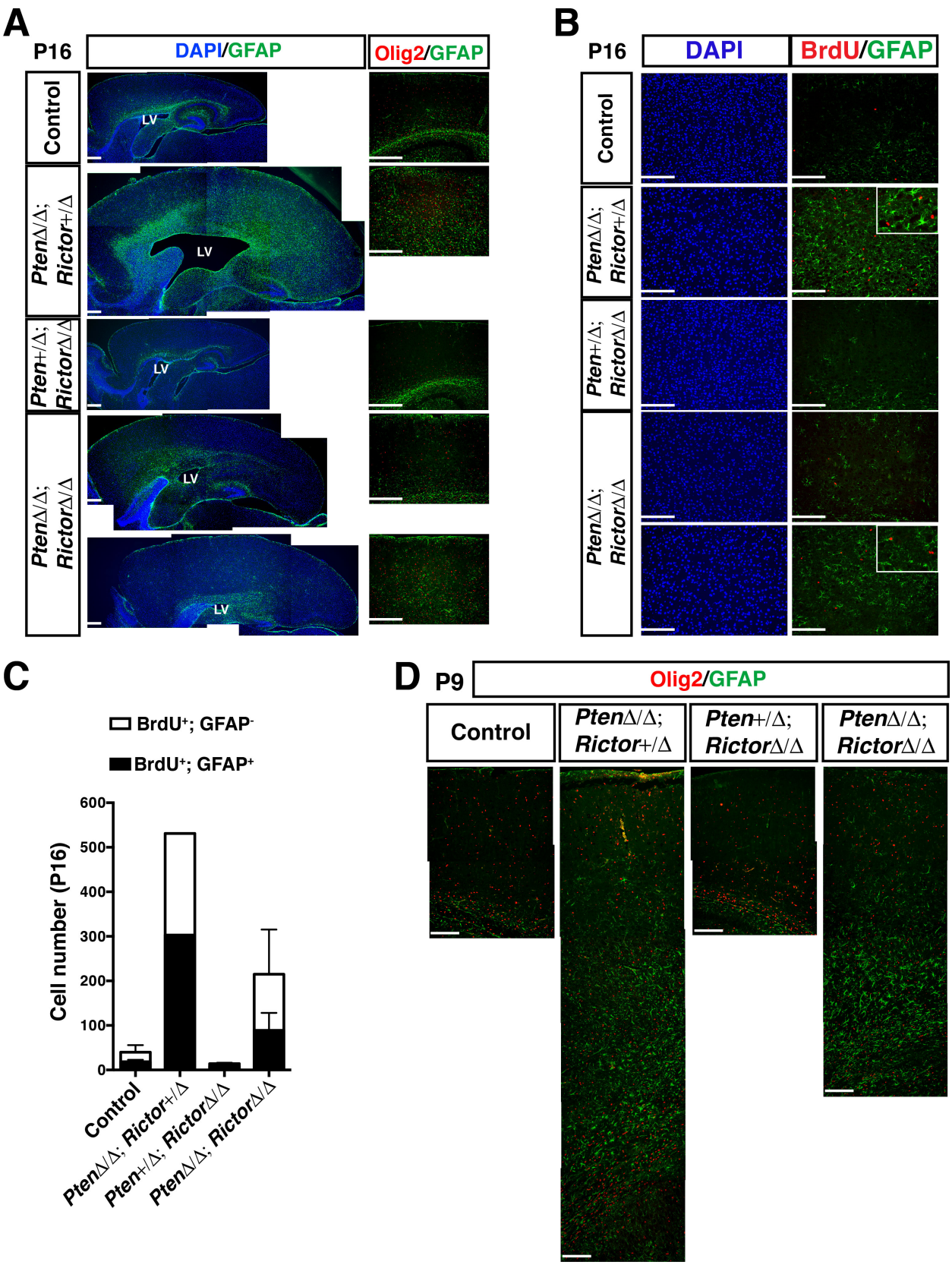
A
P16
DAPI/GFAP
Olig2/GFAP
Control
PtenΔ/Δ; RictorΔ/+
Pten+/Δ; RictorΔ/Δ
PtenΔ/Δ; RictorΔ/Δ
LV
B
P16
DAPI
BrdU/GFAP
C
BrdU+; GFAP-
BrdU+; GFAP+
Cell number (P16)
600
500
400
300
200
100
0
Control
PtenΔ/Δ; RictorΔ/+
Pten+/Δ; RictorΔ/Δ
PtenΔ/Δ; RictorΔ/Δ
D
P9
Olig2/GFAP
Control
PtenΔ/Δ; RictorΔ/+
Pten+/Δ; RictorΔ/Δ
PtenΔ/Δ; RictorΔ/Δ

Figure 28. *Pten* deficiency causes increased gliogenesis and cellular proliferation.

(A) Glial cells in P16 brains are labeled with GFAP (astrocytes) and Olig2 (oligodendrocytes).
(B) Proliferation ability of the $GFAP^+$ cells is tested with BrdU labeling. P16 mice are injected with BrdU twice. Two hours after the last injection, brains are collected, followed by analyses of cellular proliferation. White insets show the higher magnification.
(C) $GFAP^+$ and $GFAP^-$ proliferating cells are quantified in P16 brains. Note that only one *Pten*-deficient brain is used in this analysis, as only one mouse from this mutant group survived until P16.
(D) Glial cells in P9 brains are labeled with GFAP and Olig2. DAPI labels the cell nuclei. Images scan the cortex from the basal surface to the lateral ventricle.
Scale bars, 500 μm (A), 200 μm (B and D).

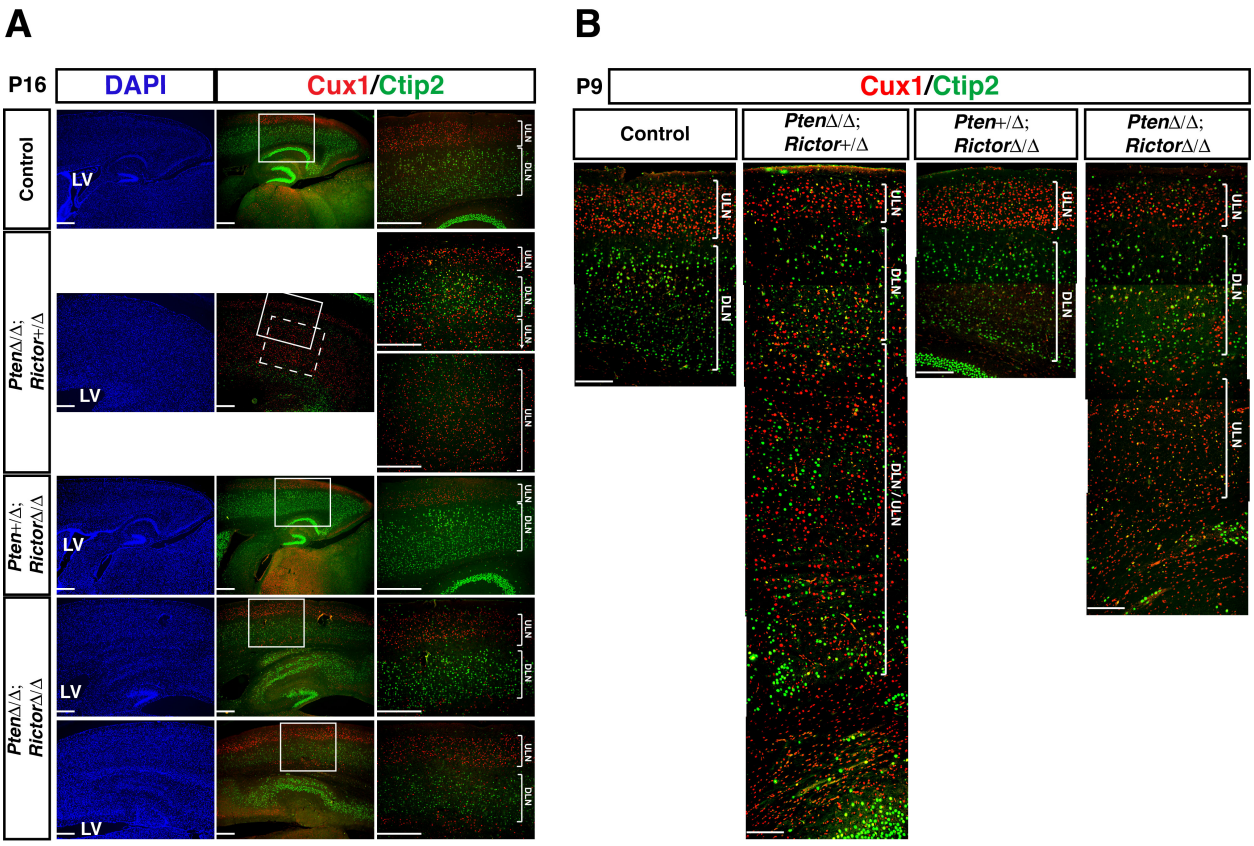

Figure 29. Neuronal layering defects in *Pten*-deficient brains persist during the postnatal stages.

(A-B) ULNs and DLNs of wild type control, *Pten*-deficient, *Rictor*-deficient and double-deficient brains are labeled with Cux1 and Ctip2 antibodies, respectively.

P16 brains are shown in (A), and P9 brains are shown in (B). White rectangles in (A) indicate the area where the higher magnification images are taken from. Images from P9 brains scan the cortex from the basal surface to the lateral ventricle.

Scale bars, 500 μm (A), 200 μm (B).

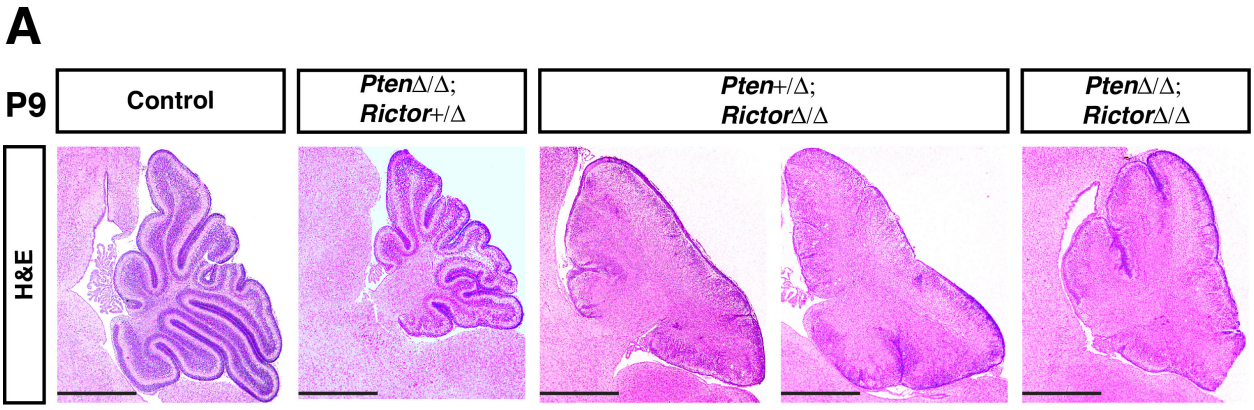
A
P9
Control
Pten Δ/Δ; Rictor +/Δ
Pten +/Δ; Rictor Δ/Δ
Pten Δ/Δ; Rictor Δ/Δ
H&E

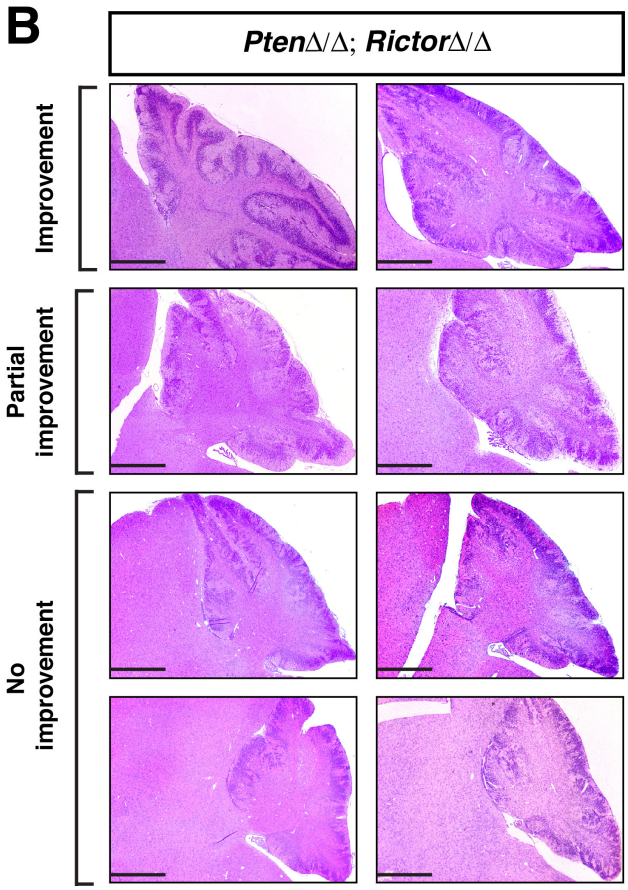
B
Pten Δ/Δ; Rictor Δ/Δ
Improvement
Partial improvement
No improvement

Figure 30. Pten regulates the formation of cerebellum via its Akt-dependent and -independent functions.

(A) H&E images of P9 cerebella from wild type control and mutant mice. Note the well-established structure in the control cerebellum. *Rictor*-deficient cerebellum is smaller than the control, but otherwise mostly normal. *Pten*-deficient cerebella are characterized by severe structural deformities. Double-deficiency has only slight improvement compared to the *Pten*-deficient cerebella.
(B) H&E images of double-deficient cerebella from eight mice with various ages. Structural improvement is evaluated by five criteria: 1) Presence of an enhancement in overall architecture or structural integrity 2) Increased cerebellar size 3) Formation of IGL-like granule neuron clusters 4) Presence of distinct lamination 5) Absence/reduction of cell clusters in ML.
Scale bars, 1 mm.

4.4 References

Backman, S. A., Stambolic, V., Suzuki, A., Haight, J., Elia, A., Pretorius, J., Tsao, M. S., Shannon, P., Bolon, B., Ivy, G. O., et al. (2001). Deletion of Pten in mouse brain causes seizures, ataxia and defects in soma size resembling Lhermitte-Duclos disease. *Nature genetics* **29**, 396-403.

Britanova, O., Alifragis, P., Junek, S., Jones, K., Gruss, P. and Tarabykin, V. (2006). A novel mode of tangential migration of cortical projection neurons. *Developmental biology* **298**, 299-311.

Britanova, O., de Juan Romero, C., Cheung, A., Kwan, K. Y., Schwark, M., Gyorgy, A., Vogel, T., Akopov, S., Mitkovski, M., Agoston, D., et al. (2008). Satb2 is a postmitotic determinant for upper-layer neuron specification in the neocortex. *Neuron* **57**, 378-392.

Butler, M. G., Dasouki, M. J., Zhou, X. P., Talebizadeh, Z., Brown, M., Takahashi, T. N., Miles, J. H., Wang, C. H., Stratton, R., Pilarski, R., et al. (2005). Subset of individuals with autism spectrum disorders and extreme macrocephaly associated with germline PTEN tumour suppressor gene mutations. *Journal of medical genetics* **42**, 318-321.

Doetsch, F., Caille, I., Lim, D. A., Garcia-Verdugo, J. M. and Alvarez-Buylla, A. (1999). Subventricular zone astrocytes are neural stem cells in the adult mammalian brain. *Cell* **97**, 703-716.

Fame, R. M., MacDonald, J. L. and Macklis, J. D. (2011). Development, specification, and diversity of callosal projection neurons. *Trends in neurosciences* **34**, 41-50.

Fraser, M. M., Bayazitov, I. T., Zakharenko, S. S. and Baker, S. J. (2008). Phosphatase and tensin homolog, deleted on chromosome 10 deficiency in brain causes defects in synaptic structure, transmission and plasticity, and myelination abnormalities. *Neuroscience* **151**, 476-488.

Fraser, M. M., Zhu, X., Kwon, C. H., Uhlmann, E. J., Gutmann, D. H. and Baker, S. J. (2004). Pten loss causes hypertrophy and increased proliferation of astrocytes in vivo. *Cancer research* **64**, 7773-7779.

Gotz, M. and Huttner, W. B. (2005). The cell biology of neurogenesis. *Nature reviews. Molecular cell biology* **6**, 777-788.

Groszer, M., Erickson, R., Scripture-Adams, D. D., Dougherty, J. D., Le Belle, J., Zack, J. A., Geschwind, D. H., Liu, X., Kornblum, H. I. and Wu, H. (2006). PTEN negatively regulates neural stem cell self-renewal by modulating G0-G1 cell cycle entry. *Proceedings of the National Academy of Sciences of the United States of America* **103**, 111-116.

Groszer, M., Erickson, R., Scripture-Adams, D. D., Lesche, R., Trumpp, A., Zack, J. A., Kornblum, H. I., Liu, X. and Wu, H. (2001). Negative regulation of neural stem/progenitor cell proliferation by the Pten tumor suppressor gene in vivo. *Science* **294**, 2186-2189.

Guerrini, R. and Dobyns, W. B. (2014). Malformations of cortical development: clinical features and genetic causes. *The Lancet. Neurology* **13**, 710-726.

Hartfuss, E., Galli, R., Heins, N. and Gotz, M. (2001). Characterization of CNS precursor subtypes and radial glia. *Developmental biology* **229**, 15-30.

Kriegstein, A. and Alvarez-Buylla, A. (2009). The glial nature of embryonic and adult neural stem cells. *Annual review of neuroscience* **32**, 149-184.

Kriegstein, A., Noctor, S. and Martinez-Cerdeno, V. (2006). Patterns of neural stem and progenitor cell division may underlie evolutionary cortical expansion. *Nature reviews. Neuroscience* **7**, 883-890.

Kwon, C. H., Luikart, B. W., Powell, C. M., Zhou, J., Matheny, S. A., Zhang, W., Li, Y., Baker, S. J. and Parada, L. F. (2006). Pten regulates neuronal arborization and social interaction in mice. *Neuron* **50**, 377-388.

Kwon, C. H., Zhu, X., Zhang, J. and Baker, S. J. (2003). mTor is required for hypertrophy of Pten-deficient neuronal soma in vivo. *Proceedings of the National Academy of Sciences of the United States of America* **100**, 12923-12928.

Kwon, C. H., Zhu, X., Zhang, J., Knoop, L. L., Tharp, R., Smeyne, R. J., Eberhart, C. G., Burger, P. C. and Baker, S. J. (2001). Pten regulates neuronal soma size: a mouse model of Lhermitte-Duclos disease. *Nature genetics* **29**, 404-411.

Leone, D. P., Srinivasan, K., Chen, B., Alcamo, E. and McConnell, S. K. (2008). The determination of projection neuron identity in the developing cerebral cortex. *Current opinion in neurobiology* **18**, 28-35.

Li, D. M. and Sun, H. (1997). TEP1, encoded by a candidate tumor suppressor locus, is a novel protein tyrosine phosphatase regulated by transforming growth factor beta. *Cancer research* **57**, 2124-2129.

Li, J., Yen, C., Liaw, D., Podsypanina, K., Bose, S., Wang, S. I., Puc, J., Miliaresis, C., Rodgers, L., McCombie, R., et al. (1997). PTEN, a putative protein tyrosine phosphatase gene mutated in human brain, breast, and prostate cancer. *Science* **275**, 1943-1947.

Lynch, N. E., Lynch, S. A., McMenamin, J. and Webb, D. (2009). Bannayan-Riley-Ruvalcaba syndrome: a cause of extreme macrocephaly and neurodevelopmental delay. *Archives of disease in childhood* **94**, 553-554.

Martynoga, B., Drechsel, D. and Guillemot, F. (2012). Molecular control of neurogenesis: a view from the mammalian cerebral cortex. *Cold Spring Harbor perspectives in biology* **4**.

McBride, K. L., Varga, E. A., Pastore, M. T., Prior, T. W., Manickam, K., Atkin, J. F. and Herman, G. E. (2010). Confirmation study of PTEN mutations among individuals with autism or developmental delays/mental retardation and macrocephaly. *Autism research : official journal of the International Society for Autism Research* **3**, 137-141.

Molyneaux, B. J., Arlotta, P., Menezes, J. R. and Macklis, J. D. (2007). Neuronal subtype specification in the cerebral cortex. *Nature reviews. Neuroscience* **8**, 427-437.

Mori, T., Buffo, A. and Gotz, M. (2005). The novel roles of glial cells revisited: the contribution of radial glia and astrocytes to neurogenesis. *Current topics in developmental biology* **69**, 67-99.

Nieto, M., Monuki, E. S., Tang, H., Imitola, J., Haubst, N., Khoury, S. J., Cunningham, J., Gotz, M. and Walsh, C. A. (2004). Expression of Cux-1 and Cux-

2 in the subventricular zone and upper layers II-IV of the cerebral cortex. *The Journal of comparative neurology* **479**, 168-180.

Noctor, S. C., Martinez-Cerdeno, V. and Kriegstein, A. R. (2007). Contribution of intermediate progenitor cells to cortical histogenesis. *Archives of neurology* **64**, 639-642.

---- (2008). Distinct behaviors of neural stem and progenitor cells underlie cortical neurogenesis. *The Journal of comparative neurology* **508**, 28-44.

Orrico, A., Galli, L., Buoni, S., Orsi, A., Vonella, G. and Sorrentino, V. (2009). Novel PTEN mutations in neurodevelopmental disorders and macrocephaly. *Clinical genetics* **75**, 195-198.

Paul, L. K., Brown, W. S., Adolphs, R., Tyszka, J. M., Richards, L. J., Mukherjee, P. and Sherr, E. H. (2007). Agenesis of the corpus callosum: genetic, developmental and functional aspects of connectivity. *Nature reviews. Neuroscience* **8**, 287-299.

Rakic, P. (2009). Evolution of the neocortex: a perspective from developmental biology. *Nature reviews. Neuroscience* **10**, 724-735.

Salmena, L., Carracedo, A. and Pandolfi, P. P. (2008). Tenets of PTEN tumor suppression. *Cell* **133**, 403-414.

Steck, P. A., Pershouse, M. A., Jasser, S. A., Yung, W. K., Lin, H., Ligon, A. H., Langford, L. A., Baumgard, M. L., Hattier, T., Davis, T., et al. (1997). Identification of a candidate tumour suppressor gene, MMAC1, at chromosome 10q23.3 that is mutated in multiple advanced cancers. *Nature genetics* **15**, 356-362.

Sulis, M. L. and Parsons, R. (2003). PTEN: from pathology to biology. *Trends in cell biology* **13**, 478-483.

Sun, H., Lesche, R., Li, D. M., Liliental, J., Zhang, H., Gao, J., Gavrilova, N., Mueller, B., Liu, X. and Wu, H. (1999). PTEN modulates cell cycle progression and cell survival by regulating phosphatidylinositol 3,4,5,-trisphosphate and Akt/protein kinase B signaling pathway. *Proceedings of the National Academy of Sciences of the United States of America* **96**, 6199-6204.

Tarabykin, V., Stoykova, A., Usman, N. and Gruss, P. (2001). Cortical upper layer neurons derive from the subventricular zone as indicated by Svet1 gene expression. *Development* **128**, 1983-1993.

Varga, E. A., Pastore, M., Prior, T., Herman, G. E. and McBride, K. L. (2009). The prevalence of PTEN mutations in a clinical pediatric cohort with autism spectrum disorders, developmental delay, and macrocephaly. *Genetics in medicine : official journal of the American College of Medical Genetics* **11**, 111-117.

Wang, Y., Kim, E., Wang, X., Novitch, B. G., Yoshikawa, K., Chang, L. S. and Zhu, Y. (2012). ERK inhibition rescues defects in fate specification of Nf1-deficient neural progenitors and brain abnormalities. *Cell* **150**, 816-830.

Wang, Y., Yang, J., Zheng, H., Tomasek, G. J., Zhang, P., McKeever, P. E., Lee, E. Y. and Zhu, Y. (2009). Expression of mutant p53 proteins implicates a lineage relationship between neural stem cells and malignant astrocytic glioma in a murine model. *Cancer cell* **15**, 514-526.

Yue, Q., Groszer, M., Gil, J. S., Berk, A. J., Messing, A., Wu, H. and Liu, X. (2005). PTEN deletion in Bergmann glia leads to premature differentiation and affects laminar organization. *Development* **132**, 3281-3291.

Chapter V: Experimental procedures, materials and methods

5.1 Control and mutant mice

The mutant mice used in this study had various genotypic configurations. For brain tumor formation hGFAP-cre; *p53*$^{flox/flox}$, hGFAP-cre; *p53*$^{flox/flox}$; *Rictor*$^{flox/+}$, hGFAP-cre; *p53*$^{flox/flox}$; *Rictor*$^{flox/flox}$ were used. A second group of mice as a validation cohort carried additional Pten mutation as follows: hGFAP-cre; *p53*$^{flox/flox}$; *Pten*$^{flox/+}$, hGFAP-cre; *p53*$^{flox/flox}$; *Pten*$^{flox/+}$; *Rictor*$^{flox/+}$ (or *Rictor*$^{KO/+)}$, hGFAP-cre; *p53*$^{flox/flox}$; *Pten*$^{flox/+}$; *Rictor*$^{flox/flox}$. For developmental biology studies, we utilized a non-tumorigenic mutant mouse model with genotype of hGFAP-cre; *p53*$^{flox/+}$;*Rictor*$^{flox/flox}$. The control group was a collection of hGFAP-cre$^{(negative)}$ mice that were phenotypically indistinguishable and completely healthy. In addition, brain tumors from a group of Ptch1$^{+/-}$ mice (Treisman et al., unpublished data) with the genotype of hGFAP-cre; *Ptch1*$^{+/-}$, hGFAP-cre; *Ptch1*$^{+/-}$; *p53*$^{flox/flox}$, hGFAP-cre; *Ptch1*$^{+/-}$; *p53*$^{flox/R172P}$ were used as SHH medulloblastoma controls. All the mice were maintained in the mixed backgrounds of C57Bl6, 129Svj, and FVB, which improve overall health and life span of the mice. Age and littermate-matched control and mutant mice were used for the developmental analyses to minimize the impact of modifier genes. Brain tumor mice were either littermates or close relatives collected over approximately 5 years. All mice in this study were cared for according to the guidelines that were approved by the Animal Care and Use Committees of the University of Michigan at Ann Arbor and Children's National Medical Center, Washington, DC.

5.2 Genotyping and PCR

Taq 2X MeanGreen Master Mix (Empirical Bioscience) was used in PCR experiments along with the following primer sets for tail and tumor tissue genotyping:

p53

X6.5: 5’ ACAGCGTGGTGGTACCTTAT 3’

e7: 5’ CATGCAGGAGCTATTACACA 3’

e4: 5’ TGGGACAGCCAAGTCTGTTA 3’

Rictor (flox)

F1: 5’ CAAGCATCATGCAGCTCTTC 3’

F3: 5’ TGCCTCATAGCATCTCCTCA 3’

R3: 5’ AAGCATGGTAACATGGTATCAAAA 3’

Rictor (KO)

C1: 5’ AGATAGCCAGAAGTGGGCATCGGACCC 3’

C2: 5’ CATCTAGGACTTCTCTCTGCAACAGATGCAGATCAC 3’

C3: 5’ TGGGGTTCGTGTCCTACAACACACACTCC 3’

Pten

A: 5’ GTCACCAGGATGCTTCTGAC 3’

C: 5’ CTCCTCTACTCCATTCTTCCC 3’

E: 5’ ACTATTGAACAGAATCAACCC 3’

Cre

ICres: 5’ CCGTTTGCCGGTCGTGGG-3’

ICreas: 5’ CGTATATCCTGGCAGCGATC 3’

Rosa-26 LacZ (R26R)

R26R-1: 5’ AAAGTCGCTCTGAGTTGTTAT 3’

R26R-2: 5’ GCGAAGAGTTTGTCCTCAACC 3’

R26R-3: 5’ GGAGCGGGAGAAATGGATATG 3’

5.3 Tissue preparations, histopathology and tumor diagnosis

Approximately 70% of the mice were sacrificed due to observable neurological symptoms including enlarged head, tremor, seizure, ataxia, or lack of balance indicating the presence of an end-stage brain tumor. One set of these mice were perfused using 4% paraformaldehyde (PFA), brains were collected and kept in 4% PFA for at least one day. The second set of mice sacrificed based on cervical dislocation procedure after anesthesia with 3.5 % Tribromoethanol (Avertin). The brains were collected in cold environment, soaked in cold PBS and cut sagittally along the midline. One half of the brain was kept in 4% PFA while the other half was used for SNAP-frozen tissue collection in liquid nitrogen and cell culture preparation. Processed and paraffin embedded brain samples were sectioned sagittally at 5 μm and collected on Superfrost Plus microscope slides (Fisher Scientific). Hematoxylin and eosin (H&E) staining was performed approximately every 10 slides and adjacent sections were subjected to immunohistochemical analysis using the antibodies for p53, Olig2, GFAP, Synaptophysin and Pax6. Samples were analyzed under a light microscope by two investigators (SCP and SA) based upon the World Health Organization (WHO) criteria of the classification of tumors in the CNS (Louis et al., 2007). Final diagnoses were reached as a consensus of H&E staining findings and immunohistochemical analyses.

High-grade gliomas included anaplastic astrocytoma, glioblastoma, anaplastic oligoastrocytoma and anaplastic oligodendrioglioma. The multinucleated and/or horseshoe-shaped giant cells and atypical pleomorphic tumor nuclei, including elongated, bent and dark stained nuclei characterizing neoplastic cells were noted in the malignant tumors. The anaplastic tumor cells had increased mitotic activity with abnormal mitotic spindle and coarse nuclear chromatin. The malignant tumors exhibited aggressive growth patterns and some of them displayed secondary structures of Scherer, including perineuronal satellitosis, perivascular growth and subpial aggregates. The dome tumor had a more nodular and relatively sharp demarcated growth with the surrounding parenchyma. Microvascular proliferation and/or necrosis (pseudo-palisading, geographic or coagulation necrosis) were required for a GBM diagnosis. Oligodendrioglioma cells had round nuclei and clear cytoplasm (“fried egg” appearance). Regardless of their

location and type, majority of the glioma cells had nuclear p53 and Olig2 staining while Pax6 immunoreactivity was very low or none. GFAP staining around the irregularly shaped nuclei labeled the tumor cells, though, many reactive astrocytes were $GFAP^+$ as well. Synaptophysin staining was absent within the tumor cells and highlighted the entrapped neuropil.

Medulloblastomas had a higher nuclear/cytoplasm ratio with scant cytoplasm. Classic medulloblastomas had dark small nuclei while large cell/anaplastic tumors were characterized by the carrot-shaped nuclei with nuclear molding or cellular wrapping. Both types of medulloblastomas were mitotically very active and occasionally displayed subarachnoid spread. Homer-Wright rosette (neurofibrillary rosette) and the apoptotic cells were observed in several samples. On the contrary of the high-grade gliomas, medulloblastomas had a very prominent Pax6 immunoreactivity while Olig2 staining was minimal. Synaptophysin was usually weak and granular in tumor cells, though, isolated cases had easily noticeable Synaptophysin staining. Of note, a subset of the medulloblastomas showed a proportion of tumor cells with GFAP immunoreactivity, suggestive of glial differentiation. Nuclear p53 staining was easily detected in many tumor cells.

Final diagnoses were reached as a consensus of H&E staining findings and immunohistochemical analyses. In rare cases where a clear diagnosis was hard to reach, Olig2 and Pax6 staining were taken as conclusive criteria as Olig2 was very characteristic to high-grade gliomas while Pax6 labeled the medulloblastomas distinctively.

5.4 Immunohistochemistry and immunofluorescence

Histological and molecular experiments were performed as described before (Wang et al., 2009). Adjacent paraffin sections were used in immunohistochemistry and immunofluorescence analyses. Slides were first deparaffinized through a series of Xylene, Ethanol and PBS treatments, boiled in Retrieve-All antigen unmasking system

(Covance), permeabilized in 0.3% Triton X-100 (Sigma-Aldrich) and blocked with 5% normal goat serum or normal donkey serum prior to overnight primary antibody incubation in cold room. The visualization of the primary antibodies in immunohistochemistry was performed with the avidin/biotin-based peroxidase system (Vectastain Elite ABC System, Vector Laboratories), except for $pAkt^{S473}$ and Pten, for which SignalStain Boost IHC Detection Reagent HRP-rabbit (Cell Signaling) was used. The dilutions of the primary antibodies used on paraffin sections in immunohistochemistry study were: p53 (1:500, rabbit, Leica), Olig2 (1:2,000, rabbit, Millipore), GFAP (1:1,000, rabbit, Dako), Synaptophysin (1:200, rabbit, Covance), Pax6 (1:500, rabbit, Covance), Ki-67 (1:500, rabbit, Abcam), $pAkt^{S473}$ (1:200, rabbit, Cell Signaling) and Pten (1:400, rabbit, Cell Signaling). In addition to aforementioned antibodies, Cleaved caspase-3 antibody (1:500, rabbit, Cell Signaling) is used in immunohistochemistry study of the brain development project. Sections were examined under a light microscope (Olympus BX51 or BX53). The visualization of the primary antibodies in immunofluorescence was performed with the use of the Alexa488, Alexa555 and Alexa647 conjugated secondary antibodies (1:400, Invitrogen, Life Technologies). The dilutions of the primary antibodies used on paraffin sections in immunofluorescence study were: p53 (1:500, rabbit, Leica), BrdU (1:500, rat, Abcam), Olig2 (1:2,000, rabbit, Millipore), Ki-67 (1:500, rabbit, Abcam), Ascl1 (1:100-1:200, mouse, BD PharMingen), GFAP (1:1,000-1:2,000, rabbit, Dako), Nestin (1:100, mouse, Millipore), Sox2 (1:250, goat, Santa Cruz Biotech), Pax6 (1:500, rabbit, Covance) and NeuN (1:500, mouse, Millipore). DAPI was used to label individual cell nucleus. In addition to aforementioned antibodies, following antibodies are used in immunofluorescence study of the brain development project: Ctip2 (1:500, rat, Abcam), Cux1 (CDP) (1:100, rabbit, Santa Cruz), and Pten (1:400, rabbit, Cell Signaling). Sections were examined under a fluorescent microscope (Olympus BX53).

5.5 BrdU assay for the analyses of proliferation and differentiation

For the proliferation assay, mice were injected with 50 μg/g (gram, body weight) of BrdU

every two hours. Embryonic and newborn mice received only one, pups and neonatal mice up to 30 days old received two, mice around two months old received three and adult mice older than two months old received five injections every two hour-intervals. All of the mice were perfused with 4% PFA two hours after the last pulse. For the differentiation assay, P15 mice were injected with 50 μg/g (gram, body weight) of BrdU only once and perfused with 4% PFA 48 hours later. In both assays, brains were dissected and processed for either paraffin-embedded or cryostat sections. BrdU immunofluorescence was performed as described previously (Wang et al., 2009).

5.6 Western blotting

Snap-frozen tissue samples from wild-type control brains and tumors were homogenized in Pierce RIPA Buffer (Thermo Scientific) (10 μl buffer/1 mg tissue), mixed 1:1 with Laemmli Sample Buffer (BioRad) and boiled at 100°C for 8 minutes. Samples were then subjected to SDS-PAGE using the Criterion TGX Precast gels (BioRad) and transferred onto PVDF membranes (Millipore). The membranes were blocked in 5% non-fat milk prepared in TBST and incubated with primary antibodies at 4°C overnight. Next day, the membranes were washed with TBST and incubated in horseradish peroxidase (HRP)-conjugated secondary antibodies at room temperature for 1 hour. The membranes were then exposed to Pierce ECL western blotting substrate (Thermo Scientific) for 3 minutes and the signals were detected by film development in dark room. The primary antibodies used in this study were as follows: $pAkt^{S473}$ (1:1,000, rabbit, Cell Signaling), $pAkt^{T308}$ (1:1,000, rabbit, Cell Signaling), Akt (1:1,000, rabbit, Cell Signaling), $pNDRG1^{T346}$ (1:1,000, rabbit, Cell Signaling), Pten (1:1,000, rabbit, Cell Signaling), Rictor (1:500, rabbit, D. Fingar), mTOR (1:1,000, rabbit, Cell Signaling), β-Actin (1:5,000-10,000, mouse, Sigma-Aldrich), $pS6K^{T389}$ (1:1,000, rabbit, Cell Signaling), $p4E\text{-}BP1^{T37/46}$ (1:1,000, rabbit, Cell Signaling), $pTSC2^{T1462}$ (1:1,000, rabbit, Cell Signaling), $pS6^{S240/244}$ (1:2,000, rabbit, Cell Signaling), S6 (1:2,000, rabbit, Cell Signaling), Olig2 (1:4,000, rabbit, Millipore), cMyc (1:1,000, rabbit, Cell Signaling), $pErk1/2^{T202/Ty204}$ (1:1,000, rabbit, Cell Signaling), Erk1/2 (1:1,000, rabbit, Cell Signaling), $pGSK\text{-}3\beta^{S9}$ (1:2,000,

rabbit, Cell Signaling), P120 (1:1000, mouse, BD Biosciences), Pax6 (1:1,000, rabbit, Covance), Gli1 (1:500, rabbit, Cell Signaling) and Ezh2 (1:1,000-1:2,000, rabbit, Cell Signaling). HRP-conjugated secondary antibodies were anti-mouse (1:5,000-1:10,000, goat, BioRad) and anti-rabbit (1:5,000-1:10,000, goat, BioRad).

5.7 Tumor-sphere cell culture and chromosome assay

End-stage tumors were dissected in cold environment and the tissues were transferred into DMEM medium, followed by enzymatic cell dissociation using Accutase (Innovative Cell Technologies). Cell cultures were then prepared in self-renewal medium based on a previously published protocol (Molofsky et al., 2003). Cell density was quantified on a cell-counter plate and approximately 20,000-100,000 cells/well were plated into 6-well ultra-low attachment surface polystyrene plates (Corning) for primary tumor-sphere cultures. The medium was changed every 3-5 days and the cultured cells were passaged into two new 6-well plates after 1-2 weeks based on the growth rate and passage number. The first plate was used to propagate the cell line while the second one, containing approximately 1-2 million cells, was used for chromosome analyses based on a Metaphase preparation protocol from Dr. David Ferguson's laboratory (Ferguson et al., 2000). According to this protocol, cells were grown for 24 hours, treated with 100 ng/ml KaryoMax Colcemid solution (Gibco, Life Technologies) for 1 hour to arrest proliferation at metaphase. Cells were then treated with 0.4% KCl at 37°C, fixed in ice cold Methanol:Glacial acetic acid (3:1) solution overnight and dropped on Superfrost Plus microscope slides (Fisher Scientific). The chromosomes were stained with DAPI for visualization. Passage 1 and passage 2 were considered as "early passage" and the subsequent passages were considered as "late passage".

5.8 RT-PCR for copy number analyses

Total genomic DNAs were extracted from wild-type control brain tissue, high-grade gliomas and medulloblastomas by using AllPrep DNA/RNA Mini Kit (Qiagen). Depending on the sample concentration, various amounts of template DNA (average 100 ng/reaction) along with the SYBR Select Master Mix (Applied Biosystems) and the following primers were used in RT-PCR:

Pten (Exon 5)

Forward: 5' AGACCATAACCCACCACAGC 3'

Reverse: 5' TACACCAGTCCGTCCCTTTC 3'

Pten (Exon 9)

Forward: 5' GGTTCACGTCCTACCCCTTT 3'

Reverse: 5' TCTGAGCATTCCCTCCATTC 3'

Dmbt1

Forward: 5' GTGAAGAAGCCAGCAAGCTC 3'

Reverse: 5' CACGGTCAATGTGTGTCCTC 3'

Gli1

Forward: 5' GCTCCGCAAACACGTGAAGA 3'

Reverse: 5' GCCGGATCCTCCTTCCCTTT 3'

Gli2

Forward: 5' TCTAGTCCACGTGTGACCCC 3'

Reverse: 5' AGGTCCGAATCATGCGTTGT 3'

N-Myc

Forward: 5' AGGAAGCACTCCCCCATATT 3'

Reverse: 5' CCGCCGAAGTAGAAGTCATC 3'

Gapdh

Forward: 5' ACCCAGAAGACTGTGGATGG 3'

Reverse: 5' CACATTGGGGGTAGGAACAC 3'

β-Actin

Forward: 5' GACGTTGACATCCGTAAAGACC 3'

Reverse: 5' AGGAGCCAGAGCAGTAATC 3'

The CT values of the each gene listed above were normalized to the CT values of one of the internal control genes *Gapdh* and *β-Actin.* The average of the normalized readings from wild-type control tissue were set to "2" and all of the samples were calculated accordingly. The estimated copy numbers based on *Gapdh* and *β-Actin* were compared to each other to confirm the accuracy of the copy number calculations.

5.9 RT-PCR for gene expression analyses

Total RNAs were extracted from wild-type control brain tissue, high-grade gliomas and medulloblastomas by using AllPrep DNA/RNA Mini Kit (Qiagen). cDNA synthesis was performed using QuantiTect Reverse Transcription Kit (Qiagen) a long with approximately 300ng of RNA for each sample. RT-PCR experiments were carried out using the SYBR Select Master Mix (Applied Biosystems) and the following primers:

Gli1

Forward: 5' CCAAGCCAACTTTATGTCAGGG 3'

Reverse: 5' AGCCCGCTTCTTTGTTAATTTGA 3'

Gli2

Forward: 5' CGCACTCACTCCAATGAGAA 3'

Reverse: 5' GGACATGCACATCATTACGCCT 3'

N-Myc

Forward: 5' AGGAAGCACTCCCCCATATT 3'

Reverse: 5' CCGCCGAAGTAGAAGTCATC 3'

Atoh1

Forward: 5' GAGTGGGCTGAGGTAAAAGAGT 3'

Reverse: 5' GGTCGGTGCTATCCAGGAG 3'

Ptch1

Forward: 5' CTCAGGCAATACGAAGCACA 3'

Reverse: 5' GACAAGGAGCCAGAGTCCAG 3'

Gapdh

Forward: 5' ACCCAGAAGACTGTGGATGG 3'

Reverse: 5' CACATTGGGGGTAGGAACAC 3'

The CT values of the each gene listed above were normalized to the CT values of the internal control gene *Gapdh*. The average of the normalized readings from the $Ptch1^{+/-}$ model medulloblastomas were set to "100" and all of the samples were calculated accordingly. Wild-type control brain tissue and gliomas were used as negative controls for medulloblastoma samples.

5.10 Quantification and statistical analyses

Kaplan-Meier survival curves were used to compare the survivorship of the mice sacrificed due to brain tumors, soft tissue sarcomas and/or other health concerns. The Mantel-Cox (Log-rank) test was used to compare the curves statistically. Anatomically comparable sections from control and mutant brains were visualized at 20X and 40X magnifications using Olympus BX51 or BX53 microscopes. Multiple images were captured, and subjected to double-blinded analysis to measure the specific areas (i.e. cerebellar surface area) and to quantify the number of the cells using ImageJ software. At least three animals were used from each group and two-tailed Student's t-test was used to compare the number and percentage of the different cellular populations (i.e. $Pax6^{+}$ cells, [$Ki\text{-}67^{+}$/ DAPI], etc.). Fisher's exact test was used to compare the mouse models in terms of the tumor location and tumor spectrum. Linear regression analysis was performed in RT-PCR experiments for copy number estimates comparing the readings based on two different reference genes. The coefficient of determination (R^2) and p-values were calculated. Data were presented as mean ± Standard Deviation (SD) and $p < 0.05$ was considered to be statistically significant in all of the statistical analyses.

5.11 Bioinformatics

Gene expression profiles and copy number analyses of GEM glioma samples and the detailed analyses of the human glioblastoma samples were performed by Dr. Roeland G.W. Verhaak and Dr. Siyuan Zheng at the University of Texas MD Anderson Cancer Center, Houston, TX. Gene expression profiles and low-coverage copy number analyses of GEM medulloblastoma samples were carried out by Dr. Stefan M. Pfister, Dr. Marcel Kool, Dr. Sebastian Stark and Susanne Gröbner at the German Cancer Research Center (DKFZ), Heidelberg, Germany.

5.12 References

Ferguson, D. O., Sekiguchi, J. M., Chang, S., Frank, K. M., Gao, Y., DePinho, R. A. and Alt, F. W. (2000). The nonhomologous end-joining pathway of DNA repair is required for genomic stability and the suppression of translocations. *Proceedings of the National Academy of Sciences of the United States of America* **97**, 6630-6633.

Louis, D. N., Ohgaki, H., Wiestler, O. D., Cavenee, W. K., Burger, P. C., Jouvet, A., Scheithauer, B. W. and Kleihues, P. (2007). The 2007 WHO classification of tumours of the central nervous system. *Acta neuropathologica* **114**, 97-109.

Molofsky, A. V., Pardal, R., Iwashita, T., Park, I. K., Clarke, M. F. and Morrison, S. J. (2003). Bmi-1 dependence distinguishes neural stem cell self-renewal from progenitor proliferation. *Nature* **425**, 962-967.

Wang, Y., Yang, J., Zheng, H., Tomasek, G. J., Zhang, P., McKeever, P. E., Lee, E. Y. and Zhu, Y. (2009). Expression of mutant p53 proteins implicates a lineage relationship between neural stem cells and malignant astrocytic glioma in a murine model. *Cancer cell* **15**, 514-526.

Chapter VI: Discussion and future directions

The main objective of my thesis work is to determine the cell-specific roles of Rictor/mTORC2, and by extension PI3K/Akt signaling, during the mutant-*p53*/*Pten* induced brain tumorigenesis and brain malformations. My projects can be described in three parts: In the first part, I aimed to understand the potential tumor suppressive activity of *Rictor* loss in mouse gliomas, which are characterized by their detrimental genomic alterations mimicking human glioblastoma. Second part was dedicated to uncovering a novel role of Rictor/mTORC2 signaling in the development of mutant-*p53* driven medulloblastoma (Figures 17 and 22). Lastly, I studied the interplay between Pten and Rictor during the embryonic cortical development, and how loss of *Pten* leads to neuronal and glial defects that might reflect to the malformations of cortical development in PTEN Hamartoma Tumor Syndrome (PHTS) patients.

6.1 Tumor suppressive activity of *Rictor* loss in high-grade gliomas

6.1.1 Distinctive genomic aberrations in mutant-*p53* GEM gliomas provide insights into the complexity of human glioblastoma

Glioblastomas exhibit extreme degrees of genomic instability accompanied by gene amplifications/deletions, detrimental mutations, epigenetic deregulations, genomic rearrangements, and chromosomal loss/gain (Brennan et al., 2013; Cancer Genome Atlas Research, 2008; Noushmehr et al., 2010; Sturm et al., 2012). Of those, one particular attention has been drawn to large deletions in chr10, which was reported in as early as

1980s, and currently known as the most frequent genomic alteration (~90%) in glioblastomas regardless of their molecular subgroup (Bigner et al., 1984; Verhaak et al., 2010). These deletions in chr10 exhibited losses that are either confined to 10q, or included essentially the entire chromosome. Entire chromosomal loss is observed in non-G-CIMP (primary) glioblastomas, while restricted 10q loses are observed mostly in G-CIMP (secondary) glioblastomas (Ozawa et al., 2014; Phillips et al., 2006). Consequently, loss of several tumor suppressor genes normally located on this chromosome has been thought to contribute to a greater malignancy in glioblastoma. Although *PTEN* gene (located at 10q.23) is considered to be the main target of chr10 deletions, additional studies have also shown the presence of other putative tumor suppressor genes, including *LGI1* (10q.24), *MXI1* (10q.24-25), *DMBT1* (10q.26), and *WDR11* (10q.26), that might be involved in gliomagenesis (Chernova et al., 2001; Ichimura et al., 1998; Wechsler et al., 1997). Homozygous deletion of *DMBT1*, particularly, was associated with unfavorable clinical outcomes in glioblastoma patients (Motomura et al., 2012). In light of these findings, we aimed to reveal the genomic alterations in our mouse models carrying mutant-*p53* genes with or without *Nf1* mutations. It should be considered that human chr10 is distributed into several different chromosomes in mouse genome. The human 10q loci that contain the aforementioned tumor suppressor genes mostly correspond to mouse chr19 and chr7. More specifically, while *Pten*, *Lgi1*, and *Mxi1* genes are located in mouse chr19, *Dmbt1* and *Wdr11* are located in mouse chr7. Remarkably, our current study has demonstrated that mutant-*p53 driven* high-grade gliomas undergo simultaneous deletions of genomic loci in chr7 and chr19 corresponding to human chr10q. I additionally showed that *Pten* and *Dmbt1* genes are indeed concurrently lost in mutant-*p53* GEM gliomas. Therefore, the independent but simultaneous deletions of mouse chr19 and chr7 in mutant-*p53* GEM gliomas have three main interpretations: 1) Mouse models that allow the sporadic genomic alterations comparable to human counterparts are essential to understand the complexity of glioblastomas. 2) Our mutant-*p53* glioma models, with or without *Nf1* gene mutations, mimic human disease not only by gene expression profile but also at the genomic level. 3) Concurrent loss of at least two tumor suppressor genes, which are located in human

chr10q and independently distributed to mouse chr19 and chr7, might exert an additive oncogenic effect that results in malignancy in glioblastomas.

It should be noted that we did not detect simultaneous deletions of chr19 and chr7 in our other mouse models that already had a genetically mutated *Pten* allele. Similarly, previously reported GEM gliomas generated by deletions of *p53* and *Pten* genes with or without *Rb* deletion did not exhibit noticeable losses in either of the chromosomes. These results suggest that despite the probable additional oncogenic effect of deletions in various tumor suppressor genes, the major target of chr10 loss in glioblastomas is *PTEN* gene. This finding also indicates a fine line between successfully inducing tumorigenesis by genetic modifications and nullifying the necessity to acquire critical genomic alterations frequently observed during the natural progression of human glioblastomas. Our mutant-*p53* models are then unique in that they gain spontaneous genomic alterations that are equivalent to human counterparts.

While providing novel insights, our findings here also raise new questions: If the simultaneous deletion of multiple tumor suppressor genes in human chr10q provides only a minor tumorigenic advantage, why then do the majority of the glioblastoma samples undergo whole chromosomal loss rather than confined deletions in *PTEN* gene? Is it possible that the oncogenic gain by loss of these tumor suppressor genes is masked by the *PTEN* alterations? If so, can recovering their function have more dramatic affect than their loss? Would this then imply a therapeutic approach?

6.1.2 Rictor/mTORC2 activity is essential, but not absolutely required, for formation and progression of high-grade gliomas

Several lines of evidence have shown that PI3K/RTK signaling is an essential survival pathway in many cancer types, and it is activated in approximately 90% of the glioblastomas regardless of their molecular subgroup (Brennan et al., 2013; Cancer Genome Atlas Research, 2008). There are multiple mechanisms for PI3K/RTK pathway

activation, and the most frequent ones include the loss of PTEN function (as described above), amplifications of or gain of mutations in *PIK3CA* and *AKT* genes, and hyperactivation of growth factor receptors (e.g. EGFR, PDGFR) via mutations or amplifications. As it serves as a convergence point for many growth stimuli, and activates a divergent set of downstream components that function in cell survival, cell proliferation, cell metabolism and angiogenesis, several studies investigated the potential therapeutic benefits of targeting PI3K/RTK signaling pathway and its major effector AKT (Bellacosa et al., 2005). Two of those studies took advantage of the fact that mTORC2, along with PDK1, is a kinase that directly phosphorylates and subsequently activates AKT. Accordingly, deletion of *Rictor*, which normally serves as a critical component of mTORC2, inhibited *Pten* deficiency driven tumorigenesis in mouse prostate epithelial cells and also hematopoietic stem cells (Guertin et al., 2009; Magee et al., 2012). These studies not only provided evidences for the essential role of Rictor/mTORC2 signaling in adult tumors, but also confirmed a previously raised theory addressing the oncogene addiction of tumor cells. According to this theory, tumor cells exhibit "oncogene addiction" to a signaling pathway for their malignancy, proliferation and/or survival, and identification of "Achilles' heel" of the tumor cells is critical to attack cancer effectively (Sharma and Settleman, 2007; Weinstein, 2002).

Supported by these findings, I aimed to test whether *Rictor* loss would provide similar anti-tumor activity in high-grade gliomas. As discussed earlier, high-grade gliomas of mutant-*p53* mouse models recapitulated the key genomic events that are frequently observed in human glioblastomas. Since genetic removal of *Pten* gene nullified the necessity to go through these genomic abnormalities, I decided to test my hypothesis using mouse models that had tissue-specific mutation in *p53* gene only. This was a different approach from the prostate cancer and leukemia studies performed by *Guertin et al.* and *Magee et al.*, which relied on *Pten* deficiency driven tumorigenesis. In the present study, I showed that simultaneous loss of *Rictor* in mutant-*p53* mice indeed exerts a tumor suppressive activity in mutant-*p53* driven high-grade gliomas, as evidenced by a significant drop in the frequency of glioma formation, and the extended life span in the

remaining mutant mice that eventually formed high-grade gliomas. My subsequent early-stage analyses aiming to understand the cellular mechanisms by which *Rictor* loss exerted an anti-glioma affect relied on the previous findings showing that tumor cells and early tumor-forming cells express mutant-p53 protein (Wang et al., 2009): Mutant-*p53* gene in our mouse model has an in-frame deletion of exon-5 and -6, which normally express DNA-binding domain of p53 protein. Truncated *p53* gene is still translated into protein, yet does not have a transcription factor activity. Therefore, both the cells that experience cellular stress and the end-stage tumor cells continuously express truncated mutant-p53 protein - a phenomenon that was uncovered long ago in many human tumors that carried mutations in their *TP53* gene (Anker et al., 1993). Based on this information, my colleague Dr. Yuan Wang previously demonstrated a linage relationship between mutant-p53 expressing ($p53^+$) "tumor-incipient" cells and the end-stage gliomas (Wang et al., 2009). My additional analyses revealed that *Rictor* deficiency does not affect the generation of the $p53^+$ cells within the germinal zone, which is defined by the Subventricular zone and Rostral migratory stream. But interestingly, it blocks the spreading of these $p53^+$ cells into the surrounding areas, including corpus callosum, cerebral cortex, hippocampus, and olfactory bulb. Thus, these findings suggest that an intact Rictor/mTORC2 signaling is essential for the invading expansion of the $p53^+$ cells throughout the brain, which is one of the central steps in gliomagenesis. In addition to the early stages of tumor formation, I analyzed the high-grade gliomas that formed even in the absence of functional *Rictor* gene. It should be noted that these glioma bearing *Rictor*-deficient mice lived significantly longer (~50%), which suggests that *Rictor* loss still has a tumor suppressive effect on end-stage gliomas. As suggested by my following experiments, this suppression might be exerted by a reduction in tumor cell proliferation that is accompanied by alleviated mTORC2 and mTORC1 signaling pathways. Together, we believe that combinatory treatment strategies that involve Rictor/mTORC2 inhibitors will improve the clinical outcome during both the early and late stages of glioblastomas (Figure 22).

Despite the presence of promising preclinical data, clinical trials utilizing PI3K/AKT/mTOR pathway inhibitors produced mostly infrequent and short-lived responses (Wen et al., 2012). There might be several reasons that led to this disappointment. 1) Regulation of numerous genes and networks is disrupted in glioblastomas, suggesting that targeting several molecular pathways is more likely to improve the clinical outcomes. For instance, a recent study showed that both AKT-dependent and –independent mechanisms underlie the drug resistance in *PTEN*-deficient glioblastoma samples (Mellinghoff et al., 2005). 2) Patient selection is proven to be a critical step to reach the maximum benefit from a therapeutic agent. 3) Drug delivery through the blood-brain barrier can build further challenge. 4) Toxicity concerns are still a drawback, as evidenced by lipid-based AKT inhibitors exerting gastrointestinal toxicity (LoPiccolo et al., 2008; Wen et al., 2012). Our data in the present study confirm the first two issues, and provides future directions addressing them. As described earlier, a relatively lower percentage of *Rictor*-deficient mice succumbed to high-grade gliomas, despite a significant increase in their overall survival. This finding suggests that Rictor/mTORC2/Akt signaling pathway is essential for the development of high-grade gliomas, however, it is not absolutely required. Consistently, our parallel analyses of human glioblastomas showed that there is a significant variation among the samples with regards to their AKT activation, implying different levels of dependence to this oncogenic signal. Our findings, then, open up several future directions: 1) It is essential to uncover the predominant oncogenic pathway(s) in *Rictor*-deficient high-grade gliomas to design new therapeutic agents, especially for PI3K/AKT-resistant glioblastomas. 2) Comparison of several molecular signatures of *Rictor*-deficient high-grade gliomas to human glioblastoma samples will allow us to determine whether these mouse tumors represent a subgroup in their human counterparts. 3) Based on this information, we aim to stratify glioblastoma patients based on their plausible response to Rictor/mTORC2 pathway inhibition, which will not only increase the potential of novel Rictor/mTORC2 inhibitors, but also improve the success rate of the existing PI3K/AKT inhibitors.

6.2 *Rictor* deficiency facilitates mutant-*p53* mediated medulloblastoma formation

6.2.1 *Rictor* loss predisposes cerebellar progenitor cells to mutant-*p53* mediated medulloblastoma formation

Numerous studies have provided several lines of evidence that stem/progenitor cells are one of the major populations that can give rise to various tumors (Chaffer and Weinberg, 2015). A recent study has also demonstrated a strong correlation between the total number of divisions in various stem cell pools and the lifetime risk of cancers in corresponding organs. Accordingly, medulloblastoma was considered as a "replicative" cancer, for which the risk factors are mostly determined by the stochastic events, such as errors during DNA replication, in contrast to "deterministic" cancers (e.g. lung cancer in smokers), for which the environmental mutagens or hereditary predispositions constitute the major risk factors. (Tomasetti and Vogelstein, 2015). Consistently, many of the well-characterized mutations in medulloblastoma occur in genes that normally function in the proliferation and/or self-renewal of the cerebellar stem/progenitor cells (e.g. *PTCH1*, *GLI1*, *GLI2*, *SMO*, *CTNNB1*, *N-MYC*) (Gajjar and Robinson, 2014; Northcott et al., 2012). However, the great portion of the cerebellar stem/progenitor cells exit cell cycle and differentiate into mature cells in a very rapid manner, leaving the cerebellum relatively a quiescent organ throughout the life of the organism. This biological phenomenon might also be responsible for the largely pediatric nature of medulloblastoma, as approximately 88% of the cases are observed in patients younger than 16 years of age (Kool et al., 2012). Therefore, both the presence and the replicative ability of the cerebellar stem/progenitor cells are among the main predispositions for medulloblastoma formation. In light of the knowledge listed here, I further demonstrated that inhibition of Rictor/mTORC2 can delay the natural differentiation of a pool of cerebellar progenitor cells, and provide a short but essential window leading to an increased incidence of mutant-*p53* driven medulloblastoma formation (Figure 17). More specifically, I presented that *Rictor*-deficient cerebellar GNPs fail to differentiate and continue their temporary but abnormal proliferation in the EGL when wild type control

cells already generated fully differentiated neurons and disappeared. In the presence of a concurrent *p53* mutation, a minor population of these ectopically proliferating cells acquires cellular stress, evidenced by their mutant-*p53* expression, and accumulates over time resulting in malignant medulloblastomas. *Rictor* deficiency alone, however, does not cause medulloblastoma, which suggest that p53-dependent mechanisms induce cell cycle exit and differentiation of ectopically proliferating GNPs. It should be noted that despite the increased lifetime risk, medulloblastoma formation in Li-Fraumeni syndrome patients, who harbor germline *TP53* mutations, is still a rare event. Similarly, medulloblastoma development in mutant-*p53* mice is also a rare event (5-10%), as shown here and before (Wang et al., 2009). Therefore, it is remarkable that loss of Rictor/mTORC2, a well-known oncogenic molecule, predisposes cerebellar progenitor cells to mutant-*p53* mediated medulloblastoma formation.

My subsequent aim was to identify the downstream components of the mTORC2 signaling, by which *Rictor* loss led to a temporary delay in GNP differentiation. mTORC2 activates several members of the AGC subfamily of kinases, including AKT, SGK1 and PKC-α (Foster and Fingar, 2010; Laplante and Sabatini, 2012), though AKT is considered to be the major mediator of the RTK/PI3K signaling pathway (Sparks and Guertin, 2010). Interestingly, $pAkt^{S473}$ levels were almost absent in the EGL, where GNPs are actively proliferating, however exhibited high/intermediate levels in ML and IGL – two layers that are occupied by newly differentiated neurons and mature neurons, respectively. Based on these findings, one likely explanation is that absence of Akt signaling is required for the continuous proliferation of the cerebellar progenitor cells, nevertheless its activity is essential for at least a subset of these cells to exit cell cycle and differentiate into mature neurons. We should note that other aforementioned downstream components of mTORC2 might also have roles in this phenomenon. Furthermore, recent studies have suggested that Rictor has mTORC2-independent roles, which includes, surprisingly, SGK1 ubiquitination and destruction (Gao et al., 2010). It is, therefore, likely, and remains to be tested, that multiple downstream effectors of Rictor and

previously identified signaling pathways (e.g. Fgf, Shh) function synergically to regulate the proper lineage progression of GNPs towards mature neurons.

6.2.2 *Rictor* loss promotes mutant-*p53* driven SHH medulloblastomas with unique genomic and chromosomal alterations

Molecular categorization of medulloblastomas has been proposed to improve our understanding of the molecular nature of the disease, which would then allow us to tailor precise therapies based on the genetic makeup that defines individual cases (Gajjar and Robinson, 2014). Two independent analyses, one performed by me and the other one by our collaborators at the German Cancer Research Center (DKFZ), indicated that regardless of the *Rictor* status, mutant-*p53* mediated medulloblastomas have prominent Shh signature, and they actually resemble SHH medulloblastoma models that were generated in earlier studies. This finding is also consistent with the fact that *TP53* mutations are enriched in SHH medulloblastomas (~21%), and these tumors have been shown to arise from cerebellar GNPs (Northcott et al., 2012; Zhukova et al., 2013). SHH medulloblastoma is probably the most studied subtype among the four molecular groups, and the mouse models recapitulating human counterparts have been the main tools of medulloblastoma research for more than a decade (Northcott et al., 2012). Virtually all of these SHH models were generated by genetic manipulations in *Ptch1* (deletion) or *Smo* (constitutive activation) genes resulting in elevated Shh signaling pathway. These models have been shown to be inherently sensitive to SMO-inhibitors, supporting several clinical trials and pharmaceutical research that involve SMO-inhibitors (Berman et al., 2002; Ng and Curran, 2011; Romer et al., 2004). However, it should be noted that approximately half of the SHH medulloblastomas acquire Shh signaling activation without an alteration in *PTCH1*, *SMO* or *SUFU* genes. Furthermore, even in the patients or mouse models that showed initial response to SMO-inhibitors, tumors acquired resistance to these agents, leading to lethality (Ng and Curran, 2011; Rudin et al., 2009). It is, therefore, important to utilize novel mouse models for SHH medulloblastoma that do not rely on genetically engineered *Ptch1* or *Smo* mutations in order to uncover the divergent complexities of

human medulloblastomas, and design therapeutic agents that are independent of Smo activation. We believe that the mutant-*p53* driven medulloblastomas presented here, especially those that are facilitated by concurrent *Rictor* loss, fulfill this need, as they do not have initial mutations in Shh pathway, and undergo spontaneous genomic alterations over the long course of the tumor initiation and progression. The future directions based on our findings would include; 1) testing whether mutant-*p53* medulloblastomas are actually resistant to SMO-inhibitors, and 2) determining whether there is a cross talk between Shh and Akt signaling pathways that may correlate with the tumor response to Shh antagonists. Pertinently, absence of Akt activation in medulloblastoma is our particular interest, as I surprisingly observed that the majority of the mouse medulloblastomas available in our laboratory exhibited very low levels of $pAkt^{S473}$ regardless of their *Rictor* status. As shown previously by Kool et al. (2014), even though almost half of the childhood SHH medulloblastomas undergo 10q loss accompanied by *PTEN* mutations and deletions, pAKT is detected in less than 10% of the cases. These two observations suggest that inactivation of PTEN signaling in childhood SHH medulloblastomas has AKT-independent consequences leading to tumorigenesis. For instance, loss of nuclear functions or protein phosphatase functions of PTEN might have roles in medulloblastoma development. 3) Lastly, we aim to test whether Akt signaling exerts a tumor suppressive effect in a certain group of medulloblastomas.

Approximately 10% of the human medulloblastomas carry *TP53* mutations, which are almost exclusive to WNT (~16%) and SHH (~21%) subgroup tumors. Interestingly, while *TP53* mutations do not produce an observable effect on the overall survival of the WNT patients, its presence has been implicated as the most important risk factor leading to early recurrence and extremely poor outcome in SHH patients (Tabori et al., 2010; Zhukova et al., 2013). Parallel studies with regards to the role of *TP53* mutations in medulloblastoma revealed a strong link between SHH/$TP53^{mut}$ tumors and "tetraploidy" (having a chromosome number four times the monoploid number), and "chromothripsis" (concurrent severe fragmentation of chromosomal regions and a subsequent reassembly in an imperfect or random manner) (Jones and Jallepalli, 2012; Rausch et al., 2012).

Despite the presence of *TP53* mutations, virtually none of the WNT medulloblastomas exhibited tetraploidy or chromothripsis, underlining the context dependent role of *TP53* mutations and subsequent genomic abnormalities (Rausch et al., 2012). These findings are also consistent with the aforementioned observations that the presence of *TP53* mutation is associated with a poor clinical outcome only in SHH, but not in WNT medulloblastomas. Functional consequences of these chromosomal aneuploidies and catastrophic DNA rearrangements uncovered the presence of gene amplifications in Shh signaling downstream components, including *N-MYC*, *GLI1*, *GLI2*, and *BOC*. These genomic events are further correlated with inherent resistance to SMO-inhibitors and consequential poor clinical outcome (Gajjar and Robinson, 2014; Northcott et al., 2012). In light of these findings, I investigated whether our mutant-*p53* medulloblastomas exhibited similar genomic alterations. My results suggested that while approximately 80% of the *Rictor*-deficient/mutant-*p53* medulloblastomas exhibited noticeable amplifications in *N-Myc* gene, almost none of the other mutant-*p53* mice (i.e. with an intact *Rictor* allele(s)), including $Ptch1^{+/-}$ models, displayed similar genomic alterations. Furthermore, I also detected *Gli2* amplifications in approximately 30% of the mutant-*p53*-*Rictor* medulloblastomas. Our collaborators in DKFZ analyzed another set of mutant-*p53* mediated medulloblastomas and showed comparable results, though *Gli2* amplification was more noticeable than *N-Myc* amplification. It should, however, be noted that their findings were based on low-coverage copy number analyses, which may represent less accurate results. Having shown that *Rictor*-deficient/mutant-*p53* medulloblastomas carry gene amplifications in key Shh components, I analyzed the chromosomal status of these tumors. Remarkably, approximately 65% of the *Rictor*-deficient/mutant-*p53* medulloblastomas had noticeable increase in their chromosome number, reminiscent of tetraploidy. Based on these results, I concluded that *Rictor* deficiency facilitates the formation of mutant-*p53* mediated medulloblastomas, which exhibit characteristic genomic and chromosomal abnormalities that are associated with poor clinical outcome and resistance to SMO-inhibitor therapy.

While these findings provide novel insights into the role of Rictor/mTORC2 and p53 signaling in medulloblastoma formation, they also open up several future directions: 1) I showed that *Rictor*-deficient/mutant-*p53* medulloblastomas have increased numbers of chromosomes similar to tetraploidy. The question is, then, whether they also exhibit the features of chromothripsis that might explain their gene amplifications. 2) My copy number analyses and our collaborators' results suggested that *N-Myc* amplification is an exclusive event for *Rictor*-deficient medulloblastomas. Does particular absence of Rictor signaling promote *N-Myc* amplification and possibly other key oncogenes involved in Shh signaling? 3) As the previous studies suggested, are these mouse medulloblastomas with gene and chromosome amplifications resistant to SMO-inhibitors? If so, can we use them in *in vivo* and *in vitro* drug screening analyses to identify novel agents for SMO-inhibitor resistant medulloblastomas?

6.3 Intact Pten signaling regulates cortical neuronal layering and maintains neuronal subpopulations

Apart from its role in brain tumorigenesis, I also studied Rictor/mTORC2 and Pten signaling pathways in cortical development during the embryonic stages. The starting point of my research was based on three previous findings: 1) *Pten* deficiency in mice causes severe increase in head circumference (macrocephaly) (Fraser et al., 2004; Groszer et al., 2001). 2) Macrocephaly is the most consistent physical characteristic of children with autism. 18-24% of the autism patients exhibited macrocephaly, and 80% of the patients had head circumferences above the mean (Davidovitch et al., 1996; Orrico et al., 2009; Stevenson et al., 1997). 3) *PTEN* mutations in PHTS patients are strongly associated with autism spectrum disorders (ASD), developmental delay, and macrocephaly. Accordingly, macrocephaly is the most common abnormality in PHTS patients, 20-50% of whom are also diagnosed with ASD (Lynch et al., 2009; Varga et al., 2009). In light of these studies, I aimed to understand how elevated Akt signaling as a result of *Pten* deficiency affect different neuronal populations in the cerebral cortex that

might be relevant to the cognitive defects observed in PHTS patients. I also investigated the therapeutic impacts of simultaneous *Rictor* loss on *Pten* deficiency phenotypes.

In addition to severely increased size, my initial observation in *Pten*-deficient brains was the presence of blood spots that were randomly distributed on the cortex. I subsequently found that large areas of tissue degeneration and apoptosis accompanied these blood spots. I also detected significant number of reactive astrocytes infiltrating the cerebral cortex, which might have contributed to the progressive brain enlargement during the neonatal stages. One likely explanation for all these observations is that initial increase in brain size as a result of *Pten* loss leads to an elevated intracranial pressure due to the physical limitations of the skull, which in turn causes tissue bleeding and cell death. These brain abnormalities may then trigger a tissue healing process accompanied by an increase in astroglial population. It is, therefore, essential to examine not only the PHTS patients but also the other syndromes associated with macrocephaly (e.g. Neurofibromatosis type 1 - NF1) to determine whether a traumatic tissue injury leads to an irreversible loss in certain neuronal and/or glial populations. It is only surprising that such loss in essential brain cells will not result in neurodevelopmental deficits. Of note, these brain abnormalities, including increased brain size, cortical bleeding and infiltrative reactive astrocytes were noticeably alleviated by simultaneous *Rictor* loss. These results implicate a therapeutic potential of targeting Rictor in megalencephaly syndrome (abnormally large brain) patients, who carry mutations in *PTEN*, *PIK3R2*, *PIK3CA*, *MTOR*, *AKT*, *TSC1/2*, and *FGFR3* genes (Guerrini and Dobyns, 2014).

In order to understand how distinct populations of cortical neurons are affected by the brain defects listed above, I specifically examined pyramidal neurons of the cerebral cortex. These neurons are glutamatergic projection neurons, and they are arranged into morphologically distinguishable six layers (I: surface of the brain – VI: inner cortex). Late-born superficial cortical layers (II-IV) comprise corticocortical "upper layer neurons" (ULNs), and early-born more apical layers (V-VI) consist of subcortical "deeper layer neurons" (DLNs) (Britanova et al., 2008; Leone et al., 2008). It should be

noted that the majority of the cortical neurogenesis takes place between E12-E17 (Hartfuss et al., 2001), therefore, my results were mainly based on P0.5 brains and to a lesser extent neonatal stages. The pyramidal neurons are generated in an inside-out manner - formation of DLNs is followed by addition of more superficial ULNs on top of the existing neurons (Britanova et al., 2006; Tarabykin et al., 2001). In *Pten*-deficient brains, I found that a great portion of the ULNs failed to migrate to more superficial layers, and they were located below or mixed with the DLN populations. Consequently, proper neuronal layering was severely damaged, as *Pten*-deficient brains appeared to have three abnormal layers from the surface of the brain to the inner cortex: ULN-DLN-ULN. My subsequent analyses indicated that neuronal layering defects were accompanied by a glial scaffold collapse in *Pten*-deficient brains. These long fibrous processes normally stretch from the lateral ventricle (LV) to the meninges at the surface of the cortex, and they serve as a migratory scaffold for newly generated neurons during their migration to more superficial layers (Molyneaux et al., 2007). My findings are then more consistent with a model where destruction in fibrous glial scaffold as a result of *Pten* loss blocks the proper migration of the ULNs, leads to their abnormal accumulation surrounding or below the DLN population, and consequently causes neuronal layering defects. Having shown that ULNs are properly generated but failed to migrate up to more superficial layers, I aimed to examine how DLNs, the second major population of pyramidal neurons, are affected by *Pten* loss. Interestingly, *Pten*-deficient brains exhibited a significant loss in DLN populations, despite their proper localization. Concurrent *Rictor* loss rescued some, but not all, of the neuronal phenotypes in *Pten*-deficient brains, suggesting that both Akt-dependent and -independent functions of Pten regulate migration and maintenance/generation of pyramidal cortical neurons. Together, my findings reveal distinct roles of Pten in different neuronal populations of the cerebral cortex: While ULNs require intact Pten signaling for their proper localization but not formation, positioning of DLNs is unaffected by *Pten* loss, however their generation and/or maintenance is severely disrupted. It is, therefore, important to isolate the specific neuronal defects in PHTS patients prior to applying an “all-in-one” treatment plan.

This part of my thesis provides novel findings that will considerably increase our understanding of the neurological and cognitive deficits in PHTS patients, however, many questions remain to be answered: 1) What is the main event that stimulates the extensive glial response in *Pten*-deficient brains? 2) Are ectopically located ULNs construct functional neural networks? 3) Can we reestablish the fibrous network to facilitate the migration of *Pten*-deficient ULNs, or are there other cell-autonomous mechanisms behind this defect? 4) Which of the neurogenic paths does *Pten* mutation affect that leads to a substantial loss in DLNs, direct or indirect? 5) Do the layer V and VI DLNs respond the same to *Pten* loss? Addressing these questions is also essential for understanding the other malformations of cortical development and paving the way for novel therapeutic strategies.

6.4 References

Anker, L., Ohgaki, H., Ludeke, B. I., Herrmann, H. D., Kleihues, P. and Westphal, M. (1993). p53 protein accumulation and gene mutations in human glioma cell lines. *International journal of cancer. Journal international du cancer* **55**, 982-987.

Bellacosa, A., Kumar, C. C., Di Cristofano, A. and Testa, J. R. (2005). Activation of AKT kinases in cancer: implications for therapeutic targeting. *Advances in cancer research* **94**, 29-86.

Berman, D. M., Karhadkar, S. S., Hallahan, A. R., Pritchard, J. I., Eberhart, C. G., Watkins, D. N., Chen, J. K., Cooper, M. K., Taipale, J., Olson, J. M., et al. (2002). Medulloblastoma growth inhibition by hedgehog pathway blockade. *Science* **297**, 1559-1561.

Bigner, S. H., Mark, J., Mahaley, M. S. and Bigner, D. D. (1984). Patterns of the early, gross chromosomal changes in malignant human gliomas. *Hereditas* **101**, 103-113.

Brennan, C. W., Verhaak, R. G., McKenna, A., Campos, B., Noushmehr, H., Salama, S. R., Zheng, S., Chakravarty, D., Sanborn, J. Z., Berman, S. H., et al. (2013). The somatic genomic landscape of glioblastoma. *Cell* **155**, 462-477.

Britanova, O., Alifragis, P., Junek, S., Jones, K., Gruss, P. and Tarabykin, V. (2006). A novel mode of tangential migration of cortical projection neurons. *Developmental biology* **298**, 299-311.

Britanova, O., de Juan Romero, C., Cheung, A., Kwan, K. Y., Schwark, M., Gyorgy, A., Vogel, T., Akopov, S., Mitkovski, M., Agoston, D., et al. (2008). Satb2 is a postmitotic determinant for upper-layer neuron specification in the neocortex. *Neuron* **57**, 378-392.

Cancer Genome Atlas Research, N. (2008). Comprehensive genomic characterization defines human glioblastoma genes and core pathways. *Nature* **455**, 1061-1068.

Chaffer, C. L. and Weinberg, R. A. (2015). How does multistep tumorigenesis really proceed? *Cancer discovery* **5**, 22-24.

Chernova, O. B., Hunyadi, A., Malaj, E., Pan, H., Crooks, C., Roe, B. and Cowell, J. K. (2001). A novel member of the WD-repeat gene family, WDR11, maps to the 10q26 region and is disrupted by a chromosome translocation in human glioblastoma cells. *Oncogene* **20**, 5378-5392.

Davidovitch, M., Patterson, B. and Gartside, P. (1996). Head circumference measurements in children with autism. *Journal of child neurology* **11**, 389-393.

Foster, K. G. and Fingar, D. C. (2010). Mammalian target of rapamycin (mTOR): conducting the cellular signaling symphony. *The Journal of biological chemistry* **285**, 14071-14077.

Fraser, M. M., Zhu, X., Kwon, C. H., Uhlmann, E. J., Gutmann, D. H. and Baker, S. J. (2004). Pten loss causes hypertrophy and increased proliferation of astrocytes in vivo. *Cancer research* **64**, 7773-7779.

Gajjar, A. J. and Robinson, G. W. (2014). Medulloblastoma-translating discoveries from the bench to the bedside. *Nature reviews. Clinical oncology* **11**, 714-722.

Gao, D., Wan, L., Inuzuka, H., Berg, A. H., Tseng, A., Zhai, B., Shaik, S., Bennett, E., Tron, A. E., Gasser, J. A., et al. (2010). Rictor forms a complex with Cullin-1 to promote SGK1 ubiquitination and destruction. *Molecular cell* **39**, 797-808.

Groszer, M., Erickson, R., Scripture-Adams, D. D., Lesche, R., Trumpp, A., Zack, J. A., Kornblum, H. I., Liu, X. and Wu, H. (2001). Negative regulation of neural stem/progenitor cell proliferation by the Pten tumor suppressor gene in vivo. *Science* **294**, 2186-2189.

Guerrini, R. and Dobyns, W. B. (2014). Malformations of cortical development: clinical features and genetic causes. *The Lancet. Neurology* **13**, 710-726.

Guertin, D. A., Stevens, D. M., Saitoh, M., Kinkel, S., Crosby, K., Sheen, J. H., Mullholland, D. J., Magnuson, M. A., Wu, H. and Sabatini, D. M. (2009). mTOR complex 2 is required for the development of prostate cancer induced by Pten loss in mice. *Cancer cell* **15**, 148-159.

Hartfuss, E., Galli, R., Heins, N. and Gotz, M. (2001). Characterization of CNS precursor subtypes and radial glia. *Developmental biology* **229**, 15-30.

Ichimura, K., Schmidt, E. E., Miyakawa, A., Goike, H. M. and Collins, V. P. (1998). Distinct patterns of deletion on 10p and 10q suggest involvement of multiple tumor suppressor genes in the development of astrocytic gliomas of different malignancy grades. *Genes, chromosomes & cancer* **22**, 9-15.

Jones, M. J. and Jallepalli, P. V. (2012). Chromothripsis: chromosomes in crisis. *Developmental cell* **23**, 908-917.

Kool, M., Korshunov, A., Remke, M., Jones, D. T., Schlanstein, M., Northcott, P. A., Cho, Y. J., Koster, J., Schouten-van Meeteren, A., van Vuurden, D., et al. (2012). Molecular subgroups of medulloblastoma: an international meta-analysis of transcriptome, genetic aberrations, and clinical data of WNT, SHH, Group 3, and Group 4 medulloblastomas. *Acta neuropathologica* **123**, 473-484.

Laplante, M. and Sabatini, D. M. (2012). mTOR signaling in growth control and disease. *Cell* **149**, 274-293.

Leone, D. P., Srinivasan, K., Chen, B., Alcamo, E. and McConnell, S. K. (2008). The determination of projection neuron identity in the developing cerebral cortex. *Current opinion in neurobiology* **18**, 28-35.

LoPiccolo, J., Blumenthal, G. M., Bernstein, W. B. and Dennis, P. A. (2008). Targeting the PI3K/Akt/mTOR pathway: effective combinations and clinical considerations. *Drug resistance updates : reviews and commentaries in antimicrobial and anticancer chemotherapy* **11**, 32-50.

Lynch, N. E., Lynch, S. A., McMenamin, J. and Webb, D. (2009). Bannayan-Riley-Ruvalcaba syndrome: a cause of extreme macrocephaly and neurodevelopmental delay. *Archives of disease in childhood* **94**, 553-554.

Magee, J. A., Ikenoue, T., Nakada, D., Lee, J. Y., Guan, K. L. and Morrison, S. J. (2012). Temporal changes in PTEN and mTORC2 regulation of hematopoietic stem cell self-renewal and leukemia suppression. *Cell stem cell* **11**, 415-428.

Mellinghoff, I. K., Wang, M. Y., Vivanco, I., Haas-Kogan, D. A., Zhu, S., Dia, E. Q., Lu, K. V., Yoshimoto, K., Huang, J. H., Chute, D. J., et al. (2005). Molecular determinants of the response of glioblastomas to EGFR kinase inhibitors. *The New England journal of medicine* **353**, 2012-2024.

Molyneaux, B. J., Arlotta, P., Menezes, J. R. and Macklis, J. D. (2007). Neuronal subtype specification in the cerebral cortex. *Nature reviews. Neuroscience* **8**, 427-437.

Motomura, K., Mittelbronn, M., Paulus, W., Brokinkel, B., Keyvani, K., Sure, U., Wrede, K., Nakazato, Y., Tanaka, Y., Pierscianek, D., et al. (2012). DMBT1 homozygous deletion in diffuse astrocytomas is associated with unfavorable clinical outcome. *Journal of neuropathology and experimental neurology* **71**, 702-707.

Ng, J. M. and Curran, T. (2011). The Hedgehog's tale: developing strategies for targeting cancer. *Nature reviews. Cancer* **11**, 493-501.

Northcott, P. A., Jones, D. T., Kool, M., Robinson, G. W., Gilbertson, R. J., Cho, Y. J., Pomeroy, S. L., Korshunov, A., Lichter, P., Taylor, M. D., et al. (2012). Medulloblastomics: the end of the beginning. *Nature reviews. Cancer* **12**, 818-834.

Noushmehr, H., Weisenberger, D. J., Diefes, K., Phillips, H. S., Pujara, K., Berman, B. P., Pan, F., Pelloski, C. E., Sulman, E. P., Bhat, K. P., et al. (2010). Identification of a CpG island methylator phenotype that defines a distinct subgroup of glioma. *Cancer cell* **17**, 510-522.

Orrico, A., Galli, L., Buoni, S., Orsi, A., Vonella, G. and Sorrentino, V. (2009). Novel PTEN mutations in neurodevelopmental disorders and macrocephaly. *Clinical genetics* **75**, 195-198.

Ozawa, T., Riester, M., Cheng, Y. K., Huse, J. T., Squatrito, M., Helmy, K., Charles, N., Michor, F. and Holland, E. C. (2014). Most human non-GCIMP glioblastoma subtypes evolve from a common proneural-like precursor glioma. *Cancer cell* **26**, 288-300.

Phillips, H. S., Kharbanda, S., Chen, R., Forrest, W. F., Soriano, R. H., Wu, T. D., Misra, A., Nigro, J. M., Colman, H., Soroceanu, L., et al. (2006). Molecular

subclasses of high-grade glioma predict prognosis, delineate a pattern of disease progression, and resemble stages in neurogenesis. *Cancer cell* **9**, 157-173.

Rausch, T., Jones, D. T., Zapatka, M., Stutz, A. M., Zichner, T., Weischenfeldt, J., Jager, N., Remke, M., Shih, D., Northcott, P. A., et al. (2012). Genome sequencing of pediatric medulloblastoma links catastrophic DNA rearrangements with TP53 mutations. *Cell* **148**, 59-71.

Romer, J. T., Kimura, H., Magdaleno, S., Sasai, K., Fuller, C., Baines, H., Connelly, M., Stewart, C. F., Gould, S., Rubin, L. L., et al. (2004). Suppression of the Shh pathway using a small molecule inhibitor eliminates medulloblastoma in Ptc1(+/-)p53(-/-) mice. *Cancer cell* **6**, 229-240.

Rudin, C. M., Hann, C. L., Laterra, J., Yauch, R. L., Callahan, C. A., Fu, L., Holcomb, T., Stinson, J., Gould, S. E., Coleman, B., et al. (2009). Treatment of medulloblastoma with hedgehog pathway inhibitor GDC-0449. *The New England journal of medicine* **361**, 1173-1178.

Sharma, S. V. and Settleman, J. (2007). Oncogene addiction: setting the stage for molecularly targeted cancer therapy. *Genes & development* **21**, 3214-3231.

Sparks, C. A. and Guertin, D. A. (2010). Targeting mTOR: prospects for mTOR complex 2 inhibitors in cancer therapy. *Oncogene* **29**, 3733-3744.

Stevenson, R. E., Schroer, R. J., Skinner, C., Fender, D. and Simensen, R. J. (1997). Autism and macrocephaly. *Lancet* **349**, 1744-1745.

Sturm, D., Witt, H., Hovestadt, V., Khuong-Quang, D. A., Jones, D. T., Konermann, C., Pfaff, E., Tonjes, M., Sill, M., Bender, S., et al. (2012). Hotspot mutations in H3F3A and IDH1 define distinct epigenetic and biological subgroups of glioblastoma. *Cancer cell* **22**, 425-437.

Tabori, U., Baskin, B., Shago, M., Alon, N., Taylor, M. D., Ray, P. N., Bouffet, E., Malkin, D. and Hawkins, C. (2010). Universal poor survival in children with medulloblastoma harboring somatic TP53 mutations. *Journal of clinical oncology : official journal of the American Society of Clinical Oncology* **28**, 1345-1350.

Tarabykin, V., Stoykova, A., Usman, N. and Gruss, P. (2001). Cortical upper layer neurons derive from the subventricular zone as indicated by Svet1 gene expression. *Development* **128**, 1983-1993.

Tomasetti, C. and Vogelstein, B. (2015). Cancer etiology. Variation in cancer risk among tissues can be explained by the number of stem cell divisions. *Science* **347**, 78-81.

Varga, E. A., Pastore, M., Prior, T., Herman, G. E. and McBride, K. L. (2009). The prevalence of PTEN mutations in a clinical pediatric cohort with autism spectrum disorders, developmental delay, and macrocephaly. *Genetics in medicine : official journal of the American College of Medical Genetics* **11**, 111-117.

Verhaak, R. G., Hoadley, K. A., Purdom, E., Wang, V., Qi, Y., Wilkerson, M. D., Miller, C. R., Ding, L., Golub, T., Mesirov, J. P., et al. (2010). Integrated genomic analysis identifies clinically relevant subtypes of glioblastoma characterized by abnormalities in PDGFRA, IDH1, EGFR, and NF1. *Cancer cell* **17**, 98-110.

Wang, Y., Yang, J., Zheng, H., Tomasek, G. J., Zhang, P., McKeever, P. E., Lee, E. Y. and Zhu, Y. (2009). Expression of mutant p53 proteins implicates a lineage

relationship between neural stem cells and malignant astrocytic glioma in a murine model. *Cancer cell* **15**, 514-526.

Wechsler, D. S., Shelly, C. A., Petroff, C. A. and Dang, C. V. (1997). MXI1, a putative tumor suppressor gene, suppresses growth of human glioblastoma cells. *Cancer research* **57**, 4905-4912.

Weinstein, I. B. (2002). Cancer. Addiction to oncogenes--the Achilles heal of cancer. *Science* **297**, 63-64.

Wen, P. Y., Lee, E. Q., Reardon, D. A., Ligon, K. L. and Alfred Yung, W. K. (2012). Current clinical development of PI3K pathway inhibitors in glioblastoma. *Neuro-oncology* **14**, 819-829.

Zhukova, N., Ramaswamy, V., Remke, M., Pfaff, E., Shih, D. J., Martin, D. C., Castelo-Branco, P., Baskin, B., Ray, P. N., Bouffet, E., et al. (2013). Subgroup-specific prognostic implications of TP53 mutation in medulloblastoma. *Journal of clinical oncology : official journal of the American Society of Clinical Oncology* **31**, 2927-2935.